A tensor network approach to non-chiral topological order

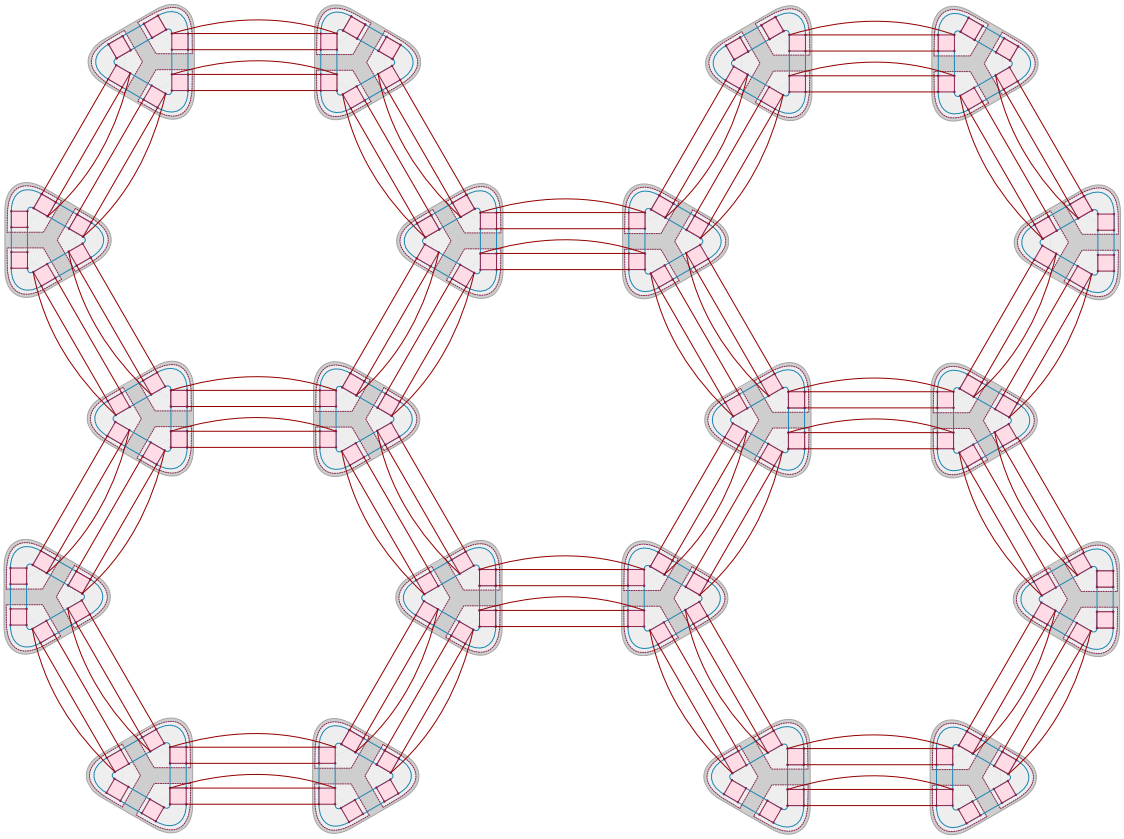

Carolin Wille

Im Fachbereich Physik der Freien Universität Berlin eingereichte Dissertation zur Erlangung des Grades eines Doktors der Naturwissenschaften. Berlin, 2019

Erstgutacher: Prof. Dr. Jens Eisert
Zweitgutachter: Prof. Emil Bergholtz, Ph.D.
Tag der Disputation: 15.5.2020

Peer-reviewed publications

[1] C. Wille, O. Buerschaper, and J. Eisert, "Fermionic topological quantum states as tensor networks," Phys. Rev. B **95**, 245127 (2017).

[2] C. Wille, R. Egger, J. Eisert, and A. Altland, "Simulating topological tensor networks with Majorana qubits," Phys. Rev. B **99** (2019).

Pre-prints

[3] A. Bauer, J. Eisert, and C. Wille, "Towards a mathematical formalism for classifying phases of matter," (2019), arXiv:1903.05413.

Contents

Part I.

Introduction

1. Overview

This Thesis discusses how non-chiral topological order in two-dimensions can be accessed within a tensor network framework. The approach is two-fold. On the one hand, we extensively discuss how tensor networks can be used as a tool to characterize topological order [1, 4–11] and how this approach blends in with other mathematical frameworks, such as string-net models [12], state sum constructions [3, 13–17] and the abstract algebraic theory of anyons formulated using category theory [18, 19]. On the other hand we use the tensor network description as a conceptual tool in the design of synthetic topological quantum matter built from mesoscopic devices, concretely networks of tunnel coupled Majorana Cooper boxes [2].

Topological order

Topological order is undoubtedly one of the most intriguing subjects studied in modern condensed matter physics. Its discovery and theoretical investigation throughout the last decades has profoundly changed our understanding of phases of matter and the mechanisms underlying their formation [20] – an achievement only recently rewarded by the Nobel prize [21]. States of matter baptized "novel" or "exotic" due to their puzzling properties in the early 80's are nowadays understood well enough to attempt harvesting their fundamental "quantumness" for applications in quantum computation [22] – a technology with revolutionary potential [23–26].

At the heart of this remarkable development is the insight, that the formation of different phases of matter can not only be attributed to the breaking of different physical symmetries – as captured beautifully by Landau's theory of symmetry breaking [27, 28] – but also to a purely quantum mechanical properties captured by the *entanglement* structure of the system [20]. Entanglement characterizes the information shared between subsystems which exceeds the information captured by classical correlations [29]. As such it is a genuine *quantum many body* phenomenon and relies on strong interactions. Topological ordered states of matter are characterized by *long-range entanglement* [30] which means that information is shared in a particular non-local fashion. As a consequence a system with topological order is sensitive to global properties of its environment which can not be detected locally – more precisely it is sensitive to the *topology* of the manifold on which it resides. The simplest example of such a dependency is the *topological ground state degeneracy*, i.e., the dimension of the ground state space depends on topological manifold invariants, e.g. the genus of a two-dimensional surface [31].

Topological order in two dimensions is of particular interest, because of the theoretically predicted point-like quasi-particle excitations which behave neither as bosons nor as fermions when exchanging the position of identical particles. These so-called anyons [31–34] feature the curious property that the wave-function is not uniquely defined by the position of the particles and instead there is a certain Hilbert space compatible with the presence of a number of such particles. For certain systems, exchanging the position of two such particles has the effect of performing a unitary rotation in this Hilbert space [18, 35, 36]. This unconventional property can again be attributed to the systems sensitivity to *topological* properties. An intuitive

interpretation of the latter statement is to consider the particle trajectory as knotted world-lines. Picturing the world-lines as defect of a 2+1 dimensional manifold, we recognize a conceptual similarity to the topological ground state degeneracy.

The theory of anyonic excitations and how the latter can be used to implement *quantum algorithms* is not the only, but perhaps the most exciting intersection of condensed matter theory and quantum information science [20]. Just as in classical computation, a quantum computation is performed by running a sequence of logical gates on some computational input state. While classical gates amount to binary operations on binary strings, quantum gates consist of local unitary operations acting on qubits, i.e., two-dimensional bosonic degrees of freedom, such as spin-1/2 particles. For some anyon models (e.g. Fibonacci anyons [12, 37, 38]) the unitary operations that result from exchanging anyonic particles are sufficient to realize arbitrary quantum gates and thus, such a system could be used as a *universal topological quantum computer* [36, 39–43].

While aiming at a universal topological quantum computer is an extremely ambitious goal, there is a more near-term application of topological order in quantum error correcting codes. A simple, paradigmatic model of topological order known as the toric code [31] has extremely beneficial properties for storing quantum information. The key idea is to use the ground states space as code space, i.e., the orthogonal basis states of the ground state space are identified with code words of logical qubits. As states in the ground state space are long-range entangled, the information is stored non-locally and robust against local noise. Due to the fact, that the toric code is an exactly solvable lattice model, i.e., its Hamiltonian is a sum of commuting projectors, it is possible to locate and identify the effects of local perturbations called "errors". A concise mathematical understanding of the system is the key to devise operations on the system that can also correct such errors in an efficient way [31, 44, 45].

The availability of commuting projector lattice Hamiltonians is one of the features that separates *non-chiral* topological order from *chiral* ones [3, 46]. While chiral topological order – characterized by gapless chiral edge modes – is the kind of topological order present in the fractional quantum Hall states [47–51] and thus observed experimentally, it is incompatible with a description in terms of commuting projector Hamiltonians [52]. On the contrary, non-chiral topological order, for which edge modes are also gapped, is beautifully captured by commuting projector Hamiltonians [12], however, as of today, no material has been found that clearly exhibits this kind of topological order[1].

A tensor network approach

The existence of commuting projector Hamiltonians (Levin–Wen string net models [12]) for non-chiral topological order can be understood on a profound mathematical level. General anyon models (including chiral theories) can be classified on an abstract mathematical level by unitary braided modular fusion categories, also called modular tensor categories [18]. On such a coarse gained level an anyon theory is a set of particle labels together with a set of rules how these particles "interact" with each other. Starting from a less structured mathematical object – a fusion category one can construct the so-called *Drinfeld center* which is a modular tensor category, which is non-chiral. It turns out, that this abstract mathematical recipe can be turned into a lattice Hamiltonian construction. Here, the fusion category is used to define degrees of freedom on a lattice and their interactions. The excitation of this Hamiltonian can then be identified with the Drinfeld center of the fusion category [19].

[1] It is still debated whether Herbersmithite is a gapless spin liquid or has non chiral $\mathbb{Z}_2$ topological order [53, 54]

This peculiar mechanism can be reinterpreted on the level of ground states within a tensor network approach [4, 6, 7, 9]. We have explained in the preceding Section that topological order is a consequence of a particular entanglement structure. Tensor network states are a class of ansatz states that exhibit the entanglement pattern of a state very clearly [55]. While they have been applied predominantly as a numerical tool [56–58], analytical studies using tensor networks can reveal fundamental conceptual insights on the structure of phases of matter. For instance, a full classification of gapped quantum phases in one dimensions has been successfully carried out using matrix product states [59–61] – a particular kind of tensor network state.

In the realm of non-chiral topological order, it was first found that the toric code ground state can be represented exactly as a tensor network state [62], a projected entangled pair state (PEPS). It became clear very soon, that the topological properties of the system can be interpreted as a consequence of *virtual symmetries* of the tensor network state [4]. These symmetries can be understood as acting in the "parameter space" of the ansatz class, which can be interpreted as the space parametrizing the entanglement. This remarkable finding can be extended to the tensor network ground states of general non-chiral topologically ordered systems [63, 64] and it has been shown that a particular structure of the virtual (entanglement) space is present in the tensor network description of all Levin–Wen string net model ground states [7]. This finding is not coincidental, but can be understood as originating from the same underlying mechanism. To be more precise, the symmetries of the virtual (entanglement) space can be capture by matrix product operators (MPOs), which bare the structure of a fusion category [8]. A unified description of these two findings can be obtained by interpreting both the Hamiltonian as well as the tensor network state within a topological state-sum construction. While it is beyond the scope of this introduction to outline this correspondence in detail, we note that a topological state sum construction assigns a topological invariant to a manifold. This is achieved by choosing a manifold triangulation and calculating quantities conceptually similar to the Euler characteristic. Per definition these quantities are invariant under retriangulations. It is this retriangulation invariance which is essentially at the core of the virtual symmetries in the tensor network and which implies that local Hamiltonian terms of the corresponding Hamiltonian are mutually commuting.

It is an interesting question whether the insights mentioned above carry over to fermionic systems [1]. While we can provide an affirmative answer to this question, we find that several adaptations to the bosonic formalism are required [1, 9, 11]. The anticommutativity of fermionic degrees of freedom makes it necessary to describe fermionic states with a different class of ansatz states, so-called *fermionic tensor network states* [65, 66]. In addition, fermionic parity is a fundamental symmetry and has to be incorporated in the mathematical formalism on an elementary level [67–69]. We explore the connection between fermionic matrix product operator symmetries in fermionic projected entangled pair states and fermionic string net models and highlight how the respective formalism are modified with respect to the bosonic setting.

Apart from an extension of the tensor network formalism to fermionic systems, our main contribution to the field presented in this Thesis is an unconventional application of the tensor network formalism – it is used as a guideline for the design of synthetic quantum materials in which topological order is realized [2]. As addressed earlier non-chiral topological order has not been found in any existing materials. This is an unfortunate situation, since non-chiral topologically ordered systems provide ideal platforms for topological quantum codes and fault-tolerant topological quantum computation [44, 70–72]. Several attempts have been undertaken to simulate or engineer non-chiral topological matter artificially [73–77]. However, most of the effort has focused on the comparably simple toric code phase [78–84]. While the

capabilities of the toric code as an error correcting quantum code are not in any doubt, it is not suited as a platform for universal quantum computation unless it is supplemented with additional hardware and protocols, which are rather costly [85–88]. To avoid the latter an alternative approach is to implement topological phases which are intrinsically more complex, in the extreme case, hosting anyons with which universal topological quantum computation can be performed. Levin-Wen string net models – a particular class of commuting projector Hamiltonians describing all known instances of non-chiral topological order – contain both extremes and the middle ground between them. In this Thesis we investigate how the latter could be realized in a concrete physical hardware platform and how the intrinsic complexity of the model interferes with and poses limits to the possible realizations. In doing so we built upon insights of the theoretical tensor network framework.

The platform we use are the so-called Majorana Cooper boxes (MCB) [89, 90] – mesoscopic units composed of several nanowires attached to a superconductor such that Majorana zero modes emerge at the boundaries of the wires. The latter are subject to a parity constraint which arises from the charging physics of the combined device and allows to identify the simplest such unit (called tetron) with a single qubit. The low-energy effective theory of tunnel coupled MCBs then gives rise to an interacting many body spin Hamiltonian acting on the effective qubits [85–87, 91]. Aided by the mindset of tensor network states and operators we present how small arrays of tunnel coupled MCBs form basic building blocks, which can be assembled to more complicated structures. In the design of the latter we investigate several mechanisms that allow to design effective Hamiltonians in a systematic fashion and make use of so-called *Hamiltonian gadgets* ideas [92–95] – a tool developed originally in quantum information theory to tackle the Hamiltonian complexity problem.

We show, how the double semion model [12, 96, 97], a string-net model of intermediate complexity, can be realized following this approach. The anyonic excitations of the double semion model are too simple to allow for universal quantum computation by braiding. Thus, we investigate how difficult it would be to engineer the simplest Levin–Wen model which is sufficient for universal topological quantum computation – the double Fibonacci model [12]. We find that the tensor network approach still reduces the required resources measured in terms of auxiliary qubits needed to design the actual phase significantly compared to a naive direct approach for which the required amount of wires and auxiliary qubits is entirely out of the question. However, the scheme we employ still relies on intricate wiring of tunnel connections and a staggered separation of energy scales which makes it experimentally hard to design and sensitive to finite temperature effects.

Results and further directions

We conclude that the tensor network formalism for non-chiral topological order is not only useful to gain a concise and profound understanding of topological phases of matter, but in addition can serve as a guiding principle in the design of artificial quantum matter. The power of the design mechanisms is partially limited by the chosen physical platform and we strongly suggest to investigate further how tensor network based schemes can be employed in other physical platforms or how the presented ideas can be elevated by employing additional hardware. We emphasize that the building blocks developed here can in principle be used in the design of other non-topological Hamiltonians as well and constitute a possible toolbox for analog quantum simulation. This direction should be explored further in the future. On a more theoretical note we remark that a tensor network description for non-chiral topological order is well explored and understood. However, it is an open question how (generalized)

tensor network constructions can access chiral topological order. Exploring the latter could lead to a unified and generalized understanding of phases of matter as a whole [3, 46].

Scope

We would like to briefly sketch the location of this work within the vast landscape of theoretical physics in order to avoid confusion and misunderstandings. This Thesis is concerned with *closed quantum systems at zero temperature*, which can be modeled by *lattice Hamiltonians*. We do not restrict ourselves to non-interacting systems described by quadratic Hamiltonians, but consider genuine strongly *interacting* many-body systems. However, we do require that interactions are short-ranged (i.e., they are *local*) and restrict ourselves to Hamiltonians that are *translation invariant* neglecting effects of disorder. We focus on Hamiltonians that are *gapped*, i.e., systems for which there exists an energy difference between the ground state space and the excited states that remains finite in the limit of infinite system size. This setting brings us into the realm of gapped *quantum phase* and their classification. The latter depends on the dimensionality and the underlying microscopic constituents. We consider mostly systems of *spins* (*or bosons*), but take a short excursion into the *fermionic* realm at some point and restrict our focus to *two dimensions*.

It is a common approach to *classify phases of matter* according to their physical symmetries or to classify different phases subject to a specific symmetry restriction, e.g. to list and label all possible time-reversal fermionic phases in one dimension. In this Thesis, we are interested in the classification of phases that emerge, when we do *not consider physical symmetries* except for fermion parity which we assume to be a fundamental. As a result the phase classification discussed here distinguishes states of matter only according to the qualitative amount of *entanglement*.

The phenomenon we are interested in is *topological order*. We aim at a deeper understanding of the latter and approach it with different mathematical formalisms partially motivated by the perspective of quantum information science, i.e., with a focus on entanglement structures. Among them are *tensor network states* – a particular class of ansatz states suitable to describe ground states of local Hamiltonians and a class of commuting projector Hamiltonian – the *Levin–Wen string-net models*. We discuss general properties of the latter two and how they are related, however, we do not perform any concrete exploratory studies of specific Hamiltonians such as mapping out phase diagrams or calculating transport properties. The focus is more on a development and interpretation of a *suitable mathematical formalism* to capture this phenomenon than on concrete instances of the latter.

In the last part of this Thesis we shift our perspective from explaining and describing phases of matter to *engineering* the latter. This brings about a change in methodology as well. We discuss the use of *low-energy effective theories* in gapped spin systems as a design principle. I.e., instead of calculating the effective Hamiltonian H_{eff} of a given Hamiltonian H, we ask how we need to design H such that a given H_{eff} emerges as the low-energy effective description. The concrete recipes are discussed for a specific physical platform (networks of tunnel coupled Majorana Cooper boxes) and are thus tailored to this setting.

Contents

While we aim to contribute to the general understanding and classification of gapped quantum matter as such, we would also like to bring this dominantly theoretical subject in closer contact

with applied sciences. In order to reach a broader audience we try to make the material presented here as accessible as possible and aim to be self-consistent. As a consequence, large parts of this Thesis are concerned with reviews of varying depth on the background material needed to understand and appreciate the topic at hand.

We start with a general introduction to *gapped local quantum phases* in Chapter 2 and present the main tools used to study the latter – entanglement and tensor network states. As an example for the usability of the latter and as a conceptual introduction to methods used later on, we review the classification of gapped local quantum phases using matrix product states.

We do not expect the reader to be familiar with *topological order* and thus present a conceptual introduction to the topic guided by the paradigmatic example of the toric code in Chapter 3. In preparation to the core material in Chapter 5 we discuss the toric code not only as a Hamiltonian model, but also its tensor network state description as a G-injective projected entangled pair state.

The introduction to topological order is completed by a general review of the abstract *algebraic theory of anyons* presented in Chapter 4. The Chapter is formulated in the language of modular unitary braided fusion categories and highlights the mathematical backbone of non-chiral topological order – the Drinfeld center construction [19].

Chapter 5 is one of the two main Chapters of this Thesis. We discuss in great detail the connection between Levin–Wen string-net models and projected entangled pair states with so-called matrix product operator isometric (MPO-isometric PEPS). As an illustrative example, we present the twisted-quantum double models in the two aforementioned formalisms and highlight how MPO-isometric PEPS are related to state-sum constructions and manifold invariants. In order not to digress to far from the tensor-network formalism and concrete Hamiltonian implementations, we refrain from reviewing state-sum constructions in full generality and only highlight certain aspects and provide an outlook to open questions, in particular addressing the question of chirality. We conclude the Chapter by presenting an extension of MPO-injective PEPS and string-net models in the fermionic realm.

In the last Chapter we propose a scheme to realize topological order via the low-energy effective Hamiltonian of a network of tunnel coupled Majorana Cooper boxes. We review different variants of low-energy effective theories and how the latter are used for *Hamiltonian design* referred to as "gadget" constructions. We continue with a discussion of Majorana Cooper box networks and the design of specific functional units composed of the latter. Finally, we show how those building blocks can be assembled to yield effective Levin–Wen string-net phases and discuss the double semion model as a detailed example and sketch how a double Fibonacci phase could be implemented. We summarize our results in Chapter 7.

2. Gapped local quantum phases

What states of matter can emerge from local interactions in a purely quantum mechanical regime at zero temperature and how can we characterize the latter in a sensible way? This question of classifying *quantum phases* is formalized in the study of gapped local Hamiltonians. A system is called *local* if the interactions between its microscopic constituents are short-ranged, i.e., they decay exponentially with the distance between sites. *Gapped* means that the ground state space is separated from the excited state space with a finite energy distance (the gap) in the infinite system size limit, also referred to as *thermodynamic limit*. Gapped local quantum systems exhibit remarkable universal properties which can be derived directly and rigorously from their definition.

Perhaps most fundamentally, there are strict bounds on the Lieb–Robinson velocities [98], which characterize the speed at which information can propagate in a local quantum systems. These so-called *Lieb–Robinson bounds* [99–101] imply several other universal properties of gapped local quantum phases. For example the entanglement entropy in gapped local systems follows a so-called *area law* [55] (cf. Section 2.1.3) which states that the entanglement shared between a subsystem and its environment grows proportional to the size of its boundary and not its volume. Lieb–Robinson bounds also allow to infer that ground states of one-dimensional gapped Hamiltonians can be approximated efficiently by a particular class of sates with low complexity [102] – so-called *matrix product states* (cf. Section 2.3.2).

An immediate physically observable consequence of Lieb–Robinson bounds is the *clustering of correlations* [99–101] stating that the correlation functions of local observables at different sites decay exponentially with the distance between them. This property can be considered as a defining feature of gapped systems and is in stark contrast to gappless systems where correlation functions decay algebraically.

It is a common point of view to regard gapless Hamiltonians as the phase transition "lines" separating different gapped Hamiltonians phases. While approaching the phase transition the correlation length of a gapped system diverges and the correlation function transitions from an exponential to an algebraic decay. The divergence of the correlation length is typically characterized by a power law with an exponent referred to as *critical exponent*. Remarkably the scaling properties close to a phase transition are often independent of the microscopic details and fall into *universality classes*. The mathematical framework for the analysis of gapless phases, also referred to as *critical systems* is largely complementary to the framework used for gapped phases and mainly employs renormalization group methods and conformal field theory. For reviews on quantum criticality see e.g. Refs. [103–105].

A few comments regarding the picture sketched above are in order. We presented the property of being gapped as generic and gaplessness as the exception, however, the question whether a "typical" local quantum systems is gapped or gapless is far from settled and largely depends of the mathematical fine-print. For systems, which are not translation invariant not even the definition given here applies as there is simply no canonical recipe how to take the thermodynamic limit. Recent work addresses this question and indicates that systems without translation invariance are generically not gapped [106]. For translation invariant systems a sequence of growing system size can be defined naturally and the definition above is meaningful.

Indeed recent results indicate that generically the latter are gapped [107, 108]. However, even in this case, there are examples of translation invariant nearest-neighbor Hamiltonians in one and two dimensions for which the question whether the gap remains finite in the thermodynamic limit is undecidable [109, 110] and one can easily imagine settings where the thermodynamic limit is not meaningful despite the system being translation invariant. For example consider a spin chain which has a ground state degeneracy that depends on the number of sites being even or odd.

To avoid problems of the kind addressed above we will assume in the following that the states of matter considered here possess a sufficient amount of homogeneity such that sequences of growing system size do not show any "discontinuous" behavior [111]. These so-called *quantum liquids* are general enough to exhibit one of the most intriguing phenomena of modern condensed matter physics – topological quantum order[1].

Topological quantum order is not detectable via local observables (cf. Section 3.1.3) and distinguished from non-topological order via its distinct entanglement structure (cf. Section 3.2.4). As a consequence, the definition of a gapped quantum phase can not be guided by local order parameters and thus goes beyond Landau's theory of symmetry breaking. Instead the definition of a quantum phase starts from scratch with the phenomenologically motivated assumption that a phase transition should be observable by a discontinuity in some local observable. Such a singularity can only occur if the gap of the Hamiltonian closes at the transition point and thus it is concluded that whenever the Hamiltonian gap is preserved along some path in the parameter space, all Hamiltonians along this path are within the same phase. This definition can be reformulated on the level of ground states and reveals the non trivial fact that two gapped Hamiltonians are in the same phase if their ground states show the same qualitative amount of entanglement.

In the remainder of this Chapter we introduce *gapped quantum phases* [20, 30, 61, 117–119] more formally. We briefly review the concept of entanglement in Section 2.1 with its different quantifiers as a prerequisite for a deeper understanding of gapped quantum phases. In Section 2.2 we present a more formal definition of a gapped quantum phase and discuss the emerging dichotomy of short- and long-range entangled phases. The crucial role of entanglement motivates the introduction of tensor network states in Section 2.3, which are optimally suited to classify states of matter according to their entanglement structure. To showcase the strength of the tensor network formalism we review the classification of gapped quantum phases in one dimensional systems via matrix product states (MPS) – a special class of tensor network states – in Section 2.4.

2.1. Entanglement

Entanglement is the source of correlations in measurement outcomes that can not be explained classically [29, 120, 121]. It is present whenever a state can not be factorized into a *product state*, i.e., a state where the many body wave function factorizes into a tensor product of the wave functions of the individual constituents

$$|\Psi\rangle = |\Psi\rangle_1 \otimes |\Psi\rangle_2 \otimes \ldots \otimes |\Psi\rangle_N \ . \tag{2.1}$$

[1] However, it is unclear, if the relatively recently discovered fracton phases [85, 112–116] can be addressed in the context of quantum liquids [111].

2.1.1. Measures of entanglement

The inspection of entanglement often relies on the concept of *density matrices*. Recall, that a general quantum system is characterized by a density matrix ρ capturing both classical probabilities of the ensemble as well as quantum mechanical probabilities. Density matrices which have more than one eigenvalue and thus more than one entry if diagonalized are called *mixed states*. In contrast, if the density matrix has only one non-zero eigenvalue (of magnitude one), i.e., it is described by a single state vector, the state is called a *pure state*. At zero temperature it is natural to work with pure states (ground states) and consider their density matrices $\rho = |\Psi\rangle \langle\Psi|$. For a system that can be partitioned into two parts A and B one then defines the *reduced density matrix* by tracing out the degrees of freedom of one of the subsystems, i.e., the reduced density matrix of a subsystem A is given by

$$\rho_A = \mathrm{Tr}_B \rho \ . \tag{2.2}$$

The reduced density matrix provides information about the amount of information shared between the two subsystems and is used to define several entanglement entropies. The one most commonly used is the von Neumann entanglement entropy

$$S(\rho_A) = -\mathrm{Tr}\left(\rho_A \log \rho_A\right) \ . \tag{2.3}$$

Unless the pure state factorizes into a tensor product of two pure states $|\Psi\rangle = |\Psi\rangle_A \otimes |\Psi\rangle_B$ defined on A and B the reduced density matrix is a mixed state and has at least two non-zero eigenvalues, which add up to one and thus are both smaller than one. Consequently, the von Neumann entanglement entropy is larger than zero and zero only for a factorizing state. For a two qubit state the maximal amount of entanglement ($\log 2$) is reached when the reduced density matrix of the remaining spin is maximally mixed, i.e., it is given by a diagonal matrix with entries $1/2$. The maximum is reached for so-called Bell states[2]

$$|\mathrm{Bell}\rangle = |00\rangle + |11\rangle \tag{2.4}$$

also referred to as maximally entangled pairs.

Another measure of entanglement derived from the reduced density matrix is the α-Renyi entropy

$$S_\alpha(\rho) = \frac{\log \mathrm{Tr}\, \rho^\alpha}{1-\alpha} \tag{2.5}$$

which approaches the von Neumann entropy in the limit $\alpha \to 1$ (from above) and is identical to the rank of the reduced density matrix for $\alpha = 0$.

A different measure of entanglement, not derived from the reduced density matrix, is the geometric entanglement entropy which quantifies the maximal possible overlap of a given state with a product state

$$E_G(|\Psi\rangle) = -\log \Lambda_{\max}(|\Psi\rangle) \ , \tag{2.6}$$

where

$$\Lambda_{\max} = \max_{\Phi} |\, \langle \Phi|\Psi\rangle \,| \tag{2.7}$$

and $|\Phi\rangle$ is a product state.

[2] It goes without saying that all states obtained by applying a factorizing unitary $U_1 \otimes U_2$ to a Bell state are maximally entangled as well.

2.1.2. Entanglement vs. correlation

It is worthwhile to emphasize the difference between entanglement and correlations. Consider the correlations of local Pauli operators σ_α ($\alpha = x, y, z$) in a spin system defined as

$$C_{i\alpha,j\beta} = \langle\Psi| \sigma_{i,\alpha}\sigma_{j,\beta} |\Psi\rangle - \langle\Psi| \sigma_{i,\alpha} |\Psi\rangle \langle\Psi| \sigma_{j,\beta} |\Psi\rangle \ . \tag{2.8}$$

The product state $|0 \dots 0\rangle$ is neither entangled nor correlated. In contrast, the GHZ state

$$|\mathrm{GHZ}\rangle = |00 \dots 0\rangle + |11 \dots 1\rangle \ . \tag{2.9}$$

(named after Greenberger, Horne and Zeilinger) is strongly correlated with respect to measurements in the z-basis and its entanglement entropy S_A is given by $\log 2$ for any connected region A. While for the last two examples entanglement and correlations coincide, we mention that for the ground states of the toric code (discussed in detail in Secs. 3.1 and 3.2.4) each spin shares a finite amount of entanglement with its environment, i.e., $\rho_{|A|=1} = \log 2$, but all spin correlations vanish identically $C_{i,\alpha,j,\beta} = 0$ for all i, j, α, β[3]. As a conclusion, we note that entanglement and correlations can occur independently and are in general different quantities describing different physical properties.

2.1.3. Area law

The scaling of the (von Neumann) entanglement entropy $S(\rho_A)$ with the size of the subsystem A is a characteristic property of a quantum phase. While in principle the rank of the reduced density matrix could grow exponentially with the number of degrees of freedom covered by the region A and thus the entanglement entropy could grow proportional to the volume of A, there are many known cases where it grows only proportional to the boundary of A. Such a scaling is called the *area law* [124]. The area law is rigorously proven for unique ground states of one dimensional gapped local Hamiltonians [125], where it implies the efficient representability of the state by matrix product states introduced in Section 2.3.2 [102] as well as for gapped free (non-interacting, quadratic) fermionic and bosonic systems [124]. The area law is conjectured to hold also for ground states of higher dimensional gapped local Hamiltonians. While this conjecture is still unproven in general, it is known to hold for important subclasses of gapped local Hamiltonians in two dimensions. In particular it holds for all states that can be represented by a certain type of tensor network state – a projected entangled pair state (cf. Sec. 2.3.3) as shown in Section 2.3.4. The latter include non-chiral topological ordered[4] and symmetry breaking states.

An interesting property of the area law is that if it holds for a ground state of some gapped Hamiltonian, it holds for all ground states of Hamiltonians within the same phase [127, 128]. Thus, it is a property of a phase rather than a property of a single state.

The area law is often invoked to justify the efficient representability of ground states of gapped local Hamiltonians with tensor network states. While it is true, that tensor network states feature an entanglement area law by construction (cf. Section 2.3.4), the converse is not true. It was shown that the area law alone is not sufficient to guarantee that a state can be efficiently represented as a tensor network state [129]. However, this does not contradict the intuition that gapped ground states are efficiently representable with tensor network states per

[3] The calculation of the entanglement entropy can be found in Refs. [122, 123].

[4] For topologically ordered states the area law holds up to a topological correction [126] to be discussed in more detail in the Section 3.2.4.

se, since there are indications[5] that being the ground state of a gapped local Hamiltonian is a much stronger condition than simply fulfilling an area law. Thus, it might very well be that states that fulfill an area law *and* are the ground states of local gapped Hamiltonians are indeed efficiently representable by tensor network states. However, this is an open problem as of today [133].

2.2. Definition and classification

Acquainted with entanglement as a general concept we now return to the definition of gapped local quantum phases closely following Refs. [30] and [111]. As we consider discrete systems such as spins or fermions on a lattice (or graph) and all finite systems have discrete energy levels, it is only sensible to define a gap as the energy difference between ground and excited states in the limit of an infinite system size – the so-called *thermodynamic limit*. In order to define a thermodynamic limit we need to specify a sequence of Hamiltonians for growing systems sizes. To construct such a sequence it is most natural to assume that the Hamiltonian is fully translation invariant. However, translation invariance alone does not guarantee that the thermodynamic limit is well defined. In contrast, there might be systems which show an alternating behavior for example in the number of ground states depending on the number of sites being even or odd. For most practical purposes one can easily detect and exclude such problematic cases, however, a more careful approach presented in Ref. [111] is to adapt the definition of a quantum phase and restrict to systems with a sufficient amount of homogeneity referred to as *gapped quantum liquid*. For the latter the ground states of Hamiltonians of increasing system size are related by a generalized local unitary circuit (introduced below) which prohibits that drastic changes occur between systems of different size.

To define phase transitions between gapped quantum liquids we invoke the phenomenological definition of a phase transition. Suppose there is a family of Hamiltonians (defined for all system sizes) which depends on a parameter g, e.g., a magnetic field strength or an interaction strength. A *phase transition* is characterized by the existence of a point g_c for which the expectation value of some observable has a singularity. The concept of *adiabatic evolution* states that for two local gapped Hamiltonians H_0 and H_1 connected by a smooth path H_g, $g \in [0,1]$ a phase transition can only occur, if the Hamiltonian H_g is not gapped or not local at some point g_c along the path [30]. Thus, two Hamiltonians are said to be in the same phase, if there exists a smooth path of local gapped Hamiltonians connecting the two.

Since the definition is tailored to gapped Hamiltonians it is reasonable to introduce a notion of a quantum phase not on the level of Hamiltonians but on the level of their ground states. We first consider the case where the ground states are unique. If there exists a gapped local Hamiltonian path $H(g), g \in [0,1]$ and $|\Phi(0)\rangle$, $|\Phi(1)\rangle$ are the unique ground states of $H(0)$ and $H(1)$, respectively, we say that the two states $|\Phi(0)\rangle$ and $|\Phi(1)\rangle$ are in the same phase. If the ground state space for $H(0)$ is degenerate, we say that two ground state spaces $\mathcal{E}(0)$ and $\mathcal{E}(1)$ are in the same phase, if their dimensionality is the same and there is a Hamiltonian path connecting $H(0)$ and $H(1)$. The existence of a Hamiltonian path is equivalent to the existence of a finite local unitary time evolution [30] transforming $|\Phi(0)\rangle$ into $|\Phi(1)\rangle$ as

$$|\Phi(1)\rangle = \mathcal{T}[e^{-\mathrm{i}\int_0^1 \mathrm{d}\, g \tilde{H}(g)}]\,|\Phi(0)\rangle \ , \tag{2.10}$$

[5] For example while contracting general PEPS is in the complexity class #P [130, 131], PEPS that are ground states of local Hamiltonians can be contracted efficiently [132]. Also, gapped local ground states fulfill a clustering of correlations that is not true for area law states in general [129].

where $\mathcal{T}$ is the time ordering operator and $\tilde{H}(g)$ is a local Hamiltonian. A finite local unitary time evolution can be approximated by a finite depth local unitary quantum circuit (essentially via writing the time evolution as a sequence of small Trotter steps). A local unitary circuit of depth M is defined as an operator $U_M = \prod_m U^{(m)}$ composed of M layers of piece wise local unitary operators $U^{(m)}$. A piece wise local unitary operator is a product of local unitary operators supported on different non-overlapping sites, i.e., $U^{(m)} = \prod_i U_i^{(m)}$. A finite depth local unitary quantum circuit is defined as a circuit that does not scale with the system size. Thus, we conclude that two (sequences of) states $|\Phi_N(0)\rangle$ and $|\Phi_N(1)\rangle$ are in the same phase if there exists a constant depth M and a (sequences of) circuits $U_{M,N}$ such that

$$|\Phi_N(1)\rangle = U_{M,N} |\Phi_N(0)\rangle \ , \tag{2.11}$$

for all system sizes N (larger than some finite value N_f). Note, that a local unitary operator acting on a finite number of spins can always be decomposed into a finite depth circuit of piece wise local unitary two-qubit gates (i.e., unitary operators acting on two spins), and thus it suffices to consider circuits composed out of two-local operators. The essential effect of a two-qubit gate (apart from changing the local basis of the individual spins) is that it can entangle or disentangle two spins. For example by performing a controlled-not (CNOT) gate we can rotate the product state $|+\rangle |0\rangle$ to a maximally entangled Bell state $|0\rangle |0\rangle + |1\rangle |1\rangle$. Thus, the depth of the local unitary quantum circuit is a measure of the maximal amount of entanglement that can be added or removed.

If by the application of a quantum gate a single spin is completely disentangled from all other spins, we can safely remove it from the system without affecting any other spins. Likewise, the definition of a quantum phase should be robust against adding unentangled spins to a given state. This motivates the introduction of generalized local unitary circuits instead of local unitary circuits, where the unitary operators are replaced by local partial isometries, i.e., operators W that are not full rank, but unitary on the support space of the state $|\Psi\rangle$ to which the circuit is applied ($W^\dagger W |\Psi\rangle = |\Psi\rangle$). A partial isometry is nothing but a unitary rotation of the multi-qubit state to a basis in which some degrees of freedom are disentangled from the rest followed by omitting the now disentangled degrees of freedom. With this notion of generalized local unitary circuits we are able to apply the definition of a quantum phase to states whose local degrees of freedom are not of the same dimension.

2.2.1. Short-range vs. long-range entangled states

According to the definition given above all product states are in the same phase as they can be deformed into each other by a single layer of on-site generalized local unitary operations. Thus, one might ask whether there exist states that are not in the product state phase, i.e., that can not be transformed to a product state with a constant depth generalized local unitary circuit. The latter are termed *long-range entangled* (*LRE*) *states* while states in the product state phase are called *short-ranged entangled* (*SRE*). Note, that all SRE phases of matter collapse to one phase according to the above definition and only long-range entangled phases of matter can be further classified.

Intuitively SRE states are states where entanglement is only shared locally. On the contrary LRE states share entanglement globally and thus need global operations (scaling with the system size) to be disentangled. One can easily write down states that are short-range entangled by starting from a product state and applying a finite layer of unitary gates to it. Examples of long-range entangled states are less obvious to construct. A prominent example for an LRE state is the GHZ state defined in Eq. (2.9). One can proof using Lieb–Robinson bounds [134]

that it can not be transformed to a product state. An intuition for this fact can be obtained if we try to disentangle spins by applying CNOT gates. While it is easy to disentangle one spin at a time (i.e., using a circuit that scales with N), it is not possible to parallelize the disentangling operations. Applying a layer of CNOT gates on pairs of sites reduces the state to a GHZ state on every second site, but than disentangling the latter requires the application of gates which are 3-local or equivalently a layer of 2-local gates. Iterating this procedure we see that the depth of the circuit inevitably scales with the system size.

Just as the GHZ state can not be transformed to a product state different GHZ states

$$|\mathrm{GHZ}\rangle_D = \sum_{\alpha=1}^{D} |\alpha, \alpha, \ldots, \alpha\rangle \tag{2.12}$$

distinguished by the number D of uniform states in the superposition belong to different phases and can not be transformed into each other. We will come back to this point once we have introduced tensor network states in Section 2.4.

In the following we will be concerned with the question whether there exist additional LRE states that are not of GHZ-type. The answer to this question depends on the dimensionality of the system and on the underlying degrees of freedom (bosons vs fermions). While for one dimensional gapped local Hamiltonian systems one can show that all LRE states are of GHZ-type, the situation gets more interesting for fermions in one dimensions [67, 68] or for higher dimensions in both fermionic and bosonic system[20]. LRE states that are not of GHZ type include the family of topologically ordered states. Those feature patterns of entanglement that is more complex than that of GHZ states and intricately linked to topological properties. We will discuss topological order and its entanglement structure in great detail in the following Sections.

Let us spent a few words on "GHZ phases" and consider the transversal field Ising model

$$H_{TI} = \sum_j -h\sigma_{x,j} - J\sigma_{z,j}\sigma_{z,j+1} \tag{2.13}$$

as an example for a Hamiltonian with GHZ type ground states. For a finite system in the phase $J > h$, the ground state is given by an adiabatic continuation of the GHZ state. However, in the infinite system size limit the ground state space becomes two-fold degenerate as the (adiabatic continuation) of the GHZ state $|00\ldots0\rangle - |11\ldots1\rangle$ becomes arbitrarily close in energy. However, this ground state space degeneracy is unstable with respect to arbitrarily small local perturbations that break the $\mathbb{Z}_2$-symmetry, i.e., that do not commute with $\prod_j \sigma_{x,j}$. Motivated by this example we interpret "GHZ phases" (i.e., the Hamiltonians with GHZ type ground states) as symmetry breaking phases where the number of states in the superposition corresponds to the number of symmetry breaking ground states of the corresponding Hamiltonian and is given by the size of the symmetry group. This perspective is further emphasized and explored in the classification of one-dimensional gapped local Hamiltonians in terms of matrix product states, discussed in Section 2.4 below.

In contrast to symmetry breaking phases, the ground state degeneracy of Hamiltonians with LRE ground states that are not of GHZ type, i.e., topologically ordered states, is robust against arbitrary local perturbations. This remarkable feature will be emphasized repeatedly throughout this text. We note, that this implies that topologically ordered states are in a sense more entangled than GHZ states. This statement can be made more precise by introducing the concept of *local stochastic quantum circuits LSCs* as presented in Ref. [111], where the unitarity of the circuit is relaxed and one finds that GHZ states can be transformed into product states via LSCs while topologically ordered states can not.

(**a**) Tensors: a scalar, a vector, a matrix, a rank-4 tensor.

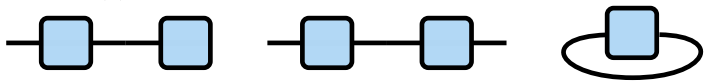

(**b**) Contracted tensors: matrix-vector multiplication, matrix multiplication, matrix trace.

Fig. 2.1. ⋆ Examples of (a) tensors and (b) tensor contractions in Penrose notation.

As it was hinted at already in the context of symmetry breaking phases, symmetries of the Hamiltonian can stabilize certain ground state degeneracies. Thus, if one restricts the space of all possible Hamiltonians $H(g)$ (or equivalently the allowed generalized unitary circuits) to those respecting certain symmetries, the phase classification is significantly refined. As certain connecting paths are now ruled out Hamiltonians that were connected previously now belong to different phases. Interestingly, the classification obtained with respect to certain symmetries (e.g. finite groups represented by global projective or linear representations) contains additional phases on top of the different symmetry breaking phases. Those symmetric phases exhibit features of topological order as long as their protecting symmetry is preserved and are therefore called *symmetry protected topological ordered* (*SPT*) phases. We will briefly address SPT phases in one dimension in Section 2.4.4.

2.3. Tensor network states

We have seen in the previous Section that entanglement plays a key role in the classification of gapped quantum phases and that the classification can be carried out on the level of states instead of Hamiltonians. A particular class of states that capture the entanglement structure of a quantum state in a concise and transparent fashion are *tensor network states* [57, 58, 135] introduced and discussed in the following Section.

A system of N local d-level systems with local Hilbert space basis $|i\rangle$, $i = 1, \ldots, d$ is generically described by a many-body wave function

$$|\Psi\rangle = \sum_{i_1, i_2, \ldots, i_N} c_{i_1 i_2 \ldots i_N} |i_1, i_2, \ldots, i_N\rangle \ , \tag{2.14}$$

i.e., by specifying all d^N coefficients in the many body basis. A tensor network state is a state for which those coefficients are given by a tensor network. That is, $c_{i_1,\ldots,i_N}$ is computed by contracting several tensors[6] arranged in a specific network that often resembles the structure of the underlying lattice. We will see momentarily that tensor network states can be used to parameterize states according to the amount of entanglement in the system. Before we so we introduce a convenient and widely used pictorial notation.

2.3.1. Penrose notation

A rank-r tensor is depicted as a box with r legs corresponding to the indices of the tensor (cf. Fig. 2.1a). Joining the index lines of two tensors denotes a contraction of the two indices, i.e., they are summed over (cf. Fig. 2.1b). Indices that are not contracted (not joined) are called open indices. This notation is most easily understood by considering the examples given in Fig. 2.1.

It is convenient to introduce additional less-standard notation for certain special cases and special tensors summarized in Fig. 2.2. First, we use the convention that index lines can go through boxes as shown in Fig. 2.2a to indicate that the tensor is diagonal with respect to the vector space associated to this index line, i.e., all tensor entries vanish if the indices at the end of the index going through the box do not assume the same value. A particularly simple and important tensor is the *delta tensor* given by the Kronecker-δ defined for an arbitrary number of indices $a, b, \ldots, n$

$$\delta_{ab\ldots} = \begin{cases} 1 & a = b = \ldots = n \,, \\ 0 & \text{otherwise.} \end{cases} \tag{2.15}$$

We will denote the delta tensor by a black filled circle as shown in Fig. 2.2b. The delta-tensor has the property that contracting several delta tensors yields a single delta tensor.

It will be convenient to represent matrices with respect to a particular block-structure. Let the row and column index of a matrix be denoted by r and c. We can introduce block-row and block-column indices, b_r and b_c and the row and column indices per block $r_{b_r,b_c} = 1, \ldots, b_r$ and $c_{b_r,b_c} = 1, \ldots, b_c$. We require that the number of rows in each block only depends on the block-row index and the number of column in each block only on the block-column index. It is then possible to represent the row index by the block-row index b_r and the row index of the respective block r_{b_r} (analogous for column indices) and use a double index line representation as in Fig. 2.2c. Since the bond dimension of the row index per block r_{b_r} depends on the block-index b_r, we use the convention that the block index is marked by a dashed line and the bond dimension of index lines parallel to dashed lines depend on the index value of the dashed-line index. A block-diagonal matrix can then be conveniently represented by a a dashed line going through the matrix-box or by using the block-index as a third index that is forwarded to row and column index lines by a delta tensor as in Fig. 2.2d. This notation will simplify calculations with block diagonal matrices.

Aside: faithful diagrams and complex conjugation

Many abstract calculations as e.g., the calculation of the entanglement entropy performed later in Section 2.3.4 can be performed in Penrose notation without ever specifying the tensors explicitly. However, if one wants to eventually relate the diagrams to explicit tensors one has to be careful that the pictograms contain all the information needed to do so. The rest of this Section deals with and resolves this issue. It is slightly technical and not essential for the understanding the rest of this Chapter.

The third pictogram in the top panel of Fig. 2.1 is invariant under rotation by 180°. Thus, if we want to identify it with a matrix A, there is an ambiguity which index represents the row and which one the column index. This implies that the given pictogram can only specify a symmetric matrix. To see this, assume the top index line in the pictogram corresponds to the row index. After a 180° rotation, top and bottom index lines are interchanged, but the diagram

[6] In this context a tensor is nothing but a data structure, i.e., a rank r-tensor is an r-dimensional array used to store complex numbers and it is not required to have any transformation properties.

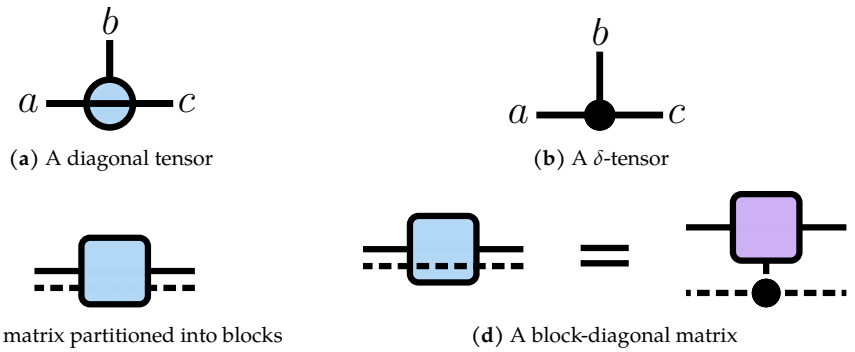

(**a**) A diagonal tensor (**b**) A δ-tensor

(**c**) A matrix partitioned into blocks (**d**) A block-diagonal matrix

Fig. 2.2. ⋆ (a) A tensor "diagonal" in the horizontal index line, i.e., $A_{abc} = a_{ab}\delta_{ac}$ (no summation convention). (b) An instance of the delta tensor δ_{abc} defined in Eq. (2.15). (c) A block matrix with square blocks on the diagonal. (d) A block-diagonal matrix.

is still the same. Thus the matrix has to be the same when permuting the row and column index $A_{ij} = A_{ji}$. To represent non-symmetric matrices we thus need pictograms that are not invariant under rotation. For general higher rank tensors we need a way to know which index line represents which index in the sequence $A_{ijk\ldots}$. If the tensor is embedded in a two-dimensional plane, this can be done by specifying which index line corresponds to the first index (e.g. by highlighting the point where the index line leaves the box) and using the convention that the second, third, etc, index corresponds to the index line that comes next when traversing the boundary of the box in clockwise or counter clockwise direction. Which of the two directions should be used is irrelevant for matrices and we could fix it by convention. However, it turns out that it is more sensible to decorate boxes with their individual clockwise or counter clockwise orientation and read off the mapping between index line and index position depending on the given direction.

As we work with tensors whose entries are complex numbers, the pictorial notation introduced so far is inconvenient, because we do not know how to represent complex conjugation pictorially. However, we would like to define Hermitian conjugation and check whether a given matrix is Hermitian or not on the level of diagrams. Since complex conjugation is an operation meaningfully defined already on the level of scalars, it makes sense to introduce its pictorial implementation as an operation defined on a box and not on the index lines. By definition this operation should be involutive. We thus need to add a decoration to the box which can be "flipped" to go back and forth between the complex numbers z and $\bar{z}$. Clearly, this decoration needs to be an unambiguous signifier for any rotated version of the diagram, since we do not want to force ourselves to specify a preferred direction on the sheet of paper that we draw on. A natural candidate for such a decoration is a handedness. For diagrams embedded in the two-dimensional plane, this can be represented by decorating the boundary of the boxes with a clockwise or anticlockwise orientation. Then complex conjugation is defined as flipping the handedness, i.e., inverting the orientation.

We can now check whether a matrix is Hermitian by permuting its row and column index (transposition) achieved by a 180° rotation and inverting the orientation of box boundary. Combining these operations we realize that this is nothing but a mirror reflection of the diagram. The convention chosen above, i.e., complex conjugation changes the way that index lines and index positions are identified allows us to define Hermitian conjugation as a reflection also for matrices that are given by contracted tensor networks embedded in the two-dimensional plane. To see this consider a diagram where all indices are labeled and the indices i and j

are (a collection of) open indices that are permuted during Hermitian conjugation. If we perform a reflection on that labeled diagram, the algebraic expression $f(i,j)$ changes by a complex conjugation $\bar{f}(i,j)$ and the indices i and j are inverted with respect to the position of the original diagram. If we now want to compare the two matrices corresponding to the original and reflected diagram, we need to relabel the open index lines, i.e., $\bar{f}(i,j) \to \bar{f}(j,i)$ and we identify the reflected tensor (network) with the Hermitian conjugate of the original. We emphasize, that defining Hermitian conjugation as a reflection would not be consistently defined, if complex conjugation did not invert the "read-off"-direction of the index positions[7]. While these consideration may seem technical, they have relevant implications. For example if we want to represent Hamiltonians as tensor networks, we need to ensure their Hermiticity. In practical terms that means, we need to check that their diagrams are invariant under reflections. In most applications considered in this Thesis, pictorial notation only serves as an illustration and we will not use the somewhat stricter notational conventions explained here.

2.3.2. Matrix product states

We consider tensor network states where the tensor network is aligned with an underlying physical lattice (cf. Fig. 2.3). For a physical system defined on a lattice with d-level systems located at the sites $j = 1, \ldots, N$, a tensor $A^{(j)}$ is placed at every physical site. Each tensor has one open physical index i_j of dimension d and is connected by virtual indices of a chosen bond dimension D along the edges of the physical lattice to all its neighbors. Fig. 2.3 shows two examples of such a construction for a regular one-dimensional and two-dimensional lattice.

The coefficients $c_{i_1,\ldots,i_N}$ of the tensor network state are calculated by contracting the tensor network. While the algebraic expression becomes cumbersome to write down for higher dimensions, in one dimension we can state it explicitly as

$$c_{i_1 \ldots i_N} = \sum_{v_1,\ldots,v_{N-1}} A^{(1)i_1}_{v_1} A^{(2)i_2}_{v_1 v_2} \ldots A^{(N)i_N}_{v_N} = A^{(1)i_1} A^{(2)i_2} \ldots A^{(N)i_N} , \tag{2.16}$$

i.e., a product of matrices and hence the tensor network state is called *matrix product state* (*MPS*).

In Eq. (2.16) a row and a column vector $A^{(1)}$ and $A^{(N)}$ are placed at the first and last sites, respectively. This is a natural choice for a system with open boundary conditions. It is also common to use only matrices and take the trace to contract the first and the last virtual index – a natural ansatz for periodic boundary conditions.

A particular example for an MPS is the δ-tensor MPS, where the tensor δ^i_{ab} with bond dimension D is chosen for every A-tensor. This MPS represents the GHZ state $|GHZ\rangle_D$ defined in Eq. (2.12) and shown in Fig. 2.4. Both delta-tensor and the GHZ state take on an important role in the classification of one-dimensional gapped local phases as discussed in Section 2.4.

In the following we provide an intuitive understanding of MPS, while a rigorous mathematical analysis is given in Section 2.4. Consider a translation invariant MPS for the sake of notational simplicity, i.e., $A^{(j)} = A$, $j = 1, \ldots, N$. The diagrammatic structure of the MPS shows that each physical spin is connected to its neighbor by an index with bond dimension D. The bond dimension D limits the amount of information that can be transmitted from one site to the next site. I.e., if $D = 1$ the matrices A^i reduce to scalars and the state collapses to a product state with no entanglement shared between sites. This factorization is visualized by the pictorial

[7] An alternative approach to represent complex numbers is to use the so-called complex-number tensors as defined in Ref. [3]. In this approach real parts and imaginary parts of a tensor are treated separately and auxiliary tensors with oriented index lines are included to mediate the multiplication of complex numbers occurring during tensor network contractions. In this formalism, it is also obvious that reflections of two-dimensional diagrams can be identified with Hermitian conjugation.

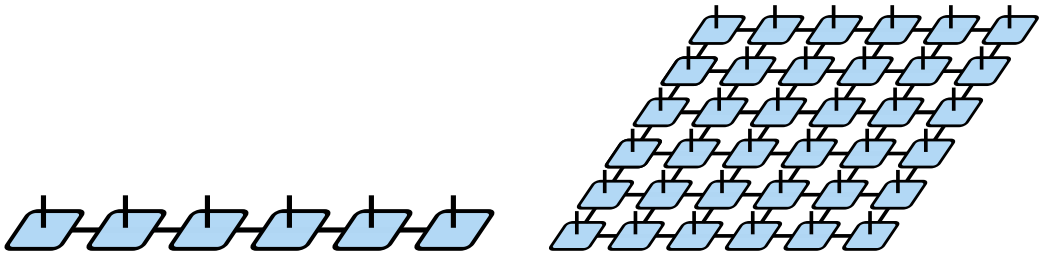

(**a**) MPS (**b**) PEPS

Fig. 2.3. ⋆ Tensor network states where the tensor network is aligned with an underlying physical lattice. (a) A matrix product state (MPS) as in Eq. (2.16) (cf. Section 2.3.2) on a one-dimensional regular lattice. (b) A projected entangled pair state (PEPS), cf. Section 2.3.3, on a two-dimensional regular lattice.

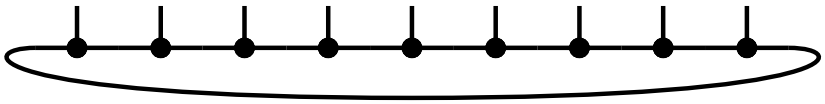

Fig. 2.4. ⋆ A GHZ state written as an MPS using delta-tensors.

notation showing N unconnected boxes. To see how information can be transferred in MPS with $D > 1$ let us consider as an example a spin-chain with local basis $|0\rangle, |1\rangle$. With $D = 2$ we can design an MPS where a spin on site j dictates the state of the spin on site $j + 1$. E.g, if we want to enforce an alternating spin pattern, we can choose $A^0_{01} = A^1_{10} = 1$ and all other entries equal to zero. With this choice of matrices, the left virtual index determines the physical index and sets the right virtual index to its opposite value. This index is passed on to the next site where it ensures the orthogonality of the spin state to its left neighbor. As a second example consider the case where $D = 2^2$. Here, we can imagine the virtual index as a double index each with dimension 2. In this case, one index line could be used to communicate the physical spin value to the nearest neighbor as in the previous example, while the other index line could fast-forward the spin value directly to the next nearest neighbor. Thus, by increasing the bond dimension spins are able to communicate directly with spins at larger distances. However, the doubling of the index lines in the example indicates that to communicate directly with a spin k sites away, a bond dimension $D = d^k$ is required.

MPS as ground states of local gapped Hamiltonians in one dimension

So far, we have introduced tensor network states as abstract tools which can store information about a wave function and with which calculations can be performed, but we have not yet related them to Hamiltonians or phases of matter. However, the great strength and justification of the wide use of MPS lies in the fact that MPS provably describe gapped local systems in one dimension very well. To explain this statement, first of all note that any state can be written as an MPS, if one allows for large enough bond dimension. In particular, for a system of size N choosing $D = d^N$ one can immediately write down an MPS given $c_{i_1,\ldots,i_N}$. The crucial question is whether a state can be represented with a bond dimension that does not scale exponentially with the system size N. For the ground states of one dimensional gapped, local spin Hamiltonians the answer is affirmative. In fact, the ground state of a gapped local Hamiltonian of system size N can be approximated by an MPS with a bond dimension that grows sub-linearly with the system size to an accuracy of $\mathcal{O}(1/poly(N))$ [136]. Moreover, there exists a polynomial time algorithm (the time needed to compute scales polynomially with the system size) to find

such an MPS, again to an accuracy $\mathcal{O}(1/poly(N))$.[8]

This approximability statement is very strong as it tells us that there exists an extremely efficient representation of the ground state. Note, that instead of specifying d^N complex numbers, the wave function of an MPS is represented by only $N \times d \times D^2$ complex numbers – an exponential reduction in the amount of storage needed on a computer. In addition, one can efficiently compute expectation values on MPS by performing matrix multiplications of small $\mathcal{O}(D^4)$ matrices. While a sublinear scaling of the bond dimension is beneficial, it is not sufficient to guarantee that any ground state of a gapped local Hamiltonian can be approximated well with an MPS of *finite* bond dimension. However, in practical calculations one often sees that the bond dimension saturates, i.e., increasing the bond dimension of the ansatz state any further does not result in an improvement (lowering) of the ground state energy. For the classification of phases of matter in one-dimensional gapped local systems it is thus a reasonable starting point to classify all MPS with constant bond dimension. Recent results [102] further support this line of thought. In Ref. [102] it is shown that MPS can approximate ground states of gapped local Hamiltonians locally (i.e., on a region of size l) to a given precision ϵ with a bond dimension that depends on l and ϵ, but is constant with respect to the system size.

Parent Hamiltonians

For any MPS there exists a so-called *parent Hamiltonian* which has the MPS as its ground state. It is given by the following construction [59, 60]: The reduced density matrix ρ_R of the MPS defined on a region of suitable size R is supported on the space $\mathcal{S}_R$. Defining the projector h_R projecting onto the complementary space one obtains the parent Hamiltonian as a sum of local projectors

$$H = \sum_R h_R \,, \; \ker(h_R) = \mathcal{S}_R \,. \tag{2.17}$$

If the MPS is translation invariant, one can show [59, 60] that the parent Hamiltonian is gapped and frustration-free. We will comment on the ground state degeneracy of the parent Hamiltonian in more detail in Section 2.4.

2.3.3. Projected entangled pair states

The generalizations of matrix products states for higher-dimensional systems are called projected entangled pair states (PEPS) [57, 124, 140, 141]. PEPS are often introduced as tensor network states for spins on a regular lattice where one tensor is located at every physical site and virtual bonds connect tensors along the edges of the physical lattice (cf. Fig. 2.3). Thus, MPS are nothing but PEPS in one dimension. While PEPS sometimes also refers to PEPS in three dimensions, it is mostly used for PEPS in two dimensions. In the context of phases of matter it is sensible to use a definition for PEPS that takes into account systems of growing size: A PEPS is a tensor network where – after blocking of a finite number of tensors – the tensor network consists of one tensor per physical site and the tensor network graph forms a lattice matching the dimensionality of the physical system. The rank of the tensors are bounded and the bond dimensions do not increase with the system size.

To understand the meaning of this definition, consider a kind of tensor network state that is very different from MPS and PEPS in both structure and purpose: The multi-scale entanglement renormalization ansatz (MERA) for one-dimensional systems is a hierarchical tensor network

[8] This algorithm is based on approximate ground state projections (AGSP) [137] and the MPS structure of the ground state. It is more rigorous and less heuristic than the more widely used density-matrix renormalization group (DMRG) method [138, 139] and thus also called RRG (rigorous renormalization group algorithm).

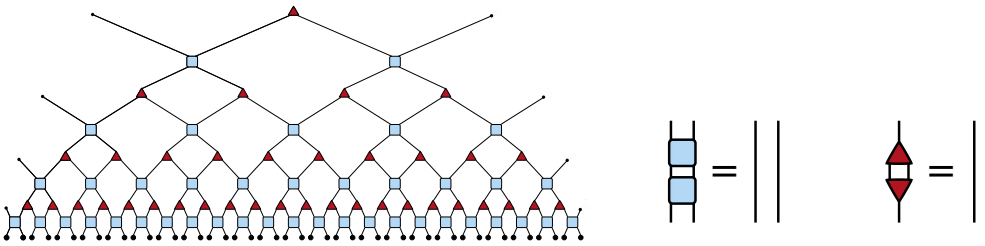

(a) MERA in one dimension. (b) Isometries and disentanglers.

Fig. 2.5. ⋆ A one-dimensional MERA state composed of isometries (blue) and disentanglers (red).

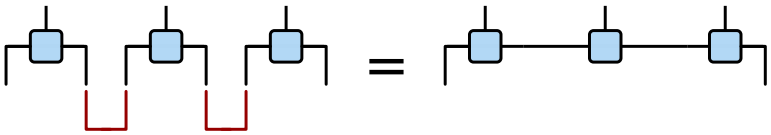

Fig. 2.6. ⋆ A one-dimensional PEPS (MPS) written as a "projected entangled pair state".

state consisting of $\log_2 N$ layers of virtual tensors and only the outermost (bottom) layer has open indices describing the physical state (cf. Fig. 2.5). One dimensional MERAs have been developed to efficiently describe critical (i.e., gapless) systems and are as such clearly distinct from MPS that describe ground states of gapped Hamiltonians. By inspection of the MERA network we note that the number of tensors used to describe N spins is still proportional to N (i.e., $2N-1$), but we can not distribute and block the tensor network in such a way that we obtain an MPS with a size-independent bond dimension [142]. A simple intuition for this can be gained by considering the effective bond dimension between one half of the chain and the other. Counting the number of crossed bonds we roughly estimate it as $\chi^{\log_2 N}$, where χ is the bond dimension of the MERA tensors. To represent such a state by an MPS the bond dimension D of the MPS needs to increase with the system size and can not remain constant. Thus, the definition above is designed to distinguish a "MERA in disguise" from a true MPS.

The name projected entangled pair state can be understood by a reinterpretation of the tensor network. To this end, consider a $D = 2$ PEPS[9] on a regular lattice of N sites and k edges per site. Place two virtual qubits at each virtual index line and maximally entangle them, such that they are in a Bell state as given in Eq. (2.4). Now apply operators $A^{(j)} : \mathbb{C}^k \to \mathbb{C}$, $j = 1, \ldots, N$

$$A^{(j)} = |i\rangle A^{(j)i}_{a_1 a_2 a_k} \langle a_1, a_2, \ldots, a_k| \tag{2.18}$$

to each site, i.e., the operator A acts on k virtual qubits located at the site j. The emerging state

$$|\Psi\rangle = \prod_{j \in \text{sites}} A^{(j)} \prod_{e \in \text{edges}} |\text{Bell}\rangle_e \tag{2.19}$$

is a projected entangled pair state. This can be easily seen if we disregard the bra-ket-structures (Choi–Jamilkowsi isomorphism) and note that $|\text{Bell}\rangle \simeq |0\rangle\langle 0| + |1\rangle\langle 1| \simeq \mathbb{1}_2$. Fig. 2.6 shows the construction above for a one-dimensional PEPS, i.e., an MPS in Penrose notation.

[9] For $D > 2$ qubits have to be replaced by qu-D-dits, but the construction is completely analogous.

PEPS as ground states of gapped local Hamiltonians in two dimensions

Similar as in the case of MPS and one-dimensional gapped local Hamiltonians, one can show that PEPS approximate ground states of local gapped two-dimensional Hamiltonians, although the statement is severely weaker [133, 143]. Under the assumption that the density of states grows at most polynomially with the system size one can prove that a PEPS approximates the ground state to accuracy $\mathcal{O}(polyN)$ with a bond dimension that scales subexponentially, i.e., $D < e^{\mathcal{O}(\log^2 N)}$. Whether this scaling can be improved to polynomial scaling is an open question [133].

Another difficulty of two-dimensional PEPS is that calculating local observables requires the contraction of the tensor network just as in the case of MPS. While the contraction of an MPS boils down to several matrix multiplications and is thus both efficient in theory and practice, contracting a PEPS is more difficult. It is known that contracting PEPS is in the complexity class #P. However, this theorem does not apply to the contraction performed for the calculations of local observables of local gapped ground states given by a PEPS [132]. Nevertheless, the practical implementation is still difficult and requires heuristic truncation techniques. To see this, note, that when a $L \times L$ PEPS grid is contracted column by column, one obtains a row of matrices with bond dimension D^L and thus a naive contraction approach scales exponentially with the system size. State of the art algorithms use physically motivated partial contractions that are then subjected to a singular value decompositions and only the matrix entries corresponding to the highest singular values are kept (truncation), such that an exponential blow up of the bond dimension of the partially contracted tensor network is avoided [58, 144, 145].

Variational numerical algorithms similar to DMRG for ground state searches using PEPS as ansatz states exist [144, 146–148] and are still evolving rapidly [149–151]. Compared to the "rival algorithms" – so-called Monte Carlo methods based on random sampling – PEPS algorithms do not suffer from the so-called sign problem [152, 153] which hinders the usage of Monte Carlo methods for frustrated spin and fermionic systems. In these cases PEPS based algorithms are often claimed to be superior [154–156].

Parent Hamiltonians. – The parent Hamiltonian construction for MPS can be adapted to PEPS in a straightforward fashion. Eq. (2.17) still applies. However, an important difference to the MPS setting is, that the Hamiltonian obtained by this construction can be gapless [62, 157]. Conditions under which the parent Hamiltonian is gapped are discussed in more detail in Section 3.2.3 and Section 5.2.2.

Exact fix point PEPS. – While the general representability of ground states of local gapped Hamiltonians in two-dimensional with PEPS is still debated [158], it is clear that a large class of fix-point models (i.e., models with zero correlation length) have exact PEPS representations. In particular, a large class of quantum phases with topological order have exact PEPS ground states. Formulating the last statement more strongly, there is no phase of matter known that has a particular kind of topological order, namely *non-chiral* topological order, which does not have a fixed-point Hamiltonian with an exact PEPS ground state. This indicates that there is a rather deep connection between PEPS and non-chiral topological order. This connection will be the subject of Chapter 5.

2.3.4. Entanglement area law for tensor network states

We have claimed that tensor network states exhibit the entanglement structure of a state very clearly. To convince ourselves of this fact and to get familiar with the way in which calculations for tensor network states are performed on a diagrammatic level, we compute the area law

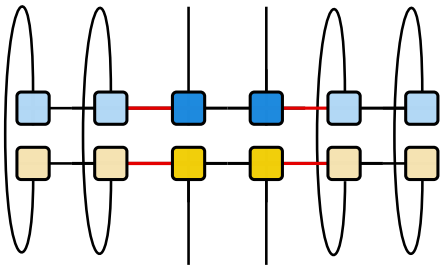

Fig. 2.7. ⋆ The reduced density matrix ρ_C as described in the text in Penrose notation. The matrices C_1, C_2 and R marked in green, orange and blue, respectively. Virtual bonds crossing the region C marked in red.

scaling of the von Neumann entanglement entropy (cf. Section 2.1.3) in PEPS. Consider a connected convex region C of a PEPS depicted in Fig. 2.3 for the one-dimensional case. The boundary of C is denoted by ∂C and the size of a region (denoted by $|C|$) is measured by the number of local degrees of freedom contained in$C$. The reduced density matrix ρ_C can be expressed conveniently in Penrose notation. To this end, we write $|\Psi\rangle$ and $\langle\Psi|$ in pictorial notation. The trace over the complement of C corresponds to connecting the open indices of the ket state in the complement of C with their bra-counterparts.

By inspection of the diagram (shown for a one-dimensional lattice in Fig. 2.7) we realize that the reduced density matrix can be decomposed into a product of matrices $\rho_C = C_1 R C_2$. Here C_1 corresponds to the C-region of the ket-state and is a $d^{|C|} \times D^{|\partial C|}$-matrix and C_2 represents the C-region of the bra-state is a $D^{|\partial C|} \times d^{|C|}$-matrix. Finally, the matrix R represents the rest of the reduced density matrix and its dimension is given by the number of bonds that cross the boundary of C, i.e., $D^{|\partial C|} \times D^{|\partial C|}$. As the rank of a matrix product is bounded by the smallest dimension occurring in the multiplication, we conclude that for a sufficiently large region the rank is bounded by $D^{|\partial C|}$. It is then straightforward to calculate that the von Neumann entropy is bounded by $\mathcal{O}(|\partial C| \log D)$, i.e., it scales with the boundary of C and we have verified that tensor network states with a 'physical' lattice structure, i.e., MPS and PEPS, fulfill the area law.

2.4. One dimension – A full classification via matrix product states

Motivated by the findings that MPS approximate ground states of gapped local Hamiltonians in one dimension very well, a classification of gapped local quantum phases based on MPS has been developed in the past years [4, 61]. The key insight is that translation invariant matrix product states with a finite bond dimension can be brought into a block-diagonal (canonical) form [60][10] such that individual matrices form a finite dimensional C^*-algebra under multiplication and addition.

Using the fact that for each finite dimensional C^*-algebra there is a finite group G and a unitary representation $U(g)$ such that U_g commutes with all elements of the C^*-algebra, one can relate the canonical form to *virtual symmetries* of the individual tensors. The virtual-symmetry approach can be carried over and extended to the two-dimensional case, where a canonical form is no longer available. Thus, we review the classification of one-dimensional gapped local quantum phases via MPS with a two-fold motivation. First, to show the power of tensor network methods and second to introduce the concepts which are fundamental to the analysis of non-chiral topological order in PEPS in Chapter 5.

[10] A more recent and more general *irreducible form* is presented in Ref. [159].

This Section is a shortened and condensed review of Refs. [4] and [61], which in turn relies on the seminal work of Refs. [59] and [60].

2.4.1. Overview of the result

The canonical form [60] is obtained by applying a gauge transformation

$$A^i \to UA^iU^{-1} \tag{2.20}$$

at every site j which leaves the state invariant. In this canonical form the matrices A^i are simultaneously block diagonalized, i.e., all A^i are decomposed into blocks of the same shape and for each block b of dimensions $B_b \times B_b$, the matrices A^i_b span the space of all complex $B_b \times B_b$ matrices, i.e., $\mathrm{span}(\{A^i_b\}_i) = \mathbf{L}(\mathbb{C}^{B_b})$.

It directly follows that the A^i span a direct sum of the vector spaces of B_b-dimensional linear operators $\mathrm{span}(\{A^i\}_i) = \oplus_b \mathbf{L}(\mathbb{C}^{B_b})$ which is a finite dimensional C^* algebra. Apart from the position of the blocks in the decomposition and unitary basis changes within each block, the canonical form is unique and thus, each translation invariant MPS can be uniquely classified by its corresponding finite dimensional C^*-algebra.

Fundamental theorems of representation theory (in particular Schur's lemma) relate the C^*-algebra structure to a discrete symmetry group G acting on the virtual level. One distinguishes between the single-block case, where the symmetry group is trivial, the MPS tensors are injective and the ground state of the parent Hamiltonian is unique and the general case, called the G-injective case. Both are reviewed in detail in the next Sections as they can be seen as the conceptual foundation of the tensor network approach to gapped quantum phases in general including the higher dimensional cases. The main result is the following. The number of conjugacy classes of the group G determines the ground state degeneracy of the parent Hamiltonian and G-injective MPS are LRE states with GHZ-type entanglement. As a consequence, the existence of topological ordered states in one dimensional gapped spin systems is ruled out and as long as (physical) symmetries are not taken into account, there are only trivial and symmetry-breaking phases classified by different ground state degeneracies.

2.4.2. Injective MPS

If the most refined block decomposition of the matrices A^i for a bond dimension D MPS is a single block of size $D \times D$, the MPS is called injective, as there is a one-to-one correspondence between the physical and the virtual vector spaces and in particular, there exist an inverse $\tilde{A}$, such that

$$\sum_i \tilde{A}^i_{ab} A^i_{cd} = \delta_{ac}\delta_{bc} \tag{2.21}$$

as visualized in the left panel of Fig. 2.8. The existence of the inverse can be seen as follows. Consider the space $\mathbf{L}(\mathbb{C}^D)$ as a vector space. A scalar product between the vectors of $\mathbf{L}(\mathbb{C}^D)$ is defined by $\mathrm{Tr}(A^\dagger B)$ and linear operators $K : \mathbf{L}(\mathbb{C}^D) \to \mathbf{L}(\mathbb{C}^D)$ are given by rank-4 tensors with two double line input and two double line output indices (each of bond dimension D). In particular the identity element $\mathbb{1} : A \mapsto A$ acting on vectors in $\mathbf{L}(\mathbb{C}^D)$ is a double line of identities $\mathbb{1} \simeq \mathbb{1}_D \otimes \mathbb{1}_D$. Since the A^i span a (non orthonormal) basis of $\mathbf{L}(\mathbb{C}^D)$ a resolution of the identity can be constructed from them $\mathbb{1} = \sum_i |\tilde{A}^i\rangle\langle A^i| = \sum_{ij} |A^j\rangle b_{ji} \langle A^i|$ for appropriately chosen b_{ij} defining the $\tilde{A}$. In the special case where the basis A^i is orthonormal, the MPS is called isometric and the resolution of the identity is simply given by $\mathbb{1} = \sum_i |A^i\rangle\langle A^i|$, i.e., $\sum_i \bar{A}^i_{ab} A^i_{cd} = \delta_{ac}\delta_{bc}$.

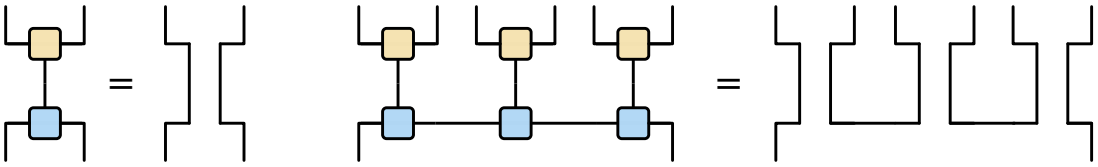

Fig. 2.8. ⋆ The inverse of an injective left MPS (left) can be used to disentangle the state to a product state (right).

Note, that injectivity requires that the physical dimension d exceeds D^2. This can be achieved by blocking matrices on neighboring sites in a region l and treating the l index lines as a single index of dimension d^l such that $d^l > D$. Generically, i.e., if the A^i are chosen randomly and do not posses additional structure, the blocked matrices on regions of size l will be injective.

Once injectivity is reached, it is stable under blocking, i.e., if A^i is injective also A^iA^j is injective.

Parent Hamiltonian

The parent Hamiltonian for injective MPS has a unique ground state which is shown in the following. It is constructed as defined in Eq. (2.17) and it suffices to choose two neighboring sites as the region R. The support space of the reduced density matrix can be spelled out explicitly and is given by

$$\mathcal{S}_2 = \mathrm{span}\{\mathrm{Tr}(A^iA^jR)\,|ij\rangle\}_{R,ij}\,, \tag{2.22}$$

where $R \in \mathbf{L}(\mathbb{C}^D)$. The parent Hamiltonian of an injective MPS can then be constructed from local projectors onto the 2-site support space $\Pi_{\mathcal{S}_2}$ by projecting onto the orthogonal compliment on every pair of sites, i.e.,

$$H = \sum_i h_i\,, \tag{2.23}$$

where

$$h_i = 1 - \Pi_{\mathcal{S}_2}(i, i+1) \tag{2.24}$$

and we assume periodic boundary conditions (i.e., $i \simeq i + L$). It is crucial to check that the Hamiltonain constructed this way is gapped. A proof of the gap property for parent Hamiltonians of general MPS is provided in Ref. [60]. Here, we will only show that the Hamiltonian in Eq. (2.23) is frustration free and has a unique ground state given by the MPS. To see this, note that it is a sum of local projectors and thus, there are two cases. Either the intersection of all local ground states $\mathcal{S}_2$ on different pairs of sites vanishes. In this case, the Hamiltonian is frustrated, because not all local constraints can be fulfilled simultaneously. Or the intersection of all $\mathcal{S}_2$ is the ground state space. We will show, that the latter is the case.

To see this, we first consider the Hamiltonian on an open chain of length L and convince ourselves, that the intersection of all $\mathcal{S}_2$ is equal to $\mathcal{S}_L$, i.e., the physical state space spanned by an MPS of length L with open boundary conditions. This is done by noting that

$$\mathbb{C}^d \otimes \mathcal{S}_{k-1} \cap \mathcal{S}_{k-1} \otimes \mathbb{C}^d = \mathcal{S}_k\,, \tag{2.25}$$

and applying this identity inductively to $\mathcal{S}_L$. Eq. (2.25) can be proven by writing any element in $\mathcal{S}_{k-1} \otimes \mathbb{C}^d$ as a three site MPS

$$\mathrm{Tr}[A^iB^jN^k]\,|ijk\rangle \tag{2.26}$$

where the first site corresponds to the first physical site,the second site corresponds to sites $2, \ldots, k-1$ blocked together, i.e., $B^j = A^{i_2} \ldots A^{i_{k-1}}$ and the third site corresponds to the k-th

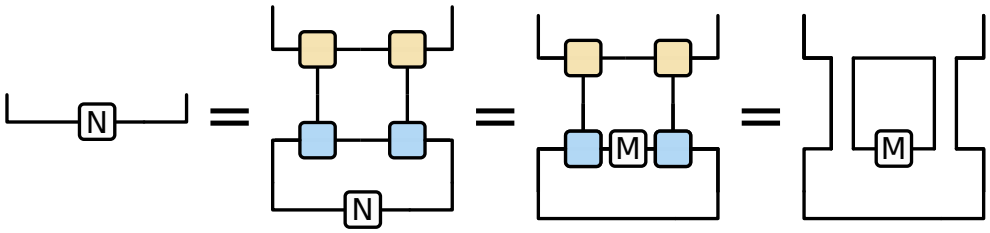

Fig. 2.9. ✦ Closure for injective MPS. Any tensor N for which there exists M, such that $|\Psi\rangle_N = \sum \mathrm{Tr}[A^i B^j N]\,|ij\rangle = \sum \mathrm{Tr}[A^i M B^j]\,|ij\rangle = |\Psi\rangle_M$ is proportional to the identity in the case that A^i and B^i are injective.

physical site, where an appropriate tensor N has been placed. The representation of $\mathbb{C}^d \otimes \mathcal{S}_{k-1}$ is done analogously and the intersection is calculated by using that

$$\{\sum_{i,j,k} \mathrm{Tr}[A^i B^j N^k]\,|ijk\rangle\}_M \cap \{\sum_{i,j,k} \mathrm{Tr}[M^i B^j A^k]\,|ijk\rangle\}_N = \{\sum_{i,j,k} \mathrm{Tr}[A^i B^j A^k X]\,|ijk\rangle\}_X\,, \tag{2.27}$$

which can be proven diagrammatically by using the inverse of A and B. Thus, we know that the ground state space on an open chain is not empty. It is given by $\mathcal{S}_L$, which contains the MPS of length L with open boundary conditions.

The interesting point is the closing of the chain. Here, the analysis of injective MPS deviates from the non-injective case. The ground state space on a closed chain can be calculated by the intersection space of two "overlapping" chains. To see this, we split the Hamiltonian in Eq. (2.23) according to $H = H_L + H_R$ where H_L does not contain $\Pi_{\mathcal{S}_2}(1,2)$ and H_R does not contain $\Pi_{\mathcal{S}_2}(L,1)$. The ground state space of H is then given by the intersection of the ground state spaces of H_L and H_R. The latter can be represented as open-chain MPS with closure tensors between sites L and site 1 or sites 1 and 2 respectively, i.e.,

$$\mathcal{S}_{L,\mathrm{closed}} = \{\sum_{\{i\}} \mathrm{Tr}[A^{i_1} B^{i_{2\ldots L}} N]\,|i_1 \ldots i_L\rangle\}_N \cap \{\sum_{\{i\}} \mathrm{Tr}[A^{i_1} M B^{i_{2\ldots L}}]\,|i_1 \ldots i_L\rangle\}_M\,. \tag{2.28}$$

The intersection of the two spaces parametrized by the two MPS does only contain the MPS with trivial closure tensor $M = N = \lambda \mathbb{1}$ in the injective case, i.e., $\mathcal{S}_{L,\mathrm{closed}}$ is one-dimensional and

$$\mathcal{S}_{L,\mathrm{closed}} \ni \sum_{\{i\}} \mathrm{Tr}[A^{i_1} A^{i_2} \ldots A^{i_L}]\,|i_1 \ldots i_L\rangle\ . \tag{2.29}$$

It is the closure property which changes in the non-injective case and opens up the possibility for grounds state degeneracies. The proof of the closure property in the injective case proceeds in two parts. First, the one-dimensional space given by $N = M = \mathbb{1}$ is trivially contained in the intersection. Second, if there is an M-tensor for which one can find an N-tensor such that the state determined by N is equal to the state given by M (i.e., the state is in the intersection), one can show, that the tensor M is proportional to the identity (cf. Fig. 2.9).

For isometric MPS the parent Hamiltonian can be easily constructed from the matrices A^i. Consider the operator $\Pi_{\mathcal{S}_2}$ defined in Fig. 2.10. One easily checks using the isometry property that it leaves the MPS invariant when applied to any two adjacent sites, i.e., $\Pi_{\mathcal{S}_2}\,|\mathrm{MPS}\rangle = |\mathrm{MPS}\rangle$. Using manipulations on diagrams it is also not difficult to check that $\Pi_{\mathcal{S}_2}$ is a projector and that two $\Pi_{\mathcal{S}_2}$ acting on overlapping sites commute. Thus, the Hamiltonian defined in Eq. (2.23) with h_i defined as in Eq. (2.24) and $\Pi_{\mathcal{S}_2}$ defined in Fig. 2.10 is a mutually commuting projector Hamiltonian that has $|\mathrm{MPS}\rangle$ as ground state with zero energy. To show that it is the unique

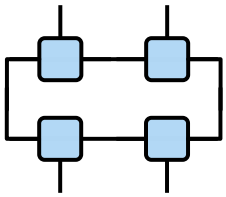

Fig. 2.10. ⋆ The projector $\Pi_{\mathcal{S}_2}$ onto the support space of 2-sites for an isometric MPS.

ground state, first note that Π_2 is a rank-D^2 projector by calculating its trace again in pictorial notation. In addition, the 2-qubit space spanned by $\{|i\rangle\,|j\rangle\,A^i_{ab}A^j_{bc}\}_{ac}$, i.e., spanned by two MPS matrices with open virtual indices is also D^2 dimensional. Thus, there is no other local space that survives the projection $\Pi_{\mathcal{S}_2}$ and thus $|\mathrm{MPS}\rangle$ is the unique ground state.

All isometric MPS are in the same phase since they can be deformed into a product state by applying $A^\dagger$ on every site as demonstrated in Fig. 2.8 (right). This result can be extended to show that all injective MPS are in the same phase [61] by using the fact that every matrix can be decomposed into a positive matrix Q and an isometric matrix W[11]. The positive part can then be smoothly tuned to zero. To be more precise, one considers the parent Hamiltonians of the MPS with matrices $A = Q_A W$ and its isometric cousin $A = W$. One can then define an adiabatic path of local gapped Hamiltonians interpolating smoothly between $Q = Q_A$ and $Q = \mathbb{1}$.

2.4.3. G-injective MPS

The case where the matrices A^i can be decomposed into a non-trivial block structure is more interesting. Insights from the representation theory of finite groups yield a connection between the block structure and a symmetry on the virtual space. To see this, we start with rearranging the block structure of

$$\mathcal{D} = \mathrm{span}(\{A^i\}_i) = \bigoplus_b \mathbf{L}(\mathbb{C}^{B_b})\,. \tag{2.30}$$

If there are several blocks with the same dimension m, we can permute the blocks by a unitary transformation acting on the virtual indices[12] such that some of them, say $\tilde{d}$, occur next to each other in the block decomposition. This can be represented as $\mathbb{1}_{\tilde{d}} \otimes \mathbf{L}(\mathbb{C}^m)$. We now permute the blocks such that d_i blocks of dimension m_i occur next to each other and perform a direct sum over i to arrive at

$$\mathcal{D} = \bigoplus_{i=1}^{I} \mathbb{1}_{d_i} \otimes \mathbf{L}(\mathbb{C}^{m_i})\,. \tag{2.31}$$

It is clear that we can write $\mathcal{D}$ in this form for appropriately chosen d_i and m_i, however, it is not yet clear what the meaning of d_i and m_i is. This becomes clear, if we recall Schur's lemma from representation theory as stated for the simple case of finite groups: Consider a irreducible representation ρ_g of a finite group G with elements $g \in G$ of dimension d. If a non-zero element of $\mathbf{L}(\mathbb{C}^d)$ commutes with all ρ_g, it has to be proportional to the identity.

On the other hand we know that every unitary representation of a finite group U_g can be decomposed by unitary transformations into a direct sum of irreducible representations, where

[11] This decomposition is called polar decomposition by comparison with the usage of polar coordinates of complex numbers to which it reduces in the case of one dimensional matrices.

[12] These so-called gauge transformations do not affect the physical state and are a standard tool for calculations with tensor networks.

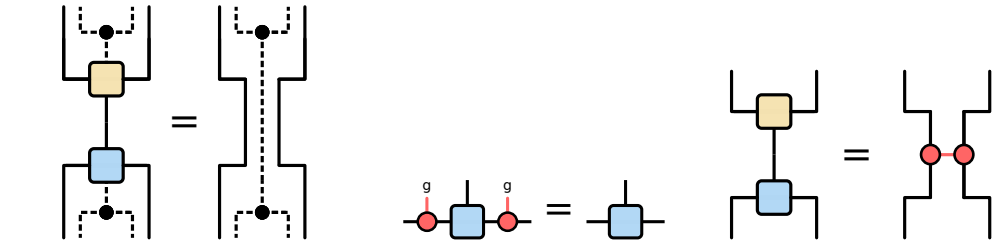

(**a**) G-injectivity (block representation) (**b**) G-symmetry (**c**) G-injectivity

Fig. 2.11. ⋆ G-injective MPS. (a) restricted injectivity in the space of block-diagonal matrices. (b) G-symmetry and (c) G-injectivity as defined in Eqs. (2.33) and (2.35), respectively. Note, that the normalization factor $1/|G|$ is not represented in the diagram on the right in (c).

the same irreducible representation can appear several times (multiplicity). We can thus write a unitary representation of a group U as a direct sum of irreducible representations ρ_i with dimension d_i and multiplicity m_i as

$$U_g = \bigoplus_{i=1}^{I} \rho_i(g) \otimes \mathbb{1}_{m_i} \,. \tag{2.32}$$

If an element of $\mathbf{L}(\mathbb{C}^D)$ commutes with all U_g given in the form of Eq. (2.32) it thus follows by Schur's lemma that it must be an element of $\mathcal{D}$ as given in Eq. (2.31). Thus, we have established a relation between a unitary representation U_g of a symmetry group G and the C^*-algebra $\mathcal{D}$. Conversely, given the C^*-algebra $\mathcal{D}$, we can construct a group G and a unitary representation U_g such that every element of $\mathcal{D}$ commutes with every element U_g. This can always be achieved, e.g., by choosing I in general different groups that have irreducible representations $\tilde{\rho}_i$ of dimension d_i. Then G is constructed as $G = G_1 \times \ldots \times G_I$ and the representation ρ_i is given by $\rho_i(g_1, \ldots, g_I) = \tilde{\rho}_i(g_i)$. In general, given a C^*-algebra, the choice of G and U_g is not unique. However, the *number* of different irreducible representations occurring in the decomposition of U_g must be the same independent of which group G and representation U_g is chosen. This number will take on the role of an invariant, classifying the quantum phase.

The block diagonal structure of the MPS gives rise to a group symmetry and a restricted injectivity condition, which together define the notion of *G-injective PEPS*. For a unitary representation U_g, the commutation property above $U_g A^i = A^i U_g$ can be recast into the form

$$U_g A^i U_g^\dagger = A^i \tag{2.33}$$

by applying the inverse group element to the right (cf. Fig. 2.11b) and we see that the A^i posses a virtual group symmetry.

The restricted injectivity can be best understood, when we convince ourselves, that the block-diagonal matrix A viewed as an operator from $\mathbb{C}^2 \times \mathbb{C}^2 \to \mathbb{C}^d$ has a non-trivial kernel, given by all block-off diagonal matrices. Thus, we cannot find a general inverse $\tilde{A}$. However, we have injectivity per block and thus, it is possible to find an inverse on the subspace of all block-diagonal matrices (cf. Fig. 2.11a). The block-diagonal matrices are exactly the one which commute with the symmetry, i.e., the subspace they span is given by all G-symmetric matrices

$$\mathcal{S}_G = \{X | [X, U_g] = 0, \forall g\} \tag{2.34}$$

and there exits $\tilde{A}$ such that

$$\tilde{A}A = \mathbb{1}|_{\mathcal{S}_G} \tag{2.35}$$

and the projector onto $\mathcal{S}_G$ (cf. Fig. 2.11c) is given by a sum over all group elements acting on the virtual indices

$$\mathbb{1}|_{\mathcal{S}_G} = \frac{1}{|G|}\sum_g U_g \otimes U_g^\dagger \,. \tag{2.36}$$

Note, that the symmetry alone is not enough to find the restricted inverse, since any subgroup of G is also a symmetry group, but injectivity is only possible after projecting onto the largest symmetry group. Thus, the symmetry and the injectivity condition come as two separate criteria which together define

Definition 2.1. *G-injective MPS*
An MPS is G-injective for a given group G and a unitary representation U_g, if it is G-symmetric and there exists an inverse on the symmetric subspace, i.e., Eqs. (2.33) and (2.35) are fulfilled.

Using representation theory and diagrammatic calculus (cf. Ref. [4]), one can derive that just like injectivity, also G-injectivity is robust under blocking. I.e., if A and B are G-injective then also AB defined as $(AB)^{ij}_{ac} = A^i_{ab}B^j_{bc}$ is G-injective.

Parent Hamiltonian

The parent Hamiltonians of G-injective MPS defined as in Eqs. (2.24) and (2.23) have a ground state degeneracy given by the number of different irreducible representations occurring in U_g. If U_g is semi-regular, i.e., every irreducible representation occurs at least once, this number is equal to the number of conjugacy classes of the group G. We refer to the general proof of this theorem to Ref. [4] and provide some intuition instead.

We can proceed analogously to the case of injective MPS and first consider the parent Hamiltonian defined on an open chain of length L. The intersection of all 2-site ground state spaces is parametrized by MPS that are closed with an arbitrary matrix, but since all non G-symmetric matrices are in the kernel of the MPS tensors, we can restrict ourselves without loss of generality to closure matrices which are G-symmetric.

The ground state space on a periodic chain is again given by the intersection of the ground state spaces of two open chains, shifted by one site, i.e., by considering the intersection of two MPS with different closure tensor positions. By using the restricted inverse, i.e., the projector onto the G-symmetric subspace instead of the inverse for injective MPS, we obtain that all closure tensors can be written as $\sum_g \lambda_g U_g$, where λ_g is a scalar. Thus, the intersection of the two open chain spaces is spanned by MPS closed with U_g and we find that every state

$$|\Psi\rangle_g = \sum \mathrm{Tr}[A^{i_1}\dots A^{i_l}U_g]\,|i_1\dots i_L\rangle \tag{2.37}$$

is an element of the ground state space. From this, we directly see, that different group elements in the same conjugacy class yield the same state, since $U_{h^{-1}gh} = U_{h^{-1}}U_gU_h$ and the h-element can be absorbed by the G-symmetric A matrices. Proving that $|\Psi\rangle_g$ with g from different conjugacy classes are linearly independent can be done easily for regular representations using $\mathrm{Tr}[U_g^\dagger U_h] = \delta_{g,h}$ and calculating the overlap $\langle\Psi|_g\,|\Psi\rangle_h = \delta_{\mathcal{C}(g),\mathcal{C}(h)}$, where $\mathcal{C}(g)$ denotes the conjugacy class of g.

Fig. 2.12. ⋆ General structure of MPS written with the explicit use of the block index (dashed line) in conventional notation (left) and in a notation highlighting the entanglement structure in the virtual space (right).

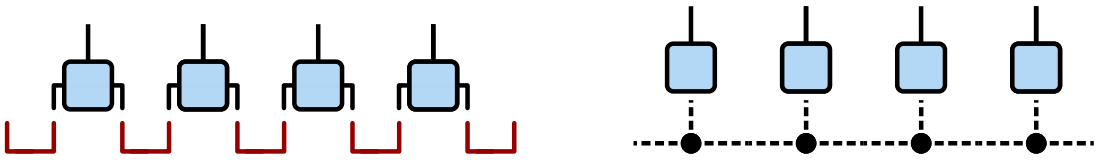

Fig. 2.13. ⋆ Left: Case 1) A single-block, i.e., injective MPS with only local entanglement in the product state phase. Right: Case 2) A G-injective MPS with D blocks of size one, corresponding to the GHZ state $|GHZ\rangle_D$ defined in Eq. (2.12).

2.4.4. Phase classification

We have seen that the parent Hamiltonians of G-injective PEPS have a ground state degeneracy determined by the (conjugacy classes of the) symmetry group G or likewise by the number of blocks in the canonical form. We will next show that this number uniquely classifies the phase.

To this end, we make use of the block diagonal structure of MPS in the canonical form. When multiplying two matrices with the same block structure the resulting matrix will again have the same block structure. Thus, we find it is useful to capture this property also diagrammatically and use the block label as another index of the tensor A and let the other two virtual indices label the rows and columns of individual blocks. Note, that in general the bond dimension of those row and column indices depend on the block index. This dependency is left implicit as it is not relevant for the statements made below. With this considerations we represent a block-diagonal MPS tensor as in Fig. 2.12. The MPS can then be deformed such that its entanglement structure becomes apparent: It can be written as a GHZ state with additional maximally entangled pairs of qubits to which the tensors A are applied (cf. Fig. 2.12 right panel). With this representation we can now perform the phase classification for general MPS.

There are two special cases (shown in Fig. 2.13) that help to understand the general situation.

I. Injective MPS (Fig. 2.13 left). The dimension of the block index is one, i.e., there is only a single block for the A^i and the MPS is injective. In this case, we can omit the block index line (it is one dimensional) and we can directly see from the structure of the virtual space, that the MPS corresponds to a product state. More explicitly, we can apply the MPS map A and its inverse to obtain unentangled pairs of two qubits at each physical site.

II. GHZ states (Fig. 2.13 right). The dimension of the block index is I (cf. Eqs. (2.31) and (2.32)) and all blocks are one-dimensional, i.e., $d_i = 1 \forall i$. In this case, we can omit all index lines except for the block index line and we see that the virtual space corresponds to a GHZ state with the MPS map A applied on each site. Decomposing A using the polar decomposition and removing the non-isometric part per block as in the case for injective MPS, we obtain a GHZ state and its parent Hamiltonian given by local terms $h_i = \mathbb{1} - \sum_{\alpha=1}^{I} |\alpha\alpha\rangle \langle\alpha,\alpha|$. The ground state degeneracy of this parent Hamiltonian is I, i.e., the number of blocks, since every state $|\alpha,\alpha,\ldots,\alpha\rangle$ is a ground state.

The general case, where the block index dimension is I and the dimensions of the other

index lines are d_i with $i = 1, \ldots, I$ can be understood as a combination of case I and II. I.e., there is global GHZ state like entanglement coming from the block index. Additionally, there is locally removable entanglement resulting from the index lines of bond dimension d_i. This entanglement can be removed by a local unitary circuit as in the case of injective-MPS, but the GHZ part remains. Thus this MPS is in the same phase as an MPS from case II which has the same number of blocks I as the given MPS.

We conclude that MPS-phases are classified by the number of blocks in the canonical form or likewise by the ground state degeneracy of their parent Hamiltonian.

Symmetries

As pointed out earlier, the phase definition in Section 2.2 does not take into account physical symmetries of the Hamiltonians. To obtain a notion of phase classification that can distinguish between phases of different symmetry one can restrict the allowed Hamiltonian path by requiring that certain symmetries of the Hamiltonian are preserved. The same can be done on the level of states by only allowing quantum circuits that respect the physical symmetry. This yields a more refined phase diagram [20]. Interestingly, it turns out that there exist cases where two Hamiltonians respect the same symmetry, but nevertheless can not be connected by a symmetry respecting adiabatic path [117]. Phases for which this is the case are called *symmetry protected topological* (*SPT*) phases, since their their long-range entanglement (a property associated with topological order) is protected by the presence of a symmetry. If the symmetry restriction is lifted, they can no longer be distinguished as distinct phases and in this sense they are not stable against arbitrarily small perturbations that violate the symmetry. Long-range entangled phases can also be subject to symmetry restrictions. In this case, one obtains a refined classification of long-range entangled phases, referred to as *symmetry enriched topologically* (*SET*) order.

Both SPT and SET phases can be classified with MPS [61] when the physical symmetry of the state is represented by an on-site linear unitary representation U_g of a group G acting as

$$\otimes U_g \, |\Psi\rangle = |\Psi\rangle \tag{2.38}$$

for SPT phases, i.e., Hamiltonians that have a unique ground state and likewise as

$$\otimes U_g \mathcal{E}_0 = \mathcal{E}_0 \, , \tag{2.39}$$

where $\mathcal{E}_0$ denotes the ground state space for SET (symmetry broken) phases.

Again making use of the canonical form, one can infer that the symmetry action on the physical space can be represented by a group action on the virtual space given by a projective representation that is defined up to a phase and depends on the MPS tensor A. Different projective representations correspond to different MPS that can not be deformed into each other and thus SPT phases in one dimension with a physical symmetry U_g are classified by the second cohomology group $H^2(G, U(1))$ determining the phase factor of the projective representation.

For SET phases in one dimension, the physical symmetry can also permute different ground states as it only needs to preserve the finite dimensional ground state space and the phases are classified by both, the permutation action and the cohomology group classifying the symmetry actions within individual ground states.

2.4.5. Limitations of the approach for higher dimensions

In higher dimensions the understanding of gapped quantum phases is much less complete. There are two immediate obstacles that prohibit us from extending the tensor network approach

described in the previous Section to higher dimensions. First, it is only conjectured, but not proven that all ground states of gapped local Hamiltonians can be well approximated by projected entangled pair states [133]. Second, even if we restrict ourselves to PEPS states, it is not possible to obtain an exhaustive classification. This is due to the fact, that there is no canonical form for general PEPS. Due to these severe limitations the study of gapped quantum phases is mainly a study of exact fix point models.

Apart from the symmetry breaking phases constructed in complete analogy to the one dimensional case, non-chiral topologically ordered phases (discussed in detail in Chapter 5) are well understood in higher dimensions. The latter are accessible via commuting projector Hamiltonians, have exact PEPS representations and are classified by modular tensor categories.

Slightly less accessible are topologically ordered phases that are chiral. Chiral phases are only fully gapped on closed manifolds and feature gapless edge modes when defined on open manifolds. There are strong indications that they can not be represented by commuting projector Hamiltonians [46, 160] and it is not clear if they can be represented by PEPS. However, on an abstract level chiral topologically ordered phases are still (per definition) classified by modular tensor categories which describe the theory of their (anyonic) excitations.

Even more exotic than chiral topologically ordered phases are so-called fracton phases, characterized by excitations that are completely immobile or mobile only in certain directions [116]. The latter two types of topological order will not be addressed further in this Thesis.

3. A conceptual introduction to topological order

Gapped quantum phases in two dimensions are profoundly more complex and interesting [20] than the one dimensional phases discussed in the previous Chapter. Most of all they include phases with *topological order* – a kind of quantum order characterized by a series of rather exotic phenomena including a topology dependent ground state degeneracy and quasi-particle excitations called *anyons* that are neither bosons nor fermions [31]. While the essential concept of topological order can be understood on an elementary level, the general theory of (non-chiral) topological order is rich and highly evolved while being fairly abstract as well. Before we discuss the abstract formalisms, i.e., the algebraic theory of anyons and non-chiral topological order of string-nets and MPO-injective PEPS in general terms in Chapter 5, this Section is devoted to a two-fold conceptual introduction to topological order. On the one hand, we review the paradigmatic toric code model [31] – a particular exactly solvable lattice Hamiltonian. On the other hand, we explain how the G-injective MPS formalism introduced in the previous Chapter can be generalized to two-dimensional tensor network states yielding the notion of G-injective PEPS [4]. We review how the latter correspond to topologically ordered states and show that the ground state of the toric code Hamiltonian is a G-injective PEPS with symmetry group $G = \mathbb{Z}_2$. Both the toric code as well as the tensor network construction can be generalized to address non-chiral topological order in full generality (cf. Chapter 5) yielding string-net Hamiltonians and MPO-injective PEPS, respectively.

The material presented in this Section is a condensed version of the first Chapter of Kitaev's seminal paper Ref. [31] and the G-injective PEPS formalism introduced by Schuch et al. in Ref. [4].

3.1. The toric code

The toric code [31] is an exactly solvable[1] spin-$\frac{1}{2}$ lattice Hamiltonian that is paradigmatic for (non-chiral) topological order in two dimensions. Its Hamiltonian can be defined on any two-dimensional lattice with spins on the edges. The Hamiltonian is a sum of local mutually commuting terms given by star (vertex) and plaquette operators A_v and B_p

$$H_{TC} = -\sum_v A_v - \sum B_p \,. \tag{3.1}$$

The star (vertex) operators measure the parity of all spins around a vertex

$$A_v = \prod_{j \in v} \hat{z}_j \tag{3.2}$$

and the plaquette operators flip the spins around each plaquette

$$B_p = \prod_{j \in p} \hat{x}_j \,. \tag{3.3}$$

[1] Exactly solvable in the sense that the Hamiltonian can be written as a sum of locally commuting projectors.

One can rewrite the Hamiltonian as a sum of commuting projectors by adding an energy shift and rescaling the A and B operators

$$H_{TC} \simeq \sum_v \frac{1}{2}(1 - A_v) + \sum_p \frac{1}{2}(1 - B_p) \,. \tag{3.4}$$

Most of the defining features of topological order are found in the toric code and can be calculated on an elementary level from the Hamiltonian. Moreover, it is fair to say that all known models exhibiting non-chiral topological order can be seen as generalizations of the toric code (cf. Section 5.1. Also, the connection between non-chiral topological order and PEPS can be understood well using the example of the toric code. We review most of the theory of topological order in the light of the toric code. Before we do so we briefly explain why the Hamiltonian model in Eq. (3.1) is called a code.

3.1.1. The toric code as a quantum code

The origins of the toric code model can be traced back to constructions in lattice gauge theory by Wegner [161] and Kogut [162] in the 70's, however, its importance was only fully realized when Kitaev proposed the model in 1997 [31] as a *topological quantum code* robust against local noise. The last statement needs explanation: One of the main properties of topologically ordered systems is that the ground state degeneracy depends on the topology. The toric code Hamiltonian defined on a two-dimensional lattice with periodic boundary conditions, i.e., a torus, has a 4-fold degenerate ground state space. Furthermore, different ground states can not be distinguished by local measurements and can only be deformed into one another by global operations – another hallmark of topological order. As a consequence, the information which particular ground state the system is in, is protected against local noise.

This suggest to interpret the 4-dimensional ground state space as a so called *code space*

$$\mathcal{E}_0 = \mathcal{C} = \mathrm{span}\{|00\rangle, |10\rangle, |01\rangle, |11\rangle\} \tag{3.5}$$

spanned by two *logical qubits* which can be used to store quantum information. One can furthermore construct *logical operators* acting globally on the system that act as Pauli spin operators on the logical qubits.

If a single spin changes its state, the system is no longer in the ground state space and we cannot identify the state immediately with an element of the code space. We say that an *error* has been created. However, since the error occurred locally it should be possible to also detect and correct it locally. The question under which conditions errors can be detected and corrected is the topic of *quantum error correction* [163]. For the toric code model, the local Hamiltonian terms are mutually commuting and thus they can be measured without the effect that the measurement of one affects the measurement of the other. Their eigenvalues are 1 or -1, respectively and the spatial pattern of -1s and 1s obtained from measuring all local operators contains information about the possible error configurations, i.e., the position and the type of local errors, that have occurred in the system. This spatial pattern of measurement outcomes is called the *error syndrome*. If for a system on a $L \times L$ square lattice, the number of errors is smaller than L, the error syndrome contains enough information to undo the errors. The task to infer the error pattern from the syndrome and to undo the error is not trivial. One has to devise a *decoder*, i.e., an algorithm that performs the task. Finding good or even optimal decoders, proving their existence or non-existence and similar questions constitute a large research area. For the toric code, one can prove that if errors occur independently and not too often, a decoder exists whose chance of succeeding in preserving the quantum information approaches unity

in the limit of infinite system size (cf. Chapter "Topological codes" in [163] or [164]). This renders the toric code an ideal candidate for a quantum memory. Variants of the toric code with open boundary conditions named *surface codes* are still considered a state of the art approach to fault-tolerant quantum memories [165, 166], however they compete against a plethora of similar codes, most prominently color codes [167], and it is not settled yet which (if any) of the codes emerges as actually suited for practical implementations.

3.1.2. Topological ground state degeneracy

A characterizing feature of topologically ordered Hamiltonians is that their ground state degeneracy $|\mathcal{E}_0|$ depends on the topology of the lattice. For the toric code, this can be understood by analyzing the structure of the ground states explicitly. We can count the number of independent projectors N_P and compare it with the total number of qubits N_q. As every independent projector projects out half of the Hilbert space dimensions, we are left with $|\mathcal{E}_0| = 2^{N_q - N_P}$. For a square lattice on a torus we have $N_q = 2L^2$ qubits and $2L^2$ projectors, however two of them are already determined by all others, so we have $N_P = 2L^2 - 2$ and the ground state degeneracy is given by 4. The counting of projectors and degrees of freedom resembles the calculation of the Euler characteristic. Indeed, we need to count the number of edges (spins) minus the number of vertices (vertex projectors) minus the number of faces (plaquette projectors) and add 2, because two of the projectors are already determined by all other ones

$$|\mathcal{E}_0| = 2^{E-V-F+2} = 2^{-\chi+2} = 2^{-(2-2g)+2} = 4^g \,, \tag{3.6}$$

where we have used the definition of the Euler characteristic $\chi = V - E + F$ and the well known fact that the Euler characteristic is related to the genus g by $\chi = 2 - 2g$. Since the Euler characteristic is a topological invariant, also the ground state degeneracy is.

3.1.3. Local indistinguishability of ground states

We have already mentioned above that different ground states can only be transformed into one another by global operations. To see this, consider the possible effects of a spin flip (σ_x) on vertex operators and note that the model is self-dual under exchanging x and z and the role of vertex and plaquette operators. Thus, the effects we observe for spin flips on the vertex operators can be mapped to the effect of σ_z operators on plaquette operators. As all operators in the Hilbert space can be represented as a sum of products of Pauli operators, these considerations will allow us to make very general statements.

Consider the effect of a single spin flip. The state is still an eigenstate of the Hamiltonian, but the two vertex operators adjacent to the edge where the flip has occurred yield -1. We say that the vertex constraint is violated at two vertices and conclude that the state is an excited state with energy 2. We can now flip another spin on one of the vertices where the vertex constraint is violated to "heal" the violation at this vertex, however, now a neighboring vertex will be violated. We have moved the violation one site further. The energy of this state is still 2. We see, that we can move excitations in this manner at no energy cost. Only, if we move the excitation back to its origin we end up in the ground state space again. If the excitation is moved back to its origin along a contractible loop, the ground state does not change. To see this, note that a contractible loop of spin flips can be obtained by tiling the loop interior by plaquette operators. Since application of the latter leaves the state invariant, a closed loop is indeed trivial. If however, the excitation is moved along a homologically non-trivial loop[2] the

[2] A homologically non-trivial closed loop can not be written as the boundary of some area on the manifold.

ground state is changed to another, orthogonal, ground state.

We conclude, that a number of spin flips of the order of the system size is needed to go from one ground state to another ground state. If there are less then L spin flips, there are two cases. Either the spin flips are arranged in a closed loop pattern and leave the ground state invariant, or the spin flips form a pattern of open strings. In this case, we obtain an excited state. We conclude that for any operator $\hat{O}(S)$ supported on sites $S = \{s_i\}_i$ with $|S| < L$, we have that for $|\Psi\rangle \in \mathcal{E}_0$

$$\langle\Psi|\,\hat{O}(S)\,|\Psi\rangle = \begin{cases} 1 & S : \text{closed loop pattern,} \\ 0 & \text{otherwise.} \end{cases} \tag{3.7}$$

This implies the local indistinguishability of ground states

$$|\,\langle\Psi_1|\,\hat{O}(S)\,|\Psi_1\rangle - \langle\Psi_2|\,\hat{O}(S)\,|\Psi_2\rangle\,| = 0 \tag{3.8}$$

for $|\Psi_1\rangle \neq |\Psi_2\rangle$ as well as the statement noted earlier in Section 2.1.2 that the toric code ground states are uncorrelated with respect to local measurements. This property is so surprising and unconventional, that it can be seen as the definition of topological order. Relaxing the condition to a distinguishability of ϵ for an operator of support l, we obtain the definition of topological order as used in [134] to prove the separation of the toric code phase from the product state phase. This result has severe implications on the hardness (or likewise time needed) to prepare a topological ordered state from a product state. More refined and slightly more technical versions of the topological order conditions have been used to proof the stability of topological phases against local perturbations in rigorous terms [168–170].

3.1.4. Anyonic excitations of the toric code

We have seen that any open string of spin flips yields a state where the two vertex projectors at the end of the string are violated. Likewise, an open string of Pauli-z operators corresponds to a violation of two plaquette constraints at the end of the z-string. By the analogy of (magnetic) flux and (electric) charge violations in lattice gauge theory, these local excitations are called e and m particles. They have unconventional properties when they are braided with one another. Let us consider a state, where a pair of two e-particles is created at some location and a pair of m-particles is created at a different location. Now we move one e-particle around one of the m-particles by acting with a closed loop of Pauli-z operators that encloses the m-particle and thus intersects with the x-string. Commuting the z-loop with the x-string, we obtain a minus sign and can then evaluate the closed z-loop on a ground state where it acts trivially. Thus, braiding an e- with an m-particle has the effect of changing the phase of the wave function by π.

Next, consider bringing an e- and an m-particle close together. This new (e, m)-particle can be moved around by applying x- and z-strings in parallel. If we move it along a closed loop and bring it back to its original position, we obtain by similar reasoning as above, that the wave function changes by -1. Thus, we can identify the (e, m)-particle with a fermion. Indeed, bringing two (e, m)-particles close together, we obtain the ground state again. Identifying the ground state with the trivial particle, we obtain the expected *fusion rules* for fermions, i.e., two fermions fuse to a boson. Similarly, we can calculate the fusion properties of the other particles. Since, both two e- and two m-particles fuse to the trivial particle, there are not more than four particle types in the model and they fuse according to

$$e \times e = m \times m = f \times f = \mathbf{1}\,, \quad e \times m = f\,, \quad e \times f = m\,, \quad m \times f = e\,. \tag{3.9}$$

Note that the fusion rules are a representation of $\mathbb{Z}_2 \times \mathbb{Z}_2$, where we identify e with $(1, 0)$ and m with $(0, 1)$. Whenever the fusion of two anyons is unique, i.e., it results in the same anyon

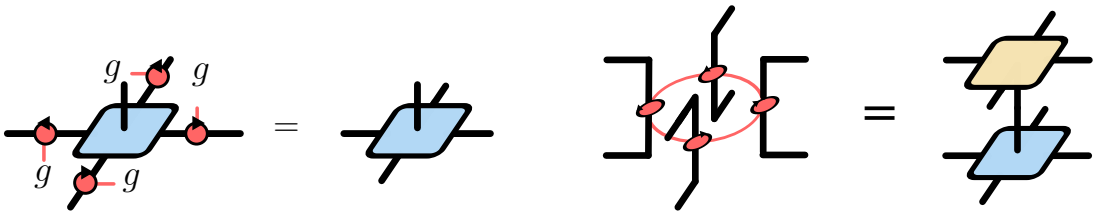

(a) G-symmetry (b) G-injectivity

Fig. 3.1. ⋆ G-injective PEPS. (a) G-symmetry and (b) injectivity on the G-symmetric subspace. We have used the convention to denote a Hermitian conjugation by a reflection as indicated by the arrows and omitted the normalization $1/|G|$ in the left-hand side of (b).

type regardless of the microscopic details of the fusion process, anyons are called Abelian. The general theory of Abelian and non Abelian anyons is presented in Chapter 4.

3.2. G-injective PEPS

The classification of gapped phases of matter in one dimension based on G-injective MPS presented in Section 2.4 can be performed solely based on the canonical form of MPS without ever invoking the group symmetry or the restricted injectivity explicitly. In contrast, for PEPS in two dimensions a canonical form is lacking and cannot be invoked. However, the concept of G-injectivity can still be adapted to the two-dimensional case in a straight forward fashion to define the notion of G-injective PEPS. G-injective PEPS already exhibit all aspects of topological order on a conceptual level and can be generalized to MPO-injective PEPS capturing all known non-chiral phases (cf. Section 5.2). In the following Section we review the basic properties of G-injective PEPS following Ref. [4] and show that they exhibit features of topological order.

3.2.1. Definition

As a first step, we generalize the symmetry and injectivity property from MPS tensors to tensors with more than two virtual indices as shown in Fig. 3.1. Note, that for translation invariant MPS there are only two indices and thus only one type of virtual index line (the horizontal one). The symmetry under $U_g \otimes U_{g^{-1}}$ then also implies symmetry under $U_{g^{-1}} \otimes U_g$. In contrast, PEPS have different index lines (e.g. horizontal and vertical on a square lattice) and it is not clear a priori how to represent the group G on different index lines. For example on a triangular lattice one could choose $U_g \otimes U_{g^{-1}} \otimes U_g$ as well as $U_g \otimes U_{g^{-1}} \otimes U_{g^{-1}}$ and the two representations are generically different. In fact, there is even more freedom in the choice of representations than in the example given: the only condition that restricts the choice of local representation is the stability under blocking[3]. Stability under blocking requires that for any link type, e.g., the horizontal link, we define a pair $U_g, U_{g^{-1}}$ acting on the left and on the right virtual index, such that the two representations cancel when two G-injective tensors are blocked along a horizontal line. The same applies for vertical lines and we see, that in general each index line type can have its own representation. We will not specify which representation is used on which index line, but will assume that every representation used is semi-regular and unitary.

[3] Considering a system in the thermodynamic limit, we do not want to loose a characteristic property of the system while zooming out.

The existence of an inverse on the symmetric subspace can also be adapted to the two-dimensional case (cf. Fig. 3.1a). Here, the choice of the representation in the definition of the symmetric projectors needs to be consistent with the choice of representations in the symmetry condition. With the preceding considerations, we arrive at the following

Definition 3.1. For a group G represented by semi-regular, unitary representations, a PEPS is called G-injective, if it is symmetric under G and an inverse exists on the G-symmetric subspace, i.e., it fulfills the equations given in Fig. 3.1.

It is not hard to prove that G-injectivity is stable under blocking. The stability of the G-symmetry follows directly from the definition and the stability of the restricted injectivity can be proven using representation theory and diagrammatic calculus.

3.2.2. Parent Hamiltonian

Recall, that parent Hamiltonians of PEPS are in general not gapped (cf. Section 2.3.3). Even for injective PEPS, which are contained in the definition of G-injective PEPS by choosing the trivial group, the parent Hamiltonian can be gapless [62]. To ensure that the parent Hamiltonian is gapped, the PEPS map has to be close enough to the *G-isometric* point.

G-isometric PEPS

The special case when the projector onto the G-invariant subspace is given by

$$\frac{1}{|G|} A^\dagger A = \frac{1}{|G|} \sum_g U_g \otimes U_g \otimes U_g^\dagger \otimes U_g^\dagger \,, \tag{3.10}$$

i.e., the inverse in Fig. 3.1b is given by $A\dagger$ and the representation U_g is the left-regular representation $U_g |h\rangle = |gh\rangle$ is called G-isometric PEPS.

Analogously to the one-dimensional case we find that the projector onto the physical subspace on four adjacent sites is given by blocking four A tensors into a 4-site tensor A_4 and contracting $A_4^\dagger$ and A_4 along the virtual indices, similar to the one-dimensional case shown in Fig. 2.10

$$\Pi_{\mathcal{S}_4} = A_4 A_4^\dagger \,. \tag{3.11}$$

The Hamiltonian is a sum of local commuting projector Hamiltonians as can be easily shown using diagrammatic calculus.

Like in the one-dimensional setting, we can decompose a PEPS tensor A into a positive map $Q \in L(\mathbb{C}^d)$ and an isometry $W : \mathbb{C}^D \otimes \mathbb{C}^D \to \mathbb{C}^d$. If Q is close enough to the identity, i.e., the ratio $\min \mathrm{EV}(Q) / \max \mathrm{EV}(Q)$ is close to unity, one can show that the parent Hamiltonian is gapped [61]. The discussion of the parent Hamiltonian should be regarded as a discussion of G-injective PEPS that are close to isometric.

Ground state space

Using the definition in Eq. (2.17) with a four-site region R, we find that the parent Hamiltonian of G-isometric PEPS is frustration free and has a ground state degeneracy that is topology dependent.

The characterization of the ground state space again proceeds analogously to the one-dimensional case. On an open patch of $L \times L$ sites the ground state space of the parent Hamiltonian is spanned by all PEPS with a G-symmetric closure.

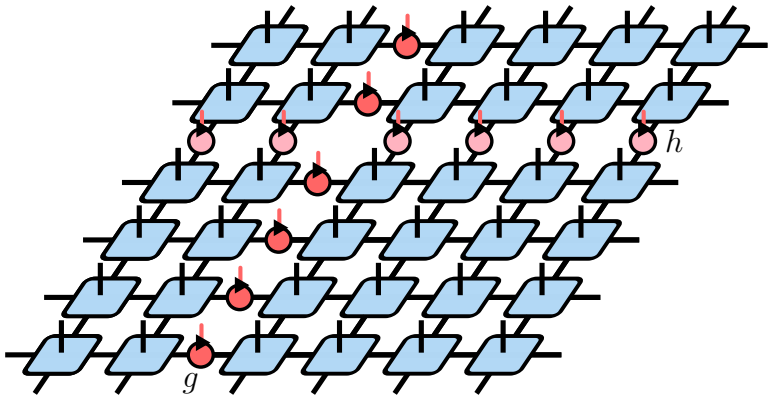

Fig. 3.2. ⋆ The ground state $|\Psi_{(g,h)}\rangle$.

The ground state space on a closed manifold, e.g., a torus is given by the intersection of the ground state spaces of all possible Hamiltonians on different open patches that jointly cover the full manifold. Thus, we consider patches closed with G-symmetric closure tensors along the two homologically non-trivial loops placed at different positions. By using the axioms of G-injectivity, one can show that the intersection of the latter is spanned by states $|\Psi_{(g,h)}\rangle$ with $[g,h]=0$, which are given by inserting a g-string, i.e., a line of U_g operators along one homologically non-trivial loop and an h-string along the other (cf. Fig. 3.2). This is analogous to the G-symmetric closure tensors in the one-dimensional setting. Note, that the commutativity of g and h is required to ensure that the closure tensor can be deformed freely which is required to yield a state in the intersection space of closures located at different positions.

We will see that the insertion of a g-string along a non-trivial loop can be identified with the action of a logical operator on the physical level, when we discuss the $\mathbb{Z}_2$-injectivity of the toric code PEPS ground state in Section 3.2.3.

Again in analogy to the one-dimensional case, not all $|\Psi_{(g,h)}\rangle$ with $[g,h]=0$ are linearly independent. Instated we find that a pair of elements (g',h'), which is equal to a pair (g,h) up to conjugation results in the same ground state. More formally, we denote the pair conjugacy class

$$\mathcal{C}(g,h)=\{(g',h')|(g',h')\sim(g,h)\} \tag{3.12}$$

as an equivalence class with the equivalence relation, $(g,h)\sim(g',h')\Leftrightarrow\exists x\in G: xgx^{-1}=g', xhx^{-1}=h'$ and find that the two ground states $|\Psi\rangle_{g,h}$ and $|\Psi\rangle_{g',h'}$ are identical if $(g,h)\sim(g',h')$. Moreover, we can prove that ground states obtained from different pair conjugacy classes are linearly independent and thus arrive at the result that the ground state space is spanned by the conjugacy classes $\mathcal{C}(g,h)$ for which $[g,h]=0$.

Local indistinguishability of ground states

Let us analyze the structure of the states $|\Psi\rangle_{\mathcal{C}(g,h)}$. It is clear, that the two loops given by an element g and an element h, which are representatives of $\mathcal{C}(g,h)$ can be deformed freely as a property of the G-symmetry of the local tensors. Furthermore, the intersection of the h- and the g-loop does not restrict the deformability since $U_gU_h=U_hU_g$, i.e., the h loop can pass trough the g-loop and vice versa. Thus, if we measure a local operator on the state $|\Psi\rangle_{\mathcal{C}(g,h)}$, we can move the g and the h loop arbitrarily far away from the point of measurement. Unless the correlation length in the system is infinite, the measurement result should not be influenced

by the loop at a far distance and thus the measurement outcome is independent of the pair conjugacy class $\mathcal{C}(g,h)$. This is a manifestation of the local indistinguishability of different ground states in topological ordered systems.

3.2.3. The toric code as a $\mathbb{Z}_2$-isometric PEPS

The parent Hamiltonians of G-isometric PEPS are the ground states of Kitaev's group quantum double models [31] constructed from finite groups G. We have already encountered the simplest example of a Kitaev quantum double model, i.e., the toric code where $G = \mathbb{Z}_2$. Indeed, the ground states of the toric code model can be written as PEPS which are $\mathbb{Z}_2$-injective as shown by the following considerations.

Closed-loop superposition

The toric code ground state can be explicitly constructed as follows. Consider a product state $|0,\dots,0\rangle$ – referred to as "vacuum". This state is an eigenstate of all vertex projectors. Now apply all plaquette operators. The resulting state is an eigenstate of all vertex and all plaquette operators[4]. Applying one plaquette operator B_{p_1} to the vacuum, one obtains a superposition of the vacuum and a state with one closed loop of flipped spins around the plaquette p_1. Applying another plaquette operator at a plaquette p_2, that is not in the vicinity of p_1, we obtain a superposition of four states, the vacuum, one loop at p_1, one loop at p_2 and two loops at both p_1 and p_2. If p_2 is a neighboring plaquette of p_1, we instead obtain a superposition of the first three states and the fourth one has a larger loop around $p_1 \cup p_2$. Iterating this procedure, we see that the toric code ground state is given by an equal weight superposition of all closed loops. When wrapped on a torus, we can construct four orthogonal ground states by starting from a state with only trivial loops in the superposition and apply x-flips on one or both of the two cycles.

PEPS map

The closed-loop superposition state can easily be written as a PEPS. To this end we define a tensor A on four physical sites around a vertex and implement the vertex constraint directly on the level of the tensor, i.e., the image of A as a linear operator from the virtual to the physical space is given by all parity even states. A map that generates (physical) parity even states from arbitrary virtual states can easily be devised by taking pairwise differences. Labeling the vector space basis elements by $\mathbb{Z}_2$ elements and using addition modulo 2 we use

$$\tilde{A} = \sum_{a,b,c,d} |a+b, b+c, c+d, d+a\rangle \langle a,b,c,d| \ . \tag{3.13}$$

The total parity of the four physical qubits as measured by the product of four Pauli-z operators is given by

$$\chi_1(a+b)\chi_1(b+c)\chi_1(c+d)\chi_1(d+a) = \chi_1(0) = 1 \ , \tag{3.14}$$

where we used $\sigma z |0\rangle = \chi_1(0)|0\rangle = 1|0\rangle$ and $\sigma_z|1\rangle = \chi_1(1)|1\rangle = -1|1\rangle$ and $\chi_1(g)$ denotes the character of the non-trivial 1-dimensional irreducible representation of $\mathbb{Z}_2$.

This map is inspired by a gauge symmetry, i.e., shifting the virtual indices a,b,c,d by the nontrivial group element is a symmetry of the map. We can use this insight to define a PEPS

[4] We also need to ensure that the state is not annihilated, i.e., the Hamiltonian is frustration free. This will become clear in the following.

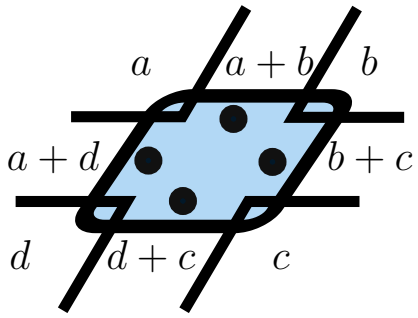

Fig. 3.3. ⋆ The PEPS map of the toric code. The four (eight, when doubled) virtual indices are denoted by lines and the four physical indices are denoted by dots. All configurations of the form depicted here yield tensor entries equal to one. All other entries are zero.

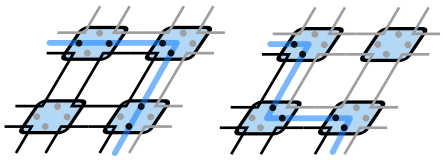

Fig. 3.4. ⋆ The two configurations of the toric code tensor network patch of four tensors for a fixed configuration of the open virtual indices are related by a spin flip of the inner spins. Grey (black) lines and dots corresponds to spin states $|0\rangle$ ($|1\rangle$) of virtual and physical indices. The blue line highlights the physical string which is deformed by a spin flip.

map A. This is most conveniently done by using $\tilde{A}$ and doubling the virtual indices as shown in Fig. 3.3. Tiling the lattice with an A tensor at every vertex, we observe, that we have twice as many physical qubits as needed. This redundancy is harmless and can be removed trivially since two spins at one physical edge are always in the same state by construction.

We observe that each tensor patch of 4 individual tensors is invariant under the application of the plaquette operator. It is cumbersome to write out all matrix elements. However, note, that there is one closed virtual index line v in the center of the 4-site tensors that is summed over and thus for a fixed configuration of the open virtual indices we obtain a superposition $|\Psi(v=0)\rangle + |\Psi(v=1)\rangle$. The physical spins of $|\Psi(v=0)\rangle$ are flipped with respect to the spins of $|\Psi\rangle_1$ and thus the space spanned by all index configuration of the open virtual indices is the $+1$ eigenspace of the plaquette operator (cf. Fig. 3.4). As a result by tiling the complete lattice with PEPS tensors and summing over all closed indices of the tensor network we obtain the closed-loop superposition ground state.

$\mathbb{Z}_2$-isometry

It is easy to check that the map given in Fig. 3.3 is $\mathbb{Z}_2$-isometric. The physical indices are insensitive to a shift of the virtual indices a, b, c, d by a group element g applied to all indices simultaneously. Thus, the map A is invariant under e.g. the left-regular representation. We next consider $A^\dagger A$ and find that it is equal to the $\mathbb{Z}_2$-symmetric projector, i.e., it fulfills Eq. (3.10), proving $\mathbb{Z}_2$-isometry. When calculating $A^\dagger A$, we sum over all physical index configurations that are in the image of A. The physical index configurations of A and $A^\dagger$ are only identical if

their virtual indices differ by a global shift. More explicitly, we find that

$$\begin{aligned} & A^\dagger A \\ &= \sum_{a,b,c,d,a',b',c'd,'} |a,b,c,d\rangle \langle a+b,b+c,c+d,d+a| \, |a'+b',b'+c',c'+d',d'+a'\rangle \langle a',b',c',d'| \\ &= \sum_{a,b,c,d,g} |a,b,c,d\rangle \langle a+g,b+g,c+g,d+g| = \sum_g U_g \otimes U_g \otimes U_g \otimes U_g \,, \end{aligned} \tag{3.15}$$

where $g = b + b' = c + c' = d + d'$ and the doubling of the virtual indices is left implicit.

Ground states on a torus

By inspection of the PEPS map we can easily verify the claim that an insertion of a g-string along a non-trivial loop corresponds to the action of a logical operator. The g-string with non-trivial group element $g = 1$, i.e., $U_g = \sigma_x$, shifts the index values of half of the virtual indices

$$\begin{aligned} A(U_g \otimes U_g \otimes \mathbb{1} \otimes \mathbb{1}) &= \sum_{a,b,c,d} |a+b,b+c,c+d,d+a\rangle \langle a+1,b+1,c,d| \\ &= \sum_{a,b,c,d} |a+b,b+c+1,c+d,d+a+1\rangle \langle a,b,c,d| = (\mathbb{1} \otimes \sigma_x \otimes \mathbb{1} \otimes \sigma_x) A \,, \end{aligned}$$

i.e., it results in a spin-flip of the two spins on the horizontal edges. Applying this identity on all PEPS maps to the left (right) of the g-string, we obtain the equivalence between virtual string-insertions and logical operators.

3.2.4. Entanglement entropy

We have seen in Section 2.3.4 that MPS and PEPS fulfill an entanglement area law. A hallmark of topological order is the so-called *topological correction* to the area law, i.e., there is a constant correction term independent of microscopic details that is given by the *topological entanglement entropy* (cf. Ref. [126, 171]). In the framework of G-isometric PEPS the entanglement entropy can be calculated explicitly: Blocking tensors on a topological trivial region C yields a tensor that is equivalent (up to local unitary transformations) to the G-symmetric projector on the virtual boundary indices. We infer that the reduced density matrix ρ_C is a projector onto the G-symmetric subspace on the boundary indices. The bond dimension of each index is $|G|$ and thus the boundary Hilbert space is $|G|^{|\partial C|}$-dimensional. The image of the symmetric projector is given by all symmetrized states. Since symmetrizing $|a,b,\ldots,c\rangle$ and $|a',b',\ldots,c'\rangle$ yields identical states if the initial states are related by a shift with a constant group element, the image is $|G|^{|\partial C|}/|G|$ dimensional. The spectrum of ρ_C is flat (as it is a projector) and thus, we find that the entanglement entropy of ρ_C is given by

$$S(\rho_C) = -\mathrm{Tr}[\rho_C \log \rho_C] = (|\partial C| - 1) \log |G| \,. \tag{3.16}$$

This result is in agreement with the scaling of the entanglement entropy of a region C in a general topologically ordered system (i.e., one that is not necessarily described by G-isometric PEPS) derived by Preskill and Kitaev [126]

$$S(\rho_C) = \alpha |\partial C| - \gamma + \ldots \,. \tag{3.17}$$

Here $\ldots$ refers to terms that vanish in the limit $|\delta C| \to \infty$ and α is a numerical prefactor as expected from the area law that is typical for gapped local systems. The constant correction term to the area law γ is called the topological entanglement entropy.

Eq. (3.17) is derived using the conjecture that in the low-energy (far infrared) limit, a topological ordered system should be characterized by a topological quantum field theory (TQFT) and in this case, the topological correction is given by the so called total quantum dimension $\mathcal{D}$ (cf. Section 4.2.1)

$$\gamma = \log \mathcal{D} \,. \tag{3.18}$$

The total quantum dimension $\mathcal{D}$ is an invariant of the phase and related to the number N and types of anyonic excitations a as

$$\mathcal{D} = \sqrt{\sum_{a=1}^{N} d_a^2} \,, \tag{3.19}$$

where d_a is the quantum dimension of the anyon a (cf. Section 4.2.1). In the simplest topological models, where the fusion of anyons is unique (Abelian anyons), we have $d_a = 1$ and thus $\mathcal{D}^2$ is equal to the number of anyons.

For the toric code, the entanglement entropy can also be calculated explicitly [122, 123] and one obtains

$$S(\rho_C) = (|\partial C| - 1) \log 2 \,, \tag{3.20}$$

in agreement with Eq. (3.16) for $|G| = 2$. By comparison with Eq. (3.17), we find

$$\gamma_{TC} = \log 2 \tag{3.21}$$

as expected since the toric code has four Abelian anyons, $1, e, m, f$ and thus $\mathcal{D}_{TC} = 2$.

3.2.5. Local excitations

Placing an open string of U_g operators on virtual bonds results in a state with an interesting property. First, due to the deformability of the U_g-string, the state does only depend on the two end points of the string and not on the string position. Second, it is not a ground state of the parent Hamiltonian, since it is not G-symmetric at the two end points of the string. Instead it corresponds to an excited state with local quasi-particle excitations. The energy of the state does not depend on the position of the string end-points, thus, it does not cost energy to move excitations around – the excitations are deconfined.

One can show that measuring the product of the physical spins around a plaquette reveals the conjugacy class of g (cf. Theorem 6.15 of [4]). By analogy to magnetic fluxes in electromagnetism this type of excitation is called a fluxon[5].

Similar to the fluxons one can define another local excitation called chargon. In the simplest case, a chargon arises if we place the diagonal tensor χ_c on a virtual link. The matrix elements of the tensor χ_c are given by the characters of the irreducible representation c. To see why the excitation is called a charge excitation, we think of the group elements as carrying charge. A state (on one qubit) is charge neutral, if all types of charges are equally present, i.e., it is an equal weight superposition of all states $|g\rangle$. Note, that in the ground state we can think of χ_0 as being placed on all edges, since the characters of the trivial irreducible representations are always equal to one and thus χ_0 is the identity $\mathbb{1}_{|G|}$. Intuitively this means, that the ground state does not favor any charge type over the other and is indeed charge neutral. Now replacing χ_0 with χ_c, the equal weight superposition is lost, since for some g we have $\chi_c(g) \neq 1$ and thus a charge is created locally. Similar to the fluxons, chargons are deconfined excitations in the sense that there is no energy cost associated to moving them.

[5] The analogy is as follows: the line integral of the magnetic vector potential along the boundary of a surface is equal to the magnetic flux through the area. This line integral is analogous to multiplying all group elements on the boundary of the plaquette. Note, that group multiplication is the natural generalization of addition in the $\mathbb{Z}_2$ case discussed in detail.

Part II.

Non-chiral topological order

4. The algebraic theory of anyons

Most signatures of topological order such as the topological ground state degeneracy, the local indistinguishability of ground states and exotic excitations with fractional statistics can be discussed using the paradigmatic example of the toric code. However, the anyonic excitations of the toric code are more simple than general anyonic excitations. Recall that bringing an e-particle in proximity to an m-particle results in a state that behaves as if a fermion was located at the position of the (e,m)-particle pair. Hence, we say that the e and m particle *fuse* to a fermion. In the toric code the fusion outcome of two particles is always unique. Anyons with this property are called *Abelian anyons*. In contrast, for non-Abelian anyons the fusion outcome is not unique. An example for such non-Abelian anyons are the *Ising anyons* with particle types $1, \sigma, \Psi$, where 1 is the trivial particle, Ψ is a fermion and σ is a non-Abelian anyon as signified by the property that two σ particles can fuse to the vacuum or to a fermion. This is formally written as

$$\sigma \times \sigma = 1 + \Psi \,. \tag{4.1}$$

For a concrete lattice implementation of a system exhibiting Ising anyons this means that a state with two σ-particles can be identified with a superposition of states with a particle 1 or Ψ at the position of the two σ-particles. One can apply different microscopic operators on the region to project into a definite particle content state.

For non-Abelian anyons detecting a certain number of anyons at several distinct positions is not enough to uniquely determine the state. For example four σ-particles could have emerged as two pairs out of the vacuum. Alternatively, they could be the result of two fermions which decayed into two σ particles. We could distinguish the two states by observing how the two pairs braid with each other. In the first case, they would behave as bosons, while in the latter, they would behave as fermions.

In general we can associate a multi-dimensional Hilbert space to a given configuration of several non-Abelian anyons. The dimension of such a space is determined by the number of different possible ways in which the given anyon configuration can be obtained from the vacuum by a sequence of particle creation processes (cf. Section 4.2.1 for a more precise definition). As the particle positions do not uniquely specify the state, moving anyons around each other such that they eventually return to their original position does not need to be an identity operation, but instead can in principle be an arbitrary unitary operator acting within the multi-dimensional Hilbert space associated to the mutli-anyon configuration. In contrast, for Abelian anyons the state space is one dimensional and thus a braiding process can change the wave function only by a phase factor. Thus, braiding operations commute, which justifies to call these types of anyons Abelian.

Non-Abelian anyons are interesting due to their potential application in *topological quantum computation* [36, 40, 42, 43], where the ability to implement unitary operators by braiding anyons is used to perform quantum gates. As the latter only depend on the topology of the braiding paths, they are robust against local noise and hence *topologically protected*. An important question is what type of anyons allow to implement a universal gate set, i.e., a set of gates that can be used to express any quantum circuit. While Ising anyons mentioned in the example above only allow for a non-universal subset of gates (Clifford gates), universal anyon theories exist. A

particularly simple example of universal anyons are the so called Fibonacci anyons[1] with the fusion property $\tau \times \tau = 1 + \tau$ [12, 36, 37, 172].

In the following Section we present the theory of anyons on an abstract mathematical level disregarding the concrete physical implementations in terms of Hamiltonians. This so called algebraic theory of anyons starts out from proposing the existence of a finite number of distinct anyonic particle types (also called anyonic charges) labeled by $a, b, c, \ldots, n$, and Hilbert spaces associated to fusion outcomes of particles $a \times b \to c$, i.e., the Hilbert space associated to two particles a and b which are in proximity and behave like a particle type c (one says that they have total charge c). Usually these spaces are one-dimensional (multiplicity free). One can then infer consistency conditions on the fusion and the braiding of anyonic particles which are imposed by fundamental symmetry assumption. One example is the associativity of particle fusion (pentagon equation), i.e., the Hilbert space associated to a finite number of particles with a given total charge has a unique (finite) dimension which does not depend on the order of the fusion of the individual particles. The theory of anyon fusion is essentially described by a mathematical structure known as *fusion category*. Physical assumptions such as the existence of a unique vacuum state, normalizable states and the existence of a Hilbert space associated to a particle configuration imply several additional properties for the fusion category, which are fulfilled if the fusion category is *unitary*. The braiding of anyonic particles needs to be consistent with the associativity of the fusion, which is specified in a non-trivial self-consistency equation called the hexagon equation. A unitary fusion category for which braid operations can be defined consistently is called a *unitary braided fusion category* also referred to as unitary ribbon category. At last a certain non-degeneracy condition of the braid operations termed *modularity* discussed in Section 4.2.2 is usually imposed. Hence, anyonic theories correspond to mathematical objects known as *modular unitary braided fusion categories* (*UBFCs*) which is used anonymously with *unitary modular tensor categories* (*UMTCs*).

Unitary modular tensor categories can be divided into two classes, chiral and non-chiral ones. A chiral UMTC has a non-zero total chiral central charge as defined in Eq. (4.5). While famous examples of topologically ordered systems such as the ones used to describe the fractional quantum Hall effect are chiral as signified by chiral gapless edge modes, non-chiral topologically ordered systems are more amenable within the framework of gapped fix point Hamiltonians and tensor network ground states. In particular, a large class of non-chiral UMTCs can be constructed from unitary fusion categories via the Drinfeld center construction [19] discussed in the end of this Section. Both the known exact fix point models of topologically ordered systems (i.e., the Levin–Wen string net models) as well as their PEPS description (in terms of MPO-injective PEPS) can be seen as a physical implementation of the Drinfeld center construction. In the light of this fact, the following Chapter is devoted to an introduction to fusion categories, braided fusion categories and their relation to the theory of anyons and concludes with a discussion of the Drinfeld center construction.

For a more in depth review of anyons and where to find them, we refer to Ref. [36]. The presentation here closely follows Ref. [18, Appendix E].

4.1. Fusion categories

Before we introduce the notion of a fusion category more formally, let us give a brief intuitive description. A fusion category is given by a finite number of *simple objects* that can be fused (multiplied) resulting again in an object of the fusion category. This object however, is in

[1] The dimensionality of the Hilbert spaces associated to one, two, there, etc. τ-anyons grows as the Fibonacci series, hence the name.

general not simple, but isomorphic to a decomposition into finitely many simple objects. An intuitive example for such a structure are irreducible representations $\rho_i(g)$ of finite groups G which take on the role of simple objects. Fusion then corresponds to taking the tensor product $\tilde{\rho}_{ij}(g) = \rho_i(g) \otimes \rho_j(g)$ which is again a representation but in general a reducible one. Thus, there exist a transformation U such that $U\tilde{\rho}_{ij}(g)U^{-1} = \oplus_i \rho_i(g)$, i.e., in the language of fusion categories the fusion of two simple objects is isomorphic to a finite direct sum of simple objects.

For a more formal definition we need to introduce some terminology on categories. A category $\mathcal{C}$ is an abstract mathematical object that captures mathematical structure on a very coarse grained level general enough to rephrase every mathematical theorem as a certain properties of a suitably specified category. A category is defined as a collection of objects and morphisms that map objects to objects. Morphisms can be composed as $f \circ g$ and the composition is associative. In addition, for every object $x \in \mathrm{Obj}(\mathcal{C})$ there is an identity morphism $\mathbb{1}_x : x \to x$ that maps it to itself. The definition of a fusion category is as follows: A fusion category $\mathcal{C}$ is a rigid, finite, semi-simple, k-linear monoidal category. These attributes are explained in the following. We start with the most important property – *monoidal*.

4.1.1. Monoidal categories

Monoidal categories are equipped with a product structure similar to a Cartesian product or a tensor product. In particular for a monoidal category there is a mapping, called a *tensor functor* denoted by $\otimes$ from $\mathcal{C} \times \mathcal{C}$ to $\mathcal{C}$ which maps tuples of objects in $\mathcal{C} \times \mathcal{C}$ to objects in $\mathcal{C}$. Likewise, tuples of morphisms in $\mathcal{C} \otimes \mathcal{C}$ are mapped to morphisms in $\mathcal{C}$ such that the composition of morphisms is preserved, i.e., $f \circ g \otimes k \circ l = f \otimes k \circ g \otimes l$ and the tensor product of identity morphisms on objects x and y is mapped to the identity morphism on $x \otimes y$, i.e. $\mathbb{1}_x \otimes \mathbb{1}_y = \mathbb{1}_{x \otimes y}$. Although we have used the tensor product symbol familiar from linear algebra, $\otimes$ is not strictly associative, but associative only up to a (natural) isomorphism[2] $\alpha_{A,B,C}$ that maps $(A \otimes B) \otimes C$ to $A \otimes (B \otimes C)$.

A useful intuition for this is to think of $(A \otimes B) \otimes C$ and $A \otimes (B \otimes C)$ as isomorphic vector spaces, i.e., vector spaces of the same dimension, but represented in a different basis.

Pentagon equation The natural isomorphism of a monoidal category are subject to a consistency condition known as Mac Lane's coherence theorem or pentagon equation. It arises if we compare the objects $((A \otimes B) \otimes C) \otimes D$ and $A \otimes (B \otimes (C \otimes D))$ and the two sequences of morphisms that map $(((A \otimes B) \otimes C) \otimes D$ to $A \otimes B(\otimes(C \otimes D)))$. It is required that the two sequences of natural isomorphisms are identical and thus the natural isomorphism α fulfill the pentagon equation visualized in Fig. 4.1. Remarkably, all other consistency conditions, i.e., the requirement that any two sequences of natural isomorphisms relating two objects of $\mathcal{C}$ are identical, also follows from the pentagon equation – a fact known as Mac Lane's coherence theorem [173].

For the definition of a monoidal category one additionally requires that there is an identity object I for which there are natural isomorphisms ρ and λ such that $\alpha_{A,I,B} : (A \otimes I) \otimes B \to A \otimes (I \otimes B)$ composed with $\mathbb{1}_A \otimes l_B : A \otimes (I \otimes B) \to (A \otimes B)$ is identical to $r_A \otimes \mathbb{1}_B : (A \otimes I) \otimes B \to A \otimes B$. This identity is referred to as the triangle equality.

[2] The precise definition of a natural isomorphism is the following. A natural isomorphism is a map between two functors F, G mapping from a category $\mathcal{C}$ to a category $\mathcal{D}$ (in our case $- \otimes (- \otimes -), (- \otimes -) \otimes - : \mathcal{C} \times \mathcal{C} \times \mathcal{C} \to \mathcal{C}$) such that for every object $x \in \mathcal{C}$ (in our case the tripe $(A, B, C) \in \mathcal{C} \times \mathcal{C} \times \mathcal{C}$) there is an isomorphism α_x from the object $F(x)$ to the object $G(x)$ (in our case an isomorphism $\alpha_{A,B,C} : (A \otimes B) \otimes C \to A \otimes (B \otimes C)$) such that for every morphism in $\mathcal{C}$ mapping x to y, the natural isomorphism mapping $F(x)$ to $G(x)$ and $F(y)$ to $G(y)$ are consistent with the morphisms $F(f)$ and $G(f)$, i.e., $\alpha_Y \circ F(f) = G(f) \circ \alpha_X$.

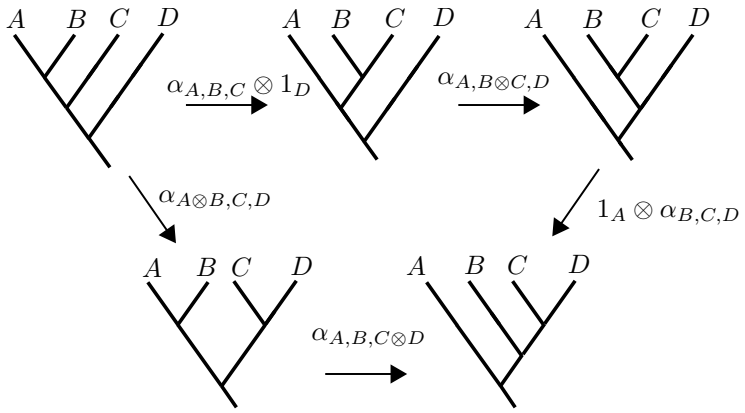

Fig. 4.1. ⋆ The pentagon equation for monoidal categories.

4.1.2. Rigidity, semi-simplicity, linearity and unitarity

The other properties of a fusion category are explained as follows. Semi-simple means that each object of $\mathcal{C}$ can be decomposed into a direct sum of *simple objects* and this sum is finite. The precise definition of a simple object is tedious, however, it agrees with the intuitive concept that a simple object can not be decomposed into other objects. It is irreducible and a good way to think of simple objects is to think of irreducible (group) representations.

Rigidity means that there is a notion of dual objects. I.e., for each object X there exists a unique dual object X^* defined by the existence of two morphisms, the unit $\eta : I \to X \otimes X^*$ and the co-unit $\epsilon : X \otimes X^* \to I$ which satisfy the so-called snake equation stating that $X \otimes (X^* \otimes X)$ is isomorphic to X. In a less rigorous language, this means that for each object there is a unique inverse with which it fuses to the identity in a unique way. Whether the isomorphism between $X \otimes (X^* \otimes X)$ and X is the identity morphism or a non-trivial morphism is an interesting property of a fusion category. It is related to the categorical definition of Frobenius Schur indicators [18][3]. The property k-linear means, that morphisms are linear and the set of all morphisms between two objects forms a vector space over a field k (in our case $k = \mathbb{C}$).

Unitarity

For the purpose of constructing physical theories from a fusion category in one way or the other, the fusion category must obey additional properties that guarantee that the resulting physical theory is compatible with the unitarity of quantum mechanical time-evolution, or likewise results in Hermitian Hamiltonians. The latter is guaranteed, if we impose unitarity of the fusion category. This means that the vector spaces of morphisms are Hilbert spaces and the natural isomorphisms, in particular the components of the natural isomorphism $\alpha_{X,Y,Z}$ used in the pentagon equation (the F-matrices) are unitary[4].

[3] A physical implication of non-trivial (higher) Frobenius Schur indicators is that they are associated to time-reversal and parity symmetry breaking as outlined in Ref. [174]

[4] Recently, non-unitary fusion categories have been considered [175], however, they give rise to non-Hermitian Hamiltonians and are beyond the scope of this thesis.

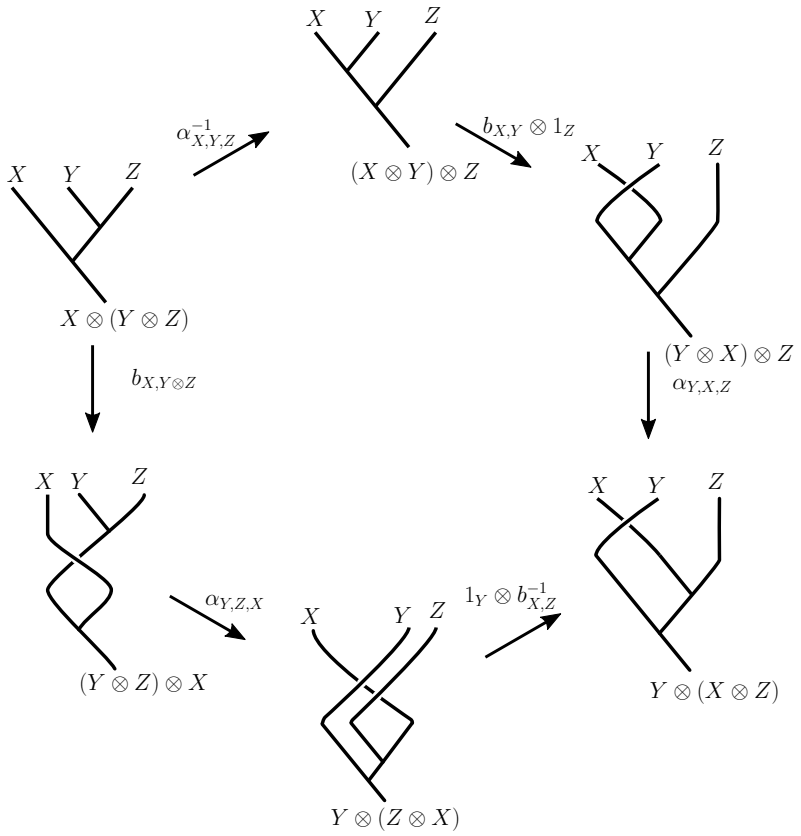

Fig. 4.2. • One of the two hexagon equations defining braided fusion categories. The other is obtained by inverting the line crossings in all figures and replacing the braid operation b by their inverses.

4.2. Modular braided unitary fusion categories and anyons

Above we discussed fusion categories without references to anyons and without discussing braid operations. Indeed, the existence of braiding operations is not part of the definition of a fusion category and for certain fusion categories it is not possible to find braid operations consistently. For an anyons theory, however, braiding is essential and is formalized as follows.

A braided fusion category is a fusion category with braiding, i.e., for all objects X and Y there are natural isomorphisms $c_{X,Y} : X \otimes Y \to Y \otimes X$ such that the braiding operation is compatible with the natural isomorphisms of the fusion $\alpha_{X,Y,Z}$ as specified by the *hexagon equations*, which states that the diagram shown in Fig. 4.2 and its counterpart obtained by replacing each braid morphism by its inverse is commutative.

4.2.1. Anyons

The simple objects of a fusion category can be identified with anyonic particles and the Hilbert space of morphisms from simple objects $A \otimes B$ to simple objects C with the physical Hilbert space V^c_{ab} – called *splitting space* –associated to particles a and b restricted to having total anyonic charge c. The dual space V^{ab}_c (of morphisms from C to $A \otimes B$) is interpreted as the Hilbert space associated to a particle c which was created by fusing particles a and b and called *fusion space*.

In the physics literature the fusion rules of anyons are often stated as $a \times b = \sum_c N_{ab}^c \, c$, where N_{ab}^c are the dimensions of the fusion (splitting) spaces and are called fusion multiplicities, i.e., $N_{ab}^c = \dim(V_{ab}^c)$.

Fusion and braiding

The associator of a unitary fusion category can be understood as a unitary isomorphism between the two Hilbert spaces associated to a triple of anyons a, b, c restricted to have total charge u. It is commonly referred to as F-symbol and defined as $F_u^{abc} : \oplus_e V_e^{ab} \otimes V_u^{ce} \to \oplus_f V_u^{af} \otimes V_f^{bc}$. Note, that to be an isomorphism the dimensionality of the two vector spaces has to be the same, i.e.,

$$\sum_e N_{ab}^e N_{ec}^u = \sum_f N_{af}^u N_{bc}^f \, . \tag{4.2}$$

The pentagon equation in Fig. 4.1 can then be written more explicitly in terms of F-symbols – the morphism $\alpha_{A,B,C} \otimes 1_D$ is replaced by F_q^{abc}, where q is the total charge of the particles a, b, c.

Similarly we can interpret the braid morphism as an actual braiding of anyonic particles and define the R-matrices $R_{ab}^c : V_c^{ab} \to V_c^{ba}$ as unitary transformations between Hilbert spaces. The hexagon equations can then be rephrased in terms of F-symbols and R-matrices.

To further analyze the anyon theory we need to introduce the concept of particles and antiparticles provided by the rigidity (i.e., the existence of duals) of the fusion category. Each particle a has a unique antiparticle a^* with which it fuses to the vacuum[5].

Quantum dimensions

An interesting quantity attributed to an anyonic particle a is its quantum dimension d_a defined as the exponential growth rate of the Hilbert space associated to an increasing number of a-particles and determined by the largest eigenvalue of the matrix N_a with $(N_a)_{jk} = N_{aj}^k$. The total quantum dimension of an anyon theory is defined as $\mathcal{D} = \sqrt{\sum_a d_a^2}$. One can easily check that for Abelian anyons, i.e., anyons for which the fusion outcomes are unique[6], the quantum dimensions are equal to one. The Hilbert space associated to a certain particle configuration is one dimensional and thus the braiding of anyons merely changes the wave-function by a phase. Thus, the order in which braidings are performed is irrelevant which justifies the given name.

In general quantum dimensions can take non-integer values. A special subclass of non-Abelian anyons are the so-called metaplectic anyons (e.g. the Ising anyons) with the property that d_a^2 is integer. It is conjectured [176] that the latter are not suitable to perform universal quantum computation via braiding. The standard example for non-Abelian anyons with non-integer quantum dimensions are the Fibonacci anyons τ with d_τ equal to the golden ratio. The quantum dimension d_a can also be expressed diagrammatically as a "closed-loop" of an a-particle. The closed-loop can be understood as the scalar product $\langle \Psi_{aa^*}^1 | \Psi_{aa^*}^1 \rangle$, where $|\Psi_{aa^*}^1\rangle \in V_{aa^*}^1$ and $\langle \Psi_{aa^*}^1| \in V_1^{aa^*}$. Attributing the value d_a to the closed loop can then be understood as a normalization convention for the basis vector $|\Psi_{aa^*}^1\rangle$.

[5] For further technical details, in particular regarding the role of potentially non-trivial Frobenius-Schur indicators, we refer to Ref. [18, Appendix E].

[6] I.e., for every pair a and b there is a unique c such that $N_{ab}^c = 1$ and $N_{ab}^{c'} = 0$ if $c \neq c'$.

(**a**) Topological twists θ_a (**b**) S-matrix

Fig. 4.3. ⋆ Twist and braiding data of an anyon theory specified by the twists θ_a and the mutual braidings S_{ab}.

S-and T-matrices

Finally, we can define the topological spin of an anyonic particle via the R-matrix (braid relation) as

$$\theta_a = d_a^{-1} \sum_c d_c \mathrm{Tr} R_c^{aa} \tag{4.3}$$

visualized in Fig. 4.3a. This expression can be understood as creating two particle-antiparticle pairs (a, a^*) braiding the particle a of one pair with the particle a of the other pair and fusing the resulting particle antiparticle pairs back to vacuum. Since we do not know how to braid two particles with arbitrary total charge, we need to evaluate the braiding for each total charge sector c and sum over all possible values.

Similarly we can characterize the braiding of two particles a and b via the entries of the *S-matrix* defined as

$$S_{ab} = \frac{1}{\mathcal{D}} \sum_c \mathrm{Tr}(R_c^{ba^*} R_c^{ab^*}) \tag{4.4}$$

and visualized in Fig. 4.3b. The entry S_{ab} of the S-matrix describes a process where two anyon particle-antiparticle pairs (a, a^*) and (b, b^*) are created, b^* and a are braided and at last, the particle-antiparticle pairs are fused to the vacuum again.

The topological charges define the total chiral charge of the theory

$$\Theta = \frac{1}{\mathcal{D}} \sum_a d_a^2 \theta_a = e^{2\pi \mathrm{i}/8c} \tag{4.5}$$

which determines the chiral central charge c (known from conformal field theory) modulo 8. The chiral central charge is a measure of the asymmetry of the topological spins. Typical non-chiral theories, i.e., theories with $\Theta = 1$ consist of two anyon theories $\mathcal{C}$ and $\bar{\mathcal{C}}$, where $\bar{\mathcal{C}}$ is the time-reversed copy of $\mathcal{C}$ with conjugated topological charges $\theta \to \bar{\theta}$.

4.2.2. Modularity

It is common to restrict the algebraic theory of anyons to a non-degenerate setting, where each particle (except for the vacuum particle) is observable by a braiding operation, i.e., for each particle $a \neq 1$ there is at least one particle which causes a change of the wave-function when moved around the particle a. This non-degeneracy condition implies that the S-matrix is unitary and the S- and T-matrices fulfill a set of equations that are – up to phase factors – identical to the defining relations for the generators of $SL(2, \mathbb{Z})$, i.e., the group of 2×2 matrices with integer coefficients and unit determinant. While $SL(2, \mathbb{Z})$ has the presentation

$$SL(2, \mathbb{Z}) = \langle S, T | S^4 = 1, (ST)^3 = S^2 \rangle, \tag{4.6}$$

the modular[7] relations for the S and T matrix in the non-degenerate setting are

$$(ST)^3 = \Theta C, \qquad S^2 = C, \qquad C^2 = 1, \tag{4.7}$$

i.e., they are identical to $SL(2,\mathbb{Z})$ for chirality free anyon models. For a more in-depth interpretation we refer to Ref. [177].

We illustrate the connection between the S-and T-matrices and the group $SL(2,\mathbb{Z})$ for non-chiral theories. It is an essential observation that each anyonic particle in the theory can be identified with a particular ground state on a torus of a suitably chosen Hamiltonian representing the theory[8] [178]. We illustrate the connection between anyonic particles and ground states on the torus on the example of the toric code. Recall, that in the toric code there are four different anyon types and four ground states on a torus. Moreover, we can express logical operators as the following process: create a particle-antiparticle pair, move one particle around a non-contractible loop and fuse it again with its antiparticle. This suggests the following picture: Imagine an anyonic flux e (i.e., a closed e-anyon world-line) inside the torus winding once around the hole. If we apply the logical operator around the other cycle which corresponds to an m-particle loop around the other cycle, this corresponds to the diagram for S_{em}. This suggests to identify eigenstates of the logical m-operator around one cycle with states of well-defined e-anyon flux through the other cycle. Generalizing this picture, we label the ground states which are also eigenstates of particular logical operators by anyon types.

As indicated above, we can than access the S- and $T-$matrices by calculating scalar products of states with well-defined anyon flux[9]. We can also change the anyon fluxes by applying Dehn-twists to the torus. A Dehn-twist is a certain global deformation which consists in cutting the manifold open along a non-contractible cycle, performing a 360° twist and gluing the cutting boundaries together again. For example, on a state with well defined anyon flux through one cycle, performing a Dehn-twist along the same cycle increases the winding number of the anyon flux. By comparing the state before and after the Dehn-twist we can calculate the topological spin of the anyonic particle corresponding to the flux. Similarly, the S-matrix entry S_{ab} can be expressed by performing a sequence of Dehn-twists on a state with anyon flux b through one cycle, such that after the deformation, the flux is transferred to the other cycle. Taking the overlap between the "rotated" b-state and the unrotated a-state coincides with the diagrammatic definition of the entry S_{ab} up to a normalization factor.

From the relations between Dehn-twists and the S-and T-matrix we can see how the latter are connected to $SL(2,\mathbb{Z})$, which is the mapping class group of the torus. To see this, we think of the torus as being parametrized by the two winding numbers (n,m) of some imaginary strings wrapped around the two non-trivial cycles. The two Dehn-twists take the tuple of winding numbers $(m,n) \to (m+n,n)$ and $(m,n) \to (m,n+m)$, respectively. Representing these actions as linear maps t_1, t_2 with integer coefficients, we obtain the standard generators of $SL(2,\mathbb{Z})$ by identifying t_1 with T and $t_1 t_2^{-1}$ with S.

4.2.3. Non-chiral anyon theories and the Drinfeld center

In this Section we consider a particular class of non-chiral braided fusion categories which are obtained from a given fusion category $\mathcal{C}$ by a particular recipe – the Drinfeld center construction. The Drinfeld center $\mathcal{Z}(\mathcal{C})$ of $\mathcal{C}$ appears as the anyon content in well-known lattice models for

[7] The projective version of $SL(2,\mathrm{Z})$, which is called the modular group $PSL(2,\mathrm{Z})$ is obtained by $SL(2,\mathbb{Z})$ when identifying A and $-A$.

[8] For non-chiral theories which are Drinfeld centers of a fusion category the Hamiltonian construction is straightforward and will be discussed in the following Section.

[9] For a procedure how this can be done explicitly, we refer to Ref. [178].

topological order, i.e. in Levin–Wen string-net models discussed in Chapter Section 5.1. Similarly, PEPS ground states of non-chiral topologically ordered systems have virtual symmetries captured by a fusion category $\mathcal{C}$ while their parent Hamiltonian host anyonic excitations given by $\mathcal{Z}(\mathcal{C})$ (cf. Section 5.2). Thus, it is fair to say that the Drinfeld center construction $\mathcal{C} \to \mathcal{Z}(\mathcal{C})$ is the mathematical backbone of non-chiral topological.

Definition 4.1. Drinfeld center (cf. Ref. [19, p. 310]) The Drinfeld center $\mathcal{Z}(\mathcal{C})$ of a fusion category $\mathcal{C}$ is a category whose objects are pairs (X, ϕ_X) where X is an object from C and ϕ_X is natural half-braid isomorphism $\phi_X : A \otimes X \to X \otimes A$ which is compatible with the tensor functor, i.e., it fulfills the hexagon equation[10] as defined in Fig. 4.2.

As a direct consequence of the definition the Drinfeld center is a braided fusion category. If the input fusion category $\mathcal{C}$ is not too exotic (i.e., it is spherical or, stronger yet, unitary), the Drinfeld center will also be modular and unitary and thus gives rise to a well defined anyon model. The anyon labels of this theory are the simple objects of the braided fusion category $Z(\mathcal{C})$. However, if we calculate the objects of $\mathcal{Z}(\mathcal{C})$ built from pairs of simple objects of $\mathcal{C}$ and appropriate braid morphisms, the resulting objects might not be simple. Finding the simple objects of $\mathcal{Z}(\mathcal{C})$ is usually done by identifying the category $\mathcal{Z}(\mathcal{C})$ with an associative $*$-algebra and calculating its irreducible representations. Depending on the specific approach used in the calculation one may arrive at different labels of the irreducible representations and it is not always apparent at first sight, if the latter are equivalent. For example in the case where $\mathcal{C}$ is given by a group G (i.e. its simple objects can be identified with group elements and the tensor functor is essentially determined by the group law), we may label the irreducible representations of the Drinfeld center either by pair-conjugacy classes as defined in Section 3.2.2 or by pairs $(C, \rho^i_{Z_C})$, where C denotes the conjugacy classes of G and $\rho^i_{Z_C}$ are the irreducible representations of Z_C, where Z_C is the centralizer for one arbitrarily chosen element of C (cf. Ref. [31]). Using representation theory, we can immediately verify that the two sets can be identified with each other.

The anyon theories associated to Drinfeld centers are always non-chiral as proven in Ref. [182] using category theory. An alternative way to see this is to show that one can always construct a gapped boundary Hamiltonian to a given bulk Hamiltonian which hosts anyons given by a Drinfeld center [46]. Note, that the converse is not true, i.e, there exist non-chiral UMTCs which are not Drinfeld centers [183].

The map $\mathcal{C} \to \mathcal{Z}(\mathcal{C})$ is not injective. There are different fusion categories that have the same Drinfeld center. Two categories with the same Drinfeld center are Morita-equivalent[11]. In physical terms this means that two seemingly unrelated Hamiltonians can give rise to the exact same anyonic excitations. An explicit example for Morita equivalent categories are the two categories which can be derived from a finite group G. The first one Vec$G$, the category of G-graded vector spaces is essentially determined by the group law itself that defines the tensor functor for simple objects as $\delta_g \otimes \delta_h = \delta_{gh}$. The other category Rep$(G)$ is the category of irreducible representations of G, where the tensor functor is given by the direct sum decompositions of the tensor product representation into irreducible representations. While we do not know how to proof this statement in elementary terms, it follows from a general theorem about Hopf algebras (which contain group algebras as the simplest examples) stating that the representations of the *quantum double* of G – which for our purpose can be used

[10] Sometimes one finds the short-hand definition $\phi_{X\otimes Y} = \mathbb{1} \otimes \phi_X \circ \phi_Y \otimes \mathbb{1}$, which does not refer explicitly to the associators. [179–181]

[11] For us, this can be seen as the definition of Morita equivalence, however the actual definition in the category theory literature is different and is given by duality relations for module categories (cf. Ref. [19, p. 289]).

synonymously with *Drinfeld center* – is equal to the quantum double of the representations of G, i.e., $\mathrm{Rep}(D(G)) = D(\mathrm{Rep}(G))$ [19, 184].

5. MPO-isometric PEPS, string-nets and state-sums

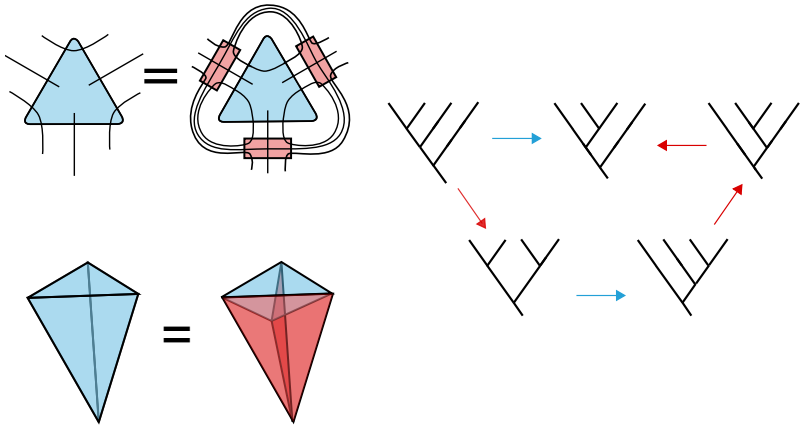

Fig. 5.1. ⋆ Equivalent manifestations of the pentagon equation in different formalisms describing non-chiral topological order. Top left: Matrix product operators (MPO) injectivity in tensor networks. Top right: Self-consistency condition for deformation rules in Levin–Wen string-nets. Bottom left: Triangulation invariance of a space time volume (1-4 Pachner move).

Non-chiral topological ordered systems exhibit hallmarks of topological order as e.g. a topological ground state degeneracy and anyonic quasiparticles. In contrast to chiral systems – such as e.g. the ones in which the fractional quantum Hall effect [47–49] is observed – they are fully gapped, meaning that their excitation spectrum is gapped not only if they are defined on a closed manifold, but also on a manifold with boundary. In contrast, chiral topological systems (cf. Section 5.4.2) are only gapped in the bulk, i.e., they are gapped on closed manifolds, but show gapless edge modes on the boundary. The latter can not be gapped out by small local perturbations. They are chiral in the sense that there is a single mode with wave-vector k and energy $\epsilon_1(k)$ without a "counter propagating" mode at $-k$ with the same energy $\epsilon_1(k) = \epsilon_2(-k)$[1]. In a conventional condensed matter perspective the connection between chirality (meaning the presence of chiral edge modes) is connected to robust gapless excitations as follows. If edge modes come in pairs $(k, -k)$ perturbations can gap out the excitation spectrum around the "band crossing" at $k = 0$ by suitably "mixing" the two bands. This is however not possible if there is only a single chiral edge mode. Thus, chiral gapless edge modes are stable against perturbations.

While the algebraic theory of the bulk anyons (discussed in Section 4.2.1) is the same for chiral and non-chiral topological order, the microscopic or field theoretic descriptions of the two are quite different [46]. We will briefly discuss this point at the end of this Chapter in

[1] This is often depicted as a circular *motion* around the edge of the system. However, the edge states are still (stationary) eigenstates of the Hamiltonian and there is a priori no "motion" associated to them.

Section 5.4.2, but the remainder of this Chapter is concerned only with non-chiral topological order.

The theory of non-chiral topological order in two dimensions is highly evolved and the range of different mathematical formalisms by which it is studied are remarkably broad and deep [11, 19, 185–188]. The most elementary description is perhaps given by exactly solvable lattice Hamiltonians similar to the toric code [31] – the *Levin–Wen string-net models* [12]. Complementary, ground states of the latter can be written as exact PEPS [63, 64] with *virtual symmetries* characterized by matrix product operators (MPOs) [6–8]. Taking a closer look at the tensor network construction one can identify individual tensors with simplices of a manifold triangulation [3, 6, 189, 190]. The virtual symmetries of the tensors can be understood as a kind of *triangulation invariance*. Thus, the tensor networks associated to string-net models give rise to *topological invariants* [14, 186, 187, 189, 191]. This relates the theory of non-chiral topological order to abstract functorial *topological quantum field theory* (TQFT) [13, 192, 193] (not addressed further in this text).

A particular subclass of non-chiral topological theories corresponds to lattice gauge theories with finite discrete gauge groups (Dijkgraaf–Witten theories) [189]. Others [12] correspond to doubled Chern–Simons theories [194], i.e., a bi-layer system with one layer described by a Chern–Simons theory and the other by its time-reversed counterpart. In a sense dual [3, 187, 195] to Levin–Wen string-net models, the toric code model can also be generalized by replacing the group $\mathbb{Z}_2$ with a general group G [31], or even more general a (finite semisimple) Hopf algebra H [5, 196, 197]. The latter models can be shown to be equivalent to string-net models and correspond to quantized Chern–Simons theories [197, 198].

We have discussed in the previous chapter that the theory of non-chiral topological order can be essentially understood – on a very abstract level – in the language of category theory. A system with microscopic degrees of freedom that interact according to rules determined by a fusion category $\mathcal{C}$ exhibits anyonic particles which are given by the Drinfeld center $\mathcal{Z}(\mathcal{C})$. Nowadays, the mathematical details, extensions and interpretation of this fundamental idea are mostly studied in the language of higher-category theory [188, 199–202]. It is our impression that the details of how the subjects mentioned here relate to each other are still not entirely understood. Moreover, it seems that the mathematical structures and their physical interpretations are only known to a small selected community.

In this Chapter we try to make the subject more accessible to a wider audience and provide an elementary introduction to non-chiral topological order. We explain the relations between Levin-Wen string-net models, virtual symmetries in topological PEPS, state sum constructions and the Drinfeld center (cf. Fig. 5.1). The connections drawn here also allow us to approach a very practical question later in this thesis. Namely, the question how non-chiral topological order can be realized in actual physical systems.

5.1. Levin–Wen string net models

In 2005 Levin and Wen proposed a class of exactly solvable models that exhibit non-chiral topological order [12] – the string-net models. Including their recent generalizations [174, 203–206] string-net models still present the largest class of known fixed point models and we will briefly review their basic theory following the original reference [12] in the following Section.

String-net models can be seen as a generalization of the toric code and are described by a

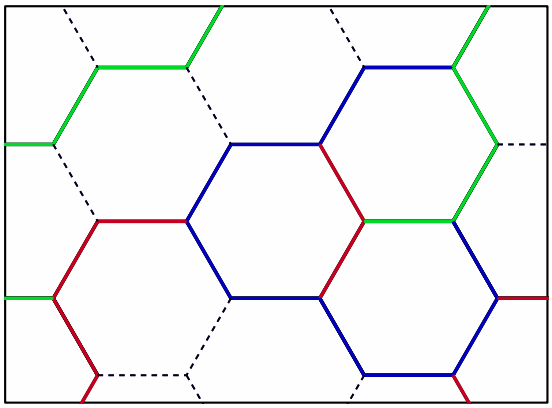

Fig. 5.2. ⋆ An example of a string-net state with four string-types. The vacuum string is drawn with dashed lines.

commuting projector Hamiltonian

$$H = \sum_v A_v + \sum_p B_p \,, \tag{5.1}$$

of vertex and plaquette operators, A_v and B_p.

The toric code ground state is given by an (equal weight) superposition of closed loops (cf. Section 3.2.3), i.e., a particular configuration of strings, where spin-up states are associated with a non-trivial string type and spin-down states are associated with the vacuum, or with the *trivial string type*. For a general string-net model there is a set of abstract *string-types* $|a_i\rangle\,, i = 1, \ldots, N_s$ that always include the trivial (vacuum) string $a_0 = 0$ and the local Hilbert spaces associated to the edges of the lattice is spanned by a basis that is labeled with the string-types.

Like in the toric code, the vertex projector projects onto the subspace of allowed vertex configurations, i.e., allowed patterns of strings that. The latter are specified by so-called *branching rules* and can be interpreted as the fusion coefficients $N_{ab}^c \in \{0, 1\}$ of a multiplicity-free fusion category (cf. Section 4.1)[2], i.e., there is only one way how two strings a and b can fuse to a string c or likewise how a string type c can split up into a string a and a string b. For the toric code there is only one non-trivial *branching rule*, stating that the non-trivial string-type is not allowed split into two strings which implies that the vertex projector projects onto states with an even number of non-trivial strings on the adjacent links of a vertex (even parity).

To distinguish fusion and splitting vertices and particles from anti-particles the edges of the lattice carry an orientation. The original string-net models [12] impose that the orientation of an edge can be reversed if the string-type associated to it is replaced by its dual string-type. This additional axiom restricts the set of non-chiral theories, which can be described by the model, but simplifies the formalism significantly[3].

For a trivalent lattice, e.g., a honeycomb lattice, the vertex constraints are immediately given by the branching rules. In general, string-net models can be defined on arbitrary graphs by

[2] Including fusion multiplicities would require to add an additional degree of freedom at every vertex, such that there is an N_{ab}^c-dimensional Hilbert space associated to a vertex where the strings a and b fuse to the string c.

[3] The condition was later relaxed to allow for more general string-net models [174, 203, 205, 207] and other even more general constructions are formulated in the language of (Turaev–Viro–Barret–Westbury) state sums [190, 208, 209] which are equivalent to string-net models [44, 185, 186]. Also, the fermionic string-net models given in [11] – restricted to the fermionic component of the theory being trivial – yield (bosonic) generalizations of the original string-net models.

the following consideration. An n-valent lattice can be decomposed into a small graph with trivalent vertices and the n-valent vertex operator is defined as the product of the respective trivalent vertex operators.

The plaquette operator performs a similar action to flipping all spins around a plaquette as in the toric code. It is given by a sum over plaquette operators associated to each string type

$$B_p = \sum_{s=1,\dots,N_s} \frac{d_s}{D} B_{p,s} \,, \tag{5.2}$$

with $D = \sum_s d_s^2$ and the factors d_s defined in Eq. (5.4) are introduced to ensure that the Hamiltonian is Hermitian. The operator $B_{p,0} = \mathbb{1}$ acts trivially. To understand the action of $B_{p,s}$ for non-trivial string-types, we need to relax the rigid notion of a lattice and consider string-types more abstractly as string-like objects living on a two-dimensional manifold. The action of $B_{p,s}$ then corresponds to inserting a closed loop of the string-type s into the interior of the plaquette p and "merging" the inserted loop with the strings on the boundary of the plaquette such that the interior of the plaquette is string-free again and the string configuration on the boundary of p has changed. For the toric code, inserting a non-trivial string type has the effect of flipping all spins, as can be seen by noting that the fusion rules are nothing but the group multiplication of $\mathbb{Z}_2$. For more general string-nets the re-integration of the inserted string into the lattice structure requires the knowledge of a set of rules specifying how string-configurations can be manipulated, which is discussed in the next Section.

5.1.1. Deformation rules

Since Levin–Wen string-net models are designed to exhibit topological order, it is required that their ground state wave function is invariant under a set of deformation rules, which do not change the topology of the string-net. A closer look reveals that the latter can be identified with the defining properties of a fusion category or correspond to additional normalization conventions. In the following we list and comment on the deformation rules proposed in Ref. [12].

The first and simplest deformation-rule motivated by topological invariance is the deformability of strings

$$\Phi\left(\quad \overset{\text{i}}{\longrightarrow} \quad\right) = \Phi\left(\quad \overset{\text{i}}{\sqsubset} \quad\right) \tag{5.3}$$

stating that the amplitude of the wave function is invariant under all topologically trivial deformations of the string-net. The second rule

$$\Phi\left(\quad \overset{\text{i}}{\circlearrowright} \quad\right) = d_i \Phi\left(\quad\right) \tag{5.4}$$

states that a topologically trivial closed loop of a string type a can be removed from the configuration (similar to the application of a generalized local unitary circuit removing disentangled degrees of freedom in Section 2.2) while the wave function amplitude changes by a scalar factor d_a. Reminiscent of the quantum dimensions in the algebraic theory of anyons (cf. Section 4.2.1) the prefactors d_s are also referred to as quantum dimensions[4] and

$$D = \sum_s d_s \tag{5.5}$$

[4] This wording is used even though the fusion category of the string types itself might not necessarily give rise to a well-defined anyon model as for some fusion categories, no consistent braid morphisms can be found.

is referred to as the total quantum dimension.

The third rule

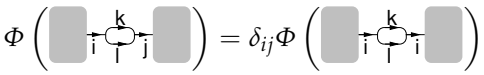

$$= \delta_{ij} \Phi$$

(5.6)

states that if a string i branches into two strings which immediately fuse again, the fusion result has to be the string i. If this was not the case and the fusion product was instead a string type p, then at the segment of the branching j, k a string type i would simply transform into a string-type p. This seems to be unphysical as the branching j, k affects the string only on a finite region and should be invisible at large distances. Thus, if such a transformation $i \to p$ would be allowed, string types i and p could freely transform into each other and would no longer correspond to distinct string-types. In other words, we require that a string type i always stays a string-type i as long as it is only "perturbed" by local string-diagrams that do not contain any outgoing or incoming strings.

The fourth rule is clearly motivated by the associativity axiom of a fusion category

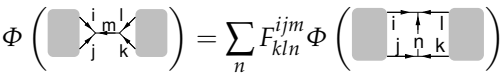

$$= \sum_n F^{ijm}_{kln} \Phi$$

(5.7)

and is referred to as *F-move*. It is a statement about a configuration where four string types i, j, k, l are fused in two different ways and expresses the fact that the wave functions associated to the two microscopically different implementations of the fusion process should be related by a linear operator, the F-symbol.

The deformation rules given above can be applied to drastically simplify a string-net configuration. A generic ground state string-net configuration can be reduced to a minimal web of strings that cannot be simplified any further due to topological obstructions of the manifold. For example, in the closed loop superposition of the toric code, one can remove every topological trivial loop and multiply the wave-function by $d_1 = 1$ until one ends up with a trivial vacuum state on a sphere. On a torus we obtain four different ground states distinguished by the number of non-trivial string types winding around the non trivial cycles.

Self-consistency equations

The deformation rules above cannot be used with arbitrary d_i, F^{ijm}_{kln}. By the analogy with fusion categories we strongly suspect that at least the associativity rule, the F-move, must be subject to a consistency condition similar to the pentagon equation. Indeed, if we require that the wave function amplitude associated to a given string configuration is unique, we obtain a pentagon equation for the F-symbols. To see this, consider the string configuration on the top left of Fig. 5.3. It can be deformed to the configuration on the bottom-right by a sequence of F-moves along the paths on the left panel. Likewise, it can be deformed to the same configuration via a different path shown on the right panel. Evaluating and equating the sequences of F-symbols along the two paths, we arrive at the pentagon equation for F-symbols of string-net models

$$\sum_{n=1}^{N_S} F^{mlq}_{kp^*n} F^{jip}_{mns^*} F^{js^*n}_{lkr^*} = F^{jip}_{q^*kr^*} F^{riq^*}_{mls^*} \ . \tag{5.8}$$

One may ask whether there are more pairs of paths given by sequences of deformation rules that connect two different string-net configurations and thus lead to additional consistency equations. However, MacLanes coherence theorem [173] (cf. Section 4.1.1) asserts that the pentagon equation is sufficient to ensure consistency, i.e., all other consistency equations are fulfilled if the pentagon equation is satisfied.

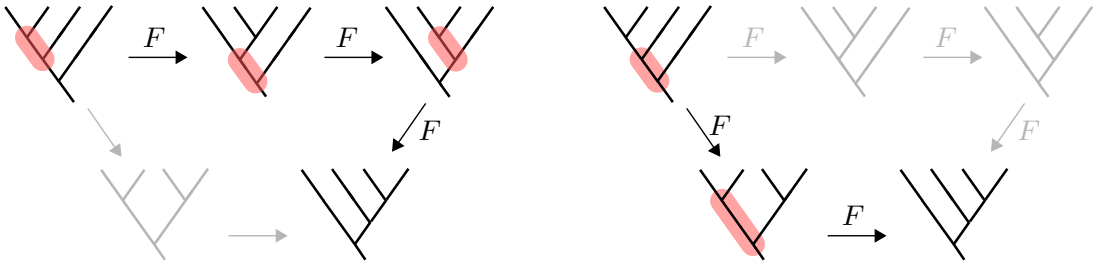

Fig. 5.3. ⋆ The pentagon equation emerges as a self-consistency equation from comparing the two different deformation paths (left and right) between an initial and a final string-configuration. Labels and arrows have been omitted in the diagram.

Normalization

Regarding the normalization of the string-net wave function, we note that there is a canonical rescaling of the wave-function: Associating a factor $f(i,j,k)$ to every vertex with string configuration i,j,k does not affect the validity of the deformation rules. As long as $f(i,i^*,0) = 1$ the rescaling only results in a gauge transformation of the F-symbols

$$\tilde{F}^{ijm}_{kln} = F^{ijm}_{kln} \frac{f(i,j,m)f(k,l,m^*)}{f(n,l,i)f(j,k,n^*)} \,. \tag{5.9}$$

Thus, we can always choose f such that the F-symbol fulfills the following *normalization condition*

$$F^{ijk}_{j^*i^*0} = \frac{v_k}{v_i v_j} \delta_{ijk} \,, \tag{5.10}$$

where

$$v_i = \sqrt{d_i} \,. \tag{5.11}$$

and δ_{ijk} is a short-hand notation for the branching rule, i.e., $\delta_{ijk} = 1$ if i, j and k are allowed to meet at a vertex and zero otherwise. We will see in Section 5.3.1 that this gauge choice can be interpreted as a generalization of gauging a 3-cocylce with a 2-cocylce.

Tetrahedral symmetry

In the original work by Levin and Wen [12] it is imposed that the wave function defined on a minimal sphere (i.e., a tetrahedron) is invariant under reflections and rotations and hence invariant under the full tetrahedral group. This additional requirement simplifies the string-net formalism while also making it less general as tetrahedral symmetry restricts the set of allowed F-symbols as follows. Applying the three generators of the tetrahedral group (reflections along three different planes) to a given string-net configuration on a minimal sphere, results in four different configurations. Each can be reduced to the vacuum configuration whereby the amplitude of the wave-function changes according to the deformation rules Eqs. (5.3), (5.4), (5.6) and (5.7). Equating the wave function amplitudes one obtains the tetrahedral symmetry conditions for the F-symbols. The latter can be used to introduce the symmetrized F-symbol – the $\tilde{G}$-symbol – which is tetrahedral symmetric by definition

$$\tilde{G}^{ijm}_{kln} \equiv F^{ijm}_{kln} v_i v_j v_k v_l = F^{lkm^*}_{jin} v_i v_j v_k v_l = F^{jim}_{lkn^*} v_i v_j v_k v_l = F^{imj}_{k^*nl} v_i v_k v_m v_n \,. \tag{5.12}$$

Plaquette operator

As discussed earlier the plaquette operator can be best understood as the sum of closed loop insertions inside a plaquette. To reintegrate the inserted string back to the hexagonal lattice, we imagine six vacuum strings inside the hexagon and apply six F-moves as in Fig 5.4a to obtain a configuration with "bubbles" at the vertices. Each bubble can be simplified according to Fig. 5.4b. Collecting all F-symbols and using Eq. (5.10) we obtain the matrix elements of $B_{p,s}$ as

$$[B_{p,s}]^{s,g'h'i'j'k'l'}_{ghijkl}(abcdef) = F^{al^*g}_{s^*g'l'^*} F^{bg^*h}_{s^*h'g'^*} F^{ch^*i}_{s^*i'h'^*} F^{di^*j}_{s^*j'i'^*} F^{ej^*k}_{s^*k'j'^*} F^{fk^*l}_{s^*l'k'^*} \,, \tag{5.13}$$

where g, h, i, j, k, l and their primed variants refer to the string types on the inner edges before and after the application of $B_{p,s}$ and a, b, c, d, e, f refer to the string types on the outer links that remain unchanged.

5.1.2. Relation to fusion categories and remarks on tetrahedral symmetry

In essence, a string-net model is defined from unitary fusion category $\mathcal{C}$. The objects of the fusion category correspond to the string-types, the fusion rules are determined by the tensor functor and the F-symbols are a concrete implementation of the natural isomorphisms $\alpha_{X,Y,Z}$ that appear in the pentagon equation for monoidal categories. The existence of a dual object a^* is implied by the rigidity of the fusion category and unitarity ensures that the F-moves correspond to unitary operations.

Tetrahedral symmetry is not a property of a general fusion category and there are in fact examples of fusion categories with non-tetrahedral symmetric F-symbols. The simplest example is the category $\mathrm{Vec}(\mathbb{Z}_3, \omega)$ where the fusion rules are given by the group multiplication and the F-symbol is given by one of the two non-trivial 3-cocycles of $\mathbb{Z}_3$ (cf. Section 5.3.1). Also, the condition that inverting edges maps a to a^* is an unnecessary restriction. What is required in order to obtain a well-defined string-net model and in particular a Hermitian string-net Hamiltonian is that the F-symbols evaluated on a sphere are subject to complex conjugation when reflected on some arbitrary mirror-plane [205][5]

5.1.3. Anyons

The theory of string-net models is designed to yield topologically ordered lattice Hamiltonians. Thus, we expect that string-net models feature anyonic excitations. As the string-net Hamiltonian is a sum of commuting projectors, all excitations are characterized by a finite number

[5] A deeper understanding of the necessity of the conjugation-mirror-symmetry of the F-symbol can be obtained in the state-sum picture and is sketched in Section 5.3.2. The latter condition is fulfilled for any unitary fusion category with the property that $a^{**} = a$ (strict pivotality) [205].

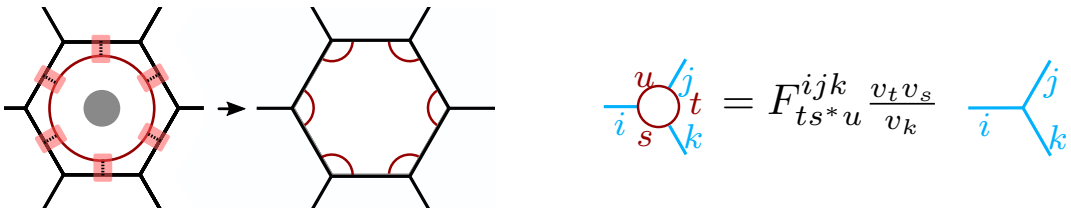

(**a**) Transforming the inserted closed loop. (**b**) Evaluation of the bubble configuration.

Fig. 5.4. ⋆ String-deformations used in the definition of the plaquette operator (cf. Eq. (5.13)).

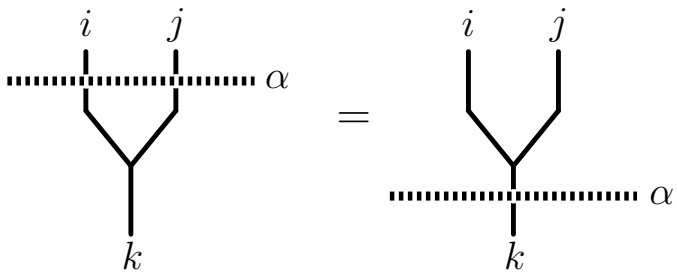

Fig. 5.5. • The deformability condition of the excitation string α expressed diagrammatically.

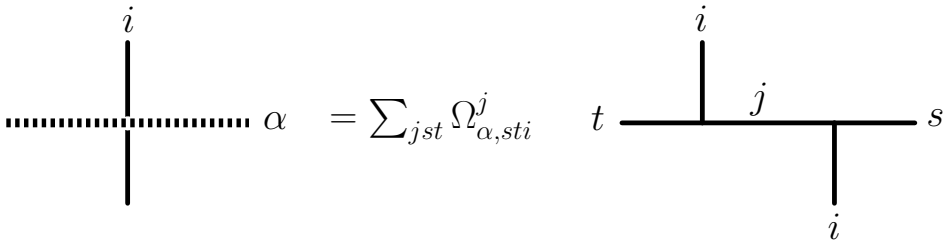

Fig. 5.6. • Definition of an excitation string-type α in terms of a string-net configuration with yet to be determined (matrix-valued) coefficients $\Omega^j_{\alpha,sti}$.

of vertex and plaquette operator violations. Motivated by the analysis of the toric code, we expect that excitations can be generated by *string-operators*. When applied to the ground state, excitations are generated at the end points of the string, while the excitation string itself can be deformed freely. A natural ansatz for these operators are matrix product operators (MPOs) where the bond dimension indicates the complexity of the string-type and the support of the MPOs should be a line-like region, i.e., of finite width. It turns out that it suffices to use an MPO that modifies the string-net configuration along a line of connected edges and whose matrix values depend only on the string types along and directly adjacent to that line. This fact can be motivated by the observation that Levin–Wen string-nets have zero correlation length.

The conditions stated above can be captured by the following ansatz for excitation string-operators expressed in a diagrammatic way. For the sake of conceptual clarity and to avoid cumbersome notation, we restrict ourselves to the case where string-types are self-dual, as is the case for several string-net models including the Fibonacci, Ising and the $\mathbb{Z}_2$ string-net. For self-dual string-types, we can omit all arrow directions in the diagrams. We introduce an abstract diagram to denote the presence of an excitation string-operator α. Without loss of generality, we pick a location that is small enough such that the excitation string only intersects with a single string-type of the lattice denoted by i in Fig. 5.6. Since, this diagram should correspond to a state in the string-net Hilbert space, we must be able to express it as a superposition of string-net configurations. These configurations should have an ingoing and an outgoing i-string and also the excitation string should be modeled by a superposition of yet to be determined of ingoing and outgoing string-types s and t. We still need to resolve the crossing of the excitation string and the i-string. With the assumptions about the locality of the excitation string, it suffices to pick a specific string segment where the i-string is changed to a (superposition of) j-strings. The coefficients of the superposition $\Omega^j_{\alpha,sti}$ in general depend on i, s, t and j. As the excitation string operator is a matrix product operator, we are free to use matrix valued coefficients $\Omega^j_{\alpha,sti}$

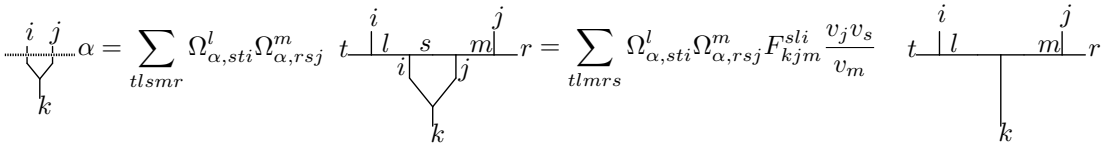

(**a**) Left-hand side of Fig. 5.5 evaluated using Fig. 5.6 and deformed using Eq. (5.7).

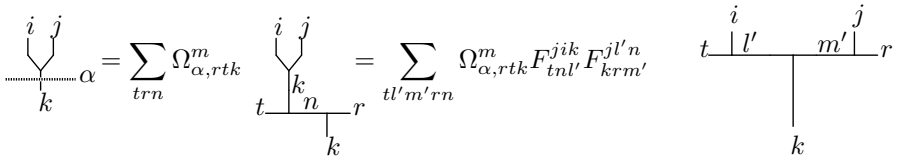

(**b**) Right-hand side of Fig. 5.5 evaluated using Fig. 5.6 and deformed using Eq. (5.7).

Fig. 5.7. ⋆ Resolving the excitation string condition (Fig. 5.5) in terms of string-net configurations.

which are multiplied if two α-segments are connected. The dimension of these matrices is not fixed a priori.

We now evaluate the condition of free deformability stated in Fig. 5.5 in diagrammatic notation. Replacing the α-strings with string-net diagrams as defined in Fig. 5.6, we can apply several F-moves to reduce both sides of the equation to a sum over string-net configurations with prefactors given by Ω- and F-symbols (cf. Fig. 5.7). From this we obtain an algebraic condition on the Ω-matrices

$$\sum_{s=0}^{N} \Omega^{m}_{\alpha,rsj} F^{sli}_{kjm} \Omega^{l}_{\alpha,sti} \frac{v_j v_s}{v_m} = \sum_{n=0}^{N} F^{jik}_{tnl} \Omega^{n}_{\alpha,rtk} F^{jln}_{krm} \,. \tag{5.14}$$

A direct sum of solutions to Eq. (5.14) is again a solution. We are thus interested in calculating the irreducible solutions to Eq. (5.14), i.e., the ones with minimal matrix dimensions. We can identify the latter with elementary anyonic particles and direct sums with superpositions.

Calculating the irreducible solutions for Ω explicitly can be tedious. However, we realize that the equations determining the excitation string types are very similar to the definition of the Drinfeld center of $\mathcal{C}$, the fusion category of string-types. Identifying each F-symbol with the associator and each Ω with the braid morphism, Eq. (5.14) is almost identical to the hexagon equation in the definition of the Drinfeld center (cf. Fig. 4.2 and Section 4.2.3). In the original string-net models, the equivalence of the quasi-particle excitations with the Drinfeld center is obvious for certain cases, e.g., when $\mathcal{C}$ is a group (cf. Section 5.3.1). A more general equivalence of quasi-particle excitations in string-net models and the Drinfeld center construction is proven in Ref. [206] using the so called Q-algebra approach.

Relating the quasi-particle content to the Drinfeld center has practical advantages. First of all, we know from fundamental category theory that the string-excitations indeed form a modular unitary braided fusion category and thus a consistent anyon model. In addition, Drinfeld centers are known in the literature for a large set of fusion categories. On top of that, known Morita equivalences allow to infer the anyon content of complicated string-net models from more simple ones. E.g., the anyon content of the fusion category $\mathrm{Rep}(S_3)$ which has three string-types with non-Abelian fusion rules and non-trivial F-symbols can be inferred from the the anyon content of the string-net model with fusion category $\mathrm{Vec}(S_3)$ which has six string-types, but trivial fusion rules given by the group multiplication and trivial F-symbols. The Drinfeld center of the latter coincides with the quantum double algebra $D(G)$ introduced

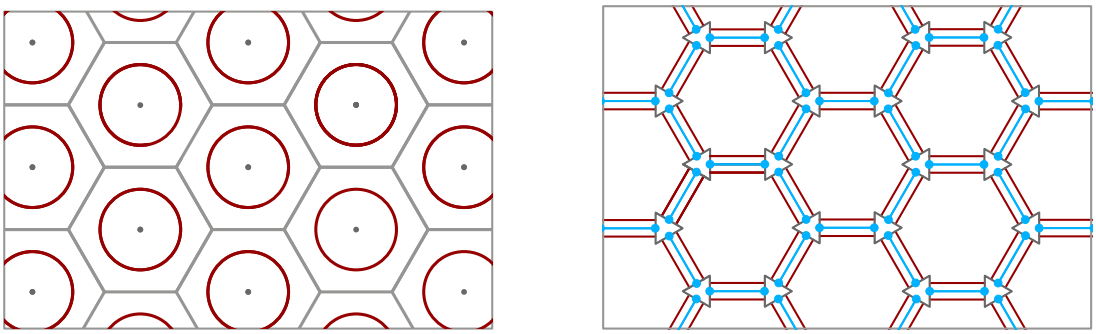

(**a**) Fat lattice picture

(**b**) PEPS representation

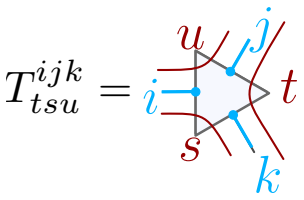

(**c**) The tensor T associated to every vertex.

Fig. 5.8. ⋆ The tensor network ground state of a string-net model obtained from (a) starting with the vacuum state and applying plaquette operators at every plaquette, deforming the string configuration (b) and replacing the string configurations at each vertex by a tensor (c). (d) shows the resulting tensor network representation.

in Ref. [31] as a generalization of the toric code model for general groups G. The equivalence of the Drinfeld center and the quantum double can be directly seen when evaluating the algebraic equations for the Ω matrices in the case where fusion is unique and specified by the group multiplication (cf. Section 5.3.1).

5.1.4. Tensor network construction

The PEPS construction for string-net ground states [63, 64] proceeds analogous to the PEPS construction for the toric code ground states. We start with the vacuum state which is an eigenstate of all vertex operators. Next, we apply the plaquette operator at all plaquettes

$$|\Psi\rangle_{\mathrm{GS}} = \prod_p B_p \, |\bar{0}\rangle \tag{5.15}$$

In the fat-lattice picture this corresponds to inserting a closed loop of a string type s weighted by a factor $a_s = d_s/D$ and summing over all string-types. The inserted loops eventually take on the role of virtual index lines (cf. Fig. 5.8).

To arrive at the concrete tensor network expression, the loop pattern is deformed to a string-configuration with strings on the edges of the hexagonal and bubble configurations at vertices (cf. Fig. 5.9). The F-symbols of the deformation move are evaluated using Eq. (5.10). The bubble configurations at the vertices are replaced with bubble-free configurations, weighted by F-symbols (cf. Fig. 5.4b). This allows us to express the string-net ground state as a sum over string configurations on the edges of the honeycomb lattice. Each of these physical configurations is weighted by a sum over all auxiliary string-type configurations that have led to the physical configurations and each addend is weighted by the product of all F-symbols and

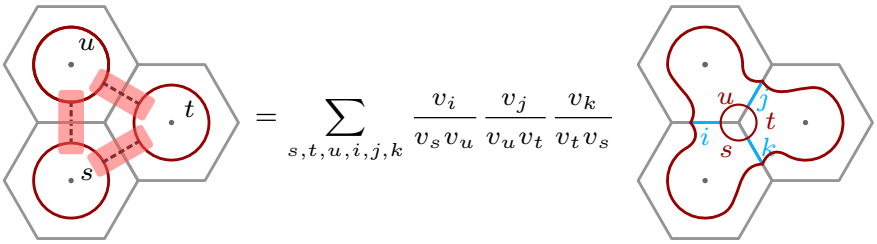

Fig. 5.9. ⋆ Reintegrating inserted loops and obtaining bubble configurations (cf. Fig. 5.4b) at the vertices.

quantum dimension factors that emerged during the string-net deformations explained above. We distribute the product of the latter evenly over all vertices, such that every vertex with physical strings i, j, k on the adjacent edges and auxiliary strings t, s, u (that were "historically" present on the adjacent plaquettes) is associated with a factor

$$T^{ijk}_{tsu} = (a_s a_u a_t)^{1/6} \sqrt{v_i v_j v_k} G^{ijk}_{tsu} \,. \tag{5.16}$$

This 6-index tensor is shown in Fig. 5.8c and is defined in terms of the G-symbol

$$G^{ijk}_{tsu} = F^{ijk}_{ts^*u} \frac{1}{v_u v_k} \tag{5.17}$$

which has a cyclic invariance under the permutation $(i,t) \mapsto (j,s) \mapsto (k,u)$. This allows us to write the ground state as a tensor network with tensors T[6] at every vertex as shown in Fig. 5.8b.

Note, that the former fat-lattice loops drawn in red have become virtual indices that form closed loops. For each closed loop u we obtain six factors $a_u^{1/6}$ from the six adjacent vertex tensors. Alternatively, one may define the tensors T without the factor $(a_s a_u a_t)^{1/6}$ and instead impose that every closed u-loop of the tensor network contributes a factor d_u. This is helpful if the tensor network is defined on lattices where the number of vertices around a hexagon is not always the same. Such lattices are interesting for the description of manifolds with locally varying curvatures. To see this, one may consider the dual lattice of any trivalent lattice formed by the triangle tensors T. Imagining that those form a regular tiling of a manifold, a varying number of vertices around a plaquette then corresponds to a varying curvature of the underlying manifold.

As a remark for later reference, we note that the G-symbols fulfill a pentagon equation that is directly derived from the pentagon equation for the F-symbols in Eq. (5.8)

$$\sum_{n=1}^{N_S} d_n G^{mlq}_{kpn} G^{jip}_{mn^*s^*} G^{js^*n}_{lk^*r^*} = G^{jip}_{q^*k^*r^*} G^{riq^*}_{ml^*s^*} \,. \tag{5.18}$$

The pentagon equation for the G-symbols constitutes an interesting symmetry of the tensor T, that we will explore in more detail in the next Section.

5.2. MPO-isometric PEPS

We have discussed a tensor network representation for string-net models [63, 64] and seen in Chapter 3.2.3 that the PEPS ground state of the simplest string-net model – the toric code –

[6] Note, that we have largely omitted arrow orientations and the distinction between a string-type a and its dual a^* in the description of the moves. To be precise, a tensor T^{ijk}_{tsu} has to be placed at every vertex of the A-sublattice of the honeycomb lattice, while a tensor T^{i*j*k*}_{tsu} is placed at the B-sublattice.

is G-injective with $G = \mathbb{Z}_2$. It is natural to ask, what kind of virtual symmetry is hidden in a general string-net ground state PEPS or the slightly more general question: What is the kind of virtual symmetry underlying non-chiral topological order?

It turns out that to characterize general non-chiral topological order in a tensor network formalism the concept of G-injectivity has to be generalized in the following way [6–8]: The group G is replaced by a fusion category $\mathcal{C}$. The symmetry operators associated to each object of the fusion category are no longer represented by factorizing operators U_g acting individually on each virtual index, but instead need to be replaced by matrix product operators (MPOs) O_a build from local tensors with finite bond dimension. Adapting the notion of symmetry and injectivity one arrives at the definition of *MPO-injective PEPS* which capture all string-net models and for which the hallmarks of non-chiral topological order can be calculated directly from the symmetry objects, i.e., the MPOs.

Before we proceed with the details of the construction let us recall the essential mechanisms that cause G-injective PEPS to be topologically ordered and try to formulate them as general axioms that can be extend beyond the group symmetry case. For G-injective PEPS the local indistinguishability of ground states follows from the deformability of the symmetry g-strings. However, there is no immediate need that the set of symmetry strings form a group, however they should form a set closed under multiplication (i.e., placing two symmetry strings parallel to each other). Further requirements on the symmetry strings emerge from considering the growth of the virtual support spaces. Recall that the topological correction to the entanglement area law follows from the fact that the symmetric projector given by the sum of all symmetry operators $P = \sum_g U_g \otimes \ldots \otimes U_g$ reduces the dimension of the virtual support space of a tensor network patch by a constant factor $1/|G|$ which is independent of the patch size (cf. Section 3.2.4 and Eq. (3.16)). We infer that in general we are looking for a set of deformable virtual symmetry strings from which we can construct a well-defined projector on all possible boundaries of a tensor network patch which reduces the growth rate of the rank of the reduced density matrix by a size independent factor, such that the topological correction to the area law emerges. We expect that this symmetry projector is given by a sum over all deformable string types. A general ansatz for such a projector is a matrix product operator with constant bond dimension. Interpreting the MPO as an MPS, the existence of a canonical form for (translation invariant) MPS directly implies a block structure of the MPO, i.e., the latter can be decomposed into a finite direct sum of single block MPOs suggesting the identification of the set of deformable string-types with the set of the single blocks of the MPO.

There are various ways to formalize the two conditions on symmetry strings stated in the previous paragraph into a set of axioms. In particular, one can formulate several local conditions that are strong enough to infer global properties of the PEPS or alternatively require global properties of the PEPS, i.e. properties valid on all tensor patches, and infer a set of algebraic conditions from the latter. The local approach is the one taken for G-isometric PEPS reviewed in Section 3.2 as well as for the slightly more general (G, ω)-injective PEPS [6] already requiring to use MPOs as symmetry objects. The most general local approach is presented in Ref. [7]. Here, one starts with a local deformability condition for MPO operators referred to as *pulling through* condition formulated for a single site of the tensor network, i.e., for a single PEPS tensor. An additional condition, namely that trivial MPO loops can be removed (cf. Eq. (3) of Ref. [7]) implies that closed single-site MPOs are projectors. A local injectivity condition, namely the invertibility on the support space of the local MPO projectors completes the set of local axioms. In order to elevate the local axioms to global properties valid on all tensor network patches one requires the existence of a local operator which can remove local degrees of freedom that are only weakly entangled with the rest of the lattice (cf. Eq. (14) and (15) of the supplemental material of Ref. [7]). This is achieved by imposing the existence of a suitable

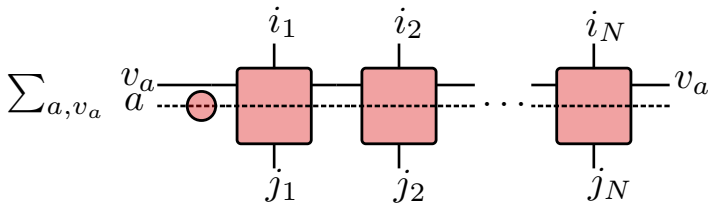

Fig. 5.10. ⋆ The MPO projector defined in Eq. (5.19) for N sites. The circle tensor diagonal in the block-index a is given by the weights w_a and the red squares correspond to the (block) matrices B_a^{ij}.

so called generalized inverse (cf. Eqs. (4) and (5) of Ref. [7]). The symmetry condition (pulling through) is automatically valid on all length scales by sequentially pulling the symmetry string through sites. While this set of local axioms is consistent and implies global MPO-injectivity, it fails to illuminate the algebraic structure of the symmetry objects and the connection to fusion categories and string-net models is not apparent at first sight.

In contrast, in the opposite, the global approach presented in Ref. [8] one requires the existence of a Hermitian projector MPO built from local tensors which determines the virtual support space of every tensor network patch of the PEPS. Employing known results about the canonical (block diagonal) form of MPS one can decompose the MPO into single blocks and derive strong algebraic conditions on the individual MPO tensors. Under a few mild additional assumptions one can show that the single blocks form a fusion category. If one additionally requires the unitarity of the fusion category, the MPO tensors can be used to define MPO-isometric PEPS on arbitrary lattices and the single block MPOs can be identified with the deformable symmetry strings fulfilling the pulling through conditions. This completes the equivalence between the local and the global approach[7]. The appearance of a fusion category strongly suggests that MPO-isometric PEPS are capable of describing string-net ground states. This can be checked explicitly and the symmetry MPOs are presented in Section 5.2.4.

5.2.1. Translation invariant Hermitian projector MPOs and fusion categories

In the following Section we review the global approach to MPO-isometric PEPS sketched in the preceding paragraph in more detail. We closely follow Ref. [8] and summarize how translation invariant Hermitian MPO projectors defined on all length scales give rise to a fusion category.

The projectors considered give rise to translation invariant MPOs. They are constructed from identical tensors B placed at every site and an additional tensor Δ, that commutes with all Bs. Using the fact that the canonical form for MPS [60] can be applied to MPOs as well, we obtain the following block diagonal form

$$P = \sum_{a=1}^{\mathcal{N}} w_a \sum_{\{i\},\{j\}}^{D} \mathrm{tr}(B_a^{i_1 j_1} B_a^{i_2 j_2} \dots B_a^{i_l j_L}) \, |i_1 i_2 \dots i_L\rangle \langle j_1 j_2 \dots j_L| \ , \tag{5.19}$$

where a is the block index and the single block tensors B_a are injective, $w_a \in \mathbb{C}$ are global weights associated to the block MPO a and result from the commuting matrix Δ. The matrix multiplication of the B_a^{ij} is left implicit (cf. Fig. 5.10).

[7] Apart from the pulling through condition, the other two local axioms, i.e., the trivial loop condition and the existence of a generalized inverse follow from the the unitary of the MPO fusion category and from sufficiently blocking individual MPO tensors, respectively.

As discussed earlier, we require that the MPO P is a Hermitian projector on all length scales. With the following abbreviation

$$O_a = \sum_{\{i\},\{j\}}^{D} \mathrm{tr}(B_a^{i_1 j_1} B_a^{i_2 j_2} \dots B_a^{i_L j_L}) \, |i_1 i_2 \dots i_L\rangle \langle j_1 j_2 \dots j_L| \tag{5.20}$$

the projector property implies

$$PP = P \;\Leftrightarrow\; \sum_{a,a'} w_a w_{a'} O_a O_{a'} = \sum_a w_a O_a \;, \tag{5.21}$$

which can only be realized for boundaries of arbitrary length of the tensor patch, if

$$O_a O_b = N_{ab}^c O_c \;, \qquad \sum_{a,b} w_a w_b N_{ab}^c = w_c \tag{5.22}$$

and N_{ab}^c takes integer values. Hence, we find that the block-MPOs possess a *fusion rule* on a global level. By the arguments in Ref. [60] this also implies the existence of a fusion rule on a local level of individual B tensors. I.e., for blocks a, b, c there exist $\mu = 1, \dots, N_{ab}^c$ *fusion tensors* X, X^+ that map the block matrices $B_a \otimes B_b$ locally to B_c via

$$X_{ab,\mu}^{c+} \left(\sum_j B_a^{ij} \otimes B_b^{jk} \right) X_{ab,\mu}^c = B_c^{ik} \;. \tag{5.23}$$

We will restrict to multiplicity-free fusion, i.e., $N_{ab}^c \in \{0, 1\}$ and omit the index μ in the following. Assuming a technical a non-degeneracy criterion[8] the stronger inverse condition

$$\sum_{c=1}^{N} X_{ab}^c B_c^{ik} X_{ab}^{c+} = \sum_j B_a^{ij} \otimes B_b^{jk} \tag{5.24}$$

holds.

Hermiticity of the projector implies the existence of a dual single block MPO O_{a^*} such that $O_a^\dagger = O_{a^*}$ and $\bar{w}_a = w_{a^*}$. Since two identical MPOs must be related by a gauge transformation of the local tensors, this implies the existence of an inversion tensor Z that relates B_{a^*} to $B_a^\dagger$. More precisely, we have

$$\bar{B}_a^{ji} = Z_a^{-1} B_{a^*}^{ij} Z_a \;. \tag{5.25}$$

A gauge transformation can be applied to simplify the matrices Z_a such that for $a \neq a^*$ we have $Z_a \bar{Z}_{a^*} = \mathbb{1}$ and for $a = a^*$, we have $Z_a \bar{Z}_{a^*} = x_a \mathbb{1}$, where $x_a = \pm 1$ is an invariant closely related to the categorical definition of a Frobenius Schur indicator (cf. Section 4.1.2). Unless the fusion algebra of block MPOs can be split into several components $A, B, \dots$ that do not talk to each other, i.e. $N_{ab}^c = 0$ if $a \in A$ and $b \in B$ for all possible c, one can identify a unique block labeled by 1 that corresponds to the unique unit element of the fusion category[9]. One can then show that the sum over c appearing in $O_a O_{a^*} = \sum N_{aa^*}^c O_c$ contains $N_{aa^*}^1 O_1$ which allows us to identify the dual element a^* with the inverse of a[10].

Associativity of the product $O_a O_b O_c$ implies $N_{ab}^e N_{ec}^d = \sum_f N_{af}^d N_{bc}^f$ (cf. Eq. (4.2)) and on a more fine grained level the existence of an F-tensor relating two fusion trees, i.e., the fusion

[8] We neglect possible off-diagonal blocks, because they do not contribute to closed MPOs.

[9] On the level of MPOs the unit element is singled out as the single-block MPO tensor that has the largest spectral radius after tracing out the vertical indices (cf. Ref. [8]).

[10] Recall, that in a fusion category, the notion of an inverse is *not* to require $O_a O_{a^*} = O_1$ but the significantly weaker condition that O_1 is contained in the fusion product of O_a and O_{a^*}.

tensors realizing the fusion $(a,b) \to e$ and $(c,e) \to d$ must be related by a tensor F^{abc}_{def} to the fusion tensors realizing the fusion $(b,c) \to f$ and $(a,f) \to d$, i.e.,

$$(X^e_{ab} \otimes \mathbb{1})\, X^d_{ec} = \sum_f F^{abc}_{def} \left(\mathbb{1} \otimes X^f_{bc}\right) X^d_{af} \,. \tag{5.26}$$

A local realization of the pentagon equation then follows from considering the product $O_a O_b O_c O_d$ and how a local segment of this MPO tensor can be fused using two different fusion trees abbreviated as $((a,b),c),d$ and $a,(b,(c,d))$. The two tensor expressions associated to them can be related in two different ways and both are given by applying a collection of F-tensors to them. This implies the pentagon equation for the F-tensor as

$$\sum_h F^{abc}_{gfh} F^{ahd}_{egi} F^{bcd}_{ihj} = F^{fcd}_{egj} F^{abj}_{efi} \,, \tag{5.27}$$

which is very similar to the pentagon equation derived for the F-symbols of string-net models (cf. Eq. (5.8)) or the pentagon equation occurring in the algebraic theory of anyons (cf. Section 4.2.1).

This concludes the survey of how translation invariant Hermitian projector MPOs correspond to fusion categories. In the next Section we discuss how the latter can be used to define a class of topologically ordered PEPS.

5.2.2. MPO-isometric PEPS

A PEPS is called MPO-isometric, if each patch of the tensor network is invertible on the space defined by the MPO projector P applied to its boundary and every single-block MPO O_a can be pulled through the tensor patch. There is one subtlety we need to take into account to complete this definition. Recall, that in the G-injective case, we defined PEPS on a square lattice and assigned to each edge of the lattice a direction specifying that the symmetry operator $U^\dagger$ is used for the virtual index associated to the starting point of the edge while U is the appropriate symmetry operator for the PEPS tensor on the end point of the edge (cf. Section 3.2.1). In the G-injective case this definition allows to pull virtual symmetry strings through the lattice by inserting a closed loop symmetry operators and then using $U^\dagger U = \mathbb{1}$ to absorb the g-string on one side of the tensor patch. This is possible only if the symmetric projectors are defined with tensors U_g and $U_g^\dagger$ depending on the edge orientations of "virtual lattice" formed by the virtual index lines. Clearly, MPO-injective PEPS should contain G-injective PEPS as a subclass. Thus, when constructing MPO-injective PEPS we again equip the lattice with directed edges and use the tensor B_a and its Hermitian conjugate $B_a^\dagger = B_{a^*}$ in the definition of the symmetry projector.

For the construction of MPO-injective PEPS the MPO tensors are restricted in such a way that the corresponding fusion category is unitary [8]. This implies that all local gauge tensors Z_a, X_{ab} are isometrics, i.e., $Z_a^{-1} = Z^\dagger$ and $X^+ = X^\dagger$ and there exists a pivotal structure (cf. Eq. (37) of Ref. [8] and Ref. [18, Section E.2.3]), which essentially allows to cyclically permute the roles of different blocks in fusion and splitting "processes" by using appropriate duals[11].

With these additional properties we can define MPO-injective PEPS by placing closed MPO projectors $\tilde{P}$ on every vertex of a lattice with oriented edges and connecting virtual indices as in Fig. 5.11a. Whether we choose B_a or $B_a^\dagger$ at each edge is determined by the direction of the edge (ingoing or outgoing). Applying an arbitrary PEPS map which is injective on the MPO

[11] Note that technicalities of this kind are avoided in the context of string-nets in the original paper by Levin and Wen [12] by restricting to fusion categories where inversion of a string-direction is identical to taking the dual and there is no clear distinction between a fusion and a splitting vertex.

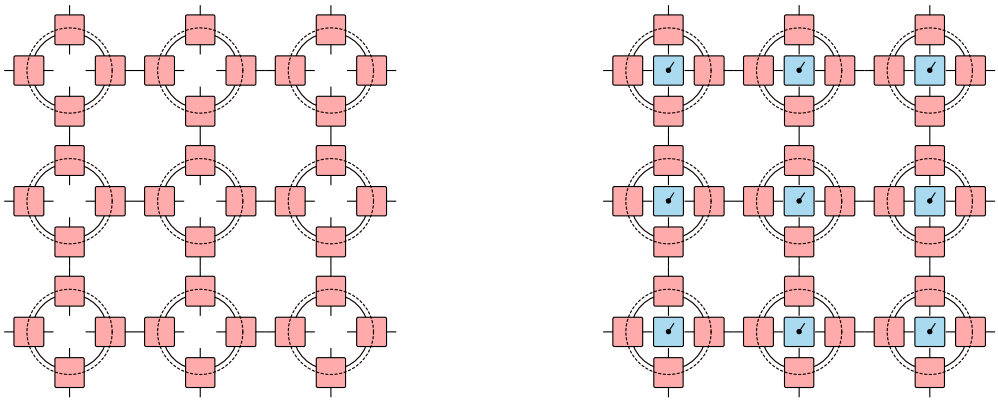

(**a**) MPO-isometric PEPS (**b**) MPO-injective PEPS

Fig. 5.11. ⋆ (a) MPO-isometric PEPS constructed from MPO projectors. An MPO-injective PEPS (b) is obtained by inserting additional local PEPS maps, which are injective on the image of the local MPO projectors.

subspace to the "interior" open indices of the MPO projector yields an MPO-injective PEPS (cf. Fig. 5.11b). One can check explicitly that the pulling through condition is valid for a single site and thus valid on arbitrary tensor network patches. Injectivity on a single site is fulfilled by definition. It can be shown that injectivity also holds on all patch sizes by explicitly constructing an inverse on two sites from the inverses on single sites and repeat the same procedure to "grow" the inverse until the desired patch size is reached (cf. Eq. (49) of Ref. [9]).

5.2.3. Parent Hamiltonians and topological order

The parent Hamiltonian of an MPO-injective PEPS with PEPS map A constructed according to Eq. (2.17) is gapped in the vicinity of the isometric point. At the isometric point itself it can be expressed as

$$H = \sum_p A_p^\dagger A_p \,, \tag{5.28}$$

where A_p denotes a blocked tensor patch on a full plaquette p, i.e., the contraction and blocking of e.g. four tensors on a square lattice or six tensors on a hexagonal lattice analogous to the G-isometric case (cf. Eq. 3.11).

If the parent Hamiltonian is gapped, it describes a (non-chiral) topological phase of matter. It has a topological ground state degeneracy with locally indistinguishable ground states and an excitation spectrum of anyonic quasiparticles. It is a remarkable feature of the MPO-injectivity formalism that the latter quantities can be calculated from the MPO tensors alone. At the core of this achievement lies the fact that the tensor network representation gives direct access to the entanglement structure of the ground state: A closed loop MPO projector can be thought of as a witness of the entanglement shared between the regions separated by it. This picture can be extended to characterize excited states which correspond to local modifications of the ground state wave function on finite disk-like regions. The anyonic charge inside a region deviating from the ground state can be detected via the entanglement that is shared between the region and the rest. An adjusted "MPO-witness" can be constructed that projects onto the entanglement space associated to a specific anyonic charge. By finding those minimal projectors, we can find out the distinct anyon types which can occur as local excitations. In the following, we will discuss the observations sketched here in more detail.

Topological correction to the area law

As a direct consequence of the MPO-injectivity axioms the rank of the reduced density matrix, i.e., the zero-Renyi entropy S_0 (cf. Eq. (2.5)) on any large enough region of an MPO-isometric PEPS is given by the rank of the Hermitian projector MPO $\tilde{P}$, which can be evaluated by taking its trace. A short calculation shows that the logarithm of the rank scales with the length of the boundary region, but with a topological correction determined by the weight w_1 of the MPO-block B_1^{ij} corresponding to the unit element of the fusion category

$$S_0 = \lambda_1 L - \log\left(\frac{1}{w_1}\right) . \tag{5.29}$$

Here λ_1 is the eigenvalue of $\sum_i B_1^{ii}$. Since the spectrum of the MPO projector P is flat, we find the same scaling for the von Neumann entropy.

Ground state degeneracy and local indistinguishability

The ground state space of the parent Hamiltonian can be characterized analogously to the G-injective case. Calculating the intersection of all local ground state spaces given by the individual local Hamiltonian terms one finds that the Hamiltonian is frustration free and the ground state space on an open patch is spanned by the PEPS tensor network with arbitrary virtual boundary tensors (that can be taken to be MPO-isometric without loss of generality). The calculation is performed by applying the generalized inverse and the pulling through conditions several times and can be found in the Supplementary Material of Ref. [7].

To calculate the ground state space on the torus one considers a minimal torus. The results obtained carry over to any torus of finite size. For a minimal torus the intersection space of the ground state spaces on four different overlapping lattice patches (that cover the whole manifold) is spanned by all states $|\Psi_{Q_1}\rangle$ defined from closure tensors Q_1 via the tensor network depicted in Fig. 5.12a. The tensor Q_1 has to be such that each state $|\Psi_{Q_1}\rangle$ can equally well be expressed in terms of other closure tensors Q_2, Q_3, Q_4 located at different lattice sites (cf. Fig. 5.12).

One can then show that two closure tensors yield the same state, if they evaluate to the same tensor when contracted with an "MPO buffer region" (cf. Eq. (40) of Ref. [7]) and further, that two tensors Q_i, Q_j with $i \neq j$ yield the same state even when they are placed at the *same* lattice site. This implies that the ground states are derived from closure tensors which can be moved freely throughout the lattice and thus the state $|\Psi(Q)\rangle$ is a ground state for all closure tensors $Q = Q_1 = Q_2 = Q_3 = Q_4$ which fulfill the pulling through condition.

The pulling through condition of the Q tensor implies that closures are not detectable locally. As a consequence different ground states arising from different closure tensors can not be distinguished locally.

The calculation of the Q-tensors can be performed analytically for certain simple cases of MP0-injectivity such as the twisted quantum double models [6, 210] and their fermionic counterpart discussed in Section 5.5.2. In general the calculation is straight forward but tedious. An alternative way to calculate the ground state degeneracy based on the identification of orthogonal ground states with distinct topological charges is presented at the end of the next Section.

Anyons

The anyonic excitations of the parent Hamiltonians of MPO-isometric PEPS can be calculated from the MPO tensors themselves. The calculation is inspired by general TQFT arguments and

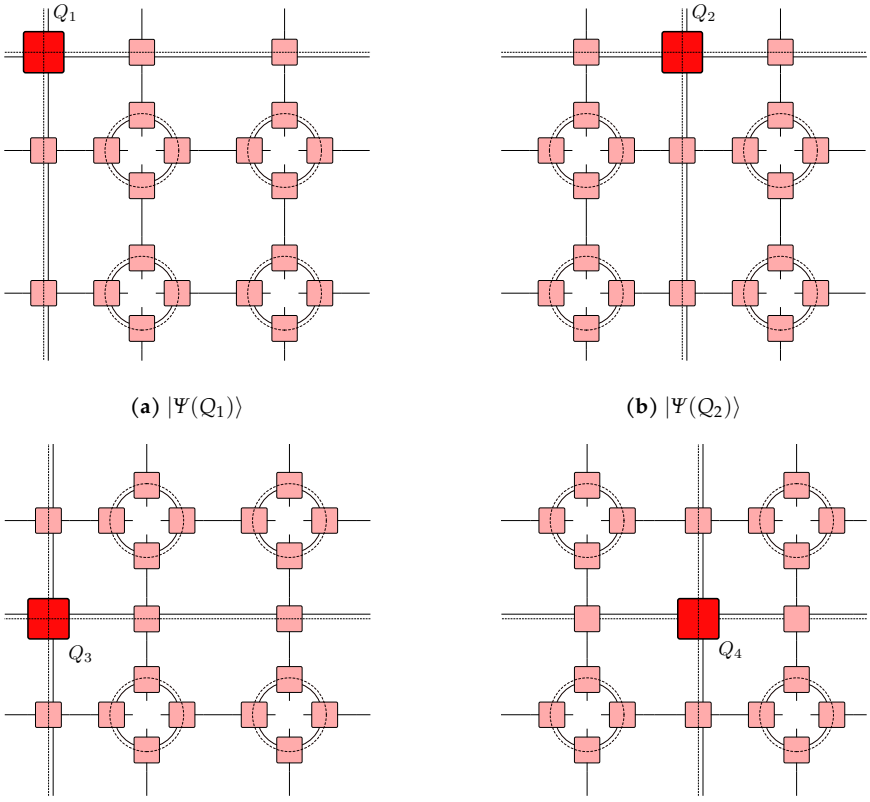

(a) $|\Psi(Q_1)\rangle$ **(b)** $|\Psi(Q_2)\rangle$

(c) $|\Psi(Q_3)\rangle$ **(d)** $|\Psi(Q_4)\rangle$

Fig. 5.12. ⋆ The four different closures on a minimal torus given by closure tensors Q_i.

related to Ocneanus tube algebra [211], also called Q-algebra in Ref. [206][12]. It is known that Ocneanus tube algebra is a presentation of the Drinfeld center [206].

Before we discuss how to obtain the anyonic charges from the MPO-isometric PEPS formalism, we first try to provide an intuitive understanding of the tube algebra and its relation to anyonic charges. It is instructive to consider a sphere with two anyons a and a^* located at the two poles. Since anyons are local excitations, the state is not distinguishable from the ground state anywhere except for two finite disk-like regions around the poles[13]. If we cut out the regions of the anyonic particles, we obtain a cylinder (a tube) or likewise an annulus with two open boundaries. The state space spanned by all possible boundary configurations is contained in the ground state space on an annulus. We conclude that an arbitrary excited state with two anyons can be expressed as a state within the ground state space on an annulus that is "closed" by appropriate states on disks, which carry come anyonic charge. We are thus looking for a partitioning of the ground state space on an annulus into sectors, which corresponds to the elementary anyon types.

This partitioning can be found using the tensor network formalism, where the cutting and gluing operations sketched in the preceding paragraph are well defined constructive operations: Cutting corresponds to cutting virtual index lines and gluing corresponds to contracting indices of two tensor network patches. With this notion of gluing and cutting in mind, we proceed to discuss the gluing of two annuli forming again an annulus. If the annuli is a segment of the tube obtained from cutting out the anyon disks a and a^* gluing together several such segments corresponds to an elongation of the tube and should have a trivial effect, since the theory is insensitive to deformations which do not change the topology (topological invariance). Thus, we claim that gluing two such segments results in an annulus segment which can be identified with a single segment. If we parameterize the ground state space on the annulus by a tensor network with open virtual indices, we obtain a linear map A from one boundary space to the other and gluing amounts to the multiplication of the two linear maps and again results in an annulus associated with a linear map. In the light of the above considerations we claim that idempotent maps ($AA = A$) can be associated with states that carry a well defined anyon flux from one boundary to the other. Concretely, the anyonic charge is transported by a deformable virtual string – a virtual version of the anyonic excitation string W_a encountered in the string-net model. In a string-net language, the idempotency of the linear map corresponds to the fact that gluing to string-configurations with a W_a such that the ends of the two W_a strings are connected, can be reduced to a single configuration with a W_a string. To obtain the anyon types, we are looking nor for arbitrary idempotents, but for minimal ones, i.e., idempotents that can not be decomposed into direct sums by a unitary basis change on the virtual indices.

The tensor network parametrization of the ground states on the annulus are the key to actually finding the latter. In Section 5.2.3, we discussed the ground state space on a torus. The ground state space on an annulus is given by cutting the torus open at a non-trivial cycle. It can be parametrized by inserting a single MPO along a cut from one boundary to the other (cf. Fig. 5.13a). By using the fusion rules for single block MPOs, we can distill the minimal virtual support space on an annulus of finite size and find represent it by a linear map A_{ac} with open block-indices a, c and additional virtual indices that are not spelled out explicitly and depend on the circumferential size of the annulus. We can further decompose the map A_{ac} into its components A_{abcd}, where b and d denote virtual block indices in the tangential direction of the annulus and specify to the case where objects are self-dual (cf. Fig. 5.13b). Evaluating the gluing operation, i.e., the multiplication of two maps is a non-trivial task and requires the

[12] For a connection between the two and the technical details between the latter we refer to Ref. [212]

[13] The size of that region depends on the correlation length. For fixed-point models discussed here, the correlation length is zero and hence, a minimal width of a few lattice sites is sufficient to shield of the effect of the anyon.

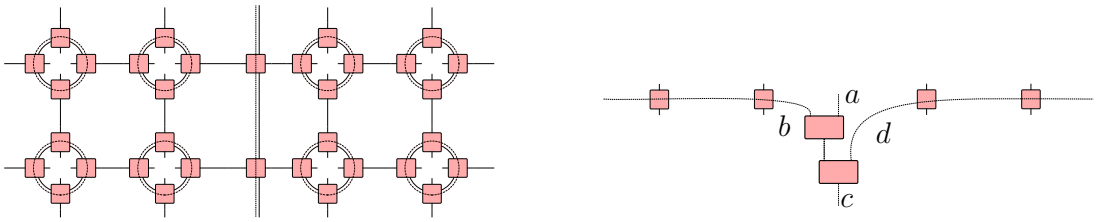

(a) Ground state space on an annulus. (b) Virtual support space.

Fig. 5.13. ⋆ (a) Ground state space parametrized by an MPO-isometric tensor network and (b) its virtual support space spanned by the tensor A_{abcd} on an annulus with boundary of length four. Indices on the left and right boundary are contracted.

application of several "F-moves" defined in Eq. (5.26) (cf. Ref. [8, Appendix B]). We finally obtain

$$A_{hegf}A_{abcd} = \delta_{ga}\sum_{ij}\mathcal{F}^{(hjci)}_{(hegf),(abcd)}A_{(hjci)}\ , \tag{5.30}$$

here $\mathcal{F}$ can be expressed essentially[14] in terms of three F-symbols much like the defining equation for string-operators (cf. Eq. (5.14)) and again resembles the definition of the Drinfeld center (cf. Fig. 4.2 and Section 4.2.3). We suspect that the A-maps from a C^*-algebra and verify this intuition by explicitly calculating $A^\dagger$. Knowing that every finite dimensional C^*-algebra is isomorphic to a finite dimensional matrix algebra, we know that we can decompose the A-(tube)-algebra into minimal idempotents (matrix blocks) using the ansatz

$$\mathcal{P}_i = \sum_{abcd} c_{abcd}A_{abcd}\ . \tag{5.31}$$

A numerical algorithm to actual perform the calculation can be found in Appendix C of Ref. [8].

5.2.4. String-net PEPS as MPO-isometric PEPS

The generalization of G-injective PEPS to MPO-injective PEPS was motivated by the finding that G-injective PEPS suffice to capture the ground states of simple models exhibiting topological order such as the toric code (and in general all group quantum double models), but fail to represent the virtual symmetries of string-net PEPS. Furthermore, we have seen that both, string-net models as well as MPO-injective PEPS are manifestations of fusion categories. In this Section we explain how string-net PEPS fall into the MPO-injectivity formalism.

The PEPS tensors of string-nets derived in Section 5.1.4 are essentially given by a G-symbol and thus the pentagon equation for G-symbols (5.18) provides a symmetry of the tensor. Indeed, one can define virtual MPO-tensors in terms of G-symbols (cf. Fig. 5.14a) such that the pulling through condition for a PEPS tensor on a trivalent lattice (cf. Fig. 5.15b) is nothing but the pentagon equation. This is most conveniently done by using the convention that a closed virtual index line u contributes a factor d_u, where d_u is the quantum dimension. In this case, the tensor T is defined without the prefactors $(a_t a_u a_s)^{1/6}$ in Eq. (5.16) and given in Fig. 5.14b (cf. Ref. [7]). Likewise, one can explicitly find a pseudo inverse of the PEPS map in terms of the G-symbol as given in Fig. 5.14c. Applying the pseudo inverse to the PEPS map we obtain the right-hand side of Eq. (5.18), while the MPO projector evaluates to the left-hand side of the pentagon equation (cf. Fig.5.15a). To see this, it is necessary to apply the tetrahedral symmetry

[14] There is an additional factor associated with taking dual block labels, which we do not discuss here.

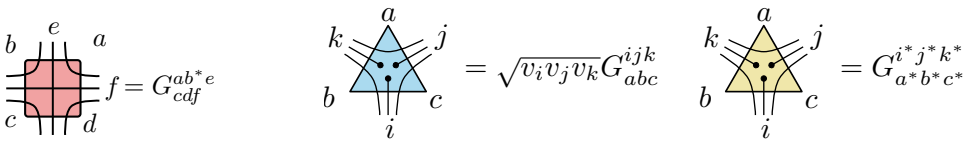

(**a**) MPO-tensors (**b**) PEPS map (**c**) Pseudo-inverse

Fig. 5.14. ⋆ MPO tensors, PEPS map and pseudo-inverse for string-net models.

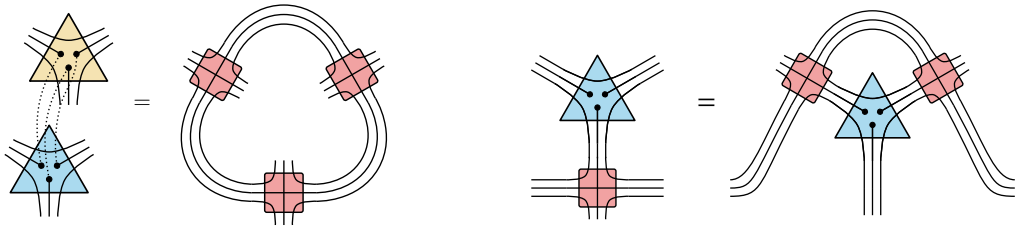

(**a**) MPO-injectivity (**b**) MPO symmetry

Fig. 5.15. ⋆ Axioms of MPO-injectivity fulfilled by the string-net tensors and their symmetry MPOs.

relations for the G-symbol which follow directly from the tetrahedral symmetry conditions of the F-symbol in Eq. (5.12).

The MPO-tensors for string-net models have a slightly different structure then the B_a^{ij} tensors introduced in the general formalism. To see that they are equivalent note that the index f in Fig. 5.14a is a block index and takes on the role of the index a in B_a^{ij}. The indices (a, b, e) are blocked to form index i and likewise (c, e, d) are blocked to form index j. The block-row and block-column indices of the matrix B_a^{ij} are given by the blocked indices (b, c) and (a, d), respectively.

Relevance and Implications

The accessibility of string-net models as MPO-isometric PEPS has several benefits. First of all, we can use the MPO-isometric PEPS formalism to calculate properties of the string-net model in a way that is perhaps easier to track (though eventually equivalent). Second, the explicit and formal use of unitary fusion categories within the MPO-formalism which does not take into account additional structure such as tetrahedral symmetry allows to generalize string-net models easily. Third, the parent Hamiltonians of string-net ground state PEPS are accessible as the low-energy effective theories of comparably simpler Hamiltonians than the original Levin–Wen Hamiltonians. This insight is prominently used in the next Chapter of this thesis, where blueprints for synthetic quantum matter realizing non-chiral topological order are devised (cf. Chapter 6).

At last, the MPO-isometric PEPS framework can be applied to study phases of matter numerically and detect topological order. Starting from a given Hamiltonian one can optimize for the best PEPS wave function with a given bond dimension using PEPS algorithms [144, 147–149]. Once a good ground state approximation is found one can investigate virtual symmetries and the virtual subspace to determine the MPO-tensors. This method is in principle superior to calculating the modular data from the ground state space of the model on a torus. In the latter

approach one calculates the S- and T-matrices from overlaps between rotated (S-matrix) and sheared (T-matrix) minimally entangled ground states (MES) on a torus (cf. Ref. [178] and Section 5.2.3). However, while it was long conjectured that the S- and T-matrices characterize an anyon model uniquely [213], a series of counterexamples provided in Ref. [214] showed that this is actually not the case and thus the method is not able to uniquely determine the topological phase. Recently, it was shown in Ref. [215] that to distinguish the topological phases with identical S- and T-matrices found in Ref. [214] it is sufficient to calculate the mapping class group representations (provided in a similar way as the calculation of S-and T-matrices) on higher genus surfaces. The construction of ground states on the latter can be done using only the MPO tensors. In fact, once the fusion category $\mathcal{C}$ of the MPO tensors is found, it uniquely determines the anyon model of the theory since the latter corresponds to the Drinfeld center $\mathcal{Z}(\mathcal{C})$. As a concluding remark we note, that very recently the method outlined above, i.e., calculating the PEPS ground state numerically and extracting the topological order from the PEPS tensors has been implemented in Ref. [216].

5.3. Example – The twisted quantum double models

To illustrate the string-net and MPO-isometric PEPS formalism discussed in the previous two Sections, we consider a particular class of string-net models as an explicit example – the twisted quantum double models [210] – characterized by a finite group G and a 3-cocylce $\omega \in H^3(G, U(1))$. Twisted quantum double models were first introduced by Dijkgraaf and Witten [189] in the context of 2+1 dimensional Chern–Simons theory with finite gauge group – later referred to as Dijkgraaf–Witten Chern–Simons theory. The path integral partition function of the latter defines a *topological invariant* on any closed 3-manifold $Z(M)$ and we will show how the latter is related to the tensor network description.

The construction of topological invariants is a subject of great interest to the mathematical community and similar constructions for topological invariants were introduced by Turaev and Viro shortly afterwards [190] and generalized later by Barret and Westbury [191]. Explicit connections between Turaev–Viro invariants (also referred to as Turaev–Viro state sums) and Levin–Wen string-net models were drawn later in the context of topological quantum computation [44] and for the special case of (untwisted) quantum double models [185]. In Ref. [186] Kirillov generalized these ideas and showed that Turaev–Viro–Barret–Westbury state sums are in one-to-one correspondence with Levin–Wen string-nets.

Due to a restriction (tetrahedral symmetry) on the F-symbols in the original paper by Levin and Wen [12] several twisted quantum double models were not accessible within the string-net formalism and the connection between Turaev–Viro state sums and string-nets did not carry over to Dijkgraaf–Witten models immediately. In Ref. [210] a Hamiltonian formulation of Dijkgraaf–Witten theories was presented and the name *twisted quantum double models* was introduced. A partial identification with string-net models was also presented. Later, generalizations of string-net models relaxing the tetrahedral symmetry conditions were presented for string-types that are given by Abelian groups G [203]. In parallel to these generalizations, Dijkgraaf–Witten theories/twisted quantum double models were characterized via MPO-isometric PEPS in Ref. [6]. For suitable gauges of the generalized string-net models, an identification with twisted quantum double models from Abelian groups is apparent.

Dijkgraaf–Witten theories represent an interesting middle ground regarding the complexity of string-net models/state-sums. The fusion rules are Abelian (coming from finite groups), yet, the F-symbols are non-trivial – given by a 3-cocycles ω – and not necessarily tetrahedral symmetric, making them sensitive to orientations (as compared to Turaev–Viro invariants [190,

217]). In addition, the PEPS ground states of twisted quantum double models do not fall within the framework of G-injective PEPS but their virtual symmetries are characterized by a *twisted* group action determined by the cocycle ω captured by an MPO-symmetry [6]. If the 3-cocylce ω is trivial the twisted quantum double models reduce to Kitaev's quantum double models introduced in Ref. [31] with the toric code ($G = \mathbb{Z}_2$) as the simplest example. An interesting consequence of the cocycle twist is that the anyonic excitations of a twisted quantum double model can be non-Abelian even for Abelian groups. The group $\mathbb{Z}_2 \times \mathbb{Z}_2 \times \mathbb{Z}_2$ with one of the non-trivial cocycles is an example [210] of such a case.

Recently, there has been interest in using twisted quantum double models as error correction codes. The simplest twisted quantum double model is known as the double semion model [12, 96, 97]. Its anyonic excitations are the trivial particle, two semions (with topological spin $\pi/2$) and a boson. It is given by $G = \mathbb{Z}_2$ and the non-trivial third cohomology class. A normalized representative is given by $\omega(1,1,1) = -1$. Since the model is tetrahedral symmetric it can be written as a conventional Levin–Wen string-net model [12]. The double semion model has been elevated to a stabilizer code [218] and a more general investigation of the code properties of twisted quantum double models is presented in Ref. [219].

In this Section, we review twisted quantum double models in their description as string-nets, MPO-injective PEPS and Dijkgraaf–Witten state sums and show how the latter three formalisms are interrelated.

5.3.1. String-net description

As mentioned before, twisted quantum double models go beyond the original Levin-Wen string-net models [12], as their F-symbols are not tetrahedral symmetric. As a consequence, arrow directions on edges have to be treated more carefully. There are different ways how to go about this issue. In Ref. [203] the authors considered generalized string-net models without tetrahedral symmetric F-symbols, but with branching rules given by Abelian groups and introduced certain lattice decorations to deal with the latter. A subsequent substantial generalization of string-net models with general non tetrahedral symmetric F-symbols can be found in Ref. [174]. The formulation presented here is tailored to elucidate the correspondence between twisted quantum double models as string-nets and state sum invariants and uses a set of decorations on the lattice (a branching structure on the dual lattice) for which this correspondence can be worked out conveniently. It is based on unpublished original and independent work.

In the string-net description of a twisted quantum double (G, ω) string-types are given by group elements $g \in G$ and their branching rules are determined by the group law in the following way. On trivalent lattices, vertices need to be oriented such that there are no three incoming or three outgoing edges, which corresponds to a branching structure on the dual lattice (cf. Fig. 5.16). The branching rule states that the three string-types meeting at a vertex have to multiply to the identity element. Outgoing edges occupied by g are evaluated as g^1, incoming edges occupied by g are evaluated with g and the group elements are multiplied in clockwise order, if the majority of edges is pointing inwards and in anti-clockwise order otherwise. In contrast to the original string-net models [12] presented in Section 5.1 it is not allowed to invert group elements and arrow directions simultaneously ad libitum.

Note, that as a consequence of the group law (Abelian fusion rules) in the ground state space the string-type on the third edge of any trivalent vertex is already determined by the string-types on the other two edges. Thus, the string-configuration subject to an F-move in Eq. (5.7) is already specified by the string-types on three of the four outer edges, e.g., i, j, k in Eq. (5.7) and consequently three of the six indices of the F-symbol are redundant. Note,

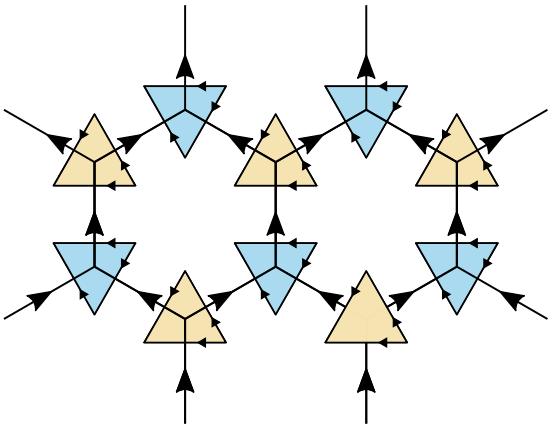

Fig. 5.16. ⋆ A lattice that has a dual lattice with branching structure.

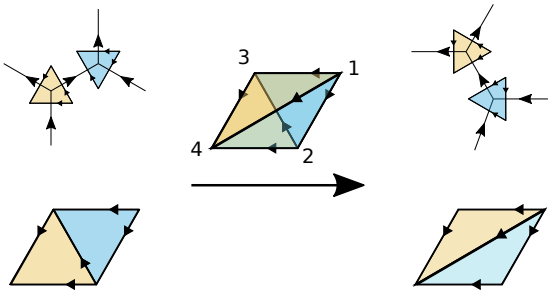

Fig. 5.17. ⋆ Assigning a simplex to an F-move via the faces associated to the dual lattice before and after the move.

that due to the fact that the arrow directions can not be flipped arbitrarily, there are a priori several distinct F-moves each corresponding to one arrow configuration before and after the move. However, due to the choice of a branching structure on the dual lattice, the faces on the dual lattices of the two configurations before and after the move can be interpreted as the front and back side of a tetrahedron as depicted in Fig. 5.17. The arrow orientations uniquely determine an ordering of the vertices[15]. The F-symbol for any move is then defined via the tetrahedron as $\omega^{\chi}(a,b,c)$, where a, b and c are the string-types associated to the edges e_{12}, e_{23} and e_{34}, respectively and χ refers to the chirality or handedness of the tetrahedron determined by whether the edges e_{12}, e_{13}, e_{14} form a left- or right-handed coordinate system.

With this definition of the F-move we can investigate the self-consistency equations as in Section 5.1.1 and find

$$\omega(i,j,k)\omega(i,jk,l)\omega(j,k,l) = \omega(ij,k,l)\omega(i,j,kl)\ . \tag{5.32}$$

This equation is well known and states that ω is a 3-cocycle[16]. Next, we consider how the gauge transformation of the F-symbol in Eq. (5.9) is simplified in the case, where the string-types are

[15] For lattices without branching structure on the dual lattice, this would not be the case and F-moves where vertices after the move do not respect the branching rules are forbidden.

[16] As a matter of self-consistency, we present a very short introduction to group cohomology of finite groups at the end of this Section.

group elements and find

$$\tilde{\omega}(a,b,c) = \omega(a,b,c)\frac{s(b,c)s(a,bc)}{s(ab,c)s(a,b)} \,. \tag{5.33}$$

We recognize a multiplication with a 3-coboundary given by the 2-cochain s associated to the four faces of the tetrahedron on the right-hand side of this equation. Thus, all 3-cocycles within the same cohomology class are related by a gauge transformation and define the same model. In particular, we can use this 3-coboundary gauge to be normalize ω and require that $\omega(a,b,c) = 1$ if a or b or c is the identity element. From now on, we will only work with these normalized representatives.

The F-symbol given by a 3-cocycle is not necessarily tetrahedral symmetric. For example the two non-trivial 3-cocycles of $\mathbb{Z}_3$ do not fulfill tetrahedral symmetry conditions. Translating the tetrahedral symmetry relations for F-symbols to 3-cocycles ω, we obtain the following equations

$$\omega(a,b,c) = \omega((abc)^{-1},c,b) = \omega(b,a,(abc)^{-1}) = \omega((ab)^{-1},b,(bc)^{-1})\frac{v_{(ab)^{-1}}v_{(bc)^{-1}}}{v_a v_c} \,, \tag{5.34}$$

where the factors v_a are defined as

$$v_a = v_a = \sqrt{\omega^{-1}(a,a^{-1},a)} \,, \tag{5.35}$$

which can be used to check if (there exist a gauge in which) the 3-cocycle is tetrahedral symmetric or not.

The definition of string-net Hamiltonian for twisted quantum double models is analogous to Eq. (5.1), however the branching structure of the lattice mildly breaks translation invariancce. The vertex projector is directly given by the branching rules and the plaquette operator is given by matrix elements which can be obtained in complete analogy to the discussion in Section 5.1.1. We will present a more elegant interpretation of the plaquette operator at the end of Section 5.3.2 (cf. Fig. 5.21a).

Concerning the anyonic excitations of twisted quantum double models, we evaluate the deformability condition for excitation strings in Fig. 5.5 with appropriately chosen arrow directions and obtain (analogous to Eq. (5.14) for general string-nets)

$$\Omega(a,s)\Omega(b,s) = \delta_{[a,s],e}\delta_{[b,s],e}\Omega(ab,s)\frac{\omega(a,b,s)\omega(s,a,b)}{\omega(a,s,b)} \,, \tag{5.36}$$

where $[a,s] = asa^{-1}s^{-1}$ is the commutator of a and s. A closer inspection reveals that

$$\phi_s(a,b) = \frac{\omega(a,b,s)\omega(s,a,b)}{\omega(a,s,b} \tag{5.37}$$

is a 2-cocycle, i.e, it fulfills

$$\frac{\phi_s(a,bc)\phi_s(b,c)}{\phi_s(ab,c)\phi_s(a,b)} = 1 \tag{5.38}$$

and hence $\Omega(\cdot,s)$ is a projective representation[17] of the centralizer $Z(s) = \{a \in G | [a,s] = e\}$, i.e. for $a,b \in Z(s)$ we have

$$\Omega(a,s)\Omega(b,s) = \phi_s(a,b)\Omega(ab,s) \,. \tag{5.39}$$

[17] A projective representation is a group representation up to a phase, i.e., $\rho(g)\rho(h) = \alpha(g,h)\rho(gh)$. Since the group multiplication is associative, it follows that $\alpha(g,h)\alpha(gh,k) = \alpha(h,k)\alpha(g,hk)$, which is nothing but a 2-cocycle condition.

We identify the anyon types with irreducible ϕ_s-projective representations of the centralizers $Z(s)$. However, we know that the centralizers of all elements within one conjugacy class are isomorphic to each other and thus the number of distinct anyon types is given by choosing one representative of each conjugacy class $s_{C_1}, \ldots, s_{C_k}$ and finding all irreducible $\phi_{s_{C_i}}$-projective representations of the centralizer $Z(s_{C_i})$.

Informal short introduction to group cohomology for finite discrete groups

In the following we sketch an interpretation of group coyclces for finite discrete groups as measures of n-dimensional volumes following a blog article by Terence Tao [220].

An n-cochain is a function $G^n \to U(1)$. We find it convenient to think of n-cochains as functions that assign a weight to n-dimensional simplices that are spanned by n group elements. I.e., the vertices of the simplices are labeled with numbers from 1 to n and the n group elements are assigned to edges in ascending order. We also define a handedness to the n-simplex by embedding it into an oriented manifold and comparing the orientation defined by its vertex ordering with the manifold orientation. We can define the weight of an n-chaincomplex (i.e., a collection of n-simplices) by multiplying all weights associated to individual simplices.

An n-cocycles is a special n-chains with the following property: An n-cocylce on a closed n-manifold triangulized by simplices evaluates to one, i.e., the trivial element of $U(1)$. It is trivial for closed chains (cycles), hence the name. A particular trivial class of n-cocycles are n-coboundaries which are constructed from $(n-1)$-cochains via multiplying the weights of all $(n-1)$-simplices of the n-simplex. We consider this setting in 3-dimensions. For a closed 3-dimensional volume, each face is encountered twice (once with a positive and once with a negative orientation) and thus as a variant of Stokes/Gauss theorem, the weight of a closed 3-dimensional volume evaluated by a 3-coboundary is trivial. Interestingly, there are cocycles which are not coboundaries, just as we know from topology that there are cycles which are not the boundary of some surface. Identifying all n-cocycles which are not n-coboundaries and classifying them up to equivalence under multiplication with a n-coboundary, we obtain the definition of $H^n(G, U(1))$ the n-th cohomology class of G with values in $U(1)$.

5.3.2. MPO-isometric PEPS and the state sum construction

Unsurprisingly, twisted quantum double models have PEPS ground states which are MPO-isometric [6]. The tensor network construction can be carried out analogous to Section 5.1.4, however, there is simpler and more intuitive way to construct PEPS ground states for twisted quantum double models, which is presented here.

Tensor network construction

We have already encountered the dual lattice which resembles the tensor network on a pictorial level. Triangles tile the manifold and their edges can be identified with the physical indices. Knowing that the twisted quantum double models reduce to quantum double models accessible with G-injective PEPS or synonymous, knowing that they arise from a local gauge symmetry, we can guess the correct virtual indices. For a physical index configuration a, b, c, we know that $ab = c$ is required by the vertex constraint. This is easily achieved, if we choose virtual indices adjacent to the vertices v, w, u of the triangle tensor and determine the physical index value at the edge as the *difference* of the two values at the vertices as in Fig. 5.18. This also implies a virtual symmetry under multiplying all vertex values by a group element. So far, we have constructed G-isometric PEPS, but we have not yet incorporated the cocycle twist ω into the

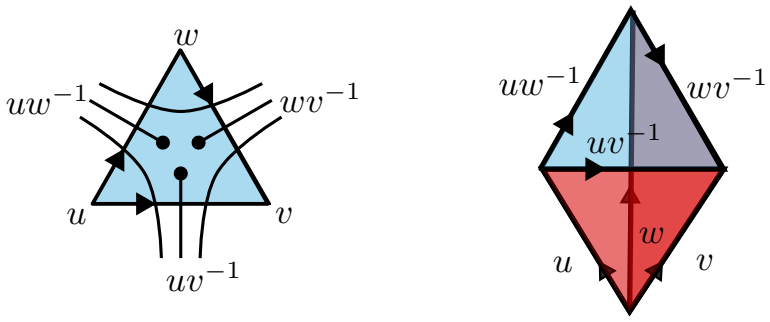

Fig. 5.18. ⋆ The PEPS map for twisted quantum double models given in Eq. (5.40).

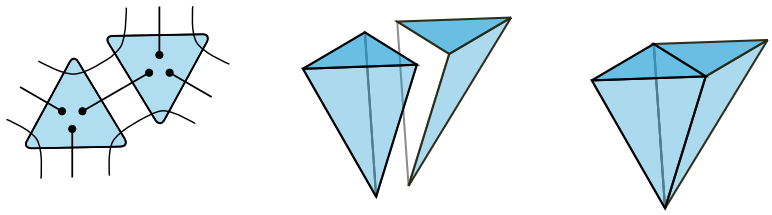

Fig. 5.19. ⋆ Contracting PEPS triangle tensors can be identified with the gluing of simplices.

tensor network construction. Thus, the tensor network obtained fulfills the vertex constraint but not the plaquette constraint. To achieve this, we need to assign the correct weight to each triangle-tensor.

In the discussion of the F-move we have already made reference to simplices whose surface was identified with a fragment of the dual lattice before and after the move. It is suggestive to identify the triangle tensor as well with a simplex, where the six indices are identified with the six edges of the simplex. The orientation of the three physical index edges originates from the physical lattice and it is a reasonable choice to orient the virtual index edges all in the same direction, e.g., pointing towards the physical plane (cf. Fig. 5.18). The weight of the tensor can then be read off from the simplex as discussed earlier and we obtain

$$A_{(G,\omega)} = \sum_{u,v,w\in G} \omega(u, uw^{-1}, wv^{-1})\, |uw^{-1}, wv^{-1}, uv^{-1}\rangle \langle u, v, w| \ . \tag{5.40}$$

This is consistent with the intuition that the PEPS map should be essentially given by an F-symbol which in the case of twisted quantum double models reduces to a 3-cocycle. Finally, we state the rule how index contractions of the tensor network are identified with the gluing of simplices. On the physical lattice two triangle tensors share a common physical edge. Translated to the tensor network formalism, the two indices need to match, but they are not contracted (i.e., summed over). Thus, we conclude that if two tetrahedra touch at an edge, the edge colorings (index configurations) have to match, but a summation over the index value is not implied. Next consider the virtual indices. All virtual indices in the interior of a tensor network patch are contracted (summed over). The corresponding virtual index edges of the associated tetrahedra are completely surrounded by simplices. I.e., they are not visible from the outside. We conclude, that internal edges of a triangulated volume have to be summed over. Note, that two triangle tensors always share three common indices (one physical and two virtual), thus, they correspond to two tetrahedra which are glued at a shared face spanned by the three index edges (cf. Fig. 5.19).

The recipe of assigning weights to triangulated volumes using the tensors of the twisted quantum double PEPS ground states is identical to the construction of the path integral partition function $Z(M)$ for Dijkgraaf–Witten theories [189, 217] on a manifold M. It is calculated from a triangulation of the manifold into simplices whose edges are colored by group elements and a weight determined by the 3-cocylce ω and the chirality χ of the simplex is associated to each colored tetrahedron. Multiplying all weights of the tetrahedra and summing over all possible edge colorings, we obtain

$$Z(M) = \frac{1}{|G|^a} \sum_{\text{colorings}} \prod_{\text{simplices}} \alpha(g,h,k)^{\pm\chi} \,, \tag{5.41}$$

where the factor $1/|G|^a$ is a normalization constant and a is the number of vertices. We will see in the following, that this number is independent of the triangulation and hence, a topological invariant [217].

MPO-symmetry as triangulation invariance

The identification of tensors with colored simplices makes it straight forward to find the correct symmetry MPOs. The left-hand side of the 3-cocycle condition in Eq. (5.32) can be identified with three simplices glued at three faces where each pair of simplices shares one common face, while the right-hand side corresponds to two simplices glued at one face, such that the two share one common face (cf. Fig. 5.20a). Both sides of the equation correspond to the same total volume whose boundary edges are colored identically. Only the interior triangulation into two or three simplices is different. Such a retriangulation *move* is well known in topology as a 2-3 Pachner move [221]. From the 3-cocycle equation we can trivially construct another equation

$$\omega(i,j,k) = \frac{\omega(ij,k,l)\omega(i,j,kl)}{\omega(i,jk,l)\omega(j,k,l)} \,. \tag{5.42}$$

The left-hand side is independent of l and thus we rewrite

$$\omega(i,j,k) = \sum_{l\in G} \frac{1}{|G|} \frac{\omega(ij,k,l)\omega(i,j,kl)}{\omega(i,jk,l)\omega(j,k,l)} \,. \tag{5.43}$$

The last equation can be expressed again neatly as a Pachner mover – the 1-4 move depicted in Fig. 5.20b. Note, that triangulation of the volume into four simplices as given by the right-hand

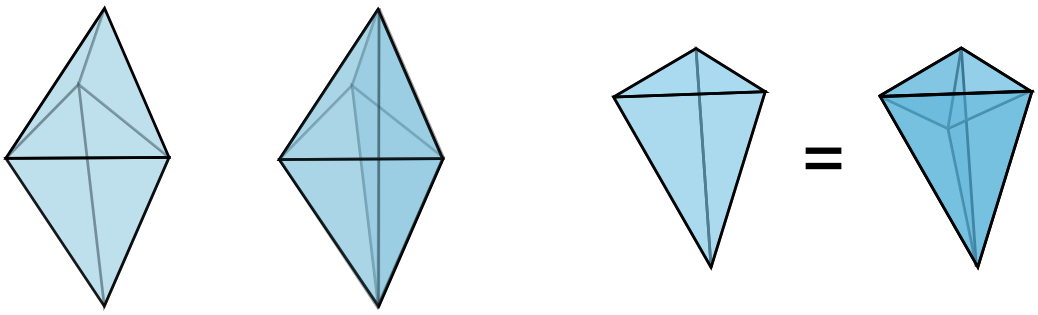

(**a**) 2-3 Pachner move (**b**) 1-4 Pachner move

Fig. 5.20. ✦ Local retriangularizations of three-dimensional manifolds.

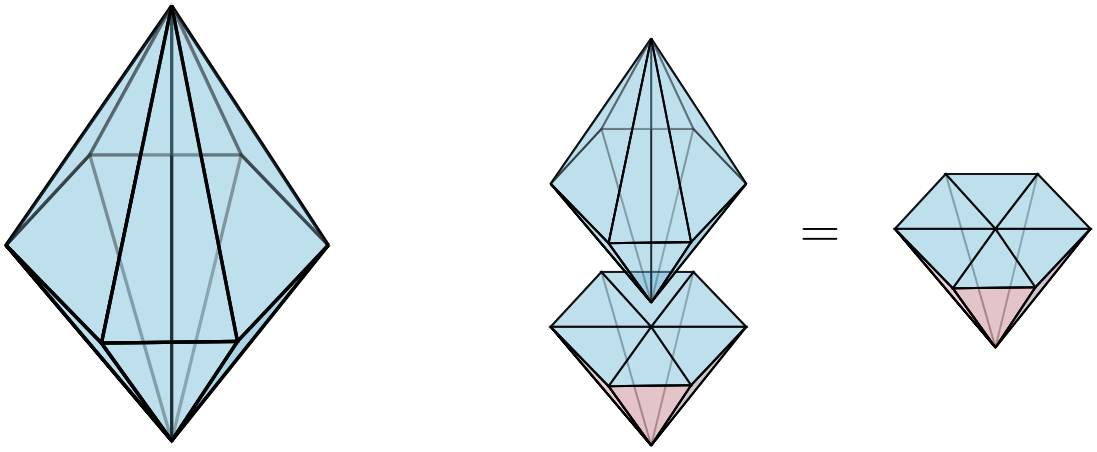

(**a**) B_p (**b**) $B_pV = V$

Fig. 5.21. ⋆ (a) The plaquette operator B_p defined in Eq. (5.2) with matrix elements given in Eq. (5.13) represented as a space-time volume of six simplices glued together, each identified with an F-symbol. (b) Applying the plaquette operator to a tensor patch V with open physical indices (red) and physical indices (blue).

side of Eq. (5.43) contains an enclosed vertex, which we have not encountered before. By comparison with the algebraic expression, we suspect that an enclosed vertex is associated with a prefactor of $1/|G|$. This concludes the mapping between arrangements of glued tetrahedra (simplicial complexes) and tensor networks. Summarizing, we have obtained a recipe how to associate a tensor network to a given triangulation. Furthermore, following from the 3-cocycle condition, we found that the evaluation of the tensor network is invariant under a 2-3 and a 1-4 Pachner move.

This finding has substantial consequences. It has been shown [217, 221], that sequences of 1-4 and 2-3 Pachner moves are sufficient to go back and forth between any two triangulations of a 3-manifold. Thus, we know that the evaluation of a tensor network associated to any 3-dimensional volume is independent of the specific triangulation. This immediately implies the pulling through condition for symmetry MPO-strings (via the 2-3 move) and the MPO-projector property

$$A = AP = A \sum_g \frac{1}{|G|} V(g) \tag{5.44}$$

via the 1-4 move. The projector property can be transformed to the MPO-isometry condition $A^\dagger A = \sum_g \frac{1}{|G|} V(g)$ by applying the pseudo-inverse $A^\dagger$.

From the triangulation invariance, we can also verify that the PEPS we constructed earlier is indeed a ground state of the twisted quantum double model Hamiltonian. To this end, we represent the plaquette operator as the volume depicted in Fig. 5.21a. An open tensor network patch is represented by a cone-shaped object with a physical surface on top and a virtual surface at the side. Gluing the plaquette operator to the physical surface, we can deform the volume such that we again obtain a flat physical surface. The internal triangulation is irrelevant and we have verified that each open tensor network patch is invariant under applying the operator B_p.

As a consequence of the remarks above, the ground state wave function can not only be written as a PEPS, but likewise as a state associated to the surface of a general 3-dimensional manifold which is triangulated with simplices. For a ball and a given lattice on the surface

the triangulation is unique and canonical. It suffices to add a single interior vertex. However, on topologically non-trivial manifolds this construction fails, which is in agreement with the observation that there is no unique ground state on a topologically non-trivial manifold and the ground state is degenerate. The different ground states on a torus are given by closure tensors in the PEPS picture as discussed in Section 5.2.3 (cf. Fig. 5.12). Translating the tensor network to a triangulated manifold, we obtain a solid torus filled with MPO-tensors. However, inside the solid torus there is another solid torus which corresponds to the closure tensor Q and gives rise to the ground state degeneracy.

5.4. General bosonic state sum constructions

We have seen in the last Section that MPO-isometric PEPS for twisted quantum double models give rise to topological manifold invariants by identifying tensors with simplices of a manifold triangulation. Constructions of this kind are known as topological state sum construction (cf. Refs. [3, 14, 46, 191, 217, 222]). We can generalize the construction for twisted-quantum double models in a straight-forward fashion to general MPO-isometric PEPS and obtain more general state-sum constructions. Essentially, every fusion category with the property that the F-symbols fulfill a mirror-conjugation symmetry can be used to define a state sum by associating the F-symbols to simplices whose edges are colored by the simple objects of the fusion category. This mirror-conjugation symmetry is required, if we want to identify manifolds with Hamiltonian terms as in the definition of the plaquette operator. Likewise, we can consider the state sum constructions as discretized imaginary time path integral partition functions. In this case, the F-tensors associated to simplices correspond to local components of a discrete time step ϵ of the imaginary time evolution under a local Hamiltonian, i.e., $F \simeq 1 - \epsilon H$, where H is a local Hamiltonian term. Thus, F needs to be Hermitian, i.e., invariant under complex conjugation followed by transposition. Depending on the specific formalism it is possible to define complex conjugation implicitly as part of the reflection operation as discussed in Section 2.3.1.

5.4.1. Tensor lattice algebras

The concept of identifying lattice structures with tensor networks can be extended significantly beyond the ideas presented here. In a general axiomatic framework presented in Ref. [3] it is discussed how different lattice types equipped with sets of allowed deformation rules (moves) and the tensor network structures associated to the latter can be used to classify phases of matter. The formalism is not restricted to simplicial complexes or to low dimensions, however, concrete examples are only worked out in one and two dimensions so far. The formalism reproduces the classification of non-chiral topological order in two-dimensional systems and provides additional insights on dualities between quantum double models (generalized to Hopf*-algebras) and string-net models (generalized to multi-fusion categories[209]). By specifying the right tensor types (e.g. fermionic, symmetric, Gaussian) and lattices (e.g. undecorated lattices, lattices with branching structure, spin lattices with a discretized spin structure) one can obtain a phase classification not only for gapped bosonic topological phases without symmetries, but also for fermionic phases, free fermionic phases or symmetry restricted phases. It is our impression that the concepts presented in this Thesis for the example of the twisted quantum double models in Section 5.3.2 provide a good basis for an understanding of the far more evolved and more technical work presented in Ref. [3, 46].

5.4.2. Chirality

At last we briefly discuss if and how tensor network methods can be used to characterize chiral topological order, i.e. phases with *chiral gapless edge modes*, which can not be gapped out by local perturbations.

There are formidable obstacles that hinder a PEPS description for systems with gapless edge modes. As pointed out by Kitaev [18] and made more explicit recently in Ref. [52] a system governed by a Hamiltonian that is a sum of commuting projectors, has zero central charge or equivalently zero thermal Hall conductance and must therefore fail to describe a model exhibiting chiral gapless edge modes. The isometric points of (G, ω)-injective PEPS give rise to parent Hamiltonians with exactly this property and thus can not be used to describe topological order with gapless edge modes exactly. As the thermal Hall conductance is a topological invariant, i.e., it can not change within a specific phase nothing is gained by relaxing the isometry condition to an injective vicinity around the isometric fix point where parent Hamiltonians are no longer necessarily given by a sum of commuting projectors.

Nevertheless, attempts towards the description of chiral systems with PEPS have been made using the construction of Gaussian fermionic PEPS (gfPEPS) [223, 224]. Numerical evidence [225–228] suggests that with the latter at least some types of states with topological order and gapless edge modes can be approximated well [229]. For the proposed tensor networks two different Hamiltonians can be constructed that both have the PEPS as their ground state. One is the usual parent Hamiltonian. It is local, frustration-free, but gapless. The other one is gapped, but has an algebraically decaying range of interaction. Thus, both Hamiltonians are not within the framework of gapped local quantum phases. It is anticipated that parent/uncle Hamiltonians of PEPS that capture chiral states will always feature one of these oddities [230, 231] due to the fact that the gaplessness of the edge implies algebraically decaying correlations on the boundary, which proliferate to the bulk.

For all topological fix-point models discussed so far, the impossibility to access chiral topological order is imminent. The existence of commuting projector Hamiltonians is guaranteed by the triangulation invariance as explained in Section 5.3.2 for the example of twisted quantum double models. It is also possible to construct gapped boundary Hamiltonians directly from the simplex tensors [46]. Thus, simple state sum constructions necessarily fail to describe chiral systems. However, there is hope that a generalized tensor network construction presented in Ref. [46] might be powerful enough to represent chiral systems. The tensor networks associated to lattices are more general in the sense, that the tensors associated to certain lattice structures depend not only on the lattice structure itself, but also on the surrounding lattice structure. I.e., instead of a rule "Associate a tensor A to each simplex." we obtain more complicated rules as e.g. "Associate a tensor A_i to a simplex with i tensors adjacent to the first vertex.". This ansatz is promising, but an example of a chiral phase described in this fashion is still missing [46].

5.5. Fermionic non-chiral topological order

In the previous Chapter we discussed the theory of non-chiral bosonic topological order extensively. In the following we will briefly discuss special instances of fermionic non-chiral topological order. The microscopic degrees of freedom of a system – being fermionic or bosonic – determine the possible phases of matter, that can emerge from local interactions. Fermionic phases of matter, i.e., phases of systems whose microscopic degrees are fermions, are richer and contain bosonic phases as a subset (cf. e.g. Refs. [67–69, 232, 233]). The latter statement can intuitively be understood by the fact that a local bosonic degree of freedom can be formed by combining two fermionic degrees of freedom, while the inverse statement is not true. The main difference which causes qualitatively distinct phases of matter for fermionic systems is that fermionic parity is an intrinsic symmetry that can not be broken. In particular, a fermionic system can never be in a superposition of fermion parity even and fermion parity odd states. A theory that allowed states of mixed fermion parity and measurements of operators whose eigenstates are of mixed fermion parity (such as the operator $f^\dagger + f$) leads to strong violations of causality as it provides mechanisms for instantaneous communication (cf. Ref. [234, Section 3.3.2]).

Preserving fermion parity is a symmetry constraint inbuilt in the definition of a fermionic quantum phase by adapting the definition in Section 2.2. To define a fermionic phases of matter a generalized local unitary circuit is replaced by a generalized *fermionic* local unitary circuit, i.e., a circuit where each local unitary preserves fermion parity. Such a circuit is composed from layers of operators that contain an even number of fermionic creation and an even number of fermionic annihilation operators.

We studied bosonic gapped quantum phases in one and two dimensions within a tensor network framework. It is natural to ask whether *fermionic quantum phases* can be studied within a tensor network framework as well. The answer to this question is affirmative: In one dimensional systems fermionic matrix product states [67, 68, 235] classify fermionic phases of matter via a *fermionic MPO* canonical form. However, due to the presence of a non-trivial fundamental symmetry – fermion parity – the phase classification is richer then in the bosonic case and contains a topologically non-trivial phase known as the Kitaev chain [236].

Likewise, two-dimensional fermionic systems exhibiting non-chiral topological order are accessible via fermionic PEPS (fPEPS) and their virtual symmetries captured by fermionic MPOs [1, 9, 10]. While in the bosonic case, the single MPO blocks form a fusion category, the fermionic version gives rise to a super fusion category [11, 237]. Analogous to the bosonic case fermionic string-net models [11, 69, 232] are in one to one correspondence with fermionic MPO-isometric PEPS [1, 9–11]. However, anticommutativity of fermionic operators has fundamental implications on the virtual symmetries and the introduction of a discretized spin-structure is required to restore robust fMPO-injectivity. The necessity of discrete spin structures appears most prominently in the state sum approach to fermionic topological order [238] and is strongly related to spin-TQFTs. While the general theory of and connections between super fusion categories [237], fermionic string-nets [11, 69], fermionic MPO-injectivity [1, 9, 10], fermionic state sums and spin-TQFT [238] is beyond the scope of this thesis, we present an in-depth discussion of a particular class of fermionic string net models, the fermionic twisted quantum double models and their fermionic MPO-injective fermionic PEPS ground states based on Ref. [1].

5.5.1. Fermionic tensor networks

Due to fermionic anticommutativity fermionic theories are more complex and require a significant amount of additional technical details compared to the bosonic theories. The fact, that the sign of a many-body wave function with several local fermions occupying certain sites depends on the order in which the fermions were created has to be reflected when fermionic states are represented as tensor network states.

There are various ways to implement the latter condition. The simplest way is to capture the weights of the fermionic many body basis states by a usual bosonic tensor network with a chosen particular order of the fermionic modes (sites) [65]

$$|\Psi\rangle = \sum_{i_1,\ldots,i_N} \mathrm{tTr}\left[A^{i_1}\ldots A^{i_N}\right] f_1^{\dagger i_1}\ldots f_N^{\dagger i_N}\,|\varnothing\rangle\ , \tag{5.45}$$

where the A^{i_j} are usual bosonic tensors. While in principle one can work with this ansatz and perform numerical simulations with it, there are several down-sites for this representation. First of all, making reference to an arbitrarily chosen global ordering of sites obscures the locality structure of the problem and obstructs the use of diagrammatic notation. In particular, a diagrammatic expression is only complete, if a directed string representing the order of sites decorates the tensor network (cf. Fig. 5.22a). More profoundly, the tensor network defined in Eq. (5.45) distinguishes very clearly between a physical and a virtual index. While a virtual index with bond dimension D labels a basis state in a D-dimensional vector space, the physical index ultimately describes a fermionic degree of freedom which can not be identified with a usual vector space due to the fundamental distinction between fermion parity even and fermion parity odd sectors and the anticommutativity of fermionic modes[18]. The structural dissimilarity of virtual and physical indices poses a significant obstacle in recovering the relation between virtual symmetries and topological order. A heuristic argument is provided by the following observation. The string-net deformation rules such as the F-move are applied to the physical degrees of freedom and we expect that for fermionic string-nets, the fermionic F-moves act on fermionic degrees of freedom. In the bosonic case, the self-consistency relations of the F-moves, i.e, the pentagon equation, directly implied a virtual symmetry of the string-net PEPS tensors. If we wish to recover a fermionic virtual symmetry from a self-consistency relation of fermionic F-moves, the symmetry objects need to act on a *fermionic virtual space* as well. It is also only in this case, that we can establish a well defined notion of *isometry* between the virtual and the physical space – a property that is desirable when constructing parent Hamiltonians from fMPO-isometric fPEPS.

In the light of the mentioned evidence, we propose to use fermionic virtual indices instead of bosonic ones, i.e., we place auxiliary fermionic modes on an underlying virtual lattice which are "integrated out" when performing the tensor network contraction. If the total parity of all virtual and all physical fermionic degrees of freedom per tensor is even, we can use a diagrammatic notation without specifying a global ordering. Restricting to total parity even tensors is advisable also because it prohibits the occurrence of states with mixed fermion parity.

There are various ways to formalize the ideas of the preceding paragraph and introduce *fermionic tensors*. The most commonly used formalisms are based either on super vector spaces [9, 67, 68], Grassmann numbers [239, 240] or the use fermionic maximally entangled pairs on which a fermion parity even fPEPS map acts on [66]. In every case, the indices of a fermionic tensor can be partitioned into parity even and parity odd ones corresponding to an even or odd number of local virtual or physical fermions. The parity of the index i is denoted by $|i| \in \{0, 1\}$,

[18] The appropriate structure to represent local fermionic degrees of freedom are *super vector spaces* [68].

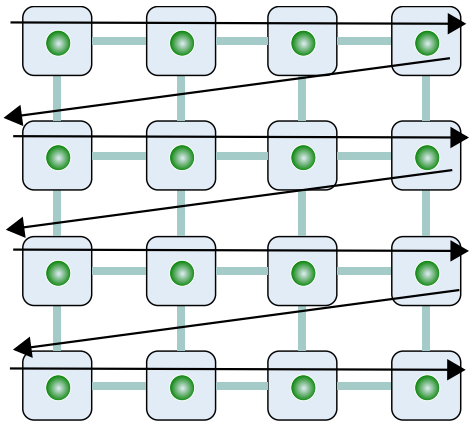

(**a**) Bosonic tensor network description of a fermionic state (cf. Eq. (5.45)).

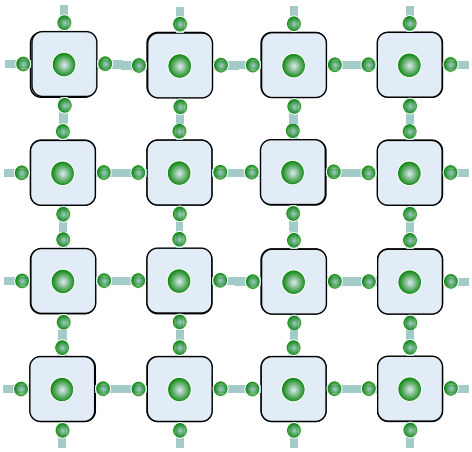

(**b**) Fermionic PEPS built from fermionic tensors.

Fig. 5.22. ⋆ Fermionic states represented as tensor networks. Green dots indicate fermionic degrees of freedom.

where $|i| = 0$ refers to *even* and $|i| = 1$ to *odd*. Specifying the tensor entry $A_{i_1 \dots i_N}$ we have to chose a *local ordering* of the fermionic indices (modes). This can be done by with the aid of a graded tensor product

$$A_{i_1 \dots i_N} \, |i_1\rangle \otimes_g \dots \otimes_g |i_N\rangle \ , \tag{5.46}$$

where $\otimes_g$ is associative and obeys

$$|k\rangle \otimes_g |l\rangle = (-1)^{|k||l|} \, |l\rangle \otimes_g |k\rangle \ , \tag{5.47}$$

or using Grassmann numbers $\theta_1, \dots \theta_N$ fulfilling the usual anticommutation relations

$$A_{i_1 \dots i_N} \theta_1^{|i_1|} \dots \theta_N^{|i_N|} \tag{5.48}$$

or using PEPS maps with a certain ordering of fermionic creation and annihilation operators. In any case, a reordering of the virtual fermionic indices can be performed by a sequence of swaps that results in a sign σ determined by the parities of the fermionic indices involved in the permutation. As an example consider the reordering a, b, c, d to d, c, b, a which results in a factor

$$\sigma(a, b, c, d \to d, c, b, a) = (-1)^{|d|(|a|+|b|+|c|)+c(|a|+|b|)+|a||b|} \ , \tag{5.49}$$

where addition is understood to be modulo two. A convenient diagrammatic notation to compute the so called Koszul signs σ (cf. Ref. [65]) is given for the example in Eq. (5.49) in Fig. 5.23a. The indices are drawn as lines connecting the initial and final position (on a horizontal line). A crossing of index lines i and j is attributed with a factor $|i||j|$ and summing over all crossings the parity of the permutation is obtained. If the total parity of all involved indices is even, e.g., if the indices are the indices of a fermionic tensor, one can use the parity even constraint to simplify the calculation. In the diagrammatic notation, we are allowed to draw index lines against the "flow of time" and revolve around the fermionic tensor to avoid index line crossings (cf. Fig. 5.23b). If an index line i takes such a detour it adds a factor i to the exponent determining the Koszul sign. This can be understood by considering the example of the index line d in Fig. 5.23 which avoids the crossing with index lines a, b and c. The factor

(**a**) General permutation

(**b**) Permutation with total parity even indices

Fig. 5.23. ⋆ Diagrammatic rules for calculating Koszul signs of reordering fermionic indices. (a) General permutation of fermionic indices calculated by drawing "world lines" along the flow of time (top to bottom). (b) Permutation of fermionic indices of an fermionic even tensor (i.e. $|a| + |b| + |c| + |d| = 0$).

$(|a| + |b| + |c|)|d| = |d||d| = |d|$ can be recovered by introducing $|d|$ as a "penalty" for the detour.

The reordering of fermionic indices is important, if we want to contract fermionic indices. To contract two fermionic indices the two fermionic modes which are integrated out have to occur next to each other and we need to specify which one comes first. Thus, the contraction of two fermionic indices is *directed* and inverting the direction of the contraction generates a minus sign, if the parity of the index is odd. Directed contractions are represented in the diagrammatic notation by placing an arrow direction on the index line. In the super vector space formalism, the directed contraction of an index l with an index r is implemented by using vectors and dual vectors depending on whether the index comes first or second in the contraction and using the scalar product $\langle l|r\rangle = \delta_{lr}$. To achieve the reordering, we note that Eq. (5.47) applies to vectors and dual vectors alike. In the Grassmann number based formalism one formally multiplies the expression with $(1 + \theta_l\theta_r)$ and performs the integral $\int d\theta_r d\theta_l$ using Grassmann numbers θ_l, and θ_r instead of vectors and dual vectors. In the maximally entangled pair picture, it is the pair itself which carries the contraction order, i.e., one distinguishes between the pair $(1 + f_l^\dagger f_r^\dagger)\,|\emptyset\rangle$ and $(1 + f_r^\dagger f_l^\dagger)\,|\emptyset\rangle$.

For concreteness we will work in a Grassmann number formalism from now on. While the ansatz in Eq. (5.48) is general, it is incomplete in the sense that the partitioning of the indices into parity even and parity odd sectors is not contained in the expression. We find it more convenient to introduce additional bosonic indices and treat "parity even" and "parity odd" as the two values of a block index. I.e, for an index $i = 1, \ldots, n_e + n_o$ with index values $1, \ldots, n_e$ even and index values $n_e + 1, \ldots, n_e + n_o$ odd, we write

$$A_{(j_1,b_1),\ldots,(j_N,b_N)}\theta_1^{b_1}\ldots\theta_N^{b_N} \tag{5.50}$$

with $\{b_i\} \in \{0, 1\}$ and the range of j_i depends on b_i consistent with the convention for block indices. The indices j can be understood as usual bosonic indices. Alternatively, we can specify the partitioning of even and odd sectors by functions $f_j : i_j \to \{0, 1\}$ and write

$$A_{i_1,\ldots,i_N}\theta_1^{f_j(i_j)}\ldots\theta_N^{f_N(i_N)}\,. \tag{5.51}$$

5.5.2. Fermionic twisted quantum double models

In the following we consider a particular class of fermionic string-net models – the *fermionic twisted quantum double models* proposed in Ref. [69] and construct fPEPS representations for the latter. In addition, we show, that they fulfill the criteria of *fermionic MPO-injectivity*.

Fermionic twisted quantum double models are the simplest examples of fermionic systems with non-chiral topological order and can be understood as fermionic generalizations of the toric code model [232]. They are a subclass of fermionic string-net models as presented in Ref. [69] and later generalized in Ref. [11]. Interestingly, fermionic parity symmetry interacts with the topological invariance formulated as string-deformation rules or as virtual symmetry in a non-trivial way as becomes apparent in the definition of F-moves and the *fermionic pentagon equation* (cf. Eq. (5.53)).

In the definition of fermionic twisted quantum double models [69, 232] fermionic degrees of freedom are introduced into a string-net model in a way that most of the bosonic formalism carries over to the fermionic case, but one still obtains new intrinsically fermionic phases of matter. Essentially, a conventional bosonic string-net model as defined in Ref. [12] and reviewed in Section 5.1 is decorated with additional fermionic sites at the vertices. The string-deformation rules have to be modified accordingly as they now affect patterns of bosonic strings with local fermions at the vertices. A particular simple ansatz is to make the presence and absence of local fermions at the vertices dependent on the bosonic string types around the vertex. Choosing bosonic string types whose fusion rules are determined by a finite group via the group multiplication, one arrives at the fermionic twisted quantum double models.

Due to the potential presence of fermions at the vertices the pentagon equation for the F-symbols is altered in such a way that the trivial F-symbol (identical to one for all allowed configurations) is no longer a solution of the fermionic pentagon equation as explained in the following Section. This is in contrast to the bosonic case, where a group G with the trivial F-symbol always defines a consistent string-net model. Thus, fermionic quantum double models are always "twisted" and are formally similar to bosonic twisted quantum double models.

The simplest fermionic twisted quantum double model is the fermionic toric code presented in Ref. [232], where the underlying group is $G = \mathrm{Z}_2$. One finds that its anyonic excitations are those of a Chern–Simons theory with diagonal K-matrix and thus give rise to a topological phase that is inaccessible for purely bosonic theories [232].

String-types and deformation rules

In the following we review the string-net description of fermionic twisted quantum double models following Ref. [69, 232].

Fermionic twisted quantum double models are defined on trivalent lattices with branching structure, i.e., the edges of the lattice are oriented and the orientations are such that no vertex has all-incoming or all-outgoing edges. Branching structures can be interpreted as a choice of a local coordinate system and appear in many topological theories that are not time-reversal symmetric[6, 174]. For the definition of the deformation rules and the ground state wave function it is central to find a consistent rule assigning fermions to vertices. We make the ansatz that for a vertex with two incoming edges occupied by sting types i, j, the occupancy of the vertex by a fermion is determined by a function $s(i, j)$. Note that due to the fusion rule being given by the group law, the tuple i, j already determines the string-type ij on the third edge. With this ansatz we can define a fermionic F-move as in Fig. 5.24 in terms of a 3-index tensor $\omega(a, b, c)$ and a product of fermionic creation and annihilation operators that remove and add fermions according to the edge occupations before and after the F-move. Note, that in order to

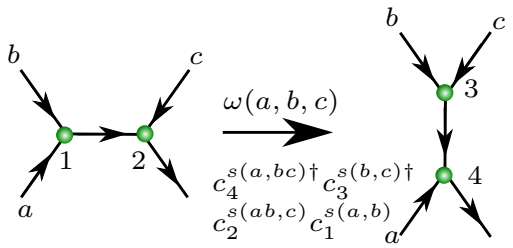

Fig. 5.24. ⋆ Fermionic F-move for a fermionic twisted quantum double. In addition to changing the wave function by a prefactor $\omega(a,b,c)$ depending on the bosonic string-types a,b,c, fermions at the old vertices are removed and added at the new vertices according to the fermion assignment function s.

conserve fermion parity the function s needs to fulfill

$$s(a,b)+s(ab,c)+s(b,c)+s(a,bc)=0\,, \tag{5.52}$$

where again addition is meant modulo two. We realize that this is the defining relation for a 2-cocycle $s\in\mathcal{H}^2(G,\mathrm{Z}_2)$.

Analogous to the bosonic case (cf. Section 5.1.1) one can derive a self-consistency equation for the fermionic F-moves – a fermionic pentagon equation – by considering two different sequences of fermionic F-moves with the same source and target configuration. Each sequence corresponds to a product of weights ω and fermionic creation and annihilation operators. Equating the two sequences and applying the usual fermionic anticommutation relations to reorder the creation and annihilation operators one obtains an equation for the weights ω

$$\begin{aligned}&\omega(a,b,c)\omega(a,bc,d)\omega(b,c,d)\\ =&(-1)^{s(a,b)s(c,d)}\omega(ab,c,d)\omega(a,b,cd)\,.\end{aligned} \tag{5.53}$$

This equation is referred to as a super 3-cocycle equation, which is a 3-cocycle equation graded by the 2-cocycle s. Formally we have $\omega\in\mathcal{H}^3_f(G,U(1),s)$. A solution to Eq. (5.53) exists, if the function $(-1)^{s(a,b)s(c,d)}$ is a coboundary $\mathcal{B}^4(G,U(1))$ viewed as a 4-cocycle.

It is an interesting observation that while for certain groups G one can construct fermionic models as a well-defined fermionic counterpart to a bosonic model (as e.g. for the fermionic toric code discussed in the next Section) this is not generically true. For example all groups $\mathbb{Z}_n$ with n odd do not admit non-trivial 2-cocycle s and hence can not be used to define a fermionic twisted quantum double model.

Hamiltonian

Given a group G and a solution to Eqs. (5.52) and (5.53) the model is fully determined and we can find a commuting projector Hamiltonian

$$H=\sum_v Q_v+\sum_p Q_p \tag{5.54}$$

given by a sum of vertex operators Q_v and plaquette operators Q_p that act on bosonic and fermionic degrees of freedom simultaneously. The vertex projector projects onto string configurations allowed by the branching rules for the bosonic string-types living on the edges δ_{ijk} and

(**a**) A_+ (**b**) A_-

Fig. 5.25. • Fermionic PEPS tensor A_+ and A_- given in Eq. (5.55) and Eq. (5.56). Solid black lines denote bosonic indices. Dashed lines denote fermionic indices.

the according fermion configurations determined by $s(i,j)$. The plaquette operator can again be represented as a sum over closed loop insertions (cf. Section 5.1.1), where the inserted loops are integrated back to the honeycomb lattice with the aid of fermionic F-moves.

Another way to construct the plaquette operator proceeds as sketched in Section 5.1.2 for the bosonic case. The fermionic F-symbols can be identified with fermionic tensors, which again can be identified with simplices, where index contraction is identified with the gluing of simplices. In addition to the bosonic indices associated to the edges of the simplices, fermionic indices are associated to the faces of the simplex. The plaquette operator can then be constructed from Fig. 5.21a completed by edge orientations (derived from the edge orientations of the physical lattice) and a convention how the latter determine the contraction direction of the fermionic indices (as e.g. provided in Ref. [240]).

Fermionic PEPS ground states

Similar to the bosonic case, fermionic string-net ground states have exact fPEPS representations [1, 9, 11]. In this Section we present a concrete fPEPS description for the fermionic twisted quantum double models and show that the fPEPS possesses virtual symmetries captured by a fermionic matrix product operator (fMPO) following Ref. [1].

As discussed in the previous Section the lattice on which we define a fermionic twisted quantum double has a branching structure, i.e., there are two types of vertices, one with two ingoing edges and one with two outgoing edges. We will use this branching structure to define two types of tensors that are placed at the positions of the respective vertex types. To define the latter it is convenient to consider the dual lattice and orient edges of the dual lattice according to the orientation of the underlying edges. We choose the convention that an ingoing edge corresponds to an edge pointing in clockwise direction and refer to the two types of tensors $A_\pm$ as positively and negatively oriented according to whether the majority of the edges are oriented clockwise or counter-clockwise. The edge orientation of the lattice are also used to define the contraction direction of the fermionic index contractions.

The concrete expressions for $A_\pm$ (cf. Fig 5.25) are motivated by the PEPS construction for string-net models and in particular twisted quantum double models[19], i.e., they are essentially

[19] See also Section 3.2.3 for an interpretation of the map between the virtual and the physical indices

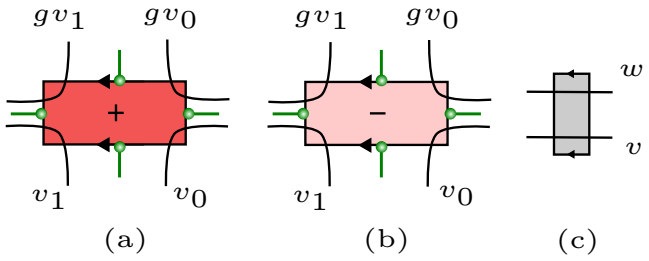

Fig. 5.26. ⋆ The MPO tensors $T_+(g)$, $T_-(g)$ and Y.

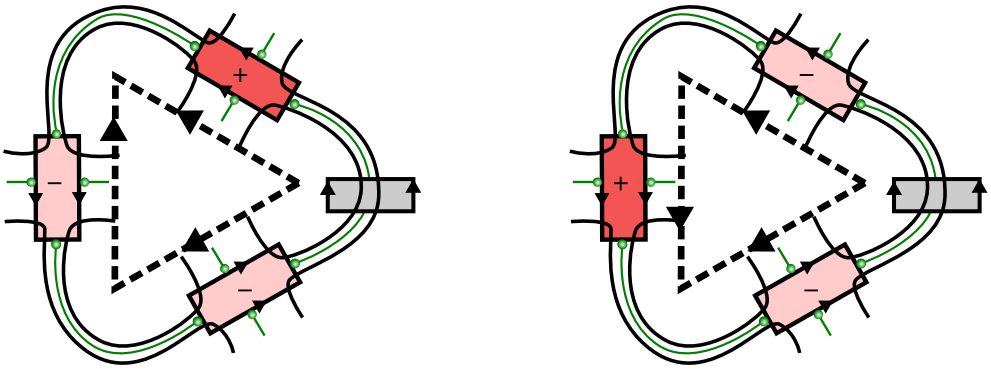

Fig. 5.27. ⋆ Symmetry fMPOs P_+ and P_- consisting of Y-tensors (grey) and tensors T_+ (blue) and T_- (red).

given by the fermionic F-symbols

$$\begin{aligned} A_+ = \sum_{v_0,v_1,v_2} & \omega(v_0, v_0^{-1}v_1, v_1^{-1}v_2) \\ & \times \theta_p^{s(v_0^{-1}v_1, v_1^{-1}v_2)} \theta_{v_{02}}^{s(v_0, v_0^{-1}v_2)} \bar{\theta}_{v_{12}}^{s(v_1, v_1^{-1}v_2)} \bar{\theta}_{v_{01}}^{s(v_0, v_0^{-1}v_1)} \\ & \times |v_0^{-1}v_1, v_1^{-1}v_2, v_0^{-1}v_2\rangle \langle v_0, v_1, v_2| \,, \end{aligned} \tag{5.55}$$

$$\begin{aligned} A_- = \sum_{v_0,v_1,v_2} & \omega^{-1}(v_0, v_0^{-1}v_1, v_1^{-1}v_2) \\ & \times \theta_{v_{01}}^{s(v_0, v_0^{-1}v_1)} \theta_{v_{12}}^{s(v_1, v_1^{-1}v_2)} \bar{\theta}_{v_{02}}^{s(v_0, v_0^{-1}v_2)} \bar{\theta}_p^{s(v_0^{-1}v_1, v_1^{-1}v_2)} \\ & \times |v_0^{-1}v_1, v_1^{-1}v_2, v_0^{-1}v_2\rangle \langle v_0, v_1, v_2| \,. \end{aligned} \tag{5.56}$$

Note, that the 2-cocycle condition on s in Eq. (5.52) implies that the tensors are fermion parity even.

In a slight variation of the contraction rule introduced above, we will use the convention that Grassmann valued indices are contracted by inserting $\int \mathrm{d}\,\bar{\theta}\,\mathrm{d}\,\theta(1+\bar{\theta}\theta)$.

Fermionic MPO injectivity

As a consequence of the fermionic pentagon equation (5.53) the fPEPS tensors defined in Eq. (5.55) and Eq. (5.56) exhibit a fermionic MPO symmetry with fermionic MPOs defined

from tensors T_+ and T_- (cf. Fig. 5.26a–b)

$$T_+(g) = \sum_{v_0,v_1} \omega(g, v_0, v_0^{-1}v_1) \quad |v_0, v_1\rangle \langle gv_0, gv_1| \tag{5.57}$$

$$\times |v_0, gv_0)(v_1, gv_1| \tag{5.58}$$

$$\times \theta^{s(v_0,v_0^{-1}v_1)}\theta^{s(g,v_1)}\bar{\theta}^{s(gv_0,v_0^{-1}v_1)}\bar{\theta}^{s(g,v_0)},$$

$$T_-(g) = \sum_{v_0,v_1} \omega^{-1}(g, v_1, v_1^{-1}v_0) \quad |v_0, v_1\rangle \langle gv_0, gv_1| \tag{5.59}$$

$$\times |v_0, gv_0)(v_1, gv_1| \tag{5.60}$$

$$\times \theta^{s(g,v_1)}\theta^{s(gv_1,v_1^{-1}v_0)}\bar{\theta}^{s(g,v_0)}\bar{\theta}^{s(v_1,v_1^{-1}v_0)}$$

We find, that in order to obtain an fMPO which is as symmetry for $A_\pm$ we need to introduce an additional purely bosonic sign factor tensor depicted in Fig. 5.26(c)

$$Y = \sum_{v,w} (-1)^{s(wv^{-1},v)} |v, w)(v, w| \,. \tag{5.61}$$

The symmetry fMPOS are than defined as

$$V_\pm(g) = \mathrm{tTr}[T_\pm(g)T_\pm(g)T_\mp(g)Y] \tag{5.62}$$

such that $A_\pm = A_\pm V_\pm(g)$, i.e., $V_\pm(g)$ is a virtual symmetry of $A_\pm$ for each group element $g \in G$.

From the symmetry MPOs $V_\pm(g)$ we can define the MPO projector as $P_\pm = \sum_g V_\pm(g)$. The projector identity $P_\pm^2 = P_\pm$ follows from the fact that $V_\pm(g)$ fulfills the group representation property $V_\pm(g)V_\pm(h) = V_\pm(hg)$. The existence of the pseudo-inverses of $A_\pm$ is verified by an explicit calculation.

To conclude that the fPEPS defined by tiling a regular honeycomb lattice with tensors $A_\pm$ is fMPO-injective, we need to investigate the stability of fMPO-symmetry and fMPO-injectivity under concatenation. We expect that the concatenation of two fMPO-symmetric fPEPS tensors is again fMPO-symmetric. However, the placement of the parity matrices for elementary MPOs depends on the edge orientations via the relations depicted in Fig. 5.28. Thus, the position of the parity matrices on a larger patch are derived from the positions of the parity matrices on elementary triangle tensors. Keeping this technicality in mind one can show that the concatenation of two MPO-symmetric tensors is again fMPO-symmetric and fMPO-injective as long as there are no vertices on the dual lattice where all edges are incoming or outgoing, i.e., the tensor network patch has a dual branching structure as well as a branching structure. A particular simple case of such an orientation pattern is a lattice where all edges point into the same direction, i.e., the angles between all pairs of edges never exceed π. In Ref. [1] we referred to this property as "global flow" property. For such a lattice one can show that the symmetry MPO acting on any tensor network patch is given by $T_\pm$ tensors placed according to the edge orientations of the boundary and parity tensors are inserted at convex source points and concave drains as explained and visualized in Fig. 5.29). Thus, there is a consistent rule for the placement of parity matrices. The proof of the consistency proceeds via straight-forward but tedious induction (cf. Ref. [1, Appendix A]). For all possibilities of attaching one additional tensor to a tensor network patch (such that the global flow property is fulfilled before and after attaching the tensor) one can check that for the larger tensor network patch the parity matrix rule is fulfilled. Details can be found in Appendix A.1.

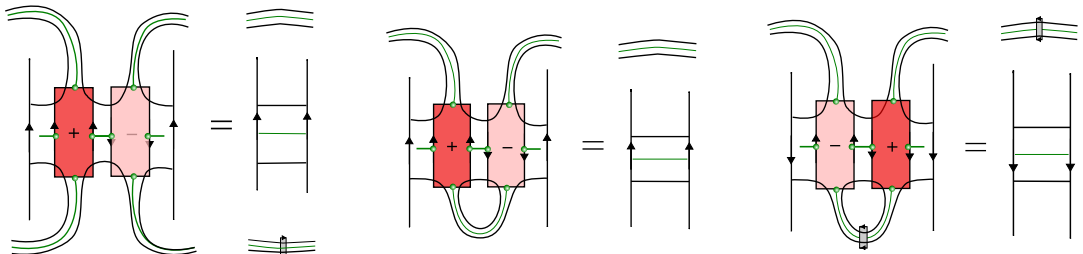

(**a**) Open boundary (**b**) Closed boundary type I (**c**) Closed boundary type II

Fig. 5.28. ⋆ Concatenation of two MPO tensors with open or partially closed radial indices.

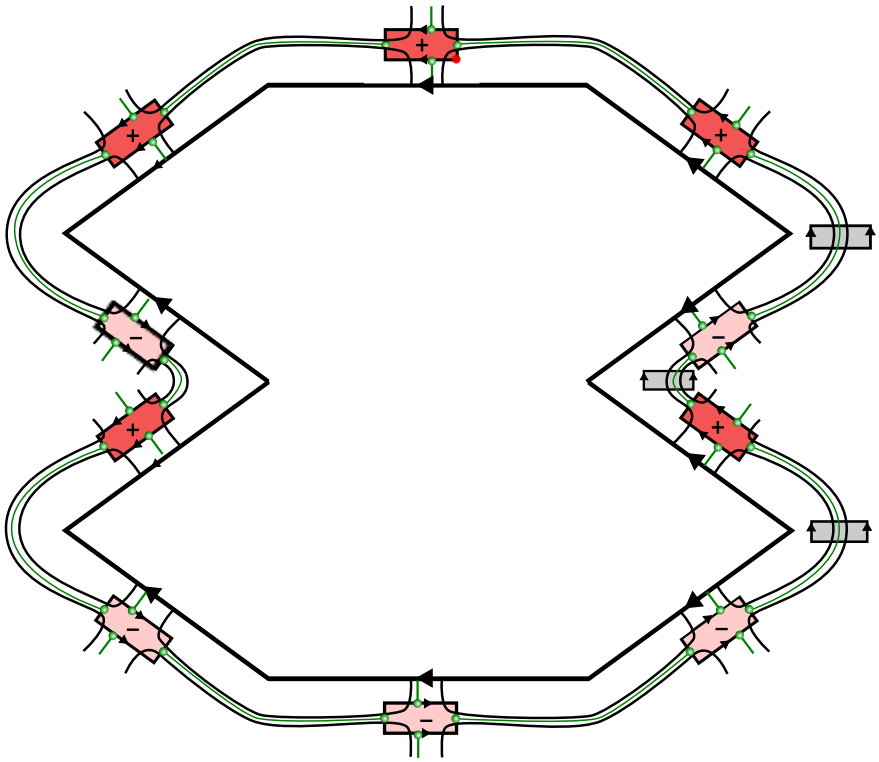

Fig. 5.29. ⋆ MPO for a generic boundary. T_+ (blue) and T_- (red) tensors are placed according to the edge orientation of the boundary and parity matrices Y (grey) are placed at convex source points (i.e., vertices around which the lattice underlying the tensor network patch is locally convex and the edges are oriented away from the vertex) and at concave drain points (i.e., vertices around which the lattice underlying the tensor network patch is locally concave and the edges are oriented towards the vertex).

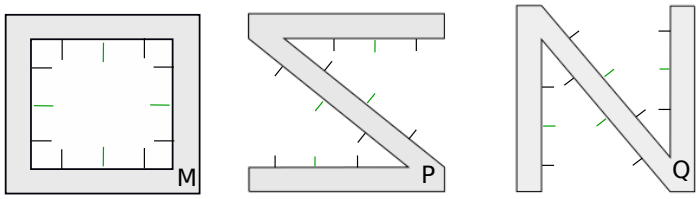

Fig. 5.30. ⋆ The three different closure tensors on a minimal torus.

Topological ground state degeneracy

We have seen in Section 5.2.3 how characteristic features of topological order can be calculated from the MPO tensors without considering the ground state or the Hamiltonian of a model explicitly. In particular, we showed how to calculate the ground state degeneracy on a torus for bosonic G-injective PEPS (a subclass of MPO-injective PEPS) in Section 3.2.2 and found that it is given by all pair conjugacy classes $C(g,h)$ defined in Eq. (3.12). For fermionic twisted quantum double models, we can obtain a similar result. To this end we focus on fMPO-injective PEPS on a torus equipped with a branching structure admitting a global flow and adapt the calculation for MPO-injective PEPS of bosonic twisted quantum double models presented in Ref. [6] to the fermionic setting.

As explained on a conceptual level in Section 2.4.3 for the one dimensional setting and in Sections 3.2.2, 5.2.3 adapted to the two-dimensional setting of G-injective and MPO-injective PEPS, to calculate the ground state degeneracy, we need to consider all locally undetectable closures on a minimal torus which are MPO-symmetric. Thus, we search for all states which can be defined simultaneously using the three different closure tensors depicted in Fig. 5.30. Similar to the bosonic setting we find the following parametrization of the space spanned by the latter

$$\operatorname{span}\{M(g,h)|\ [g,h]=0,\ s(g,h)=s(h,g)\}\ , \tag{5.63}$$

where the closure tensor M is constructed as depicted in Fig. 5.31 and given by

$$\begin{aligned} M(g,h) =& \sum_{\alpha} \lambda(\alpha;g,h)\,|\alpha, g\alpha, gh\alpha, h\alpha\rangle \\ &\times \theta^{s(g\alpha,{}^{\alpha}g^{-1})}\theta^{s(hg\alpha,{}^{\alpha}h^{-1})}\bar{\theta}^{s(gh\alpha,{}^{\alpha}g^{-1})}\bar{\theta}^{s(h\alpha,{}^{\alpha}h^{-1})}\ . \end{aligned} \tag{5.64}$$

Here, ${}^{\alpha}g = \alpha^{-1}g\alpha$ denotes conjugation by the inverse element and the coefficient λ is given by

$$\begin{aligned} \lambda(\alpha;g,h) =& \frac{\omega(h,g,\alpha)\omega(h,g\alpha,{}^{\alpha}g^{-1})}{\omega(g,h,\alpha)\omega(g,h\alpha,{}^{\alpha}h^{-1})} \\ &\times(-1)^{s(gh\alpha,{}^{\alpha}h^{-1})s(g\alpha,{}^{\alpha}g^{-1})+s(hg\alpha,{}^{\alpha}g^{-1})s(h\alpha,{}^{\alpha}h^{-1})} \\ &\times(-1)^{(s(h,\alpha)+s(h\alpha,{}^{\alpha}h^{-1}))(s(g,\alpha)+s(g\alpha,{}^{\alpha}g^{-1}))+s(hg,\alpha)}\ . \end{aligned} \tag{5.65}$$

We use MPO-symmetry by acting with a four-site MPO $V(k)$ on M and obtain a parametrization of the ground state space in terms of MPO-symmetric tensors

$$\begin{aligned} M'(g,h) =& \frac{1}{|G|}\sum_{k} V(k)M(g,h) \\ =& \frac{1}{|G|}\sum_{k} \eta_g^{\omega}(h,k)M(g^k,h^k)\ . \end{aligned} \tag{5.66}$$

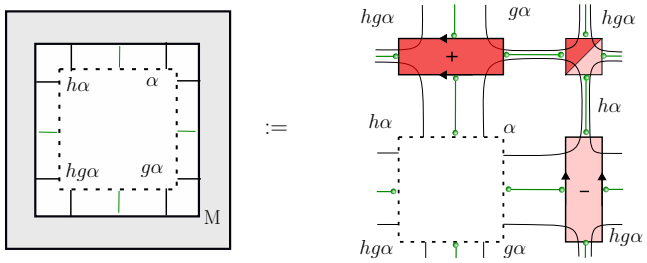

Fig. 5.31. ⋆ Closure tensor $M(g,h)$. The labels for the fermionic indices follow from the definition of $T_\pm$ and are omitted.

where $g^k = kgk^{-1}$ denotes conjugation and $\eta_g^\omega(h,k)$ is given by

$$\begin{aligned}\eta_g^\omega(h,k) =& \frac{\omega(g,k^{-1},h^k)\omega(k^{-1},h^k,g^k)\omega(h,g,k^{-1})}{\omega(h,k^{-1},g^k)\omega(k^{-1},g^k,h^k)\omega(g,h,k^{-1})} \\ & (-1)^{[s(k^{-1},kh)+s(kh,k^{-1})][s(k^{-1},kg)+s(kg,k^{-1})]} \\ & (-1)^{s(k^{-1},kgh)+s(kgh,k^{-1})} \,. \end{aligned} \tag{5.67}$$

To count the number of linearly independent elements of the ground state space, we first show that two states $M'(g,h)$ and $M'(k,l)$ are linearly dependent if (g,h) and (k,l) are in the same pair conjugacy class. This follows from the identity

$$\eta_{g^t}^\omega(x^t, yt^{-1}) = \frac{\eta_g^\omega(x,y)}{\eta_g^\omega(x,t)} \tag{5.68}$$

which holds formally as in the bosonic setting despite the fact that η^ω has additional sign factors and is given by a product of super 3-cocycles ω.

An additional subtlety to be considered is that not all pair conjugacy classes correspond to a non-vanishing state. Similar to the bosonic setting only pair conjugacy classes $\mathcal{C}(g,h)$ contribute to the total ground state space dimension for which $[g,h] = 0, s(g,h) = s(h,g)$ and where for all elements of the centralizer $k \in \mathcal{Z}(g,h)$ we have

$$c_g^\omega(h,k) = c_g^\omega(k,h) \tag{5.69}$$

where

$$c_g^\omega(h,k) = \frac{\omega(g,h,k)\omega(h,k,g)}{\omega(h,g,k)} \,. \tag{5.70}$$

We refer to this property as (c^ω, s)-regular. To see that only (c^ω, s)-regular pair conjugacy classes contribute to the ground state dimension we first note that if

$$\sum_{s \in Z(g,h)} \eta_g^\omega(h,s) = 0 \,, \tag{5.71}$$

then also

$$\sum_{s | g^s = g^{t_i}, h^s = h^{t_i}} \eta_g^\omega(h,s) = 0, \quad \forall i \,. \tag{5.72}$$

Writing out the state $M'(g,h)$ in the basis of the elements of the pair conjugacy class $\mathcal{C}(g,h)$ we make use of the fact above to conclude that

$$M'(g,h) = 0 \Leftrightarrow \sum_{s\in\mathcal{Z}(g,h)} \eta_g^\omega(h,s) = 0\,. \tag{5.73}$$

To single out the pair conjugacy classes for which Eq. (5.73) is fulfilled we note that for all elements k in the centralizer of (g,h) with $[g,h]=0$ we have

$$\eta_g^\omega(h,k) = \frac{c_g^\omega(k^{-1},h)}{c_g^\omega(h,k^{-1})}\,, \tag{5.74}$$

where $c_g^\omega(h,k)$ as defined in Eq. (5.70). For $g,h,k \in \mathcal{Z}(g,h)$ and $[g,h]=0$, i.e. g,h,k are mutually commuting $c_g^\omega(h,k)$ is a 2-cocycle. This insight is used to apply the same arguments as in Ref. [210] and show that

$$\sum_{s\in\mathcal{Z}(g,h)} \eta_g^\omega(h,s) = 0 \Leftrightarrow c_g^\omega(h,s) \neq c_g^\omega(s,h)\,. \tag{5.75}$$

In other words, only pair conjugacy classes $\mathcal{C}(g,h)$ contribute to the total ground state space dimension for which $[g,h]=0, s(g,h)=s(h,g)$ and $c_g^\omega(h,k)=c_g^\omega(k,h)$ as claimed above. In complete analogy to the bosonic setting the considerations on the minimal torus carry over to a torus of arbitrary size. We conclude that the ground state degeneracy for fermionic twisted quantum double models defined by a triple (G,s,ω) is given by the number of (c^ω,s)-regular pair conjugacy classes.

As a sanity check we confirm that whenever the 2-cocycle s is trivial, we reobtain a classification of the ground state basis in terms of c^ω-regular pair conjugacy classes as expected from the results in Ref. [6].

Example – Fermionic Toric Code

In the next Section we show how the ground state of the fermionic toric code Hamiltonian as proposed in Ref. [232] can be written as a fermionic tensor network satisfying the axioms of fermionic MPO-injectivity. The fermionic toric code model is the simplest solution of the self-consistency equations for fermionic twisted quantum double models, i.e., the simplest triple (G,s,ω).

In particular, we have $G=\mathbb{Z}_2=\{0,1\}$, i.e., the model is constructed with spin-$\frac{1}{2}$ degrees of freedom on the edges of the honeycomb lattice. $G=\mathbb{Z}_2$ has only two second cohomology classes and the trivial one results in the bosonic toric code or the double semion model depending on the choice of the (then ungraded) 3-cocycle ω. The non-trivial second cohomology class has the normalized representative $s_{fTC}(g,h)=1$ if $g=h=1$ and 0 otherwise. We find two normalized solutions to the fermionic pentagon equation

$$\omega_{fTC}(g,h,k) = \begin{cases} \pm\mathrm{i} & g=h=k=1\,, \\ 1 & \text{otherwise} \end{cases} \tag{5.76}$$

which correspond to the fermionic toric code model.

The lattice from Ref. [232] admits a global flow and thus we can write an ansatz for the ground state wave function as a fermionic PEPS with $A_\pm$ tensors defined in Eq. (5.55) and (5.56) with $G=\mathbb{Z}_2$ and s,ω defined above. The tensor network is fMPO-injective by construction. To prove that it is indeed the ground state of the fermionic toric code Hamiltonian one needs to choose

an appropriate gauge of the Hamiltonian given in Ref. [232] as discussed in Appendix A.1.1 and verify that the tensor network is an eigenstate to each local projector in the given gauge. The definition of the $A_\pm$ tensor already implies that the tensor network state is an eigenstate to all vertex projectors. Verifying that it is also an eigenstate to each plaquette operator is done by explicit calculation. An intuitive understanding of this result can be understood by interpreting the plaquette operator as inserting a closed loop around the center of the hexagon. The contraction of the inner virtual index v_0 exactly compensates for that, i,e., $Q_p A_{\text{hex}}(v_0 = 0) = A_{\text{hex}}(v_0 = 1)$ and $Q_p A_{\text{hex}}(v_0 = 1) = A_{\text{hex}}(v_0 = 0)$. Note that due to the anti-commutating Grassmann variables it is not trivial to see that all sign-factors are indeed correct but it is a result of an explicit calculation. Due to the translation invariance of the lattice it follows that the tensor network state is the ground state on any region with open virtual boundary.

As an application of the formalism developed in the previous Section, we calculate the ground-state degeneracy on a torus. Since $\mathbb{Z}_2$ is Abelian there are four pair conjugacy classes $(0,0), (0,1), (1,0)$ and $(1,1)$. All of them are (c^ω, s)-regular. This can be easily checked. The 2-cocycle s is symmetric and the super 3-cocycle is normalized. Thus, the regularity condition is trivially fulfilled whenever one of the elements g, h, k is the trivial group element. For the only other case $g = h = k = 1$ it is also fulfilled as can be verified by explicit calculation. Thus, the ground state on a torus is four fold degenerate and the result is in agreement with a direct calculation on the physical level provided in Ref. [232].

Part III.

Synthetic topological quantum matter

6. Realizing topological order in mesoscopic systems

We have seen in Chapter 5 that the theory of non-chiral topological order is rich and beautiful in its mathematical description. In stark contrast, the experimental realization of the theory is lacking almost completely [119]. While chiral topological order is found in fractional quantum Hall states [36, 47–49, 119] and thus is present in many materials under the right external conditions [51, 241, 242], for non-chiral topological order Herbertsmithite ($ZnCu_3(OH)_6Cl_2$) is the only material candidate and it is still debated whether its unconventional magnetic properties are truly a consequence of $\mathbb{Z}_2$ topological order (i.e., it is in a toric code phase) [53, 54, 243, 244] or whether the material is actually in a gapless phase (a gapless $U(1)$ Dirac liquid [245]).

Still, the interest in non-chiral topological order is not only a matter of academic curiosity, but is motivated to a large extent by the potential applications in quantum information processing, namely as topological quantum codes and platforms for fault-tolerant topological quantum computation [44, 70–72]. Thus, in the absence of material candidates an alternative approach is to simulate or engineer non-chiral topological matter artificially. Most of the experimental effort in this direction has focused on the comparably simple toric code phase (cf. Section 3.1) and its code properties. Apart from experiments that focus on preparing the ground state space and performing stabilizer measurements on it, but do not realize a Hamiltonian [78–80], the toric code phase has been simulated experimentally in minimal instances on different platforms including optical lattices [81], arrays of Josephson junctions [82], Rydberg atoms [83] and in more unconventional simulation approaches using Floquet engineering [84].

While the toric code is still considered as a state-of-the-art error correcting code, it is not suitable as a platform for (universal) quantum computation unless it is supplemented with additional "hardware" and protocols. The set of quantum gates can be completed by introducing auxiliary qubits into the system that are prepared to be in a special so-called "magic states"[246]. However, the magic states have to be of high fidelity (i.e., the state must be very close to the desired state). A protocol to distill high-fidelity magic state qubits from several low-fidelity magic state qubits is known as magic state distillation[246]. The latter is a costly additional process [85–88]. Avoiding such additional overheads one may try to implement topological phases which are intrinsically more complex, hosting non-Abelian anyons with which universal topological quantum computation can be performed. A prime candidate in this realm are Fibonacci anyons for which recent work demonstrates their capability of fault-tolerant quantum computation even under adverse conditions of finite temperature and noise [247–249]. Fibonacci anyons can be found in comparably simple string-net models with two string-types and a non-Abelian fusion rule $\tau \times \tau = 1 + \tau$.

Several proposals towards the realization of topological phases beyond the toric code have been brought forward. Among them are ideas for the implementation of topological orders with (non-Abelian) discrete gauge groups (i.e., Kitaev's quantum double models captured by G-injective PEPS) in arrays of Josephson junctions [73, 74] and optical lattices of cold atoms

[75, 76] or trapped ions [77][1]. However, none of the proposed schemes is suited for a phase of matter that hosts anyons which can be used for universal topological quantum computation. In particular, it is not investigated if and how general Levin–Wen string-net models can be realized in concrete physical platforms.

In the following Section we approach this question. As a physical platform we choose networks of tunnel coupled Majorana Cooper boxes (MCBs) [89, 90], which have been considered before as candidates to realize the toric code [85–87, 91] and color codes [88]. To give a vague intuition why we think that this platform is suitable for this task, we note that the physics of MCB networks is dominated by charging effects, which naturally give rise to a low-energy effective theory of "ring-exchange" processes – i.e., particle tunnelings that always take place in "closed loops". This vaguely reminds us of the plaquette operators in Levin–Wen models given by closed-loop insertions of virtual strings. In the preceding Sections, we have encountered yet another "closed-loop structure", namely the matrix product operator projectors of MPO-isometric PEPS. We have also seen how the latter two are connected (cf. Section 5.2.4). In the following we will argue that the low-energy effective theory of tunnel coupled MCB is naturally characterized by matrix product operators.

Combining this insight with the theoretical framework of the preceding Sections we make use of the MPO-injective PEPS formalism as a guide to devise blueprints for string-net phases in MCB architectures. We suggest that – apart from the physical dimension of the qudits, i.e., the number of string-types – the bond dimension of the matrix product operator projector determining the virtual subspaces of the PEPS ground states gives a measure of how difficult it is to realize the string-net model. We explore the limits of the given physical platform. Concretely, we present how small arrays of coupled MCBs can be used as building blocks for matrix product operators and design additional useful structures such as Bell-pair projectors, which can be assembled to more complicated structures. In doing so, we make use of several so called Hamiltonian gadgets ideas [92, 94, 251–253] – a tool developed originally in quantum information theory to tackle the Hamiltonian complexity problem – which can be seen as recipes to effectively engineer Hamiltonians with high locality from comparably simpler ones.

In our proposal the identification and characterization of low-energy subspaces is crucial in several ways. First of all, the low-energy subspace of the Majorana Cooper box – a relatively complex device – can be identified with one or several qubits (depending on the number of nanowires) [89, 90]. Second, instead of engineering the canonical parent Hamiltonian of a topological PEPS, i.e., a standard Levin–Wen fix-point Hamiltonian, we aim for a simpler Hamiltonian, the so called perturbative PEPS parent which is in the same phase.

Thus, the first Section of this chapter discusses in detail the idea of Hamiltonian gadgets and degenerate perturbation theory as a tool to engineer effective low-energy Hamiltonians that feature intricate n-body interactions from comparably simpler Hamiltonians. We recapitulate the general theory of degenerate perturbation theory, in particular the Schrieffer–Wolff (SW) transformation [254] and review specific gadget constructions, including the perturbative PEPS parent construction [94] and the Jordan–Farhi gadgets [93]. Next, we turn to the mesoscopic constituents – the MCBs – and how effective qubits emerge in the latter. We discuss the effective spin Hamiltonians in networks of MCBs and construct small well-controlled MCB networks as building blocks. Finally, we show how those buildings blocks can be combined to yield the perturbative PEPS parent Hamiltonian of the double semion model and briefly discuss the additional effort needed to implement the double Fibonacci model.

[1] For a recent review on simulation proposals for general lattice gauge theories see also Ref. [250].

6.1. Low-energy effective theories

Fixed point models of topological order are complex and feature an unnaturally high locality – typically 12-local interactions for Levin–Wen string-net models. In contrast natural Hamiltonians typically feature only 2-local interactions. It is known that in perturbation theory low-energy effective Hamiltonians H_{eff} with high locality can emerge from Hamiltonians with lower locality. This insight will be used as a design principle in the construction of systems that effectively realize string-net models. In the following Section we will briefly review different formalisms of low-energy effective theories in lattice models and design principles named *Hamiltonian gadgets*.

In all cases the starting point is to consider a Hamiltonian

$$H = H_0 + \epsilon V \,, \tag{6.1}$$

where H_0 is referred to as the unperturbed Hamiltonian and V is called the perturbation. The effective Hamiltonian H_{eff} is then derived perturbatively in the limit of small ϵ.

It is sufficient to assume that the Hamiltonian H_0 has an energy gap Δ separating the low-energy and the high energy space, i.e., all eigenstates either have energy less than δ – those span the low-energy subspace – or higher than $\delta + \Delta$. However, we will restrict ourselves to the case, where the low-energy subspace is fully degenerate, i.e., it consists only of the ground state space $\mathcal{E}_0$ with ground state energy $E_0 = 0$. This assumption simplifies the calculations and all Hamiltonians considered below will be of this form. Intuitively this case can also be seen as a good approximation for the general case, if the energy gap Δ is much larger than the level separation of the low-energy states.

When constructing the low-energy effective Hamiltonian we are interested in reproducing the energy spectrum of H in the low-energy subspace $\mathcal{E}$ that originates from the deformation of the ground state space $\mathcal{E}_0$. Intuitively, the massive ground state degeneracy of H_0 will be lifted by the perturbation V yielding a refined spectrum around the ground state energy E_0. The excited energy levels of H_0 may split and shift as well, but we can assume that if the gap Δ is much larger than ϵ, they will stay well separated from the low-energy spectrum.

The mathematical machinery to formalize the intuition sketched above is highly evolved and a research topic in its own right. While some methods do not involve a perturbative treatment at least on a formal level and are therefore exact, for practical purposes the effective Hamiltonian is usually given as a series expansion and different expansion techniques will in general not yield the same effective Hamiltonian order by order. However, in the cases considered here, different methods will agree in leading order. The main techniques used for degenerate perturbation theory are the self-energy expansion, the Bloch method and the Schrieffer–Wolff method in a global and a local version. We will review these methods in the following Sections accompanied by examples.

Traditionally, degenerate perturbation theory has been studied to analyze the low energy theory of a given physical model. More recently, low-energy effective theory analysis has been used also as a reverse engineering approach to Hamiltonian design [93–95, 252]. Here the goal is to synthesize a complicated effective low energy Hamiltonian H_{eff} from comparably simpler Hamiltonians H and V. This idea has become popular under the name of Hamiltonian gadgets. The term first appeared in the context of Hamiltonian complexity, where the authors of Ref. [92] showed that the 2-local Hamiltonian problem[2] is in the complexity class QMA [255]

[2] The k-local Hamiltonian problem is the task to decide whether given r k-local Hamiltonian terms H_i, $i = 1, \ldots, r$ and two real numbers a and b, the lowest eigenvalue of the Hamiltonian $H = \sum_{i=1}^{r} H_i$ is below a or all its eigenvalues are larger than b.

by reducing the 3-local Hamiltonian problem known to be in QMA to a 2-local Hamiltonian problem. This is done by showing that the spectrum of a given 3-local Hamiltonian is well approximated by the spectrum of an effective Hamiltonian that emerges from a specifically designed 2-local Hamiltonian of the form $H = H_0 + V$. Following up on this idea various other Hamiltonian gadgets have been constructed.

An instructive example how to apply degenerate perturbation theory is presented in the discussion of the Kitaev honeycomb model in Ref. [18] and will be reviewed briefly in Section 6.1.1. Next, we discuss a fairly general gadget construction by Jordan and Farhi [93] that can be used to design general k-local Hamiltonians from 2-local Hamiltonians in Section 6.1.2. The reduction in locality is usually paid by introducing auxiliary qubits to the system leading to a huge and possibly impractical overhead. This overhead can be reduced when the gadget construction is tailored to designing specific Hamiltonians. The perturbative PEPS parent construction by Brell et al. allows to engineer parent Hamiltonians of topologically ordered PEPS with significantly less overhead than the general-purpose gadget by Jordan and Farhi and will be reviewed in Section 6.1.4.

Notation

We introduce some notation that will be used throughout the following Sections. The projector onto the ground state space $\mathcal{E}_0$ of H_0 is denoted by P_0 and the projection onto its orthonormal complement by $Q_0 = 1 - P_0$. We assume that the Hamiltonian H_0 is local and local terms do not overlap. Therefore, the ground state space and its projector P_0 have a tensor product structure

$$P_0 = p_0^{(1)} \otimes p_0^{(2)} \otimes \ldots \otimes p_0^{(k)} \,, \tag{6.2}$$

where generically all $p_0^{(i)}$ are of rank two and the number of tensor factors grows with the system size, such that the ground state degeneracy of H_0 grows exponentially with the system size. A typical example for H_0 would be a sum of non-overlapping interacting spin pairs $\sum_i \hat{z}_{2i}\hat{z}_{2i+1}$. Another example we will encounter are disjoint clusters of spins with ferromagnetic interaction between all pairs $\sum_C \sum_{i,j\in C} \hat{z}_i\hat{z}_j$. Here, the ground state space factorizes into several giant qubits formed by clusters of single spins that are aligned.

The perturbation $V = \sum_i v_i$ is a sum of potentially overlapping 2-body terms that act either entirely on the same Hilbert space on which H_0 acts on or at least partially on that Hilbert space. In the latter case we will usually think of the total Hilbert space as being partitioned into auxiliary qubits and target qubits, where H_0 only acts on auxiliary qubits and V acts on both auxiliary and target qubits. Each local term v_i has the property that it does not preserve the ground state space, i.e., $P_0 v_i P_0 = 0$ which again simplifies the perturbative expansions.

It is convenient to split all operators according to whether they act within the ground state space, within the excited state space or between the two spaces, i.e.,

$$O_{--} = P_0 O P_0 \,, \qquad O_{++} = Q_0 O Q_0 \tag{6.3}$$

.

$$O_{+-} = Q_0 O P_0 \,, \qquad O_{-+} = P_0 O Q_0 \,. \tag{6.4}$$

6.1.1. Self-energy expansion and the Kitaev honeycomb model

We briefly review the perhaps most standard approach to degenerate perturbation theory – the self-energy method closely following Refs. [18] and [92].

In order to determine the spectrum of H in the low-energy subspace, we would like to project to $\mathcal{E}_0$ using P_0 at some point in our calculation. However, eigenvalues are usually not preserved under a projection. This is easy to see in our example as $P_0HP_0 = P_0H_0P_0 + \epsilon P_0VP_0 = 0$ is trivial. However, one can instead consider the resolvent

$$G(z) = (z - H)^{-1} \tag{6.5}$$

and its poles that are in one to one correspondence with the eigenvalues of H and perform the projection to P_0 on the resolvent. The projected resolvent $G_{--}(z)$ can then be used to define the self-energy $\Sigma(z)$ as

$$G_{--}(z) = (z - \Sigma(z))^{-1} \tag{6.6}$$

which takes on the role of an effective Hamiltonian H_{eff} if its dependency on z can be neglected. Whether this is the case or not depends on the specific form of the perturbation V. This is the most prominent downside of the self-energy method. We will now assume, that the z-dependency is small and evaluate $H_{\text{eff}} = \Sigma(0)$ perturbatively in leading order. The corrections arising from taking into account the z-dependence are usually larger than the subleading order corrections [18].

To calculate $\Sigma(z)$, we express G in terms of the unperturbed resolvent $G_0 = (z - H_0)^{-1}$ and the perturbation and express it in a block-matrix form partitioned into P_0 and Q_0, i.e.,

$$G = (G_0^{-1} - \epsilon V)^{-1} = \begin{pmatrix} G_{0,++}^{-1} - \epsilon V_{++} & -\epsilon V_{+-} \\ -\epsilon V_{-+} & G_{0,--}^{-1} - \epsilon V_{--} \end{pmatrix}^{-1} . \tag{6.7}$$

Calculating the matrix inverse and selecting the low-energy subspace contribution we obtain

$$G_{--} = \left(G_{0,--}^{-1} - \epsilon V_{--} - \epsilon^2 (G_{0,++}^{-1} - \epsilon V_{++})^{-1} V_{+-} \right)^{-1} \tag{6.8}$$

Using the series expansion $(1 - X)^{-1} = 1 + X + X^2 + \dots$ and using Eq. (6.6) we obtain

$$\Sigma(z) = H_{0,--} + \epsilon V_{--} + \epsilon^2 V_{-+} G_{0,++}(z) V_{+-} + V_{-+} G_{0,++}(z) V_{++} G_{0,++}(z) V_{+-} + \dots \tag{6.9}$$

which we summarize as

$$\Sigma(z) = H_{0,--} + \epsilon V_{--} + \epsilon^n \sum_{n=2}^{\infty} V_{-+} (G_{0,++}(z) V_{++})^{n-2} G_{0,++}(z) V_{+-} . \tag{6.10}$$

Since $G_0(z)$ only has poles at 0, we can evaluate the self-energy around $z = 0$ and use $G_0(0) = -1/H_0$. We also recall that we work under the assumption that $H_0P_0 = 0$ and thus $H_{--} = 0$ and that applying perturbations lead out of the ground state subspace, i.e., $V_{--} = 0$ and thus

$$H_{\text{eff}} = \Sigma(0) = \epsilon^n \sum_{n=2}^{\infty} V_{-+} \left(\frac{1}{-H_0} V_{++} \right)^{n-2} \frac{1}{-H_0} V_{+-} . \tag{6.11}$$

Evaluating the first addend explicitly we obtain

$$H_{\text{eff}} = \epsilon^2 P_0 V \frac{1}{-H_0} V P_0 + \epsilon^3 P_0 V \frac{1}{-H_0} Q_0 V \frac{1}{-H_0} V P_0 + \mathcal{O}(\epsilon^4) . \tag{6.12}$$

We will later compare this expansion obtained from the self-energy approximation with expansions obtained from the Bloch method and the Schrieffer–Wolff method. For now, note, that the terms in the effective Hamiltonian can be thought of as paths starting and ending in

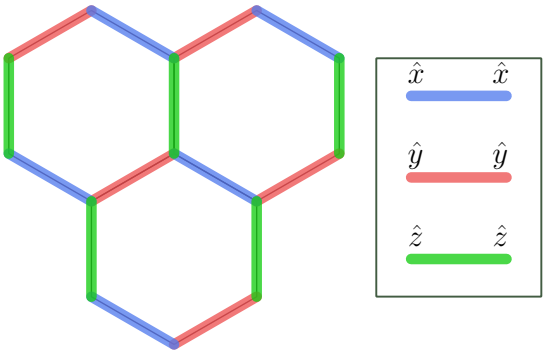

Fig. 6.1. ⋆ Kitaev honeycomb model.

the ground state space P_0 that run via intermediate virtual states in the excited state space Q_0 where the perturbation V takes us from one state to the next one. It is natural to think of the length of the path as the number of applied perturbations V. Since $1/H_0$ is evaluated only in the excited state space we have $1/H_0 < 1/\Delta$ and thus a term corresponding to a path of length n scales with ϵ^n/Δ^{n-1} which means that long excursions through the virtual excited state space are suppressed drastically.

To illustrate the formalism we consider an example how the self-energy approximation method can be used to determine the topological phase of a Hamiltonian by finding its low-energy effective description H_{eff}. The example is given in Ref. [18] and our presentation closely follows the given reference with the only difference that the notation is changed to be consistent with the rest of this Section. Although in this example the method is applied to investigate a given Hamiltonian rather than constructing a specific target Hamiltonian H_{eff} from simpler Hamiltonians H_0 and V the structure of H_0 and V is of the form that will be used in more constructive so-called gadget constructions and clearly inspired the latter.

We consider the Kitaev honeycomb model [18], i.e., a Hamiltonian defined on a hexagonal lattice with qubits on vertices and nearest neighbor interaction that depends on the orientation of the edge shared by two spins (cf. Fig. 6.1). Partitioning the three different types of edges into sets X, Y, Z we have

$$\tilde{H} = -J_x \sum_{x\in X} \hat{x}\,\hat{x}|_{\partial x} - J_y \sum_{y\in Y} \hat{y}\,\hat{y}|_{\partial y} - J_z \sum_{z\in Z} \hat{z}\,\hat{z}|_{\partial z}\,, \tag{6.13}$$

where $|_{\partial a}$ denotes the two vertices at the boundary of the edge a. We now consider the regime where $0 < J_x, J_y \ll J_z$ and define

$$H_0 = -J_z \sum_{z\in Z} \hat{z}\,\hat{z}|_{\partial c} + J_z N_z\,, \tag{6.14}$$

where we have included the energy shift to ensure $E_0 = 0$ and N_z denotes the number of z-edges

$$V = -J_x \sum_{a\in A} \hat{x}\,\hat{x}|_{\partial a} - J_y \sum_{b\in B} \hat{y}\,\hat{y}|_{\partial b}\,, \tag{6.15}$$

and $H = H_0 + V$. The ground state space of H_0 is given by all states where qubits along the z-edges are aligned, i.e., it has the tensor product structure mentioned above and is massively degenerate. We now investigate the effective Hamiltonian in Eq. (6.11). Each addend in the perturbation V flips two spins on different z-edges and thus breaks the alignment on at least

two z-edges and we have $P_0 V P_0 = 0$ as required in the initial assumptions. The first non-vanishing contribution in the series expansion occurs at second order, when the flip of two spins is reversed by flipping them back, i.e.,

$$H_{\text{eff}}^{(2)} = P_0 J_y^2 \sum_{y\in Y} \hat{y}\,\hat{y}|_{\partial y} \frac{1}{-4J_z} \hat{y}\,\hat{y}|_{\partial y} P_0 + P_0 J_x^2 \sum_{x\in X} \hat{x}\,\hat{x}|_{\partial x} \frac{1}{-4J_z} \hat{x}\,\hat{x}|_{\partial x} P_0 = -(N_x + N_y)\frac{J_y^2 + J_x^2}{4J_z} P_0 \,, \tag{6.16}$$

i.e., the effect is a lowering of the ground state energy. The third order term vanishes because after having flipped two spin pairs (breaking two different bonds) flipping one more spin pair can only "heal" one of the broken bonds. However, at fourth order we obtain terms that correspond to flipping all spins around a hexagon (plaquette). There are $4! = 24$ different permutations of those four pairs of spin flips that we need to sum over. For eight of the 24 terms the first two spin flips occur on opposite edges. They yield a sequence of intermediate virtual states with higher energy then the other terms since, after the two pairs of spin flips four bonds are broken. We label this class of terms by the number of broken bonds in the sequence of intermediate states, i.e., $(2, 4, 2)$. Terms where the two first pairs of spin flips occur on neighboring bonds are labeled by $(2, 2, 2)$. Also note, that pairs of spin flips on neighboring bonds anticommute and the 16 $(2, 2, 2)$-terms split into two halves with opposite sign which cancel each other and we are left with

$$H_{\text{eff}}^{(4)} = -8\frac{J_y^2 J_x^2}{4 \cdot 8 \cdot 4 J_z^3} \sum_p Q_p \,, \tag{6.17}$$

where the plaquette operator $Q_p = \hat{x}\,\hat{y}\,\hat{z}\,\hat{x}\,\hat{y}\,\hat{z}$ and the product is meant to follow the vertices in one plaquette in clockwise direction. If we regard the spin pairs along the z-edges as a single logical qubit with states $|\bar{0}\rangle = |00\rangle$, $|\bar{1}\rangle = |11\rangle$ we can identify the operator $\hat{x}\hat{y}$ as well as $\hat{y}\hat{x}$ acting on the two qubits of the spin pair with a logical y-operator $\hat{Y}$ acting on the logical qubit. Also, the operators $\hat{z}\mathbb{1}$ and $\mathbb{1}\hat{z}$ can be identified with the logical $\hat{Z}$ operator. The logical qubits occupy a square lattice and the plaquette operators assume the form $Q_p' = \hat{Y}\hat{Z}\hat{Y}\hat{Z}$. Applying a local unitary basis transformation (spin rotation) results in plaquette operators $\hat{Y}\hat{Y}\hat{Y}\hat{Y}$ and $\hat{Z}\hat{Z}\hat{Z}\hat{Z}$ on every other plaquette and we can identify the the two different plaquette types with the usual star and vertex operators of the toric code.

This example is instructive in several aspects. First, we see how the local ground state spaces can be identified with logical qubits on which the effective Hamiltonian can be defined. Second, the analysis of the perturbation expansion reveals that non-trivial terms correspond to closed paths of operator products. This mechanism will be encountered again in the following examples.

6.1.2. Bloch method and Jordan–Farhi gadgets

Among the various gadget ideas [92, 94, 251–253], the gadget construction by Jordan and Farhi [93] is of particular conceptual simplicity. We briefly review this method following the original reference [93].

The starting point is again a Hamiltonian $H = H_0 + V$ which is designed such that the effective Hamiltonian H_{eff} reproduces a certain target Hamiltonian H_T. Considering a general k-local qubit Hamiltonian H_T acting on n qubits we can decompose it into a sum of Pauli products

$$H_T = \sum_{s=1}^{r} c_s \sigma_{s,1} \ldots \sigma_{s,k} \tag{6.18}$$

where

$$\sigma_{s,j} = \alpha_{s,j}\hat{x}_j + \beta_{s,j}\hat{y}_j + \gamma_{s,j}\hat{z}_j \tag{6.19}$$

and $\alpha, \beta, \gamma \in \mathbb{R}$ with $\alpha^2 + \beta^2 + \gamma^2 = 1$, i.e., $\sigma_{s,j}$ is normalized. One could also restrict to the case, where $\sigma_{s,j}$ is one of the three Pauli matrices and not allow to use linear combinations of Pauli matrices. However, this might increase the number of addends r.

The following 2-local Hamiltonian can be used to simulate H_T. For each s-term in the sum, we use k auxiliary qubits, that are coupled strongly with z-z-interactions among each other or put in different words, projected pairwise to the even parity subspace,

$$H_0 = \sum_{s=1}^{r} \sum_{1 \le i < j \le k} \frac{1}{2}(\mathbb{1} - \hat{z}_{i,r}\hat{z}_{j,r}) \, . \tag{6.20}$$

The ground state space of H_0 is characterized by r clusters each containing k spins which are aligned, i.e., we can again think of r logical qubits with $|\bar{0}\rangle = |0 \dots 0\rangle$ and $|\bar{1}\rangle = |1 \dots 1\rangle$ that each consist of k individual qubits.

Next we define the perturbations V. To every auxiliary qubit in a given cluster, we associate one physical qubit – "physical" meaning the qubits on which H_T is eventually simulated – and define an interaction that simultaneously flips the auxiliary qubit while acting with $\sigma_{s,j}$ on the physical qubit , i.e.,

$$V = \sum_{s=1}^{r} \left(c_s \sigma_{s,1} \otimes \hat{x}_{s,1} + \sum_{j=2}^{k} \sigma_{s,j} \otimes \hat{x}_{s,j} \right) \, , \tag{6.21}$$

here the explicit use of the tensor product symbol indicates the separation between the physical and the auxiliary qubit and we have associated the proportionality factor c_s to one specific auxiliary/physical qubit pair. We now consider the Hamiltonian $H = H_0 + \epsilon V$.

Regardless of the specific method employed to obtain the low-energy effective theory the intuition behind the gadget construction is as follows. Each term of V flips one auxiliary spin. As the auxiliary qubits within one cluster are coupled ferromagnetically this operation is heavily penalized. Only a repeated application of spin flips or a product of spin flips acting on all auxiliary qubits of a given cluster can restore the ground state configuration. In the latter case the operators $\sigma_{s,1} \dots \sigma_{s,k}$ are simultaneously applied to the physical qubits, generating the addends of the target Hamiltonian up to proportionality. If the auxiliary qubits are initialized in the state $|\bar{+}\rangle = |\bar{0}\rangle + |\bar{1}\rangle$, the collective spin flip leaves the state of the auxiliary qubits unchanged and thus the auxiliary qubits and physical qubits remain unentangled. In essence, we expect to encounter a global energy shift due to flipping the same spins back and forth at second order and a Hamiltonian proportional to the target Hamiltonian in k-th order.

We now confirm this expectation analyzing the Hamiltonian H with the so called Bloch method named after French physicist Claude Bloch [256]. Here, the key idea is to consider the rotation

$$\mathcal{U} : \mathcal{E}_0 \to \mathcal{E} \tag{6.22}$$

from the ground state space of H_0 to the low-energy subspace of H. With that we can construct the operator

$$\mathcal{A} = \epsilon P_0 V \mathcal{U} \tag{6.23}$$

which yields the low-energy spectrum of H. To see this, denote the eigenstates of H at energy E_j by $|\Psi_j\rangle$ and their projections onto $\mathcal{E}_0$ by $|\alpha_j\rangle = P_0 |\Psi_j\rangle$. The rotation $\mathcal{U}$ is defined by $\mathcal{U}|\alpha_j\rangle = |\Psi_j\rangle$. Now a direct calculation shows that $|\alpha_j\rangle$ are the right eigenvectors of $\mathcal{A}$ at energies E_j

$$\mathcal{A}|\alpha_j\rangle = \epsilon P_0 V \mathcal{U} |\alpha_j\rangle = P_0(H - H_0)|\Psi_j\rangle = P_0 H |\Psi_j\rangle = E_j |\alpha_j\rangle \, .$$

Note, that $\mathcal{A}$ is not Hermitian and thus we need to specify to right-eigenvectors. We can now conjugate $\mathcal{A}$ by $\mathcal{U}$ to obtain an "effective Hamiltonian"

$$H_{\text{eff}} = \mathcal{U}\mathcal{A}\mathcal{U}^{-1} \,. \tag{6.24}$$

We put quotation marks to indicate that this operator is in general not Hermitian and thus should not be called a Hamiltonian. The expression Eq. (6.24) is meaningless unless we now the rotation $\mathcal{U}$. However, finding $\mathcal{U}$ exactly is as hard as diagonalizing H. Instead, we can derive an equation for $\mathcal{U}$ which can be expanded in orders of ϵ. Comparing terms order by order yields a recursive definition of the m-th order term and we can explicitly construct a series expansion for $\mathcal{U}$. The starting point is the equality

$$\mathcal{U} = P_0 - \frac{1}{H_0} Q_0 (\epsilon V \mathcal{U} - \mathcal{U}\epsilon V \mathcal{U}) \tag{6.25}$$

which can be derived in a straightforward fashion from the definitions given here[3]. The recursive definition of $\mathcal{U}^{(m)}$ is found to be

$$\mathcal{U}^{(0)} = P_0 \tag{6.26}$$

and

$$\mathcal{U}^{(m)} = S_1 \left[\epsilon V \mathcal{U}^{(m-1)} - \sum_{p=1}^{m-1} \mathcal{U}^{(p)} \epsilon V \mathcal{U}^{(m-p-1)} \right] \,, \tag{6.27}$$

where we have introduced

$$S_l = \begin{cases} \frac{Q_0}{-H_0^l} & l > 0 \,, \\ -P_0 & l = 0 \,. \end{cases} \tag{6.28}$$

The solution

$$\mathcal{U}^{(m)} = \epsilon^m \sum_{l_1,\ldots,l_m} S_{l_1} V S_{l_2} V \ldots S_{l_m} V P_0 \,, \tag{6.29}$$

where the sum is restricted to $l_1 + \ldots + l_p \geq p \; \forall 1 \leq p \leq m-1$ and $l_1 + \ldots + l_m = m$ can be proven by induction. The convergence of the series is guaranteed if $||\epsilon V|| < \frac{\Delta}{4}$ as is shown in Ref. [93, Appendix B]. Though this bound might seem generous at first sight, note that in the setting considered, the gap is constant in the system size while the operator norm of the perturbation grows linear with the system size and we need to scale ϵ with $1/N$.

From the series expansion of $\mathcal{U}$ we readily obtain a series expansion for $\mathcal{A}$

$$\mathcal{A}^{(m)} = \epsilon^m P_0 \sum_{l_1,\ldots,l_{m-1}} V S_{l_1} V S_{l_2} V \ldots S_{l_{m-1}} V P_0 \,, \tag{6.30}$$

where now the sum is restricted to

$$l_1 \geq 1 \,, l_1 + l_2 \geq 2 \,, \ldots \,, l_1 + \ldots l_{m-1} \geq m-1 \,, \tag{6.31}$$

and

$$l_1 + \ldots + l_{m-1} = m - 1 \,. \tag{6.32}$$

Note, that each term $A^{(m)}$ starts and ends with a ground state projection just as it was the case for the effective Hamiltonian obtained via the self-energy approximation. We can conclude at this state that for the gadget Hamiltonian we have

$$\mathcal{A} = c_0 P_0 + \mathcal{A}^{(k)} + \mathcal{O}(\epsilon^{k+1}) \,, \tag{6.33}$$

[3]For an explicit calculation we refer to Appendix A of [93]

i.e., $\mathcal{A}$ consists of terms proportional to the ground state projector which will result in a global energy shift that arises from contributions with $i < k$ that cannot have a non-trivial effect on the physical Hamiltonian and the non-trivial terms arising from collectively flipping all k auxiliary spins in one cluster. Consider the k-th order term. If one or more of the summation indices are zero, the product contains factors $S_0 \propto P_0$ which trivialize the operator, i.e., either it vanishes or it is proportional to P_0, since non-trivial terms of the form $P_0 \dots P_0$ can only be generated by k factors of V. If none of the $l_1, \dots, l_{m-1}$ is equal to zero, Eq. (6.32) implies $l_1 = l_2 = \dots = l_{m-1} = 1$ and we obtain

$$A^{(k)} = \epsilon^k P_0 \left(V \frac{Q_0}{-H_0} \right)^{k-1} V P_0 \, . \tag{6.34}$$

This result coincides with the k-th order of the effective Hamiltonian obtained from the self-energy approximation. Indeed, calculating $H_{\text{eff}} = \mathcal{U}\mathcal{A}\mathcal{U}^{-1}$ we find

$$H_{\text{eff}} = \mathcal{U} c_0 P_0 \mathcal{U}^{-1} + \mathcal{U} A^{(k)} \mathcal{U}^{-1} + \mathcal{O}(\epsilon^{k+1}) \, . \tag{6.35}$$

Using that $\mathcal{U} P_0 \mathcal{U}^{-1} = \Pi$ is nothing but the energy shift and $\mathcal{U} = P_0 + \mathcal{O}(\epsilon)$ we obtain in lowest non-trivial order

$$H_{\text{eff}} = \Pi + A^{(k)} + \mathcal{O}(\epsilon^{k+1}) \, , \tag{6.36}$$

which confirms that the first non-trivial order of the Hamiltonian obtained via the self-energy approximation and the Hamiltonian obtained via the Bloch method agree for this construction.

We now evaluate $\mathcal{A}^{(k)}$ explicitly. There are $k!$ addends that all contribute to the term for one cluster, i.e., the number of different permutations of applying individual spin flips. Since all terms commute and the set-up is perfectly symmetric, we can calculate one specific sequence and multiply the result by $k!$. The energy in the denominator is calculated as follows. After applying the first perturbation, i.e., flipping one spin in the k-cluster, $(k-1)$ bonds are frustrated. Flipping a second spin heals one bond (the one between the first flipped spin and the second flipped spin) and adds $(k-2)$ broken bonds, such that we have $2(k-2)$ broken bonds. Iterating this, we obtain for the energy denominator

$$(-1)^{k-1} \prod_{j}^{k-1} \frac{1}{-j(k-j)} = \frac{(-1)^{k-1}}{((k-1)!)^2} \, , \tag{6.37}$$

and finally arrive at

$$\mathcal{A}^{(k)} = \frac{-k(-\epsilon)^k}{(k-1)!} \sum_s c_s \sigma_{s,1} \dots \sigma_{s,k} \otimes \hat{x}_{s,1} \dots \hat{x}_{s,k} \, . \tag{6.38}$$

Using that the auxiliary registers are initialized in the $|\bar{+}\rangle$ state we obtain for the effective Hamiltonian (with traced out auxiliary qubits)

$$H_{\text{eff}} \simeq \Pi + \frac{-k(-\epsilon)^k}{(k-1)!} H_T + \mathcal{O}(\epsilon^{k+1}) \, , \tag{6.39}$$

i.e., the effective Hamiltonian is proportional to the target Hamiltonian up to higher order corrections.

This makes the Jordan–Farhi gadget construction a very powerful tool for designing or simulating general k-local qubit Hamiltonians. However, the number of auxiliary qubits is kr, where r is the number of linearly independent Pauli-words of length k in which the target

Hamilton has been decomposed. This number can be very large. A general Hermitian operator acting on k qubits can be decomposed in slightly less than 4^k Pauli-words, where 4 is the number of local basis vectors, i.e., $\mathbb{1}, \hat{x}, \hat{y}, \hat{z}$ and "slightly less" means that a few addends can always be grouped together as in e.g. $a\hat{x}\hat{x} + b\hat{x}\hat{y} = \alpha\hat{x}(\beta\hat{x} + \sqrt{1-\beta^2}\hat{y})$, however a simple parameter counting shows that this approach is limited to a number that scales only linear with k. Thus using the Jordan–Farhi gadget requires approximately $k4^k$ auxiliary qubits.

6.1.3. The Schrieffer–Wolff method

The Schrieffer–Wolff (SW) method [254, 257] is the most advanced technique to analyze low-energy effective theories and will be reviewed here closely following Ref. [254]. In contrast to the self-energy approximation it does not rely on an assumption that is in general hard to check, namely that the self-energy $\Sigma(z)$ does not depend strongly on z. Though it is conceptually related to the Bloch method and also relies on a suitable rotation between the low-energy subspaces, it does not suffer from the inconvenience that non Hermitian operators are used to define the effective Hamiltonian. Instead a unitary rotation $U = \exp(S)$ is used to transform the Hamiltonian H to a Hamiltonian that is block diagonal with respect to $\mathcal{E}_0$ and $\mathcal{E}_0^\perp$. Projecting this Hamiltonian to the low-energy subspace yields the effective Hamiltonian

$$H_{\text{eff}} = P_0 e^S (H_0 + \epsilon V) e^{-S} P_0 \,. \tag{6.40}$$

Perhaps the most significant drawback of the SW technique is that the series expansion obtained for the generator of the rotation S is quite cumbersome and thus also the series expansion of the effective Hamiltonian has a structure more complicated than that of the effective Hamiltonian obtained via the self-energy approximation.

The rotation U is constructed via a double reflection

$$U = \sqrt{R_{\mathcal{E}_0} R_{\mathcal{E}}} \tag{6.41}$$

where the projector onto a space $\mathcal{V}$ is denoted by $P_{\mathcal{V}}$ and

$$R_{\mathcal{V}} = 2P_{\mathcal{V}} - \mathbb{1} \tag{6.42}$$

can be understood in analogy to a double reflection applied to vectors in $\mathbb{R}^2$, i.e., a reflection along the direction of one vector a followed by the reflection along the direction of another vector b leads to a rotation of $2\angle(a,b)$. It can be proven [254] that the $\sqrt{\ }$ operation is well defined if no vector in $\mathcal{E}_0$ is orthogonal to $\mathcal{E}$ and vice versa and that the latter condition is satisfied for small enough perturbations, i.e., if $\epsilon||V|| < \Delta/2$. The rotation U is also called *direct or minimal rotation* as it is the rotation which differs least from the identity (in Frobenius norm) among all rotations V fulfilling $VPV^\dagger = P_0$.

The generator S is anti-Hermitian and block-off diagonal with respect to both $\mathcal{E}, \mathcal{E}^\perp$ and $\mathcal{E}_0, \mathcal{E}_0^\perp$ which allows to derive an expression for the transformed Hamiltonian from which a series expansion of S can be obtained. Referring for the details to Ref. [254] one finds the non-trivial relation

$$S = \mathcal{L}\hat{S}(\epsilon V_{\text{d}}) + \mathcal{L}\hat{S}\coth(\hat{S})(\epsilon V_{\text{od}}) \,, \tag{6.43}$$

where we have introduced the following short-hand notation for the diagonal and off-diagonal part of the perturbation

$$V_{\text{d}} = P_0 V P_0 + Q_0 V Q_0 \,, \qquad V_{\text{od}} = Q_0 V P_0 + P_0 V Q_0 \,, \tag{6.44}$$

and the superoperators $\hat{S}, \mathcal{L}$ defined as $\hat{O}(A) = [O, A]$ and

$$\mathcal{L}(A) = \sum_{i,j} \frac{\langle i|P_0 A Q_0 + Q_0 A P_0|j\rangle}{E_i - E_j} |i\rangle \langle j| \ , \qquad \text{with} \qquad H_0 |i\rangle = E_i |i\rangle \ . \tag{6.45}$$

The superoperator $\mathcal{L}$ "projects" the operator A to its off-diagonal part and assigns to each matrix element A_{ij} the inverse energy difference of the states $|i\rangle$ and $|j\rangle$ (the states before and after transition).

From Eq. (6.43) we can derive a series expansion of S with the ansatz $S = \sum_n S_n \epsilon^n$ and finally obtain a series expansion for the effective Hamiltonian

$$H_{\text{eff}} = H_0 P_0 + \epsilon P_0 V P_0 + \sum_{n=2}^{\infty} \epsilon^n H_{\text{eff},n} \ . \tag{6.46}$$

Again we refer for further details of the derivation to Ref. [254]. The effective Hamiltonian at orders higher than two has a rather complicated structure of nested commutators, i.e.,

$$H_{\text{eff},n} = \sum_{j \geq 1} b_{2j-1} P_0 W_{2j-1}^{(n-1)} P_0 \ , \tag{6.47}$$

where

$$W_k^{(n)} = \sum_{\substack{j_1 + j_2 + \ldots + j_k = n \\ j_1, j_2, \ldots \geq 1}} [S_{j_1}, [S_{j_2}, [\ldots, [S_{j_k}, V_{\text{od}}] \ldots]]] \tag{6.48}$$

with the property that $W_r^q = 0$ if $q < r$ and the coefficients of the expansion of S are given recursively as

$$S_1 = \mathcal{L}(V_{\text{od}}) \tag{6.49}$$

$$S_n = \mathcal{L}\left([S_{n-1}, V_d]\right) + \sum_{j \geq 1}^{\lfloor \frac{n-1}{2} \rfloor} a_{2j} \mathcal{L} W_{2j}^{(n-1)} \tag{6.50}$$

and $a_n = 2^n B_n / n!$, $b_{2j-1} = \frac{2(2^{2j}-1) B_{2j}}{(2j)!}$ are numerical prefactors defined in terms of the Bernoulli numbers B_n.

The expression stated here is general in the sense that we did not yet make use of the fact that $\mathcal{E}_0$ is fully degenerate with a single eigenvalue $E_0 = 0$ and the perturbation takes the system out of $\mathcal{E}_0$, i.e., $P_0 V P_0 = 0$. Using these simplifications we obtain a more comprehensible expression for H_{eff}.

First, note that the superoperator $\mathcal{L}$ is simplified to

$$\mathcal{L}(A) = P_0 A \frac{Q_0}{-H_0} - \frac{Q_0}{-H_0} A P_0 \tag{6.51}$$

and thus

$$S_1 = P_0 V \frac{Q_0}{-H_0} - \frac{Q_0}{-H_0} V P_0 \tag{6.52}$$

$$S_2 = P_0 V \frac{Q_0}{-H_0} V \frac{Q_0}{-H_0} - \frac{Q_0}{-H_0} V \frac{Q_0}{-H_0} V P_0 \ . \tag{6.53}$$

We find that

$$W_1^1 = [S_1, V_{\text{od}}] = 2 P_0 V \frac{Q_0}{-H_0} V P_0 - \frac{Q_0}{-H_0} V P_0 V Q_0 - Q_0 V P_0 V \frac{Q_0}{-H_0} \tag{6.54}$$

and thus

$$H_{\text{eff},2} = b_1 P_0 W_1^1 P_0 = P_0 V \frac{Q_0}{-H_0} V P_0 \,, \tag{6.55}$$

the result we already obtained via the self-energy approximation. Also in third order we obtain

$$W_1^2 = [S_2, V_{\text{od}}] = 2P_0 V \frac{Q_0}{-H_0} V \frac{Q_0}{-H_0} V P_0 - \frac{Q_0}{-H_0} V \frac{Q_0}{-H_0} V P_0 V Q_0 - Q_0 V P_0 V \frac{Q_0}{-H_0} V \frac{Q_0}{-H_0} \tag{6.56}$$

and thus

$$H_{\text{eff},3} = b_1 P_0 W_1^2 P_0 = P_0 V \frac{Q_0}{-H_0} V \frac{Q_0}{-H_0} V P_0 \,, \tag{6.57}$$

again in agreement with the self-energy approximation. The first (potential) disagreement occurs in fourth order where we find that S_3 deviates from the pattern of S_1 and S_2 and contains also addends with single factors of $Q_0/(-H_0)^2$. The expressions for $W_1^3 = [S_3, V_{\text{od}}]$ and $W_3^3 = [S_1, [S_1, [S_1, V_{\text{od}}]]]$ also show these kind of terms. They are calculated in a straight forward fashion, but are rather lengthy and thus are not stated here. We eventually find

$$\begin{aligned} H_{\text{eff},4} &= b_1 P_0 W_1^3 + b_3 P_0 W_3^3 \\ &= P_0 V \frac{Q_0}{-H_0} V \frac{Q_0}{-H_0} V P_0 - \frac{1}{2} P_0 V \frac{Q_0}{H_0^2} V P_0 V \frac{Q_0}{-H_0} V P_0 - \frac{1}{2} P_0 V \frac{Q_0}{-H_0} V P_0 V \frac{Q_0}{H_0^2} V P_0 \,. \end{aligned} \tag{6.58}$$

This Hamiltonian contains terms with intermediate P_0 in the product compensated by a power of $1/H_0^2$ at another position in the product. In more physical terms, the system returns to the ground state space for some intermediate virtual state. Those contributions are absent from the effective Hamiltonian obtained via the self-energy approximation method. Note however, that these terms are either subleading or vanishing. If they are not vanishing, they must have already occurred at second order and thus the fourth order is not the leading order. Similar arguments can be made if the first non-vanishing contribution occurs at higher orders. As a matter of fact the leading order will never contain terms with intermediate virtual ground states. Thus, we conclude that the self-energy approximation coincides with the more advanced SW result in leading order.

6.1.4. Perturbative parent Hamiltonians

Tailored to parent Hamiltonians of PEPS (cf. Section 2.3.2 and 2.3.3) which fulfill some additional constraints discussed below, the perturbative PEPS parent construction proposed by Brell et al. [95] gives a recipe how to construct a Hamiltonian

$$H = H_0 + \epsilon V \tag{6.59}$$

whose effective low-energy Hamiltonian H_{eff} obtained by the Schrieffer–Wolff (SW) method is a parent Hamiltonian for an encoded version of a given projected entangled pair state (PEPS). It plays a prominent role in the design of string-net phases in Section 6.3 and is thus reviewed in greater detail closely following the original reference by Brell et al. [95].

Encoded PEPS and encoded parent Hamiltonian

The effective Hamiltonian in the perturbative PEPS parent construction is not the parent Hamiltonian itself, but an *encoded* version thereof. To apply the construction it is thus required that the PEPS map A is a (partial) isometry on the virtual subspace, i.e., $A^\dagger A = P$ where P is a

Hermitian projector. With that we can use the following encoding. Consider a conventional PEPS obtained by placing maximally entangled pairs of virtual qudits on the edges of some lattice and applying the PEPS map $A : V_{\text{virt}} \to V_{\text{phys}}$ on all vertices of the lattice, i.e.,

$$|\Psi\rangle_{\text{phys}} = \prod_v A_v \prod_e |\text{Bell}\rangle_e \ . \tag{6.60}$$

We obtain the *encoded* PEPS by applying the pseudo-inverse $A^\dagger : V_{\text{phys}} \to V_{\text{virt}}$ on all vertices

$$|\Psi\rangle_{\text{virt}} = \prod_v A_v^\dagger |\Psi\rangle_{\text{phys}} = \prod P_v \prod_e |\text{Bell}\rangle_e \ . \tag{6.61}$$

Note, that the encoded PEPS is equivalent to the original PEPS since we can restrict the physical space to the local images of A on which we have $AA^\dagger = \mathbb{1}$ and thus we can apply the PEPS map A again locally at every site to obtain the original PEPS from the encoded one. For this reason the projector P is called the code space projector, since for all virtual states in the code space $\mathcal{V}$ defined by $P\mathcal{V} = \mathcal{V}$, we have a one-to-one correspondence between the virtual and the physical states while states in $\mathcal{V}^\perp$ do not get mapped to any physical states.

Two other properties are needed for the construction: quasi-injectivity and a gapped canonical parent Hamiltonian. Here, we review the perturbative PEPS parent construction only for the case of MPO-isometric PEPS which fulfill both of the criteria above [95]. For MPO-isometric PEPS (cf. Section 5.2.3 and Eq. (5.28)) the canonical parent Hamiltonian

$$H_{\text{phys}} = \sum_p A_p A_p^\dagger \ , \tag{6.62}$$

is gapped and the gap is not affected by applying the pseudo inverses $A^\dagger$ locally. Thus, also the encoded PEPS has a gapped canonical parent Hamiltonian

$$H_{\text{virt}} = \prod_v A_v^\dagger \left(\sum_p A_p A_p^\dagger \right) \prod_v A_v = \sum_p Q'_p \ , \tag{6.63}$$

where

$$Q'_p = \prod_{v \in p} A_v^\dagger \left(A_p A_p^\dagger \right) A_v \ , \tag{6.64}$$

and we recall that A_p is the PEPS mapped obtained from blocking the PEPS maps A around a full plaquette p.

The last property required is so-called quasi-injectivity. This is a formal criterion defined in Ref. [95] stating that the PEPS is the simultaneous eigenstate of several operators Y_i at their highest eigenvalue. While we refer for the general definition to the original work by Brell et al., we observe that for MPO-isometric PEPS quasi-injectivity is fulfilled and the Y_i are simply given by the Q'_p.

Effective Hamiltonian

We will now explain how the effective low energy description of the Hamiltonian

$$H = H_0 + \epsilon V \tag{6.65}$$

yields an effective Hamiltonian that is in the same phase as the encoded parent Hamiltonian. Here,

$$H_0 = \sum_v (1 - P_v) \tag{6.66}$$

is the sum of all local code space projectors applied at all vertices of the lattice and the perturbation

$$V = \sum_e |\text{Bell}\rangle \langle \text{Brell}|_e \tag{6.67}$$

consists of all local Bell-pair projections along the edges of the lattice To get an intuitive understanding of this fact first note that the ground state projector P_0 is given by the product of all code space projectors, i.e.,

$$P_0 = \prod_v P_v \tag{6.68}$$

and thus the effective Hamiltonian acts within the code space only. Also, note that the n-th order effective Hamiltonian obtained via the SW method is a sum of terms with the following structure

$$P_0 V G_{i_1} V G_{i_2} \dots G_{i_{n-1}} V P_0 \,, \tag{6.69}$$

where $i_1, \dots, i_{n-1} \geq 0$, $i_1 + \dots + i_{n-1} = n-1$ and

$$G_i = \begin{cases} P_0 & i = 0 \,, \\ \frac{Q_0}{(-H_0)^i} & i \geq 1 \,. \end{cases} \tag{6.70}$$

We neglect the G_i for a second and evaluate

$$P_0 V^n P_0 = \prod_v P_v \left(\sum_e |\text{Bell}\rangle \langle \text{Bell}|_e \right)^n P_v = \prod_v P_v \sum_R c_R \prod_{e \in R} |\text{Bell}\rangle \langle \text{Bell}|_e \, P_v \,, \tag{6.71}$$

where R denotes a collection of up to n Bell-pairs, which can be pictured as some region R and c_R are numerical coefficients. It is instructive to consider a collection of Bell-pair projections inside a connected region R sandwiched by code space projections (cf. Fig. 6.2). Writing the code space projections as $P_v = A^\dagger A$ we realize that the Bell-pair projections inside the region have the effect of contracting or blocking the PEPS maps A and their counterparts and thus

$$\prod_v P_v \prod_{e \in R} |\text{Bell}\rangle \langle \text{Bell}|_e \, P_v = \prod_v A_v^\dagger A_R A_R^\dagger A_v \,. \tag{6.72}$$

If the region R is large enough in the sense that $A_R A_R^\dagger = Q_p$, we can identify the term emerging on the right-hand side of Eq. (6.72) as the encoded local Hamiltonian term Q_p'. In the case of general string-net PEPS the region R_p corresponds to one full plaquette consisting of 18 Bell-pair projection edges, i.e.,

$$\prod_v P_v \prod_{e \in R_p} |\text{Bell}\rangle \langle \text{Bell}|_e \, P_v = Q_p' \,. \tag{6.73}$$

From these considerations it is clear how the encoded Hamiltonian appears in the series expansion of H_{eff}. The situation is simplified significantly if $P_0 V P_0 = 0$, since then we can evaluate $P_0 V Q_0 V P_0 = P_0 V (1 - P_0) V P_0 = P_0 V^2 P_0$ and the G_i reduce to numerical prefactors in low orders. Also at higher orders we can always express Q_0 as $(1 - P_0)$ and obtain the desired Hamiltonian at some finite order. The main problem is to ensure that the Q_p' terms are the dominant contribution, i.e., lower order terms vanish or "project" into a space that contains the ground state space of H_{virt} and higher order contributions can be regarded as small perturbations that do not drive the system towards a phase transition. We will illustrate that both of these conditions are fulfilled on the example of the double semion model in the next Section. For the full and general proof that the effective Hamiltonian is in the same phase as

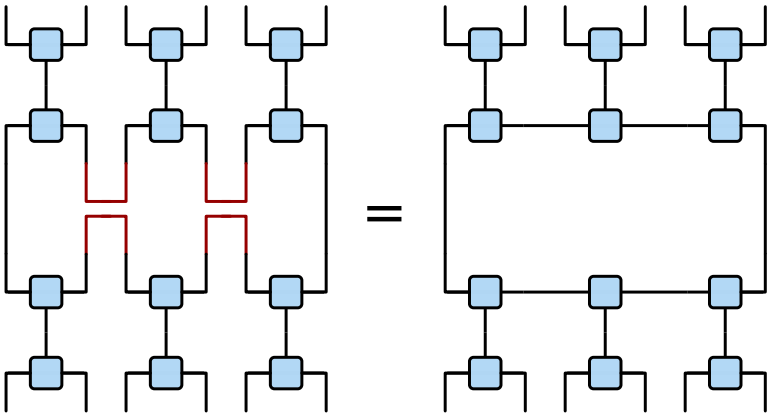

Fig. 6.2. ⋆ A one-dimensional version of Bell-pair projections sandwiched by code space projections which yields a blocking of the PEPS maps in a virtual encoding.

H_{virt} we refer to the original work by Brell et al. [95] and only summarize the proof technique used there in words.

Similar to our considerations provided to get a preliminary and intuitive understanding of the effective Hamiltonian, the proof in Ref. [95] also starts out with highlighting a particular contribution to the perturbation expansion that occurs at some finite order. It is then argued that this contribution corresponds to a sum of operators Y_i, which stabilize the PEPS (as a consequence of quasi-injectivity) and that this term can indeed be considered the dominant contribution. The proof proceeds with showing that the higher order contributions of the perturbation expansion can be considered as a small perturbation to the finite order Hamiltonian which do not change the phase of the Hamiltonian. The latter is achieved by invoking the stability of topological ordered states, i.e., the well known fact that Hamiltonians possessing the formal property of local topological quantum order (LTQO) [168–170] are stable against small local perturbations. To ensure that all higher order terms can indeed be regarded as local perturbations a local version of the SW method is used and it is shown that the effective Hamiltonian obtained via global SW is in the same phase as the effective Hamiltonian obtained via local SW.

Double semion parent Hamiltonian

As the simplest example of an MPO-isometric PEPS we consider the double semion ground state (cf. Section 5.3). The perturbative PEPS parent Hamiltonian consists of the code space projectors acting on six qubits located in a triangle around each vertex and is a matrix product operator of bond dimension two. The Bell-pair projections act on all edges and there are two parallel edges connecting each pair of vertex triangles (cf. Fig. 6.3.). To analyze the perturbation expansion first note that we have $P_0 V P_0 = 0$ which follows from the fact that sandwiching a single Bell-pair projection between code space projectors evaluates to zero. To see this, we explicitly calculate the code space projector from the PEPS map given as e.g. in Ref. [95]

$$\hat{P}_{v,DS} = \frac{1}{2}(\hat{P}_c + \hat{X}) \,, \tag{6.74}$$

here $\hat{P}_c = \sum_{a,b,c} |a,a,b,b,c,c\rangle \langle a,a,b,b,c,c|$ projects from the 2^6-dimensional space $\otimes^6 V$ of general states, $|a,a',b,b',c,c'\rangle$, onto the 2^3-dimensional space of pairwise even-parity states

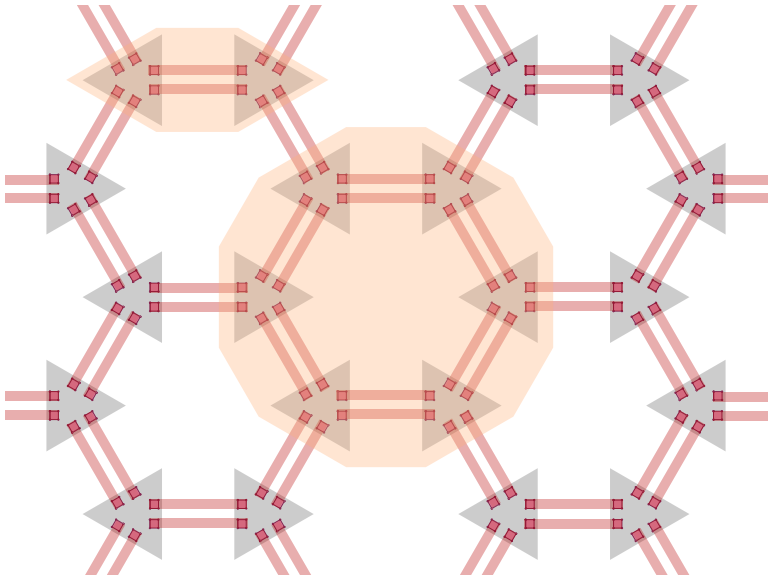

Fig. 6.3. ⋆ The perturbative PEPS parent of the double semion model with the support of the code space projectors marked by grey triangles and the support of the Bell-pair projections marked by red rectangles. The regions marked in orange correspond to the support of $H^{(2)}_{\text{eff}} \sim P_c$ and $H^{(6)}_{\text{eff}} \sim Q'_p$.

$\simeq \otimes^3 V$ and

$$\hat{X} = \sum_{a,b,c} |a \oplus 1, a \oplus 1, b \oplus 1, b \oplus 1, c \oplus 1, c \oplus 1\rangle \, X_{abc} \\ \langle a, a, b, b, c, c| \tag{6.75}$$

likewise acts in $\otimes^3 V$ where it flips all states and assigns a sign factor

$$X_{abc} = \begin{cases} -1 & a+b+c = 1, 2\,, \\ 1 & \text{otherwise.} \end{cases} \tag{6.76}$$

It is easy to see that a single Pauli operator acting on a single qubit excites the system and thus the first-order term vanishes. As a consequence the first potential non-zero contribution to the perturbation expansion is given by terms in second order where the region of Bell-pair edges consists of the two edges connecting two neighboring vertices

$$H^{(2)}_{\text{eff}} = P_0 V \frac{Q_0}{-H_0} V P_0 \propto P_0 \sum_{v_1, v_2} P_{v_1} P_{v_2} \prod_{e \in R_{v_1} \cup R_{v_2}} |\text{Bell}\rangle \langle \text{Bell}|_e \, P_{v_1} P_{v_2} P_0\,, \tag{6.77}$$

where v_1, v_2 are neighboring vertices and R_v denotes the triangle at v. Using the considerations from the above paragraph and Eq. (6.72) we find

$$H^{(2)}_{\text{eff}} = \sum_{v_1, v_2} P_0 (A^\dagger_{v_1} A^\dagger_{v_2} A_{R_{v_1,v_2}} A^\dagger_{R_{v_1,v_2}} A_{v_1} A_{v_2}) P_0\,. \tag{6.78}$$

The contracted PEPS map $A_{R_{v_1,v_2}}$ is best understood, if we recall that the physical qubits are located at the edges of the triangle tensor. Thus, if we consider two uncontracted neighboring triangle tensors, there are two independent physical qubits for each edge of the hexagonal

lattice. However, those two qubits should in the end correspond to only one physical qubit. This is guaranteed if the tensor network is contracted. It is exactly this contraction which is enforced by the second order terms stated above. Thus, we identify the ground state space of $H_{\text{eff}}^{(2)}$ with the physically consistent space of virtual qubits and denote its projector by $P_{0,c}$

$$H_{\text{eff}}^{(2)} \sim P_{0,c} \, . \tag{6.79}$$

Note, that it is reasonable to evaluate all higher order contributions within the physically consistent subspace as all states orthogonal to the latter will be penalized with an energy that exceeds the energy scale of the higher order contributions arbitrarily in the limit of $\frac{\epsilon}{\Delta} \to 0$.

The third and fifth order contributions vanish just like the first-order contribution, because three or five Bell-pair projections cause isolated spin flips. At fourth order we obtain products of second order terms which further stabilize the space of physical consistent configurations. At sixth order we obtain a term that consists of six Bell-pair projections around one hexagonal loop sandwiched by code space projections. If we evaluate this term in the physically consistent subspace enforced by the second order terms, we obtain the encoded plaquette operator, i.e.,

$$H_{\text{eff}}^{(6)} \sim \sum_p P_{0,c} \prod_{v \in p} (A_v^\dagger A_{R_p} A_{R_p}^\dagger A_v) P_{0,c} = \sum_p Q_p' \, . \tag{6.80}$$

Scaling

We want to conclude this Section by comparing the number of qubits needed to effectively realize a Levin–Wen phase via the perturbative PEPS parent method with the number of qubits needed in the Jordan–Farhi gadget construction. On a hexagonal lattice with N qubits, there are $N_v = \frac{2N}{3}$ vertex operators and $N_p = \frac{N}{3}$ plaquette operators. The vertex operators are 3 local and the plaquette operators are 12 local. The number of individual Pauli words appearing in the decomposition of the vertex and plaquette terms denoted with r_v and r_p, respectively, depends on the model and in general there are more Pauli words needed the more complex the model is. While for the toric code model there is only a single Pauli word per vertex and a single one per plaquette operator, i.e., $r_{v,TC} = r_{p,TC} = 1$ already the plaquette operator of the double semion model has $2^6 = 64$ Pauli words because the phase factor of the plaquette operator depends on the state of the outer spins and we have $r_{v,DS} = 1$, $r_{p,DS} = 64$. For the double Fibonacci model we have seven Pauli words to characterize the vertex operator $r_{v,FB} = 7$ and the Pauli word decomposition of the plaquette operator can not even be calculated naively on a usual desktop machine as it involves 4^{12} multiplications of two $2^{12} \times 2^{12}$ matrices. Recall that we can find a Pauli word decomposition of an operator acting on n sites by calculating $\text{Tr}(\sigma_{i_1 \ldots i_n} A)$, where $\sigma = \sigma_{i_1} \otimes \ldots \otimes \sigma_{i_n}$ for all $i_j = 0, 1, 2, 3$ and σ_k with $k = 0, 1, 2, 3$ labeling the 3 Pauli matrix and the identity matrix. Thus, finding the Pauli word decomposition is a computationally costly problem. A rough estimate of the number of Pauli words of the double Fibonacci plaquette operator can be obtained by realizing that the plaquette operator can be written as a sum of two MPOs, one with bond dimension two, the other with bond dimension three each acting on six sites comprised of two qubits. Thus, we obtain $2^6 + 3^6 = 793$ terms that each correspond to a different Pauli word.

The number of auxiliary qubits used for the Jordan–Farhi gadget constructions is

$$N_A = 3N_v r_v + 12 N_p r_p \tag{6.81}$$

to which the number of physical qubits has to be added, i.e., the total number of qubits is

$$N_{\text{JF}} = N_A + N = N + 2N r_v + 4N r_p \, . \tag{6.82}$$

Inserting the numbers above, we obtain

$$N_{\mathrm{JF}} \begin{cases} = 259N & \text{double semion,} \\ \approx 3187N & \text{double Fibonacci.} \end{cases} \tag{6.83}$$

However, the lower bound is a very conservative estimate and most likely the true value is orders of magnitudes higher.

Assuming that the code space projector of the perturbative PEPS parent approach can be realized without additional gadget constructions, the number of qubits used in this approach equals the number of qubits used to define the code space, which is 6 for the double semion model and 9 for the double Fibonacci model, times the number of vertices of the hexagonal lattice, i.e.,

$$N_{\mathrm{pPEPS}} = N_v N_{\mathrm{code}} = \begin{cases} 4N & \text{double semion,} \\ 6N & \text{double Fibonacci.} \end{cases} \tag{6.84}$$

Thus, the scaling is linear with the system size in both cases. However, while the number of qubits increases moderately with the complexity of the model in the case of the perturbative PEPS parent, the Jordan–Farhi gadget method is not even applicable in a straight forward fashion since already the computation of the Pauli decomposition becomes problematic.

6.2. Majorana Cooper box networks

The next Section follows Ref. [2], which is the work of the author performed in collaboration with together with R. Egger, J. Eisert and A. Altland. Figures are taken directly from Ref. [2].

In the following we will review the theory of Majorana Cooper boxes (MCBs) [89, 90] and how their low-energy state space corresponds to a Hilbert space of qubits. We show how tunnel coupled networks of MCBs [85, 86, 88, 91, 113, 258–260] give rise to an effective low energy theory of interacting spins and how we can book-keep the effective interactions in a comprehensible way. This allows us to identify mechanisms of destructive interference, i.e., conditions under which certain interactions are suppressed. These insights can in turn can be used as design principles to construct small network structures that yield well-controlled effective qubit interactions.

6.2.1. Majorana Cooper box

A Majorana Cooper box (MCB) [89, 90] is a mesoscopic device for which theoretical studies suggest that its low-energy subspace can be identified with one or multiple qubits. The essential idea is to use quantum wires which host Majorana bound states (MBS) at their ends. The charging physics of the full device – consisting of the quantum wires and a normal superconductor – gives rise to a parity constraint on the Majorana modes (corresponding to the MBS) which makes the mapping from Majorana modes to qubits possible. We will briefly review the main concepts of the MCB including the formation of Majorana zero modes in nanowires and refer for further details to Refs. [87, 261, 262].

Much thought has been spent on the question how Majorana modes can appear in condensed matter systems [263–267] and we refer for a recent review on MBS to Ref. [268]. Here, we will only briefly discuss the theoretically proposed emergence of Majorana zero modes in nanowires with strong spin-orbit coupling in a magnetic field placed in proximity to a superconductor.

Readers with a background in quantum information theory might be less familiar with Majorana physics, but know very well that the Kitaev chain [236] exhibits Majorana edge

modes in the topological phase and is used as a toy model for a superconductor of spinless Fermions (so-called p-wave superconductors). While superconductivity occurs frequently in all kinds of materials, the usual pairing term couples Fermions of opposite spin (s-wave pairing). A possible way how one can nevertheless have superconductors of spinless Fermions is to consider mechanism by which effectively spinless Fermionic bands can emerge and to "add" superconductivity by placing the system in proximity to a usual s-wave superconductor. One particular mechanism how a single effective spinless band emerges is in systems with strong intrinsic spin-orbit coupling as for example in InAs or InSb nanowires [267]. The spin-orbit coupling induces a splitting of the two spin-bands with a level crossing at the $k = 0$ point of the Brioullion zone. If now a uniform magnetic field is applied along the wire direction, the additional Zeeman splitting causes the level crossing of the two bands to disappear and a gap is opened around $k = 0$. If the Fermi energy is close to zero, an effective band of spinless Fermions emerges. The superconducting pairing term acting on those effectively spinless Fermions emerges if the nanowire is brought in close contact to a superconductor. This effective Kitaev chain can give rise to Majorana edges modes if it is in the topological phase (i.e., for appropriate parameters). Experimental evidence for the formation of MBS in systems designed as the one sketched above has been reported in Refs. [269–274]. However, it is not yet settled whether the observed phenomena would only occur for MBS or could also be caused by so called Andreev bound states [275–277]. For recent proposals for experiments to distinguish the latter see e.g. Refs. [278–280] and the references therein.

With this general setting in mind we now turn to the physics of the Majorana Cooper boxes following Ref. [2]. An MCB consists of n quantum nanowires fabricated with a superconducting shell such that they fulfill the requirements above and host Majorana edge modes. All n wires are isolated against ground but electrically connected to a superconductor island. A schematic of the setup is shown in Fig. 6.4, where the vertical dark shaded bars indicate the superconductor connected to the horizontal wires. When isolated against ground, systems of this size have small electrostatic capacitance, C, and as a consequence a large electrostatic charging energy, $E_C(N - n_g)^2$, where $E_C := e^2/2C \approx 1$ meV [270], N is the particle number on the MCB and n_g an effective background parameter tunable via side-gate electrodes. The charging effects are sensitive to the number of non-local fermions formed from the Majorana edge modes of the Kitaev wires, $n_\gamma = \sum_{\alpha=1}^{n} n_\alpha$ with $n_\alpha := c_\alpha^\dagger c_\alpha$ and conventional fermion operators $c_\alpha = (\gamma_{2\alpha-1} + i\gamma_{2\alpha})/2$ [281] and the number of Cooper pairs in the superconducting island N_C. The charging Hamiltonian is given by

$$H_C = E_C(N - n_g)^2 \,, \qquad N = 2N_C + N_\gamma \,. \tag{6.85}$$

If the back gate voltage n_g is tuned to a value such that the closest integer, N, is electrostatically favored, a parity constraint emerges as follows [89, 90, 282]. Since Cooper pairs can be created in the superconductor at no energy cost the value of N is only fixed modulo 2. And thus the ground state of the charging Hamiltonian is given by all configurations with an even or odd number of non-local Fermions N_γ depending on whether n_g is an even or odd integer. Expressing this parity constraint in terms of the Majorana modes we obtain

$$\mathcal{P} = \mathrm{i}^n \gamma_1 \dots \gamma_{2n} = \pm 1 \,. \tag{6.86}$$

The even- and odd-parity sectors are separated by a large energy gap due to the charging energy E_C of the box and we can restrict our analysis to the sector where the parity constraint is satisfied.

Due to the parity constraint Eq. (6.86) an MCB with $2n$ spatially localized MBS $\gamma_i = \gamma_i^\dagger$, $i = 1, \dots, 2n$ satisfying the anticommutation relation

$$\{\gamma_{i,a}, \gamma_{j,b}\} = 2\delta_{i,j}\delta_{a,b} \tag{6.87}$$

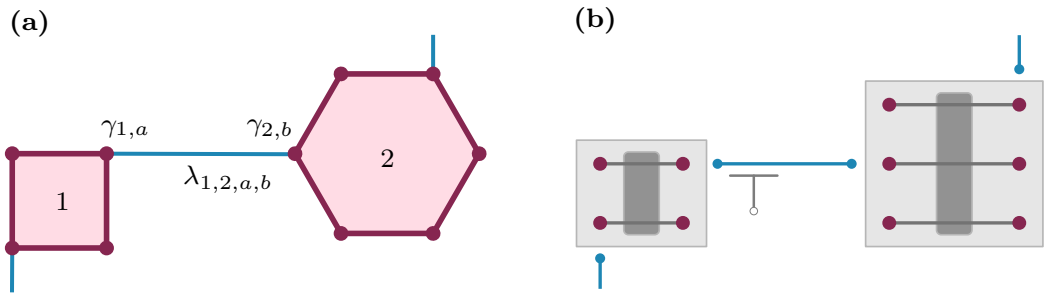

Fig. 6.4. ⋆ (a) Part of a network containing one tetron (MCB 1) and one hexon (MCB 2). In the ground state, each MCB abides in a definite eigenstate of the parity operator (6.86). Individual MBSs of different MCBs are coupled via complex tunneling amplitudes indicated in blue. (b) A somewhat less schematic representation of the same architecture, emphasizing that each MCB is a mesoscopic island comprising n parallel quantum wires proximitized by the same superconductor (shaded vertical structure). Tunneling links between neighboring MCBs are tunable via local gate voltage changes.

gives rise to a 2^{n-1} dimensional Hilbert space that can be interpreted as the Hilbert space of $(n-1)$ qubits. Products of an even number of Majorana operators can be identified with Pauli words acting on the latter. For $n = 2$, i.e., an MCB hosting four MBS called a *tetron* and for $n = 3$, an MCB hosting six MBS called a *hexon*, all Pauli words can be expressed as Majorana bilinears, while for general $2n$ MCBs some Pauli words can only be expressed by products of four or more Majorana operators. This makes tetrons and hexons particularly interesting as building blocks in the scheme to be developed below since the full Hilbert space can be explored only by Majorana bilinears. Bilinears appear quite naturally in single tunneling processes where an electron tunnels into and out of the MCB. In contrast a product of four Majoranas would correspond to two tunneling events that occur simultaneously.

One possible explicit identification of the Majorana modes in a tetron with the Pauli algebra of a qubit [89] is the following

$$\gamma_1\gamma_2 = -\mathrm{i}\hat{x}\,, \qquad \gamma_2\gamma_3 = -\mathrm{i}\hat{y}\,, \qquad \gamma_1\gamma_3 = -\mathrm{i}\hat{z}\,. \tag{6.88}$$

Combinations involving γ_4 are fixed by the parity constraint in Eq. (6.86), $\gamma_1\gamma_2\gamma_3\gamma_4 = 1$. In Fig. 6.5a this identification is visualized. For later reference, we mark one of the Majorana modes with a white dot such that the Fig. 6.5a can be used as a legend in more complicated MCB networks.

Similarly for a hexon [262] we can partition the six Majorana modes into two groups of three and Majorana bilinears formed from only one group correspond to single-qubit Pauli operators on single qubits, cf. Fig. 6.5b. In contrast, bilinears involving MBSs from different groups yield two-qubit operators which follows from the parity constraint. For instance, $\gamma_1\gamma_4 = \mathrm{i}\gamma_2\gamma_3\gamma_5\gamma_6$ and thus equals $-\mathrm{i}\hat{z}\otimes\hat{z}$ as indicated in Fig. 6.5c.

6.2.2. Tunneling Hamiltonian

Next, we consider MCBs tunnel coupled with phase-coherent connectors (e.g., normal-conducting short nanowires), indicated by blue lines in Fig. 6.4. The effective couplings $\lambda_{ij,ab}$ depend on the fabrication process and are not well controlled. However, one can tune their values by a changing the voltage at local side gates as indicated in the bottom panel of Fig. 6.4. In a one-time interferometric calibration procedure that is performed prior to the actual operation

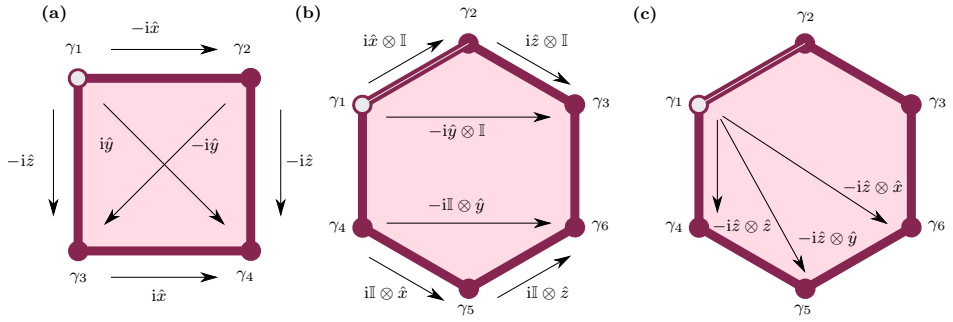

Fig. 6.5. ⋆ Pauli operator representation of Majorana bilinears on tetrons and hexons. Arrows between vertices (i.e., MBSs) identify Majorana bilinears and their associated single- or two-qubit operators. The marking of γ_1 (open circle) indicates our Majorana ordering choice. (a) Single-qubit operators for a tetron. (b) Single-qubit operators for a hexon. (c) Several two-qubit operators for a hexon.

of the system one can thus adjust their values. In particular, adjusting the complex tunneling phase is a powerful mechanism that will be used in the following, cf. Section 6.3.2 and Refs. [87, 261, 262, 281] for the general interferometry calibration protocol.

Crossing wires are difficult to implement in practice, though current fabrication technology does not exclude them in principle [267]. The coupling architectures described in the following try to minimize the number of crossing wires, although they cannot be completely avoided.

It is convenient to work in a charge fractionalized picture where all Majorana fermions are considered charge neutral and charge transferred to MCB i is expressed as $e^{\mathrm{i}\hat{\phi}_i}$ using a number-phase conjugate pair $[\hat{\varphi}_i, \hat{N}_j] = \mathrm{i}\delta_{i,j}$ [90, 281, 283]. We arrive at this fractionalized picture by applying a gauge transformation $c_{i,\alpha} \mapsto c_{i,\alpha} e^{\mathrm{i}\hat{\varphi}_i}$ to the fermion operators of the respective MCB.

Our approach will be based on perturbation theory in the parameters $|\lambda_{ij,ab}|/E_C \ll 1$. Physically, this means that state changes of the system are induced by virtual excitations out of the definite parity ground state sector.

In this formulation the tunneling Hamiltonian assumes the following form

$$\hat{H}_t = \sum_{i,j,a,b} \lambda_{ij,ab} \gamma_{i,a} \gamma_{j,b} e^{\mathrm{i}(\hat{\varphi}_i - \hat{\varphi}_j)} + \text{h.c.}\,, \tag{6.89}$$

where $e^{\mathrm{i}(\hat{\varphi}_i - \hat{\varphi}_j)}$ accounts for the fact that charge is raised/lowered by one unit on MCB i/j. The Hamiltonian of the whole system is given by a sum of all individual MCB Hamiltonians $\hat{H}_0 = E_C \sum_i (\hat{N}_i - n_{g,i})^2$ and the tunneling Hamiltonian

$$\hat{H} = \hat{H}_0 + \hat{H}_t. \tag{6.90}$$

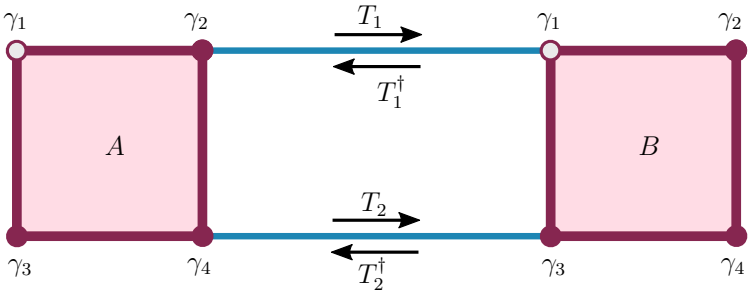

Fig. 6.6. ⋆ Example of a minimal MCB network, cf. Eq. (6.94).

6.2.3. Effective low-energy theory

In general the charging energy defines the largest energy scale of the system, i.e., $|\lambda_{ij,ab}|/E_C \ll 1$ and we can treat the Hamiltonian in Eq. (6.90) perturbatively. We seek to characterize only the low energy behavior of the system and therefore restrict our attention to the processes within the ground state space of $\hat{H}_0$. Note that the action of $\hat{H}_t$ on any element in the ground state space of $\hat{H}_0$ generates an excited state. The task of the perturbative program outlined below is then to identify the relevant virtual ring-exchange processes which take the system through a sequence of excited states and finally back to the ground state space of H_0. We will first present an intuitive picture for this. Each single tunneling process decharges the emitting MCB and charges the receiving MCB. The reverse tunneling process can undo this effect, but it has a trivial effect on the MCBs, acting as an identity operation. However, if a sequence of further tunneling processes transports the charge unit through a closed loop of MCBs back to the emitting box, charge neutrality is reached again. However, now the effect on the MCBs is non-trivial, as it causes a hybridization of all Majorana states visited, i.e., an operator given by a product of the respective Majorana modes.

In the following we show that this intuitive picture can be made more precise by applying a self-energy expansion as in Section 6.1.1. The emerging relevant tunneling processes can than be expressed as products of Pauli operators (Pauli words) acting on the low-energy Hilbert space of the system identified with a tensor product Hilbert space of qubits.

As introduced in Section 6.1.1, we consider the series expansion

$$\hat{H}_{\text{eff}} = \sum_{k=1}^{\infty} \hat{H}^{(k)} , \quad \hat{H}^{(k)} = \hat{P}_0 \left(\hat{H}_t \frac{Q_0}{-\hat{H}_0} \right)^{k-1} \hat{H}_t \hat{P}_0 , \tag{6.91}$$

where $\hat{P}_0$ is the ground-state projector of $\hat{H}_0$.

We find it convenient to represent every individual tunneling operator

$$T_{ij,ab} = \lambda_{ij,ab} \gamma_{i,a} \gamma_{j,b} e^{\mathrm{i}(\hat{\varphi}_i - \hat{\varphi}_j)} \tag{6.92}$$

as a directed arrows from $\gamma_{i,a}$ to $\gamma_{j,b}$ for different MCBs $a \neq b$. The arrow direction indicates the direction of the charge flux and the Hermitian conjugate $T^\dagger_{ij,ab}$ corresponds to the reversed arrow direction, cf. Fig. 6.6. Depicting a product of individual tunneling operators as an arrow pattern, it is easy to see, that charge neutrality now requires an equal number of incoming and outgoing arrows at each MCB. Thus, only hopping patterns that correspond to oriented closed paths contribute to Eq. (6.91) and the effective Hamiltonian is given by a sum over the

latter. Each closed path can be partitioned into a product of loops. If we consider closed paths without self-intersections, i.e., only single loops, we can easily characterize all the contributing terms. There are two possible orientations $d = \pm 1$ of the loop giving rise to a term and its Hermitian conjugate

$$O_+ = O_-^\dagger \ . \tag{6.93}$$

In addition, for a loop of length k, i.e., a loop consisting of k tunneling links and a chosen orientation, there are $k!$ different permutations of the tunneling link segments that each contribute to the expansion Eq. (6.91). Since in general individual T_i operators do neither commute with each other nor with $1/\hat{H}_0$, the summation has to be performed explicitly. We will comment on possible simplifications in the following Sections.

It is important to note, that the contributions from closed paths of length k are weighted by a factor that decays exponentially with k, since each operator $1/\hat{H}_0$ yields a factor of the order of $1/E_C$. Thus, short (and thereby relatively simple paths) dominate the theory and it is not expedient to develop a full analysis of all possible complicated patterns. However, we will briefly remark on self-intersecting closed paths at the end of this Section.

We now analyze Eq. (6.91) for a simple example – a network of two tetrons connected with two parallel wires depicted in Fig. 6.6 where no self-intersecting loops can occur. Using the notation in Fig. 6.6 the tunneling Hamiltonian is given by $\hat{H}_t = T_1 + T_2 + T_1^\dagger + T_2^\dagger$ with the hopping operators

$$T_1 = \lambda \gamma_{2,A}\gamma_{1,B} e^{\mathrm{i}(\hat{\varphi}_A - \hat{\varphi}_B)} \ , \quad T_2 = \kappa \gamma_{4,A}\gamma_{3,B} e^{\mathrm{i}(\hat{\varphi}_A - \hat{\varphi}_B)} \ . \tag{6.94}$$

The effective Hamiltonian is given by the only possible closed loop of length two summing over two possible directions and the possible permutation of $\hat{T}_1$ and $\hat{T}_2$. We obtain

$$\begin{aligned} \hat{H}_{\text{eff}}^{(2)} &= \hat{O}_{1,2,+}^{(2)} + \hat{O}_{2,1,+}^{(2)} + \hat{O}_{1,2,-}^{(2)} + \hat{O}_{2,1,-}^{(2)} \ , \\ \hat{O}_{i,j,+}^{(2)} &= \hat{P}_0 T_i \frac{1}{-\hat{H}_0} T_j^\dagger \hat{P}_0 \ , \end{aligned} \tag{6.95}$$

where the index specifies (s, d). As discussed earlier contributions where hopping occurs back and forth along the same wire, i.e., $\hat{O}_{j,j,\pm}^{(2)}$ are trivial meaning they are proportional to an identity operation and only cause an irrelevant overall energy shift. Thus, they will always be omitted.

From now on we will assume, that the MCBs are operated at the electron-hole symmetric point. In that case both charging or decharging the MCB give rise to a state with energy E_C and we can further evaluate Eq. (6.95) using the identification of Majorana bilinears with Pauli operators in Eq. (6.88) to obtain

$$\hat{O}_{1,2,+}^{(2)} = -\frac{\lambda\kappa^*}{2E_C}\gamma_{2,A}\gamma_{1,B}\gamma_{3,B}\gamma_{4,A} = \frac{\lambda\kappa^*}{2E_C}\hat{z}_A\hat{z}_B \ . \tag{6.96}$$

Note, that for a given loop the Pauli operators are the same up to a numerical prefactor independent of the orientation and the sequence of the hopping operators. We summarize this observation by expressing the operator corresponding to an oriented loop of length k and given operator ordering s by

$$\hat{O}_{s,d}^{(k)} = \mathrm{i}^k A(k, s, d)\hat{Q}^{(k)} \ , \quad \hat{Q}^{(k)} = \hat{q}_1\hat{q}_2\cdots\hat{q}_k \ , \tag{6.97}$$

where $\hat{Q}^{(k)}$ is composed of Pauli operators $\hat{q}_i$ acting on MCB i. The prefactor $A(k, s, d)$ is a product of all tunneling amplitudes of the wire segments that form the loop and the (inverse) excitation energies of all virtual intermediate states. Depending on the sequence, in some intermediate virtual states more than two boxes might be excited at the same time which is why the prefactor is only proportional to $1/E_C^{k-1}$ and not exactly given by $1/(2E_C)^{k-1}$.

6.2.4. Destructive interference mechanisms

The exponential decay of $A(k,s,d)$ with the loop length is important, as it limits the ability to engineer effective qubit operators which act on many qubits simultaneously. In the generic case short loops corresponding to few qubit operators will dominate the effective theory. This is a severe obstacle in the design of topologically ordered fix-point Hamiltonians since they generically require 12-body interactions [12, 119, 172]. We thus discuss two specific mechanisms in the next Section that can lead to the cancellation of specific loop terms. Since the effective Hamiltonian term corresponding to a certain loop $\hat{O}$ is given by the sum over both orientations and all sequences

$$\hat{O} = \sum_{s,d} \hat{O}_{s,d} \tag{6.98}$$

it is natural to ask when this sum vanishes as an effect of destructive interference. We analyze first a setting where cancellation occurs by summing the different sequences of an oriented loop. The reversely oriented loop will vanish as well since it is only the Hermitian conjugate of the former. Then we discuss how the prefactor can be tuned to be purely imaginary such that adding its Hermitian conjugate (summing over both loop directions) leads to cancellation.

Loop cancellation by symmetry

If for each sequence s of tunneling operators, there exists a *permuted sequence* $\Pi[s]$ with opposite prefactor,

$$A(k,\Pi[s],d) = -A(k,s,d) \tag{6.99}$$

the sum over all sequences is zero since we have

$$\hat{O}_d = \sum_s \hat{O}_{s,d} = \sum_s \hat{O}^{(k)}_{\Pi[s],d} = -\sum_s \hat{O}^{(k)}_{s,d} \,. \tag{6.100}$$

This condition is not necessary, but sufficient and in particular it is simple to find instances of loops that fulfill this criterion. To this end note that a sign change due to a change of the sequence can only occur if at least some of the hopping operators anticommute. This is the case if two wires are couple to the same Majorana mode, i.e., if we have overlapping hopping terms. If the permutation interchanges an odd number of overlapping hopping terms and leaves the energy prefactor invariant, i.e., the product of all inverse energies of the virtual intermediate state is the same for the sequence s and $\Pi[s]$ the condition in Eq. (6.99) is guaranteed. Since the energy of the intermediate states only depends on the charge transferred between MCBs, irrespective of precisely which MCBs are involved in the tunneling path or whether we have tetrons or hexons, we can simplify the loop to a reduced graph where MCBs are replaced by single vertices labeled by their charging energy. MCBs with overlapping hopping operators connected to them are marked. Now a practical approach to finding the permutation Π is to find suitable symmetries of the reduced graph. In particular a mirror symmetry, mapping edges to edges and vertices to vertices of the same color and same charging energy, with the mirror axis going through an odd number of marked vertices will directly yield such a permutation. This is easily seen as the symmetry guarantees that the intermediate states have the same energy and the reflection induces an odd number of sign changes. Note that for the construction of the reduced graph the coupling amplitudes are irrelevant since their product appears irrespective of the specific sequence.

We illustrate this mechanism for the MCB network in Fig. 6.7a, which has a mirror symmetry of its reduced graph (cf. Fig. 6.7b) along the vertical axis. This reflection defines a permutation $T_1 \leftrightarrow T_4$ and $T_2 \leftrightarrow T_3$ of tunneling terms. Since T_2 and T_3 anticommute, this permutation

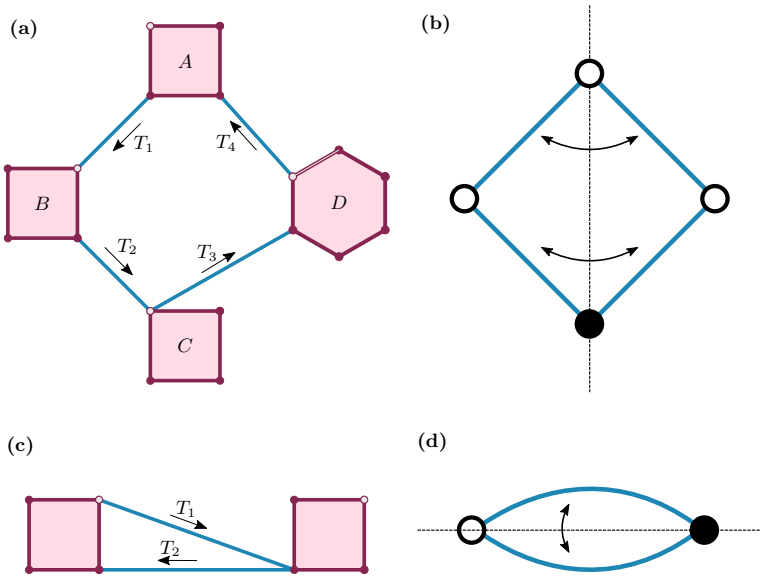

Fig. 6.7. ⋆ Two examples for loop cancellation by symmetries and anticommuting T_i terms. (a) MCB network with overlapping hopping terms T_2 and T_3, and (b) the corresponding reduced graph. The reflection symmetry defining the loop-canceling permutation $\Pi[s]$ is also indicated. (c) Another example for a network with anticommuting T_i operators and (d) the associated reduced graph.

induces a sign change. We evaluate the loop contributions for a specific sequence s and the associated permuted sequence $\Pi[s]$ to make the notation clear,

$$\begin{aligned} \hat{O}^{(4)}_{s,+} &= \hat{P}_0 T_1 \frac{1}{-\hat{H}_0} T_3 \frac{1}{-\hat{H}_0} T_2 \frac{1}{-\hat{H}_0} T_4 \hat{P}_0 \\ &= \frac{\mathrm{i}}{16 E_C^3} \hat{x}_A \hat{x}_B \mathbb{1}_C (\hat{z} \otimes \hat{z})_D \,, \\ \hat{O}^{(4)}_{\Pi[s],+} &= \hat{P}_0 T_4 \frac{1}{-\hat{H}_0} T_2 \frac{1}{-\hat{H}_0} T_3 \frac{1}{-\hat{H}_0} T_1 \hat{P}_0 \\ &= -\frac{\mathrm{i}}{16 E_C^3} \hat{x}_A \hat{x}_B \mathbb{1}_C (\hat{z} \otimes \hat{z})_D \,. \end{aligned} \tag{6.101}$$

Here we have set the tunneling amplitudes to one since they are irrelevant as explained above. We see that both contributions cancel each other as expected from the general arguments laid out above.

Loop cancellation by phase tuning

Next we consider a cancellation mechanism that occurs for a suitable tuning of the complex coupling amplitudes. We define the *loop phase* as the complex phase of the prefactor $A(k, s, d)$ which is independent of the sequence and given by

$$\Phi_{k,+} = k\pi/2 + \Phi_1 + \ldots + \Phi_k \,, \tag{6.102}$$

where Φ_i with $\lambda_i = |\lambda_i| e^{\mathrm{i}\phi_i}$ are the complex phases of the coupling amplitudes of the wires defining the loop. If $\Phi_k = \pm\pi/2$ we obtain an anti-Hermitian operator O_+ and adding its Hermitian conjugate O_- will yield zero.

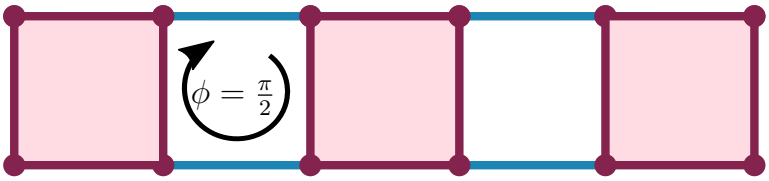

Fig. 6.8. ⋆ An example for cancellation of composed loop paths.

Let us briefly reconsider the two-tetron example in Fig. 6.6 to illustrate this mechanism. Summing over the two different sequences for a clockwise oriented loop, we obtain

$$\hat{O}^{(2)}_{+} = \frac{\lambda\kappa^*}{E_C}\hat{z}_A\hat{z}_B, \tag{6.103}$$

cf. Eq. (6.96). Now $\hat{O}^{(2)} = \hat{O}^{(2)}_{+} + \hat{O}^{(2)}_{-}$ exactly vanishes for $\mathrm{Re}(\lambda\kappa^*) = 0$ or $2\pi/2 + \phi_\lambda - \phi_\kappa = \pm\pi/2$. It is important to note that this loop phase is accessible experimentally and can be tuned via the gate voltage in an interferometric procedure (e.g., conductance or capacitance spectroscopy) measurements [261, 262]. Thus, cancellation based on phase tuning can in principle constitute a powerful tool to avoid unwanted short-loop contributions to the overall effective Hamiltonian. However, in practice, the above calibration procedure will adjust the loop phases only up to a certain accuracy level, and the suppression will not be perfect. Still, one can regard the occurring terms as small perturbations to the unperturbed effective Hamiltonian.

Composite loop patterns

We now investigate general closed paths and see how the two cancellation mechanism can be transferred to this setting. First, for disjoint unions of closed loops it is straightforward to see that their contribution factorizes into the product of the contributions from the individual loops up to a numerical prefactor. Thus, if one of the single-loop contributions vanishes, the contribution from the disjoint union will vanish as well.

Regarding the cancellation due to symmetries of the reduced graph explained above, note that we did not restrict ourselves to self-intersection free loops and the cancellation argument extends to this case.

To investigate the applicability of the cancellation mechanism based on the tuning of the loop phase consider a self-intersecting path and partition it into n non-intersecting closed sub-paths with sequences and orientations $\{(s_i, d_i)\}$. Charge neutrality requires that only orientation patterns for which the number of paths beginning and ending at a vertex is the same contribute to the effective low energy Hamiltonian. If for all these patterns there is at least one oriented sub-loop which vanishes due to its loop phase being $\pm\pi/2$ the complete parent path will vanish. In Fig. 6.8 we examine an example of this type. The left length-2 loop, $\hat{L} = \hat{L}_+ + \hat{L}_- = 0$, vanishes due to phase cancellation while the right length-2 loop, $\hat{R} = \hat{R}_+ + \hat{R}_-$, has an arbitrary loop phase and does in general not vanish by itself. However, the closed length-4 path $\hat{O}^{(4)}$ can be decomposed into two oriented segments $\hat{L}$ and $\hat{R}$ that can both have either clockwise or anticlockwise orientations. The total contribution is given by $\hat{O}^{(4)} = O^{(4)}_{++} + O^{(4)}_{+-} + O^{(4)}_{-+} + O^{(4)}_{--} \propto (\hat{L}_+ + \hat{L}_-)(\hat{R}_+ + \hat{R}_-) = 0$ and thus vanishes.

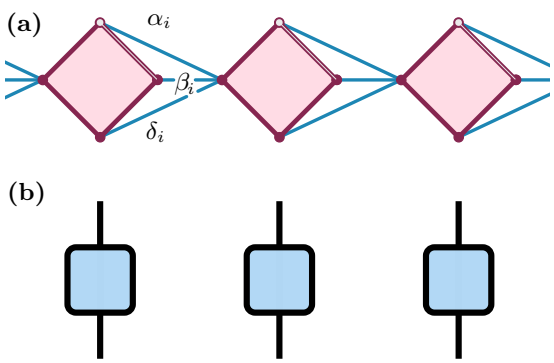

Fig. 6.9. ⋆ (a) MCB ring of tetrons (the chain has periodic boundary conditions), and (b) the leading order of the corresponding effective qubit Hamiltonian (6.104), a product operator, represented as tensor network.

6.2.5. Engineering multi-qubit operators

Next, we analyze what kind of qubit Hamiltonians can be achieved with the cancellation mechanism introduced above. As mentioned earlier generic network structures in which wires are not sparsely distributed will be dominated by 2-body interactions corresponding to the shortest possible loops. However, sparsity also severely limits the emerging Hamiltonians. In particular, in order to engineer multi-qubit operators that can generate a certain amount of entanglement, wires can not be arbitrarily sparse. If for every pair of MCBs there is only one wire connecting them, the emerging operators will be simply product operators while having more then one connecting wire creates a short loop unless a cancellation mechanism is employed. In this sense, the complexity (or ability to generate entanglement) of a multi-qubit operator is limited by the ability to suppress short loops. We will next investigate this observation in more detail.

Product operators

The symmetry based cancellation mechanism explained in the previous Section allows us to engineer product operators on a ring of MCBs of arbitrary length M, where each single qubit operator is a sum of $\hat{x}, \hat{y}$ and $\hat{z}$ with arbitrary weights. Fig. 6.9 shows the MCB network architecture for such an operator. Tunnel bridges connect neighboring MCBs, but each wire terminates at the same MBS per box. Thus, all length-2 loops cancel due to the fact that they have a mirror symmetry giving rise to a canceling permutation. All loops which are products of several length-2 loops vanish by the factorization property discussed above and the only non-vanishing loops are of length M winding once around the full ring. Thus, the leading order of the low energy theory is given by the operator

$$\hat{O}_+^{(M)} = \frac{-\mathrm{i}^M}{(2E_C)^{M-1}} \hat{q}_1 \hat{q}_2 \cdots \hat{q}_M \,, \tag{6.104}$$

$$\hat{q}_i = \delta_i \hat{x}_i + \beta_i \hat{y}_i + \alpha_i \hat{z}_i \,, \tag{6.105}$$

since tunneling from one box to another can take place via the three different wires weighted by weights α_i, β_i and δ_i and corresponds to a single qubit operator. The resulting Hamiltonian is given by summing $\hat{O}_+^{(M)}$ and its Hermitian conjugate. We observe that for loops with even

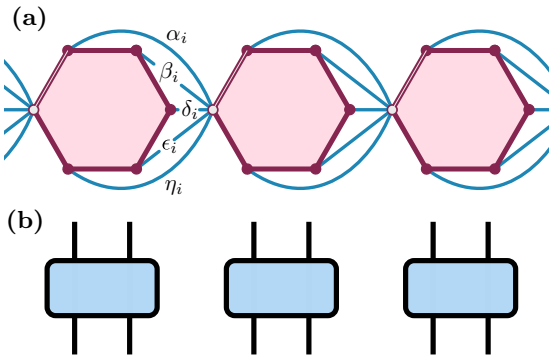

Fig. 6.10. ⋆ (a) MCB ring of hexons, and (b) the leading order of its effective qubit Hamiltonian, a product operator composed from two-qubit operators, depicted as tensor network.

(odd) length M and purely real (imaginary) tunneling amplitudes, $\hat{O}_+^{(M)}$ is Hermitian. In that case, the low-energy Hamiltonian, $\hat{H}_{\text{eff}} = 2\hat{O}_+^{(M)}$, implements a Hermitian product operator of qubits, where the associated tensor network is shown in Fig. 6.9b. Detuning the tunneling phases away from the purely Hermitian point, we have $O_+ \neq O_-$ and thus H is not a pure product operator anymore, but a sum of two product operators. I.e., it may generate some entanglement.

The same design principle can be applied to a ring of hexons or mixed hexon/tetron structures. For hexons, Eq. (6.104) describes the leading order operators, but the individual $\hat{q}_i$ operators are now replaced by two-qubit operators. For instance, for the example in Fig. 6.10a, we have

$$\begin{aligned} \hat{q}_i &= -\alpha_i(\hat{x}\otimes\mathbb{1})_i + \beta_i(\hat{y}\otimes\mathbb{1})_i \\ &+ \delta_i(\hat{z}\otimes\hat{x})_i + \epsilon_i(\hat{z}\otimes\hat{y})_i + \eta_i(\hat{z}\otimes\hat{z})_i\,, \end{aligned} \tag{6.106}$$

where $\alpha_i, \beta_i, \delta_i, \epsilon_i, \eta_i$ again refer to the five tunneling amplitudes connecting the MCB labeled by i to its left neighbor, cf. Fig. 6.10a. For the sake of completeness Fig. 6.10b shows the operator in tensor network notation, where the two-qubit nature of the compound operators $\hat{q}_i$ becomes apparent through the the two parallel vertical index lines at each tensor.

Matrix product operators

Employing the phase-cancellation mechanism we can design well controlled matrix product operators with bond dimension two. Unfortunately, the mechanism is not suited to go to higher bond dimensions. To the best of our knowledge, hierarchical gadgets constructions with more than one low-energy subspace projection are required to achieve the latter. We will comment on this in a later Section. For now, we consider again a ring structure as in Fig. 6.11a, but this time each pair of neighboring MCBs is coupled with two wires of tunneling amplitudes

$$\alpha_i = |\alpha_i| e^{i\phi_{\alpha_i}} \quad \left(\beta_i = |\beta_i| e^{i\phi_{\beta_i}}\right)\,. \tag{6.107}$$

We tune the loop phase to be

$$\phi_{\text{loop}}^{(i)} = \phi_{\alpha_i} - \phi_{\beta_i} = \pm\pi/2 \tag{6.108}$$

such that destructive interference occurs. Tuning all $\phi_{\text{loop}}^{(i)}$ to this value all length-2 loops and their products cancel and the leading order of the low-energy effective theory is given by the

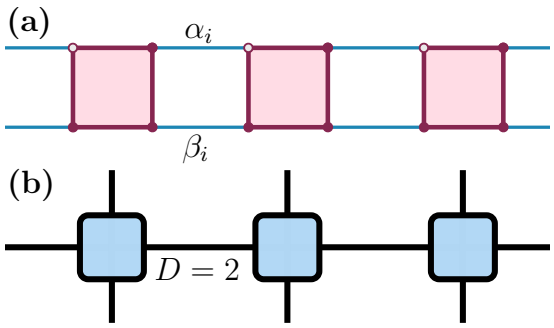

Fig. 6.11. ⋆ Matrix product operators. (a) Tetron ring of length $M = 3$. (b) Tensor network representation for case (a) as a qubit MPO. The bond dimension of this MPO is $D = 2$.

sum of all operators that emerge from a tunneling process around the full ring. Since tunneling from one box to the next one can occur via the upper or the lower wire segment it is convenient to express the operator in MPO form with bond dimension two, i.e.,

$$\begin{aligned} \hat{O}_+^{(M)} &= \frac{-\mathrm{i}^M}{(2E_C)^{M-1}} \sum_{i_1=0,1} \cdots \sum_{i_M=0,1} \hat{A}^1_{i_1 i_2} \hat{A}^2_{i_2 i_3} \cdots \hat{A}^M_{i_M i_1} \\ &= \frac{-\mathrm{i}^M}{(2E_C)^{M-1}} \mathrm{Tr}\left(\hat{A}^1 \hat{A}^2 \cdots \hat{A}^M\right) , \end{aligned} \tag{6.109}$$

where the $\hat{A}^i$ are Pauli operators acting on MCB i weighted by tunneling amplitudes,

$$\hat{A}^i_{00} = -\alpha_i \hat{x} , \quad \hat{A}^i_{01} = \beta_i \hat{y} , \tag{6.110}$$

$$\hat{A}^i_{10} = \alpha_i \hat{y} , \quad \hat{A}^i_{11} = \beta_i \hat{x} , \tag{6.111}$$

and again the Hamiltonian is given by $\hat{H}_{\text{eff}} = \hat{O}_+^{(M)} \hat{O}_+^{(M)}$. The tensor network representation of this operator is given in Fig. 6.11b.

Note, that Eq. (6.111) does not represent a general $D = 2$ MPO. While it is possible to vary the local basis and thereby replace the pair of $\hat{x}, \hat{y}$ with another pair say $\hat{y}, \hat{z}$, we can not choose all four operators independently due to the symmetry of the tetron. In addition to that, it is not straight forward to implement operators proportional to the identity. Thus, careful inspection is required when answering the question if a desired $D = 2$ MPO can be realized as an MCB network.

Next, let us discuss why adding a third parallel wire fails to yield a bond dimension three MPO in leading order. The reason is very simple. Out of the three length-2 loops formed between two MCBs, only two can be tuned to have a loop phase of $\pm\pi/2$ simultaneously. The third one is simple the sum of the the two and thus equal to 0 or π, i.e., it cannot be subject to phase based cancellation. Other mechanisms to generate $D = 3$ MPOs are much more involved and explained in Section 6.2.6.

Bell-pair projection

As mentioned earlier more complex Hamiltonians can only be achieved by combining several low energy projections. One of those hierarchical gadget construction is employed later to construct the double semion model and combines the perturbative PEPS parent gadget construction with the low energy projection of MCB networks. In addition to MPO-projections, the

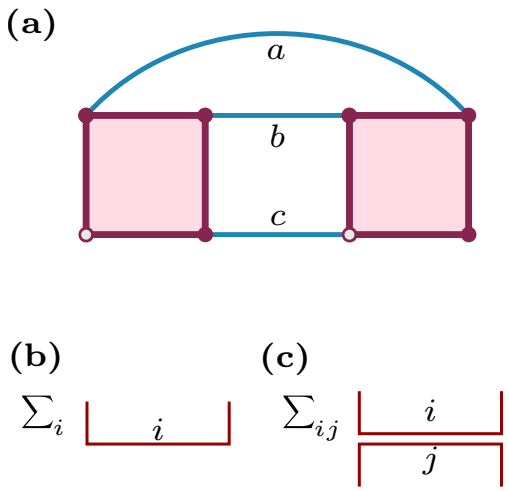

Fig. 6.12. ⋆ Bell-pairs. (a) Coupled tetron device. The ground state of the associated effective Hamiltonian (6.112) is a Bell state for real positive $a = b = c$. (b) Tensor network representation of $|\text{Bell}\rangle = |0,0\rangle + |1,1\rangle$. (c) Tensor network representation of the Bell-pair projector $\hat{P}_{Bell} = |\text{Bell}\rangle\langle\text{Bell}|$.

PEPS parent Hamiltonian is composed of several Bell-pair projections. We thus briefly show how a Bell-pair projection can be engineered in a simple MCB network. The network is given in Fig. 6.12a showing three wires with weights a, b, c connecting two MCBs. Thus, the three length-2 loops give rise to three 2-qubit operators. For $a = b = c > 0$ we obtain

$$\hat{H}_{\text{eff}} = \frac{a^2}{2E_C}\left(-\hat{x}_1\hat{x}_2 - \hat{z}_1\hat{z}_2 + \hat{y}_1\hat{y}_2\right) . \tag{6.112}$$

which has a Bell state $|\text{Bell}\rangle = |0,0\rangle + |1,1\rangle$ as its ground state. The state as well as the projector $\hat{P}_{\text{Bell}} = |\text{Bell}\rangle\langle\text{Bell}|$ are depicted in Figs. 6.12b–c in tensor network notation.

6.2.6. Hierarchical designs

The operator designs proposed above all rely on the fact that we work within a low-energy sector separated from the excited state space with a large energy gap. It is possible to think of design schemes in which additional energy scale separations are introduced, e.g. by choosing certain link weights to be much stronger than others. In these settings, we obtain a low-energy description of the low energy description. We refer to these designs as hierarchical designs or hierarchical gadgets and present several examples of the latter in the following Section.

Repetition code qubits

A particularly simple hierarchical gadget construction is the repetition code Hamiltonian operating on a chain of MCBs again connected with parallel wires with tunneling amplitude a and b shown in Fig. 6.13a, but this time, the loop phases are not tuned to the destructive interference regime. Instead, we choose $\phi_{\text{loop}} = \phi_a - \phi_b$, such that $\pi/2 < \phi_{\text{loop}} < 3\pi/2$ the and the length-2 loops yield

$$J = \frac{\text{Re}(ab^*)}{2E_C} < 0 , \tag{6.113}$$

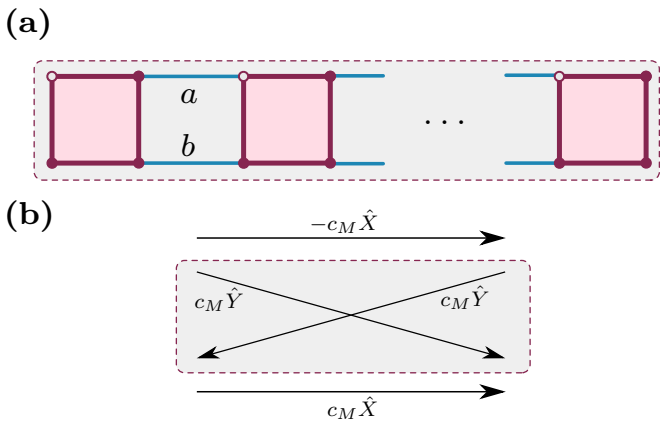

Fig. 6.13. ⋆ Logical qubit in a repetition code. (a) Chain of M tetrons with open boundary conditions. Neighboring tetrons are coupled by tunneling amplitudes a and b. (b) Logical Pauli operators $\hat{X}$ and $\hat{Y}$ emerge by pumping an electron through the entire chain, cf. Eq. (6.117).

and the effective Hamiltonian

$$\hat{H}_{\text{eff}} = J \sum_{i=1}^{M-1} \hat{z}_i \hat{z}_{i+1} \tag{6.114}$$

is nothing but a ferromagnetic Ising chain. The two-fold degenerate ground state space of this Hamiltonian can be identified with the code space of a *repetition code* [284], i.e., the logical zero state $|\bar{0}\rangle = |00\ldots0\rangle$ and the logical one state $|\bar{1}\rangle = |11\ldots1\rangle$. We can assume that the whole system will always be in the logical subspace and thus forms a logical qubit. Interestingly, this logical qubit may be operated just like a single tetron-based qubit but with enhanced error resilience.

Let us consider a process where an electron enters the MCB chain at the left side and exits at the right site. Such processes can be implemented experimentally a shown in Ref. [86]. This process corresponds to a sum of all possible paths, each corresponding to a Pauli word composed of $\hat{x}$ and $\hat{y}$ operators. Interestingly the action on the logical space spanned by $|\bar{0}\rangle$ and $|\bar{1}\rangle$ only depends on the entry and exit point of the tunneling electron and is independent of the exact path. To see this, first consider a chain of length two and a tunneling processes where the electron enters at the top left and exits at the top right. The two possible paths yield

$$\hat{S}_{00} = \frac{-1}{2E_C}\left(a\hat{x}_1\hat{x}_2 + b\hat{y}_1\hat{y}_2\right) , \tag{6.115}$$

where the first (second) index refers to the entry (exit) point and the index value 0 (1) refers to the top (bottom) MBS. On the logical space we have $\hat{y} = \mathrm{i}\hat{x}\hat{z}$ and $\hat{z}_1\hat{z}_2 = \mathbb{1}_2$ and obtain

$$\hat{S}_{00} = -\frac{a-b}{2E_C}\hat{x}_1\hat{x}_2, \tag{6.116}$$

which is proportional to the logical Pauli-$\hat{X}$ operator. We can generalize this argument by induction and arrive at the general expression for a M-qubit chain

$$\hat{S}_{00} = -\hat{S}_{11} = -c_M\hat{X} , \quad \hat{S}_{01} = \hat{S}_{10} = c_M\hat{Y} , \tag{6.117}$$

where the logical Pauli operators are defined as $\hat{X} = \hat{x}_1\hat{x}_2\cdots\hat{x}_{M-1}\hat{x}_M$ and $\hat{Y} = \hat{x}_1\cdots\hat{x}_{M-1}\hat{y}_M$. Apart from the prefactor,

$$c_M = (-\mathrm{i})^M[(a-b)/(2E_C)]^{M-1} , \tag{6.118}$$

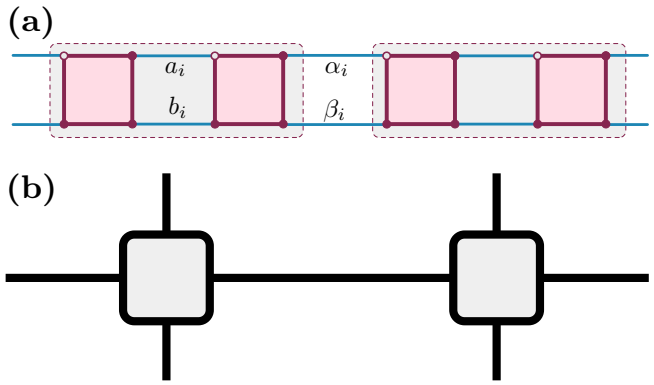

Fig. 6.14. ⋆ (a) A hierarchical structure in which units of two tetrons are first linked by tunneling amplitudes $a_i \simeq -b_i$ to define repetition qubits. These blocks are then coupled by amplitudes α_i, β_i to an MPO depicted as tensor network in (b).

this result is identical to the mapping of Majorana bilinears to Pauli operators for a single tetron, cf. Eq. (6.88).

MPOs on repetition code qubits

One can now use repetition code chains as elements in more complex networks where only the four MBS at the boundary of the chain are coupled to the rest of the network. Now, the tunneling processes corresponding to logical operations discussed above, occur as higher order contributions to the low-energy effective theory. I.e., at the energy scale J defined in Eq. (6.113), one would not be able to resolve the more structured effective Hamiltonian of the logical qubit, but only see a ferromagnetic chain. However, on the scales $< \frac{1}{2E_C}^{M-1}$, the higher order terms of the effective theory can be resolved and we discover an effective Hamiltonian acting on logical repetition code qubits. This is our first example of a hierarchical gadget constructions. To be more specific, consider the network structure depicted in Fig. 6.14 closed in a ring of length M, i.e., $M/2$ repetition code blocks formed by tunnel couplings a_i, b_i are embedded into an MPO structure with $M/2$ parallel wire pairs α, β.

We want to resolve the effective theory at energy scales $\propto 1/E_C^{M-1}$, i.e., terms corresponding to tunnelings once around the ring. However, the theory is generically dominated by length-2 loops. Tuning the loop phases of the α, β pairs such that destructive interference cancels them, we obtain three decoupled logical repetition qubits at energy scale $1/E_C$. Now the theory at scale $\propto 1/E_C^{M-1}$ can safely be evaluated projecting to the ground state space of the effective theory at scale $1/E_C$, i.e., the code space of three independent repetition code qubits and we obtain an MPO of $M/2$ logical Pauli operators acting on repetition qubits given by

$$\hat{O}_+^{(M)} \propto \mathrm{Tr}\left(\hat{B}^1 \hat{B}^2 \dots \hat{B}^{M/2}\right) , \tag{6.119}$$

with MPO matrix elements

$$\begin{aligned} \hat{B}^i_{00} &= -\alpha_i \hat{X} , \\ \hat{B}^i_{01} &= \beta_i \hat{Y} , \\ \hat{B}^i_{10} &= \alpha_i \hat{Y} , \\ \hat{B}^i_{11} &= -\beta_i \hat{Y} . \end{aligned} \tag{6.120}$$

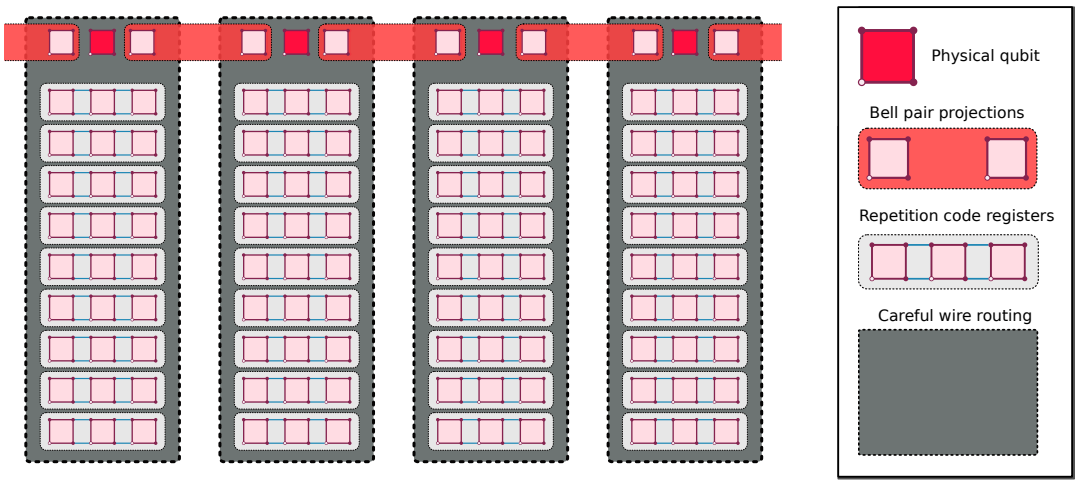

Fig. 6.15. ⋆ A design scheme for realizing $D = 3$ MPOs on physical qubits (red).

Jordan–Farhi-gadget enhancements

To overcome the limitation of the bond dimension $D = 2$ for matrix product operator designs explained in Section 6.2.5 we employ a hierarchical gadget design sketched in Fig. 6.15 sufficient to design a $D = 3$ MPO. The design idea is inspired by the Jordan–Farhi gadgets in Section 6.1.2 and the perturbative PEPS parent construction. Each physical qubit p, i.e., the qubit on which the MPO eventually acts on, is supplemented with auxiliary qubits that together form a unit cell (grey boxes in Fig.6.15). The unit cell consists of an array of of 3×3 repetition code qubits $r_{(i,j)}$, $i, j = 1, 2, 3$, each assembled form three MCBs $r_{(i,j),k}$, $k = 1, 2, 3$ and two communication qubits c_1, c_2 which are subject to Bell-pair projections with the communication qubits of the neighboring unit cells.

The repetition code qubits are used similar to the Farhi gadget construction to engineer well controlled 3-body operations on the physical qubit and its associated communication qubits. A desired Pauli word, e.g.

$$\hat{X}_{c_1} \otimes \hat{Y}_p \otimes \hat{Z}_{c_2} \tag{6.121}$$

is assembled by adding two-body interactions

$$\hat{X}_{c_1} \otimes \hat{x}_{r_{(i,j),1}}\,, \quad \hat{Y}_p \otimes \hat{x}_{r_{(i,j),2}}\,, \quad \hat{Z}_{c_2} \otimes x_{r_{(i,j),3}} \tag{6.122}$$

between the communication (physical) qubits and the auxiliary qubits of the register (i, j). Similar to the Jordan–Farhi-gadget construction the leading order term in perturbation theory is given by the shortest product of two-body terms that flips all auxiliary spins, i.e., performs a logical $\hat{X}_{(i,j)} = \hat{x}_{r_{(i,j),1}} \otimes \hat{x}_{r_{(i,j),2}} \otimes \hat{x}_{r_{(i,j),3}}$ on the repetition code register (i, j). In this way, we can design a total of 9 freely chosen three-qubit operations.

Note, that there is a massive amount of short cuts (mini-loops) generated since many wire ends are connected to one single Majorana terminal. However, non of them is harmful to the construction, as they fail to perform a logical $\hat{X}$ or $\hat{Z}$ on the repetition code qubits and thus do not contribute to the effective theory in low order.

The Pauli words on the triple (c_1, p, c_2) designed using the repetition code array (i, j) are not arbitrary, but instead of the form $\sigma^{(i)}_{c_1} \hat{B}^{(i,j)}_p \tilde{\sigma}^{(j)}_{c_2}$, where $i, j = 1, 2, 3$ and $\sigma^{(i)} = \hat{x}, \hat{y}, \hat{z}$ and

$\tilde{\sigma} = \hat{x}, -\hat{y}, \hat{z}$. The operators $B^{(i,j)}$ can be freely chosen and correspond to the MPO tensors eventually.

The choice of the Pauli matrices on the communication qubits is such that the index contraction between MPO tensors on different unit cells is carried out effectively via the Bell-pair projection. Consider two three qubit operators on two neighboring unit cells

$$\sigma_{c_1}^{(i)} \hat{B}_p^{(i,j)} \tilde{\sigma}_{c_2}^{(j)} \ , \quad \sigma_{c_1}^{(i')} \hat{B}_p^{(i',j')} \tilde{\sigma}_{c_2}^{(j')} \tag{6.123}$$

A Bell-pair projection on the right communication qubit of unit cell one (j) and the left communication qubit of unit cell two (i')

$$\hat{P}_{\text{Bell}} \tilde{\sigma}_j \otimes \sigma_{i'} \hat{P}_{\text{Bell}} = \delta_{j,i'} \tag{6.124}$$

selects only those Pauli words, where neighboring communication qubits are operated on with the same Pauli matrix.

To summarize we write down the leading order effective Hamiltonian of each layer of the construction. On the level of a single unit cell we have the repetition code registers (wired with coupling strength μ)

$$H_{r,(i,j)} = \frac{\mu^2}{E_C} \sum_{(i,j)} \hat{z}_{r_{(i,j)_1}} \hat{z}_{r_{(i,j)_2}} + \hat{z}_{r_{(i,j)_2}} \hat{z}_{r_{(i,j)_3}} \tag{6.125}$$

and the weaker couplings (λ between MCBs of repetition code registers to communication and physical qubits within each unit cell

$$H_{rcp,(i,j)} = \frac{\lambda^2}{E_c} \left(\sigma_{c_1}^{(i)} \otimes \hat{x}_{r_{(i,j)_1}} + B_p^{(i,j)} \otimes \hat{x}_{r_{(i,j)_2}} + \tilde{\sigma}_{c_2}^{(j)} \otimes \hat{x}_{r_{(i,j)_3}} \right) \tag{6.126}$$

such that the first layer of the gadget construction is

$$H_{\text{eff},1} = \sum_{i,j} H_{r,(i,j)} + H_{rcp,(i,j)} \ . \tag{6.127}$$

The energy separation between the code space of all repetition code registers and all other states is determined by the ratio μ/λ. If we assume $\mu \gg \lambda$, we obtain from the next layer of effective low energy projection the effective Hamiltonian on the unit cell k

$$H_{\text{eff,2,k}} = \beta \sum_{i_k, j_k = 1} \sigma_{c_1}^{(i_k)} \hat{B}_p^{(i_k,j_k)} \tilde{\sigma}_{c_2}^{(j_k)} \ , \tag{6.128}$$

where β is proportional to $\lambda^6/(E_C \mu^4)$. Note, that in order to neglect the operators acting on the repetition code registers, we need to initialize the registers in the logical $|+\rangle$ state, such that logical x-operations have a trivial effect which we can omit as in Eq. (6.128) above.

Next, consider the full system. Tunnel couplings with strength κ between communication qubit c_2 of unit cell k and communication qubits c_1 of unit cell $k+1$ result in effective Bell-pair projections $H_{\text{Bell,k}}$ (cf. Eq. (6.112)) proportional to $\alpha = \kappa^2/E_C$. The effective Hamiltonian on the full system then reads

$$H_{\text{eff},2} = \sum_{k=1}^{N} \alpha H_{\text{Bell,k}} + \beta H_{\text{eff,2,k}} \tag{6.129}$$

where N is the number of unit cells. For $\alpha \gg \beta$, we obtain in a third layer of low energy projection

$$H_{\text{eff},3} = \sum_{i_1, \ldots, i_N = 1} B_{p_1}^{(i_1,i_2)} \otimes B_{p_2}^{(i_2,i_3)} \otimes \ldots \otimes B_{p_N}^{(i_N,i_1)} \ , \tag{6.130}$$

acting on the physical qubits of the system and trivially on the auxiliary spins.

The idea presented here to design $D = 3$ MPOs can be easily adapted to $D > 3$ without introducing additional gadget layers. If we double the communication qubits and use two parallel Bell-pair projections between neighboring unit cells, we can realize $D = 3^2$. The repetition registers now consists of 5 qubits each such that they can generate five-qubit operators acting on all four communication qubits and the physical qubit. To generate all $3^2 \times 3^2$ MPO operators $B^{(i,j)}$ acting on a physical qubit, a total of 3^4 repetition code registers is needed. Thus, to realize a $D = 3^n$ MPO acting on N qubits, we need $N(1 + 3^{2n})(2n + 1)$ qubits. While this is a massive qubit overhead, we note that compared to a naive Jordan–Farhi gadget the scaling is still moderate[4]

Adding Hamiltonian terms

Engineering well controlled k-body interactions by tunnel coupling k MCBs is a non-trivial task as we have explained above. To avoid spin Hamiltonians dominated by nearest neighbor interactions, cancellation mechanisms have to be invoked. Another difficulty arises if these k-local Hamiltonian acting on different sites are added to form a local Hamiltonian on a larger spin system. The supports of the k-local terms have to overlap at least partially, otherwise we obtain a collection of individual subsystems that do not talk to each other. However, starting with a tunnel coupled network that gives rise to one Hamiltonian term H_1 and than adding all wires required to engineer a term H_2 will not result in the Hamiltonian $H_1 + H_2$, but generically short additional loops will be created that also cause two qubit interactions. This is the case whenever the supports of H_1 and H_2 overlap on more than one qubit as demonstrated for product operators and MPOs with $D = 2$ in Fig. 6.16. Only for special product operators as e.g. used in the construction of the MCB version of the toric code, the emergence of additional 2-body interactions can be avoided. This is essentially possible in the rare cases, when wires of the operator H_1 can be reused for the design of the operator H_2.

If the supports overlap only on one qubit, we refer to this as *tangential overlap*. In this case, one will generically encounter wire crossings that might lead to difficulties with regards to experimental realizations, but no additional short-loops are created and we can indeed obtain $H_1 + H_2$ by simply adding the wires generating H_1 and the wires generating H_2.

Note, that this constraint on the overlap severely limits the Hamiltonian design and a hierarchical gadget construction where interactions between different local parts of the system are mediated in a very controlled and specific way as e.g. in the perturbative PEPS parent design explained in Section 6.1.4 are essential to make any progress.

6.3. String-net phases in MCB networks

Having discussed the general principles of low-energy effective theories and gadgets, in particular the perturbative PEPS parent design which is tailored to engineering string-net Hamiltonians and understanding the possibilities and limitations of Hamiltonian design in MCB networks, we are now ready to return to the main question of this chapter – engineering string-net Hamiltonians.

[4]For $D > 4$ a Jordan-Farhi gadget would generically require 4^N auxiliary qubits, which is the maximum number of linearly independent Paui words on N qubits.

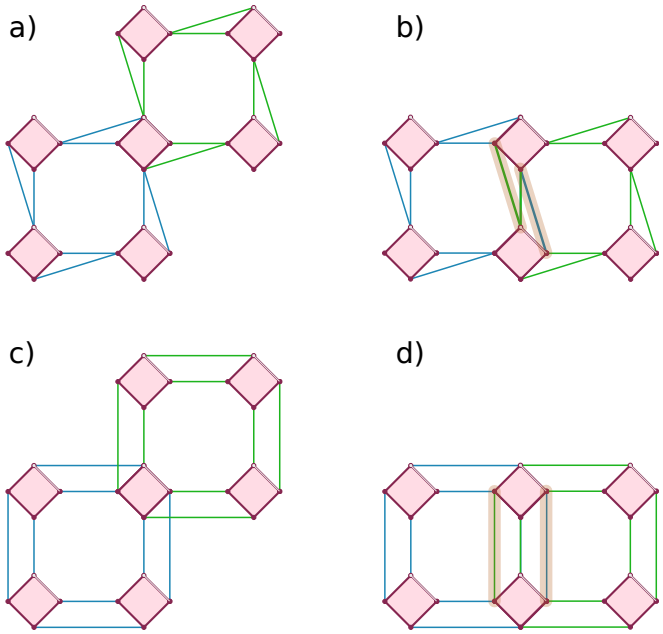

Fig. 6.16. ⋆ Adding two individual Hamiltonian operators realized with blue and green wire couplings, respectively. a) and c) show tangential overlap of the support, i.e., overlap on only one qubit for a) product operators, c) MPOs with $D = 2$. b) and d) show overlapping support on two qubits leading two additional short loops (length two) marked in red.

6.3.1. General design

The design of string-net Hamiltonians is challenging mainly because the plaquette operator is 12 local and neighboring plaquette operators have overlapping support on 5 qubits. Both features are extremely adverse to a realization in coupled MCB networks. However, for a given string-net model, we can use its MPO-isometric PEPS ground state to construct a perturbative parent Hamiltonian

$$H = \sum_v (1 - P_v) + \epsilon \sum_e |\text{Bell}\rangle \langle \text{Bell}|_e \tag{6.131}$$

as discussed in Section 6.1.4 whose low-energy effective theory is in the same phase as the original string-net model. The perturbative PEPS parent Hamiltonian (cf. Section 6.1.4) does not suffer from overlapping supports. The only overlap of supports is between vertex operators and Bell-pair projections, but here the overlap is only tangential in the language of Section 6.2.6. Implementing the Bell-pair projections on MCB qubits is straightforward and we can simply use the architecture given in Section 6.2.5.

Qudits

So far, we have mostly considered effective qubit Hamiltonians emerging in MCB networks. However, to our knowledge, there are only three string-net models that are defined with 2 string-types, the toric code, the double semion and the double Fibonacci model. All other string-net models are based on having three or more different string types. Thus, we would need to design MCB structures with a local Hilbert space dimension larger than 2. However, MCB devices are based on a parity constraint so their Hilbert space is usually of a tensor product structure and we obtain 2^n dimensional local Hilbert spaces naturally. While we can

in principle embed a d-dimensional Hilbertspace $\mathcal{H}_d$ in a 2^n dimensional one $\mathcal{H}_{2^n}$ as long as $d < 2^n$, we note, that if we do not implement any constraints that restrain the system from taking on states in $\mathcal{H}_{2^n}/\mathcal{H}_d$, we need to prepare the initial state of the system very carefully and need to have very good control over the Hamiltonian terms to avoid that the system ends up in a state that is not identifiable with a state in the string-net Hilbertspace. However, implementing constraints to penalize certain states is not trivial. E.g. if we want to obtain a 3 dimensional Hilbert space embedded into the 2^2-dim space of 2 MCBs, we need to implement an operator that is proportional to a projector onto a one-dimensional space up to some overall energy shift. However, there is no simple candidate for such an operator. Both single qubit Pauli operators acting on a single box as well as Pauli product operators acting on both effective MCB qubits will project out half the state space. Splitting this space again by another single qubit or product operator results in three or four distinct energy levels rather than a threefold degenerate ground state. Of course one can employ a Bell-pair projection to project out a one dimensional space. However, this involves three coupled wires already. It turns out that one cannot expect to do much better, since in general one needs to engineer a 1-dimensional projector by a sum of three two qubit Pauli operators. To see this, note, that two length two Pauli words always commute and thus can be simultaneously diagonalized. Weighted with coefficients α and β, the spectrum of the sum of the two is given by $\alpha+\beta, \alpha-\beta, -\beta+\alpha, -\alpha-\beta$ and thus we cannot design a threefold degenerate subspace. Adding a third length-2 Pauli word resolves the situation. Thus, we conclude that the implementation of additional constraints reducing the Hilbert space dimension is costly and cumbersome. It might also lead to the emergence of unwanted short loops in the more general setting of n MCBs. Thus, we need to restrict ourselves to string-net models with two-string types.

Vertex projector

The crucial point in designing the Hamiltonian in Eq. (6.131) is the design of the vertex operator P_v. We have already seen that the vertex projector can always be written as an MPO with relatively low bond dimension. In particular, the bond dimension is upper bounded by the number of allowed vertex configurations and thus for the same number of string-types, a string-net model with multiple fusion channels for the same pair of string types will generically have a higher bond dimension. This is reflected in the fact, that the toric code and the double semion model have bond dimension one and two respectively, while the Fibonacci model has bond dimension 5. Thus, we can implement the toric code and the double semion model without making use of Jordan–Farhi gadget enhancements by simply implementing the bond MPOs with bond dimension one or two, respectively. However, for the toric code model it is not even necessary to employ the perturbative PEPS parent since already the string-net Hamiltonian itself has only tangential overlap and consists of product operators. A concrete example for the toric code in an MCB network is presented e.g. in Ref. [91]. We will thus not investigate the construction of the toric code model but instead consider the double semion in detail and sketch a design for the Fibonacci model based on the more costly Jordan–Farhi enhanced MPOs.

Before we continue with the details of the double semion construction, we note that in general the symmetry projection MPOs of string-net PEPS act on nine virtual qudits located in a triangle and every two qudits in one corner of the triangle are forced to take the same value. This effect can be conveniently achieved by using repetition code qubits instead of uncorrelated single qubits in the construction of the effective Hamiltonian (cf. Section 6.2.6) for all string-net models with two string types, i.e., the case where the MPO acts on qubits.

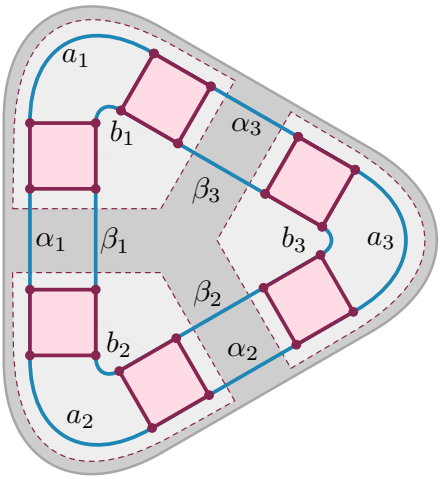

Fig. 6.17. ⋆ Tetron ring ("triangle") used for implementing the effective vertex Hamiltonian, $\hat{H}_v$.

6.3.2. $D = 2$ – The double semion blueprint

This Section is closely following the original work of the author – and co-authors – in Ref. [2].

We now turn to the implementation of the vertex operator for the double semion model defined in Eq. (6.74). There is no need to implement the operator P_c which enforces even parity on the pairs of qubits on the edges of the triangle explicitly. Instead the even parity constraint on all corner pair qubits is enforced by using a repetition code MPO as defined in Section 6.2.6. Then $\hat{P}_c$ acts as an identity operator within the parity restricted subspace and the essential information of the code space projector $\hat{P}_{v,DS}$ is carried by $\hat{X}$. In particular, we know that the local ground space of the operators $1 - \hat{P}_{v,DS}$ in the parent Hamiltonian in Eq. (6.74) coincides with that of $-\hat{X}$. Our objective is thus to engineer an MCB network whose ground space equals that of $-\hat{X}$.

To this end, note that the operator $\hat{X}$ in Eq. (6.75) can be explicitly represented as an MPO with bond dimension $D = 2$,

$$\hat{X} = -\frac{1}{32} \sum_{i,j,k} \hat{A}_{ij} \otimes \hat{A}_{jk} \otimes \hat{A}_{ki} \,, \tag{6.132}$$

where individual factors,

$$\begin{aligned} \hat{A}_{00} = &\hat{A}_{11} = \hat{x} \otimes \hat{x} - \hat{y} \otimes \hat{y} \,, \\ \hat{A}_{01} = &\hat{A}_{10} = \hat{x} \otimes \hat{y} + \hat{y} \otimes \hat{x} \,, \end{aligned} \tag{6.133}$$

act on a qubit pair at the corner of a triangle (cf. Fig. 6.3).

The operator $\hat{X}$ can be implemented using the MCB structure shown in Fig. 6.17 with $a_i \simeq -b_i$ and $\alpha = \mathrm{i}\beta$. For the chosen parameters the leading order effective Hamiltonian corresponds to an MPO acting on repetition code qubits at the corners. The length-6 loop in clock-wise direction results in an MPO

$$\hat{O}_+^{(6)} = \frac{63}{8E_C^5} \mathrm{Tr} \left(\hat{B}^1 \hat{B}^2 \hat{B}^3 \right) \,, \tag{6.134}$$

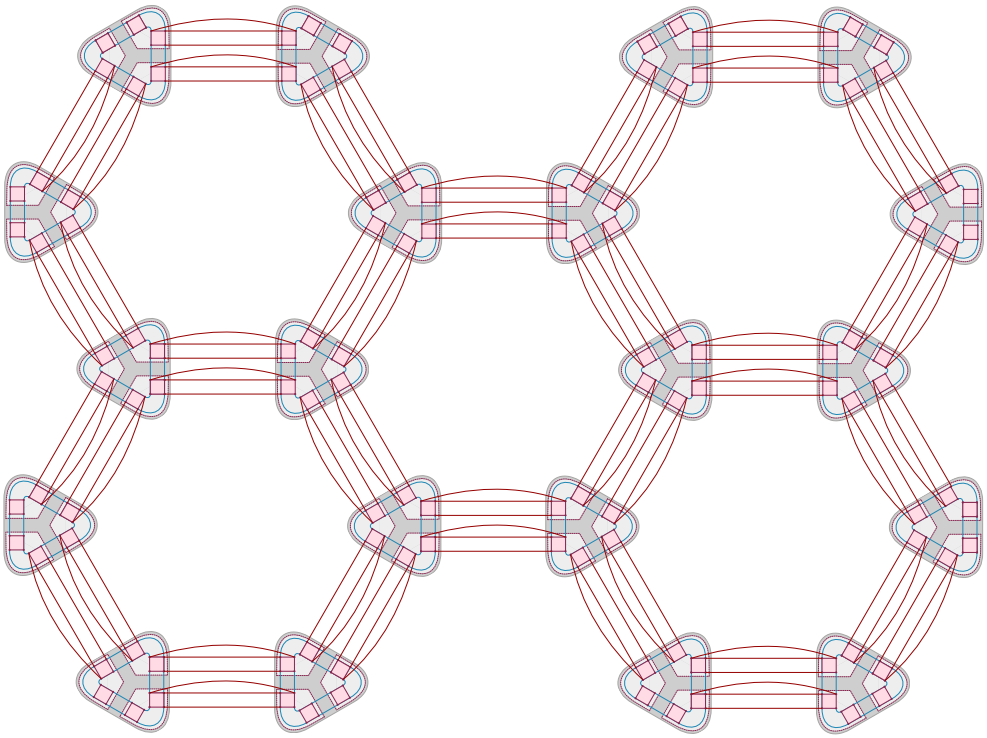

Fig. 6.18. ⋆ Double semion MCB network: Triangular 6-tetron vertices (grey triangles), cf. Fig. 6.17, are connected via Bell-pair tunneling bridges (red). Note that vertices are arranged in two different sublattices. For a magnified view of the coupling between vertices, cf. Fig. 6.19 below.

with MPO matrix elements

$$\begin{aligned}
\hat{B}^i_{00} &= -\alpha_i(a_i\hat{x}\otimes\hat{x} + b_i\hat{y}\otimes\hat{y})\,, \\
\hat{B}^i_{01} &= \beta_i(a_i\hat{x}\otimes\hat{y} - b_i\hat{y}\otimes\hat{x})\,, \\
\hat{B}^i_{10} &= \alpha_i(a_i\hat{y}\otimes\hat{x} - b_i\hat{x}\otimes\hat{y})\,, \\
\hat{B}^i_{11} &= -\beta_i(a_i\hat{y}\otimes\hat{y} + b_i\hat{x}\otimes\hat{x})\,,\,,
\end{aligned} \tag{6.135}$$

which can be evaluated further

$$\begin{aligned}
\hat{B}^i_{11} &= \pm\mathrm{i}B^i_{00} = c_i(\hat{x}\otimes\hat{x} - \hat{y}\otimes\hat{y})\,, \\
\hat{B}^i_{01} &= \mp\mathrm{i}B^i_{10} = c_i(\hat{x}\otimes\hat{y} + \hat{y}\otimes\hat{x})\,,
\end{aligned} \tag{6.136}$$

with $c_i = \beta_i a_i$. Choosing $c_i = \mathrm{i}$ (e.g. $\alpha_i = \mathrm{i}\beta_i$) we obtain the effective tunneling Hamiltonian $\hat{H}_v \propto -X$ (cf. Eq. (6.132)).

Practical implementation

In Fig. 6.18 we present a schematic of the actual hardware layout consisting of the tunnel couplings that generate the vertex-operator MPO (on triangles) and the Bell pair projections. Apart from a small amount of wire crossings, the structure does not include elements truly adverse to experimental realization. An essential point of the construction is the phase tuning of the tunnel couplings. This is achieved by an initial calibration procedure which requires

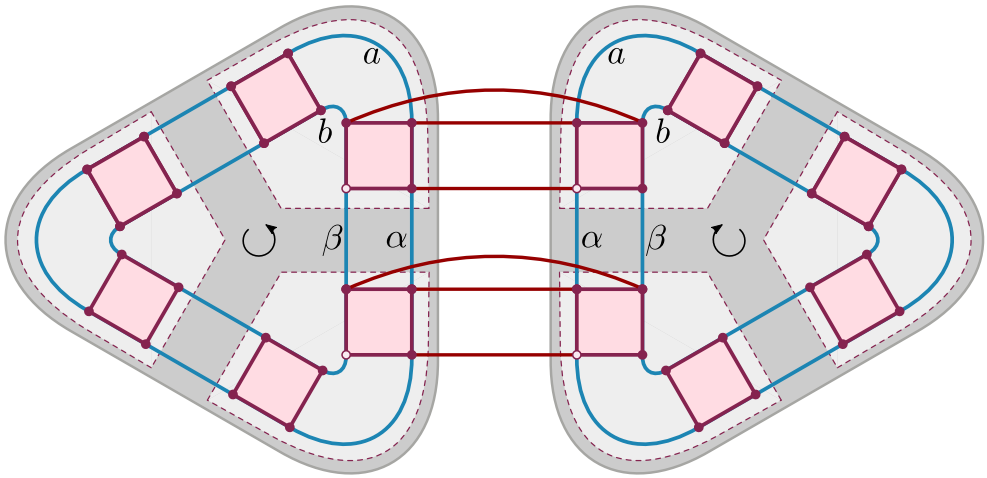

Fig. 6.19. ✦ Bell-pair tunnel bridges connecting neighboring vertices in the double semion MCB network of Fig. 6.18.

the presence of additional local gates near each tunneling link and performing interferometric measurements [261, 262] followed by subsequent gate voltage tuning.

Inaccuracies in the above calibration procedure result in small but finite contributions to the Hamiltonian $\hat{V}_i = (\lambda^2/E_C)\Delta\phi_i \hat{z} \otimes \hat{z}$ with $\Delta\phi_i$ most likely uncorrelated. The additional terms have the effect of an effective spatially varying magnetic field, since depending on the sign $\Delta\phi_i$ there is a bias towards the physical $|0\rangle$ ($|1\rangle$) state (encoded by the parity of the two qubits). In Ref. [285] the stability of the double semion model against a homogeneous magnetic fields has been studied and it was found that the topological phase persists up to a critical field strength, h_c about one tenth of the gap. It is very reasonable that the phase is even more stable against a random spatially varying magnetic field [286].

The stability of the phase against higher order terms of the perturbation series is investigated in Ref. [2, Appendix] which is reprinted in Appendix B of this Thesis for convenience. It is found that higher order terms are irrelevant and do not pose a threat to the stability of the phase.

6.3.3. $D = 5$ – A double Fibonacci candidate

The double Fibonacci model is the simplest string-net model hosting non-Abelian anyons. It is constructed from the Fibonacci fusion category $\mathcal{C}_{\text{Fib}}$ with string-types 1 and τ with the fusion rule $\tau \times \tau = 1 + \tau$. The quantum dimension d_τ is given by the golden ration. Its F-symbols are non-trivial and can be found e.g. in Ref. [12]. The Drinfeld center of the Fibonacci category is given by the Fibonacci theory itself times its time-reversed dual (cf. Ref. [12]). Thus, the particle content of the model contains Fibonacci anyons and thus can be used for universal topological quantum computation by braiding (cf. Chapter 4). Therefore, there is a strong motivation to realize this topological phase of matter.

Since the double Fibonacci model also has only two string-types, tetron MCBs giving rise to effective qubits are sufficient to represent the string types and the main obstacle for extending the approach used in the design of the double semion model is the bond dimension of the MPO projector defining the vertex projector in Eq. (6.131). We can easily calculate the bond dimension of the projector MPO by considering the F-symbols of the model and the MPO-

tensors constructed from the latter as specified in Fig. 5.15. A closer inspection of the G-symbol reveals that the index values of the indices at each edge of the MPO tensor in Fig. 5.14a have to fulfill the fusion rules. Thus, there are five possible values of the blocked horizontal index (a, f, d) in Fig. 5.14a, namely $(1,1,1), (1,\tau,\tau), (\tau,1,\tau), (\tau,\tau,1)$ and (τ,τ,τ) and likewise for the blocked index (b, f, c). As opposed to the double semion model, the vertical index value e is no longer fixed by the index values a and b as a result of ambiguous fusion results. Thus, the single MPO tensor corresponds to a three qubit operator and we need to introduce an additional MCB per triangle edge compared to the double semion model (cf. Fig. 6.17).

Applying the hierarchical gadget idea for $D = 3^2$ MPOs from Section 6.2.6, we can design the vertex operator from MPOs where individual MPO tensors are three qubit operators, i.e., we need to add two additional physical qubits and two additional communication qubits to the unit cell in Fig. 6.15. Addressing the seven qubits, we use repetition code registers of 7 MCBs each. As we are only looking for a bond dimension $D = 5$ MPO, it is sufficient to use 5^2 such registers.

It is doubtful that even if MCB units become experimental reality, the presented scheme would be feasible due to the large number of MCBs used and the enormous amount of wiring needed to engineer the couplings. Even if these technical obstacles could be overcome, it is doubtful whether signatures of a double Fibonacci phase would be observable. The multi-layer gadget construction might work in principle, however, the separation of energy scales is crucial and one needs to have access to very small energy scales that emerge from the splitting of the splitting of the splitting of the ground state energies. It goes without saying that this approach is thus also extremely sensitive to finite temperature effects.

7. Summary and discussion

In this Thesis we approached non-chiral topological order within a tensor network framework. We introduced the subject of gapped quantum phases and their distinguished properties. The fundamental role of entanglement in the formation of quantum phases beyond Landau's symmetry breaking paradigm lead us to the introduction of tensor network states as the right ansatz class to concisely capture quantum phases in the absence of symmetries. We highlighted the power of the tensor network approach by reviewing the full classification of phases of matter in one dimension and identified virtual symmetries of the individual tensors as the fundamental object that causes phases of matter to become entangled. A finite virtual symmetry group G defining G-injective matrix product states (MPS) gave rise to GHZ-like entanglement – a weak form of long-range entanglement.

Asking whether there exist even stronger forms of long-range entanglement, we turned towards topologically ordered systems in two dimensions. In an attempt to carry over the techniques from the one-dimensional setting, we introduced G-injective projected entangled pair states (PEPS) and explained how the paradigmatic model of non-chiral topological order – the toric code – can be described by the latter.

With this we concluded the introduction to the general mindset and framework of this thesis and moved on to discuss the mathematical mechanisms behind topological order on a general rather abstract level. We introduced the algebraic theory of anyons and explained that it is described by what mathematicians refer to as modular tensor category. We highlighted a particular class of anyon theories which is non-chiral and can be constructed from a fusion category by a particular construction known as the Drinfeld center.

Identifying the mathematical backbone of non-chiral topological order on an abstract mathematical level we returned to the main matter of this Thesis - the emergence of non-chiral topological order in various formalisms which can be considered equivalent. We presented a class of exactly solvable lattice Hamiltonians, the Levin–Wen string-net models, that exhibit non-chiral topological order. We showed how the latter are essentially constructed from a fusion category and that their anyonic particles correspond to the Drinfeld center of the latter. Coming back to the tensor network formalism, we showed that the ground states of Levin–Wen string net Hamiltonians are exact PEPS with virtual symmetries given by matrix product operators that again form a fusion category. We exemplified the equivalence of the latter two formalisms on the example of twisted quantum double models and showed how one can understand both the lattice Hamiltonian as well as the tensor network in terms of a state-sum perspective relating the two formalisms directly to the construction of topological manifold invariants and discretized path integrals of topological quantum field theories.

We concluded the investigation of non-chiral topological order with an excursion to fermionic systems and showed that the MPO-injective PEPS formalism can be generalized to fermionic string-net models.

The third part of this Thesis focused on applying the highly evolved and abstract tensor network formalism to a very concrete problem – the realization of topological order in synthetic quantum matter. We found that MPO-injective PEPS give rise to parent Hamiltonians that can be engineered as the low energy effective theory describing tunnel coupled Majorana

Cooper boxes in a way that is simpler and more feasible than the direct implementation of Levin–Wen string net Hamiltonians, which feature intricate 12-body interactions. The central tool of this investigation were low energy effective theories and their controlled design in the realm of Hamiltonian gadgets. We introduced several variants of low energy effective theories and elaborated on the relation between them. In particular we reviewed a general purpose gadget scheme introduced by Jordan and Farhi and a scheme tailored to realizing PEPS parent Hamiltonians proposed by Brell et al.

As a physical platform on which we sought to implement the aforementioned gadget constructions, we considered mesoscopic hybrid devices – so called Majorana Cooper boxes (MCBs) composed of nanowires and superconductors. Majorana zero modes emerging in the latter give rise to effect qubits in the low energy sector. We presented a concise and systematic way to characterize the effective spin-interaction resulting from tunnel coupling the latter and investigated different mechanisms to control and design the emerging Hamiltonian contributions. Designing small building blocks we were finally able to devise a blueprint for a topological phase of matter beyond the toric code, i.e., the double semion model. In a bold attempt to realize phases of matter which allow for universal topological quantum computation, we investigated the measures necessary to elevate the presented blueprint to give rise to a double Fibonacci phase. The scheme we presented employed hierarchical gadget designs and – though being impractical with the current state of available technologies – showed a way towards designing complex topological quantum matter in principle.

We hope that the ideas presented here are of service to the greater community of condensed matter and quantum information scientist and inspire further ideas for the design of artificial quantum matter from a tensor network perspective. In the future we would like to investigate whether the design ideas presented here can be carried over to other physical hardware platforms such as arrays of Josephson junctions or if one can devise additional control mechanisms to avoid specific Hamiltonian terms. Preliminary investigations regarding the latter have been performed in periodically driven (Floquet) systems, however no significant improvement of the flexibility of the design scheme could be found. At last we suggest to use the existing building blocks as a tool box for analogue quantum simulation and to explore which (non topological) models are available with the components developed already.

On a more theoretical note, we would like to investigate the precise obstacles in capturing chiral topological phases with a tensor network approach. The state-sum perspective presented in this Thesis seems to provide the most clear conceptual insights to this problem and it is apparent from the material presented here that MPO-injective PEPS can not be ground states of chiral Hamiltonians. However, a generalized tensor network approach could be sufficient to capture chiral phases and would potentially lead to a unified understanding of phases of matter.

Acknowledgments

I would like to thank my supervisor Jens Eisert for having been given the opportunity to work on fascinating research subjects, that I would not have dared to study without his encouragement and his persistent aura of positivity and enthusiasm. I am grateful for his valuable insights and advice on countless occasions, for providing a thriving research environment in the local QMIO group and for introducing me to the CRC 183, which lead to an exciting and fun collaboration with Reinhold Egger and Alexander Altland. I am very grateful for this experience. I would also like to thank Andi Bauer for his remarkably unorthodox and innovative ideas and his patience in sharing and discussing the latter with me. I thank all current and former members of the QMIO group who made pursuing a PhD a joyful experience. Thank you, Albert, Martin, Marcel, Dominik, Christian, Alex, Alex, Nick, Marek, Markus, Juani and most of all, Henrik and Augustine, with whom I shared an office and many thoughts about physics and life in general.

I would like to seize this opportunity to thank all the people that persuaded me to continue studying physics at various stages of my life starting with the high school teachers without whom I would not even have considered to take advanced physics classes in school and my best friend Kati Schwanstecher with whom I shared the joy of learning. I want to very warmly thank my companions in the early days of my Bachelor studies, S. Herold, S. Wolf and F. Huber, with whom my journey into the wonderful world of theoretical physics began. Without you I would not have managed to build the fundament for everything that came next – or at least it would have been severely less fun. I would also like to thank my Theoretical Physics tutor Eros Mariani who did an excellent job guiding me through the first year of studies and my former supervisor Axel Pelster, who introduced me to scientific research. I am grateful beyond words to Alexander Altland for his advice and his words of encouragement spoken at the right time. Most of all I would like to thank Sophie Herold for her continuous, invaluable support and encouragement during the last eleven years.

Last but not least, I would like to thank Louzie for her support during the last years and all my friends and my family, in particular my mother, who respect my decision to spend the larger part of my life on a subject alien to them and love me nonetheless. Thank you, Kati, Tobias, Merle, Christina, Charlotte, Isa, Mix, Eva, Robin, Sherien. At last I would like to express my gratitude towards my late father for his endless patience in answering the countless questions of a curious child and for encouraging me to trust in my own judgment and abilities.

A. Technical details on fMPO-symmetric fPEPS

A.1. Concatenation stability

To prove the concatenation stability of fMPO-injectivity for the fPEPS tensors $A_\pm$ defined in Eqs. (5.55) and Eq. (5.56) with the rules defined in Section 5.5.2 (cf. Fig. 5.29), we first introduce an abbreviated notation in Fig. A.1. Instead of drawing the full symmetry MPO, we indicate the positions of the parity matrices Y before and after the concatenation (Fig. A.1) by circles at the respective boundary vertices. Next, we consider all possible ways in which a new tensor can be attached to an existing tensor network patch.

We distinguish between an "open" concatenation depicted in Fig. 5.28a and a partially closed concatenation depicted in Figs. 5.28b–c. The latter are relevant when an outer vertex of a triangle tensor becomes an inner vertex during the concatenation process.

For the case of "open" concatenation consider a concatenation along an edge pointing towards the global flow direction. The different possible concatenation cases are then classified by the shared angle θ with the neighboring edges at the origin vertex (i.e., the source of the edge). The placement of parity matrices depends only on whether the shared angle is smaller or larger than π, while the edge orientations and the exact angles are irrelevant. Thus, there are only four different cases ($\theta = 0, \pi/2, \pi, 3\pi/2$). The global flow criterion restricts the possible geometries and making use of the mirror symmetry along the global flow direction there are only six distinct cases, which are shown explicitly in Fig. A.2a.

When two MPO-symmetric tensors are contracted along a common boundary of length two or more, two different concatenation rules apply depending on the orientation of the inner edge relative to the position of the already contracted transversal indices (cf. Fig. 5.28b and Fig. 5.28c. There are again two cases. First, the edges to be contracted share a vertex at their origin. In this case the contraction does not yield additional parity matrices (cf. Fig. A.2b upper panel). In the other case, we consider the different possible edge configurations in the vicinity of the contracted edge. Using symmetry arguments, we find three distinct cases shown explicitly in Fig. A.2b panel 2 to 4.

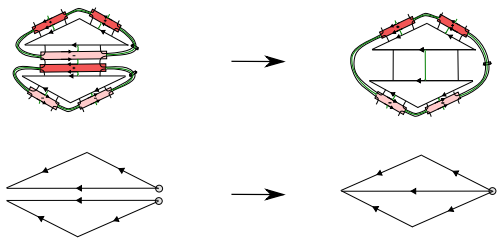

Fig. A.1. ⋆ The concatenation of two MPO-symmetric tensors written in explicit notation (upper panel) and in abbreviated notation only depicting the positions of parity matrices Y.

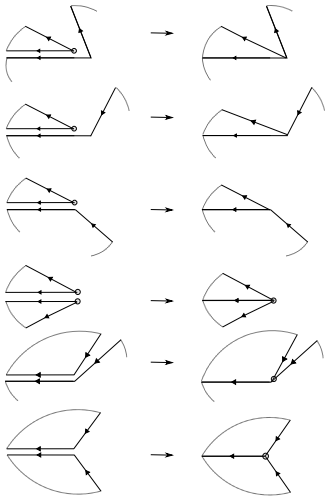

(**a**) Open concatenation.

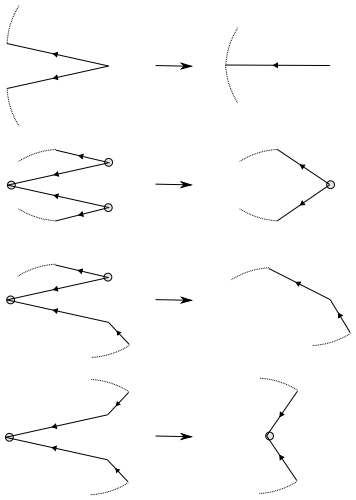

(**b**) Closed concatenation.

Having checked that the fMPO symmetry rules are remain consistent under all possible ways to attach another triangle tensor to an existing patch, the proof is completed by noting that the induction anchor is provided by the elementary triangle tensors $A\pm$.

A.1.1. Hamiltonian gauge of the fermionic toric code model

To prove that the fermionic tensor network defined in Section 5.5.2 is a ground state of the fermionic toric code model [232], we need to apply a gauge transformation on the original Hamiltonian. For fMPO symmetric fPEPS there is a also a gauge choice of ω. A natural gauge is to choose a normalized 3-cocycle. A tensor network defined with normalized 3-cocycles yields a wave-function that is invariant under adding a closed-loop, i.e. $d_i = 1$. Thus, the tensor network gauge suggests a particular Hamiltonian gauge of the corresponding string net model.

In Ref. [232], several gauge transformations were introduced and the Hamiltonian was given in a specific gauge ($\beta = 1$). Thus, we first reintroduce the gauge parameter β by performing the gauge transformation

$$c^\dagger \mapsto \frac{1}{\sqrt{\beta}} c^\dagger, \qquad c \mapsto \sqrt{\beta} c \,. \tag{A.1}$$

and then choose $\beta = -i$. In this gauge we obtain that closed loops are attributed with trivial factors. On the level of matrix elements the plaquette operator is now written as

$$\begin{aligned} Q_p = \sum_{g_1,\cdots,g_6} & p(g_1,\ldots,g_6)\mathcal{F}_p(g_1,\ldots,g_6) \\ & \times |g_1 \oplus 1,\ldots,g_6 \oplus 1\rangle \langle g_1,\ldots,g_6| \ , \end{aligned} \tag{A.2}$$

where $\oplus$ denotes addition modulo two and $\mathcal{F}_p(g_1,\ldots,g_6)$ are given in Table A.1.

Using this gauge, we can check that an open tensor network patch is an eigenstate of the plaquette operator by explicit calculation.

i,j,k,l,m,n	$p(i,j,k,l,m,n)\mathcal{F}_p(i,j,k,l,m,n)$	i,j,k,l,m,n	$p(i,j,k,l,m,n)\mathcal{F}_p(i,j,k,l,m,n)$
000000	$-\alpha/\beta c_3^\dagger c_6^\dagger$		
100000	$c_3^\dagger c_1$	010000	$1/\beta^2 c_1^\dagger c_2^\dagger c_3^\dagger c_6^\dagger$
001000	$c_6^\dagger c_2$	000100	$c_6^\dagger c_4$
000010	$-1/\beta^2 c_3^\dagger c_4^\dagger c_5^\dagger c_6^\dagger$	000001	$c_3^\dagger c_5$
110000	$-1/\beta c_2^\dagger c_3^\dagger$	011000	$-1/\beta c_1^\dagger c_6^\dagger$
001100	$-\beta c_6^\dagger c_4 c_3 c_2$	000110	$1/\beta c_5^\dagger c_6^\dagger$
000011	$-1/\beta c_3^\dagger c_4^\dagger$	100001	$\beta c_3^\dagger c_6 c_5 c_1$
101000	$-\alpha\beta c_2 c_1$	010100	$\alpha/\beta c_1^\dagger c_2^\dagger c_6^\dagger c_4$
001010	$-\alpha/\beta c_4^\dagger c_5^\dagger c_6^\dagger c_2$	000101	$\alpha\beta c_5 c_4$
100010	$-\alpha/\beta c_3^\dagger c_4^\dagger c_5^\dagger c_1$	010001	$\alpha/\beta c_1^\dagger c_2^\dagger c_3^\dagger c_5$
100100	$-\alpha\beta c_4 c_1$	010010	$\alpha/\beta^2 c_1^\dagger c_2^\dagger c_3^\dagger c_4^\dagger c_5^\dagger c_6^\dagger$
001001	$\alpha\beta c_5 c_2$		
000111	1	001110	$-c_5^\dagger c_6^\dagger c_3 c_2$
011100	$c_1^\dagger c_6^\dagger c_4 c_3$		
101100	$\alpha\beta^2 c_4 c_3 c_2 c_1$	010110	$\alpha/\beta^2 c_1^\dagger c_2^\dagger c_5^\dagger c_6^\dagger$
001011	$-\alpha c_4^\dagger c_2$	100101	$-\alpha\beta^2 c_6 c_5 c_4 c_1$
110010	$\alpha/\beta^2 c_2^\dagger c_3^\dagger c_4^\dagger c_5^\dagger$	011001	$-\alpha c_1^\dagger c_5$
010101	$-c_4^\dagger c_5^\dagger c_2 c_1$		

Table A.1. ⋆ The first 32 matrix element of the plaquette operator Q_p defined on a hexagon with physical spins i,j,k,l,m,n after ungauging the Hamiltonian given in Ref. [232]. The remaining 32 matrix elements follow by Hermitian conjugation.

B. Perturbation analysis of the double semion MCB network

This Appendix presents a detailed analysis of the perturbation series for the effective Hamiltonian in the double semion MCB network discussed in Section 6.3.2. It is a literal copy of the Appendix in Ref. [2] which is original work of and was written solely by the author.

We consider the MCB network in Fig. 6.18 where we assume that the energy scale λ^6/E_C^5 characterizing the vertex part, $\hat{H}_v$, is much larger than the scale $\varepsilon = \lambda_{\text{Bell}}^2/E_C$ corresponding to Bell-pair tunneling links between neighboring vertices. Under this assumption, the analysis of Ref. [95] applies where one treats the Bell-pair Hamiltonians $\hat{H}_{Bell}$ as perturbation to $\sum_v \hat{H}_v$. In addition, in our case, terms of order $\mathcal{O}(\varepsilon\lambda^2/E_c^2)$ arise due to loops of length 4 (and beyond) which involve MCBs on different vertices. Such contributions need to be included in a perturbative analysis aimed at checking that the low-energy Hamiltonian of the perturbative PEPS parent theory is indeed the parent Hamiltonian of the encoded PEPS. While the full analysis combining global and local Schrieffer–Wolff transformations [254] is cumbersome, a simplified calculation [95] for the double semion model considers a self-energy expansion series order by order and establishes the physical meaning of each term. As in our perturbative expansion for the low-energy physics of MCB networks in Section 6.2.3, only operators acting within the ground state space of the dominant Hamiltonian term, here the code space, are considered.

The first order gives no contribution since $\hat{P}\hat{H}_{Bell}\hat{P} = 0$, where $\hat{P}$ is the projector to the ground state of $\sum_v \hat{H}_v$. In fact, all odd orders do not contribute apart from trivial energy shifts. At second order, the simultaneous action of Bell-pair operators on two neighboring vertices yields a contribution favoring even parity states for the corresponding four qubits. This term has a clear physical meaning. Indeed, mapping the encoded state back to the physical state by applying the PEPS map A, one finds that the physical state (which used to live on the edge of the honeycomb lattice) is overdetermined. Thanks to the even parity constraint for the four qubits, this overdetermination is resolved and one recovers a consistent mapping from code space to physical space. At fourth order, products of second-order terms but no qualitatively new contributions emerge. Such contributions arise, however, in sixth order from six Bell-pairs Hamiltonians acting on 12 qubits around one plaquette. These terms correspond to encoded versions of the string-net plaquette operator and are essential to drive the system into a topological phase. Note that up to the fifth order, the effective Hamiltonian only contains (encoded versions of) vertex projections and terms ensuring consistency of different local decodings, where one does not expect a topologically ordered ground state. It is thus crucial that the effect of the plaquette operator is relevant for the system. In particular, if we repeat the perturbative analysis for the MCB network Hamiltonian, taking into account perturbations due to loops of length 4 and beyond, we have to check that no terms overwhelming the plaquette operator are present which can potentially destroy the topological order of the ground state.

The design of the MCB network overcomes this obstacle in a natural way by making use of destructive interference mechanisms. Consider a junction of two vertices connected by two Bell-pair bridges in Fig. 6.19. There are 36 different length-4 loops that emerge from tunneling from one MCB at one vertex to the neighboring MCB on the same vertex (via α or β) then to the

other vertex via one of the three Bell bridges, then (again via α or β) to the neighboring MCB and finally back to the starting point via one of the three Bell bridges. It is useful to partition these 36 loops into four different groups labeled by the loop phase $\phi_{\alpha/\beta} - \phi_{\alpha/\beta}$. Let us analyze the different $\phi_\alpha - \phi_\beta$ loops. There is one loop that is threatening the emergence of topological order. It corresponds to the $\hat{z}\hat{z}$ interactions on neighboring qubits, interactions that we needed to suppress already in the design of the vertex Hamiltonian. Because the parity of two different corner qubits determines the physical state uniquely, a system that favors a specific parity of those two qubits corresponds to a trivial product state. Since this state is part of the code space there is no chance to argue that it will not survive the code space projection P. This is why we have chosen the tunneling links on different sublattices according to Fig. 6.19. The loop phase $\phi_\alpha - \phi_\beta = \pi/2$ and likewise $\phi_\beta - \phi_\alpha$ leads to a complete cancellation of all those loops (note that the Bell-pair wires do not add phase shifts) including the one that would otherwise lead to the adverse $\hat{z}\hat{z}$ interaction. The other half of the length-4 loops does not vanish but also poses no threat to the formation of topological order. They are of the form $\hat{O}^{(4)} \propto \hat{p}\hat{p} \otimes \hat{q}\hat{q}$ where the tensor product indicates the separation into two Bell-pairs and $\hat{p}$, $\hat{q}$ denote different Pauli operators. Contributions of this form also arise in second order perturbation theory in ε from the Bell-pair Hamiltonian and therefore do not yield qualitatively new contributions. In addition they are completely outside the code space and do not contribute at all when treated as a first order correction to $\sum_v H_v$. Similar arguments apply to higher order loop terms. Prominently among them are detour-loops that wind once around a vertex ring but with a detour via two qubits of a neighboring vertex. Those detour terms either leave the code space or yield terms that correspond to a product of $O^{(6)}$ and $\hat{z}\hat{z} \otimes \hat{z}\hat{z}$. These terms cause a splitting of the ground state space degeneracy that is in agreement with the aforementioned consistency of physical qubit states and do not cause a phase transition. Detour terms involving more than one detour can be treated similarly.

To conclude, we have verified that the analysis of Ref. [95], and therefore our encoded PEPS approach to the ground state of the double semion model, also applies in the presence of higher-order terms.

Bibliography

[1] C. Wille, O. Buerschaper, and J. Eisert, "Fermionic topological quantum states as tensor networks," Phys. Rev. B **95**, 245127 (2017).

[2] C. Wille, R. Egger, J. Eisert, and A. Altland, "Simulating topological tensor networks with Majorana qubits," Phys. Rev. B **99** (2019).

[3] A. Bauer, J. Eisert, and C. Wille, "Towards a mathematical formalism for classifying phases of matter," (2019), arXiv:1903.05413.

[4] N. Schuch, I. Cirac, and D. Pérez-García, "PEPS as ground states: Degeneracy and topology," Ann. Phys. **325**, 2153 (2010).

[5] O. Buerschaper, J. M. Mombelli, M. Christandl, and M. Aguado, "A hierarchy of topological tensor network states," J. Mat. Phys. **54**, 012201 (2013).

[6] O. Buerschaper, "Twisted injectivity in projected entangled pair states and the classification of quantum phases," Ann. Phys. **351**, 447 (2014).

[7] M. B. Şahinoğlu, D. Williamson, N. Bultinck, M. Mariën, J. Haegeman, N. Schuch, and F. Verstraete, "Characterizing Topological Order with Matrix Product Operators," ArXiv e-prints (2014), arXiv:1409.2150.

[8] N. Bultinck, M. Mariën, D. Williamson, M. Şahinoğlu, J. Haegeman, and F. Verstraete, "Anyons and matrix product operator algebras," Ann. Phys. **378**, 183 (2017).

[9] N. Bultinck, D. J. Williamson, J. Haegeman, and F. Verstraete, "Fermionic projected entangled-pair states and topological phases," J. Phys. A. **51**, 025202 (2017).

[10] D. J. Williamson, N. Bultinck, J. Haegeman, and F. Verstraete, "Fermionic Matrix Product Operators and Topological Phases of Matter," (2016), arXiv:1609.02897.

[11] D. Aasen, E. Lake, and K. Walker, "Fermion condensation and super pivotal categories," (2017), arXiv:1709.01941.

[12] M. A. Levin and X.-G. Wen, "String-net condensation: A physical mechanism for topological phases," Phys. Rev. B **71**, 045110 (2005).

[13] E. Witten, "Topological quantum field theory," Commun. Math. Phys. **117**, 353 (1988).

[14] V. Turaev and O. Viro, "State sum invariants of 3-manifolds and quantum 6j-symbols," Topology **31**, 865 (1992).

[15] B. Balsam, "Turaev-Viro invariants as an extended TQFT III," (2010), arXiv:1012.0560.

[16] A. K. Jr. and B. Balsam, "Turaev-Viro invariants as an extended TQFT," (2010), arXiv:1004.1533.

[17] B. Balsam, *Turaev-Viro invariants as an extended TQFT II*, 2010, arXiv:1010.1222.

[18] A. Kitaev, "Anyons in an exactly solved model and beyond," Ann. Phys. **321**, 2 (2006).

[19] N. Andruskiewitsch, J. Cuadra, and B. Torrecillas, *Hopf Algebras and Tensor Categories*, Contemporary Mathematics (American Mathematical Society, 2013).

[20] B. Zeng, X. Chen, D.-L. Zhou, and X.-G. Wen, "Quantum Information Meets Quantum Matter," Quant. Sci. Tech. (2019).

[21] E. Gibney and D. Castelvecchi, "Physics of 2D exotic matter wins Nobel," Nature **538**, 18 (2016).

[22] E. Gibney, "Inside Microsoft's quest for a topological quantum computer," Nature (2016).

[23] P. W. Shor, "Polynomial-Time Algorithms for Prime Factorization and Discrete Logarithms on a Quantum Computer," SIAM Journal on Computing **26**, 1484 (1997).

[24] J. Preskill, "Quantum computing and the entanglement frontier," (2012), arXiv:1203.5813.

[25] M. Möller and C. Vuik, "On the impact of quantum computing technology on future developments in high-performance scientific computing," Ethics Inf. Technol. (2017).

[26] R. de Wolf, "The potential impact of quantum computers on society," Ethics Inf. Technol. **19**, 271 (2017).

[27] L. D. Landau, "On the theory of phase transitions," Zh. Eksp. Teor. Fiz. **7**, Reprint: Ukr. J. Phys.53,25(2008), 19 (1937).

[28] H. E. Stanley, *Introduction to Phase Transitions and Critical Phenomena* (Oxford University Press, 1971).

[29] J. S. Bell, "On the Einstein Podolsky Rosen paradox," Physics **1**, 195 (1964).

[30] X. Chen, Z.-C. Gu, and X.-G. Wen, "Local unitary transformation, long-range quantum entanglement, wave function renormalization, and topological order," Phys. Rev. B **82**, 155138 (2010).

[31] A. Kitaev, "Fault-tolerant quantum computation by anyons," Ann. Phys. **303**, 2 (2003).

[32] J. M. Leinaas and J. Myrheim, "On the theory of identical particles," Il Nuovo Cimento B (1971-1996) **37**, 1 (1977).

[33] F. Wilczek, "Quantum Mechanics of Fractional-Spin Particles," Phys. Rev. Lett. **49**, 957 (1982).

[34] J. Fröhlich, "Statistics of Fields, the Yang-Baxter Equation, and the Theory of Knots and Links," in , edited by G. 't Hooft, A. Jaffe, G. Mack, P. K. Mitter, and R. Stora (Springer US, Boston, MA, 1988), pp. 71–100.

[35] A. R. Stern, "Non-Abelian states of matter," Nature **464**, 187 (2010).

[36] C. Nayak, S. H. Simon, A. Stern, M. Freedman, and S. Das Sarma, "Non-Abelian anyons and topological quantum computation," Rev. Mod. Phys. **80**, 1083 (2008).

[37] S. Trebst, M. Troyer, Z. Wang, and A. W. W. Ludwig, "A Short Introduction to Fibonacci Anyon Models," Prog. Theor. Phys. Supp. **176**, 384 (2008).

[38] C. Nayak, S. H. Simon, A. Stern, M. Freedman, and S. Das Sarma, "Non-Abelian anyons and topological quantum computation," Revs. Mod. Phys. **80**, 1083 (2008).

[39] M. H. Freedman, A. Kitaev, and Z. Wang, "Simulation of Topological Field Theories by Quantum Computers," Commun. Math.. Phys. **227**, 587 (2002).

[40] M. H. Freedman, A. Kitaev, M. J. Larsen, and Z. Wang, "Topological quantum computation," Bull. Amer. Math. Soc. (N.S, 31 (2002).

[41] M. H. Freedman, M. Larsen, and Z. Wang, "A Modular Functor Which is Universal for Quantum Computation," Commun. Math. Phys. **227**, 605 (2002).

[42] V. Lahtinen and J. Pachos, "A Short Introduction to Topological Quantum Computation," SciPost Phys. **3** (2017).

[43] B. Field and T. Simula, "Introduction to topological quantum computation with non-Abelian anyons," Quantum Science and Technology **3**, 045004 (2018).

[44] R. Koenig, G. Kuperberg, and B. W. Reichardt, "Quantum computation with Turaev–Viro codes," Ann. Phys. **325**, 2707 (2010).

[45] E. Dennis, A. Kitaev, A. Landahl, and J. Preskill, "Topological quantum memory," J. Mat. Phys. **43**, 4452 (2002).

[46] A. Bauer, "Generalized topological state-sum constructions and their universality," (2019), arXiv:1909.03031.

[47] D. C. Tsui, H. L. Stormer, and A. C. Gossard, "Two-Dimensional Magnetotransport in the Extreme Quantum Limit," Phys. Rev. Lett. **48**, 1559 (1982).

[48] H. L. Stormer, "Nobel Lecture: The fractional quantum Hall effect," Rev. Mod. Phys. **71**, 875 (1999).

[49] R. B. Laughlin, "Anomalous Quantum Hall Effect: An Incompressible Quantum Fluid with Fractionally Charged Excitations," Phys. Rev. Lett. **50**, 1395 (1983).

[50] G. Moore and N. Read, "Nonabelions in the fractional quantum hall effect," Nucl. Phys. B **360**, 362 (1991).

[51] X. Lin, R. Du, and X. Xie, "Recent experimental progress of fractional quantum Hall effect: 5/2 filling state and graphene," Natl. Sci. Rev. **1**, 564 (2014).

[52] A. Kapustin and L. Fidkowski, "Local Commuting Projector Hamiltonians and the Quantum Hall Effect," Commun. Math. Phys. (2019).

[53] T.-H. Han, M. R. Norman, J.-J. Wen, J. A. Rodriguez-Rivera, J. S. Helton, C. Broholm, and Y. S. Lee, "Correlated impurities and intrinsic spin-liquid physics in the kagome material herbertsmithite," Phys. Rev. B **94**, 060409 (2016).

[54] M. Fu, T. Imai, T.-H. Han, and Y. S. Lee, "Evidence for a gapped spin-liquid ground state in a kagome Heisenberg antiferromagnet," Science **350**, 655 (2015).

[55] J. Eisert, "Entanglement and tensor network states," (2013), arXiv:1308.3318.

[56] R. Orús, "Advances on tensor network theory: symmetries, fermions, entanglement, and holography," English, Eur. Phys. J. B **87**, 280 (2014).

[57] R. Orús, "A practical introduction to tensor networks: Matrix product states and projected entangled pair states," Ann. Phys. **349**, 117 (2014).

[58] S.-J. Ran, E. Tirrito, C. Peng, X. Chen, L. Tagliacozzo, G. Su, and M. Lewenstein, "Lecture Notes of Tensor Network Contractions," (2017), arXiv:1708.09213.

[59] M. Fannes, B. Nachtergaele, and R. F. Werner, "Finitely correlated states on quantum spin chains," Commun. Math. Phys. **144**, 443 (1992).

[60] D. Pérez-García, F. Verstraete, M. M. Wolf, and J. I. Cirac, "Matrix product state representations," Quantum. Inf. Comput. **7**, 401 (2007).

[61] N. Schuch, D. Pérez-García, and I. Cirac, "Classifying quantum phases using matrix product states and projected entangled pair states," Phys. Rev. B **84**, 165139 (2011).

[62] F. Verstraete, M. M. Wolf, D. Perez-Garcia, and J. I. Cirac, "Criticality, the Area Law, and the Computational Power of Projected Entangled Pair States," Phys. Rev. Lett. **96**, 220601 (2006).

[63] O. Buerschaper, M. Aguado, and G. Vidal, "Explicit tensor network representation for the ground states of string-net models," Phys. Rev. B **79**, 085119 (2009).

[64] Z.-C. Gu, M. Levin, B. Swingle, and X.-G. Wen, "Tensor-product representations for string-net condensed states," Phys. Rev. B **79**, 085118 (2009).

[65] P. Corboz, R. Orús, B. Bauer, and G. Vidal, "Simulation of strongly correlated fermions in two spatial dimensions with fermionic projected entangled-pair states," Phys. Rev. B **81**, 165104 (2010).

[66] C. V. Kraus, N. Schuch, F. Verstraete, and J. I. Cirac, "Fermionic projected entangled pair states," Phys. Rev. A **81**, 052338 (2010).

[67] L. Fidkowski and A. Kitaev, "Topological phases of fermions in one dimension," Phys. Rev. B **83**, 075103 (2011).

[68] N. Bultinck, D. J. Williamson, J. Haegeman, and F. Verstraete, "Fermionic matrix product states and one-dimensional topological phases," Phys. Rev. B **95**, 075108 (2017).

[69] Z.-C. Gu, Z. Wang, and X.-G. Wen, "Classification of two-dimensional fermionic and bosonic topological orders," Phys. Rev. B **91**, 125149 (2015).

[70] A. Lavasani, G. Zhu, and M. Barkeshli, "Universal logical gates with constant overhead: instantaneous Dehn twists for hyperbolic quantum codes," Quantum **3**, 180 (2019).

[71] P. Webster and S. D. Bartlett, "Fault-Tolerant Quantum Gates with Defects in Topological Stabiliser Codes," (2019), arXiv:1906.01045.

[72] G. Zhu, A. Lavasani, and M. Barkeshli, "Fast universal logical gates on topologically encoded qubits at arbitrarily large code distances," (2018), arXiv:1806.02358.

[73] B. Douçot, L. B. Ioffe, and J. Vidal, "Discrete non-Abelian gauge theories in Josephson-junction arrays and quantum computation," Phys. Rev. B **69**, 214501 (2004).

[74] Sameti, Mahdi and Potočnik, Anton and Browne, Dan E. and Wallraff, Andreas and Hartmann, Michael J., "Superconducting quantum simulator for topological order and the toric code," Phys. Rev. A **95**, 042330 (2017).

[75] B. Paredes and I. Bloch, "Minimum instances of topological matter in an optical plaquette," Phys. Rev. A **77**, 023603 (2008).

[76] E. Zohar, A. Farace, B. Reznik, and J. I. Cirac, "Digital Quantum Simulation of $\mathbb{Z}_2$ Lattice Gauge Theories with Dynamical Fermionic Matter," Phys. Rev. Lett. **118**, 070501 (2017).

[77] R. Nath, M. Dalmonte, A. W. Glaetzle, P. Zoller, F. Schmidt-Kaler, and R. Gerritsma, "Hexagonal plaquette spin–spin interactions and quantum magnetism in a two-dimensional ion crystal," New. J. Phys **17**, 065018 (2015).

[78] J. K. Pachos, W. Wieczorek, C. Schmid, N. Kiesel, R. Pohlner, and H. Weinfurter, "Revealing anyonic features in a toric code quantum simulation," New. J. Phys **11**, 083010 (2009).

[79] C.-Y. Lu, W.-B. Gao, O. Gühne, X.-Q. Zhou, Z.-B. Chen, and J.-W. Pan, "Demonstrating Anyonic Fractional Statistics with a Six-Qubit Quantum Simulator," Phys. Rev. Let. **102** (2009).

[80] X.-C. Yao, T.-X. Wang, H.-z. Chen, W. Gao, A. Fowler, R. Raussendorf, T. Chen, N.-L. Liu, C.-Y. Lu, Y.-J. Deng, Y.-A. Chen, and J.-W. Pan, "Experimental demonstration of topological error correction," Nature **482**, 489 (2012).

[81] H.-N. Dai, B. Yang, A. Reingruber, H. Sun, X.-F. Xu, Y.-A. Chen, Z.-S. Yuan, and J.-W. Pan, "Four-body ring-exchange interactions and anyonic statistics within a minimal toric-code Hamiltonian," Nat. Phys. **13**, 1195 (2017).

[82] S. Gladchenko, D. Olaya, E. Dupont-Ferrier, B. Douçot, L. B. Ioffe, and M. E. Gershenson, "Superconducting nanocircuits for topologically protected qubits," Nat. Phys. **5**, 48 (2008).

[83] H. Weimer, M. Müller, I. Lesanovsky, P. Zoller, and H. P. Büchler, "A Rydberg quantum simulator," Nat. Phys. **6**, 382 (2010).

[84] C. Schweizer, F. Grusdt, M. Berngruber, L. Barbiero, E. Demler, N. Goldman, I. Bloch, and M. Aidelsburger, "Floquet approach to $\mathbb{Z}_2$ lattice gauge theories with ultracold atoms in optical lattices," Nat. Phys. **15**, 1168 (2019).

[85] S. Vijay, T. H. Hsieh, and L. Fu, "Majorana Fermion Surface Code for Universal Quantum Computation," Phys. Rev. X **5**, 041038 (2015).

[86] S. Plugge, L. A. Landau, E. Sela, A. Altland, K. Flensberg, and R. Egger, "Roadmap to Majorana surface codes," Phys. Rev. B **94**, 174514 (2016).

[87] L. A. Landau, S. Plugge, E. Sela, A. Altland, S. M. Albrecht, and R. Egger, "Towards Realistic Implementations of a Majorana Surface Code," Phys. Rev. Lett. **116**, 050501 (2016).

[88] D. Litinski, M. S. Kesselring, J. Eisert, and F. v. Oppen, "Combining Topological Hardware and Topological Software: Color-Code Quantum Computing with Topological Superconductor Networks," Phys. Rev. X **7**, 031048 (2017).

[89] B. Béri and N. R. Cooper, "Topological Kondo Effect with Majorana Fermions," Phys. Rev. Lett. **109**, 156803 (2012).

[90] A. Altland and R. Egger, "Multiterminal Coulomb-Majorana junction," Phys. Rev. Lett. **110**, 196401 (2013).

[91] B. M. Terhal, F. Hassler, and D. P. DiVincenzo, "From Majorana fermions to topological order," Phys. Rev. Lett. **108**, 260504 (2012).

[92] J. Kempe, A. Kitaev, and O. Regev, "The Complexity of the Local Hamiltonian Problem," SIAM J. Comp. **35**, 1070 (2006).

[93] S. P. Jordan and E. Farhi, "Perturbative gadgets at arbitrary orders," Phys. Rev. A **77**, 062329 (2008).

[94] C. G. Brell, S. T. Flammia, S. D. Bartlett, and A. C. Doherty, "Toric codes and quantum doubles from two-body Hamiltonians," New. J. Phys **13**, 053039 (2011).

[95] C. G. Brell, S. D. Bartlett, and A. C. Doherty, "Perturbative 2-body parent Hamiltonians for projected entangled pair states," New J. Phys. **16**, 123056 (2014).

[96] M. Freedman, C. Nayak, K. Shtengel, K. Walker, and Z. Wang, "A class of P,T-invariant topological phases of interacting electrons," Ann. Phys. **310**, 428 (2004).

[97] O. Buerschaper, S. C. Morampudi, and F. Pollmann, "Double semion phase in an exactly solvable quantum dimer model on the kagome lattice," Phys. Rev. B **90** (2014).

[98] E. H. Lieb and D. W. Robinson, "The finite group velocity of quantum spin systems," Commun. Math.. Phys. **28**, 251 (1972).

[99] M. B. Hastings, "Lieb-Schultz-Mattis in higher dimensions," Phys. Rev. B **69** (2004).

[100] M. B. Hastings and T. Koma, "Spectral Gap and Exponential Decay of Correlations," Commun. Math. Phys. **265**, 781 (2006).

[101] B. Nachtergaele and R. Sims, "Lieb-Robinson Bounds and the Exponential Clustering Theorem," Commun. Math. Phys. **265**, 119 (2006).

[102] A. M. Dalzell and F. G. S. L. Brandão, "Locally accurate MPS approximations for ground states of one-dimensional gapped local Hamiltonians," Quantum **3**, 187 (2019).

[103] P. Coleman and A. J. Schofield, "Quantum criticality," Nature **433**, 226 (2005).

[104] J. A. Hertz, "Quantum critical phenomena," Phys. Rev. B **14**, 1165 (1976).

[105] S. Sachdev, *Quantum Phase Transitions* (Cambridge University Press, 2000).

[106] R. Movassagh, "Generic Local Hamiltonians are Gapless," Phys. Rev. Lett. **119**, 220504 (2017).

[107] C. Lancien and D. Pérez-García, "Correlation length in random MPS and PEPS," (2019), arXiv:1906.11682.

[108] M. Lemm, "Gaplessness is not generic for translation-invariant spin chains," Phys. Rev. B **100** (2019).

[109] T. S. Cubitt, D. Perez-Garcia, and M. M. Wolf, "Undecidability of the spectral gap," Nature **528**, 207 (2015).

[110] J. Bausch, T. Cubitt, A. Lucia, and D. Perez-Garcia, "Undecidability of the Spectral Gap in One Dimension," (2018), arXiv:1810.01858.

[111] B. Zeng and X.-G. Wen, "Gapped quantum liquids and topological order, stochastic local transformations and emergence of unitarity," Phys. Rev. B **91**, 125121 (2015).

[112] J. Haah, "Local stabilizer codes in three dimensions without string logical operators," Phys. Rev. A **83**, 042330 (2011).

[113] S. Vijay and L. Fu, "Teleportation-based quantum information processing with Majorana zero modes," Phys. Rev. B **94**, 235446 (2016).

[114] G. B. Halász, T. H. Hsieh, and L. Balents, "Fracton Topological Phases from Strongly Coupled Spin Chains," Phys. Rev. Lett. **119**, 257202 (2017).

[115] A. Gromov, "Towards Classification of Fracton Phases: The Multipole Algebra," Phys. Rev. X **9**, 031035 (2019).

[116] R. M. Nandkishore and M. Hermele, "Fractons," Annu. Rev. Condens. Mat. Phys. **10**, 295 (2019).

[117] X. Chen, Z.-C. Gu, and X.-G. Wen, "Classification of gapped symmetric phases in one-dimensional spin systems," Phys. Rev. B **83**, 035107 (2011).

[118] X. Chen, Z.-C. Gu, and X.-G. Wen, "Complete classification of one-dimensional gapped quantum phases in interacting spin systems," Phys. Rev. B **84**, 235128 (2011).

[119] X. G. Wen, "Colloquium: Zoo of quantum-topological phases of matter," Rev. Mod. Phys. **89**, 041004 (2017).

[120] J. F. Clauser, M. A. Horne, A. Shimony, and R. A. Holt, "Proposed Experiment to Test Local Hidden-Variable Theories," Phys. Rev. Lett. **23**, 880 (1969).

[121] B. Hensen, H. Bernien, A. Dréau, A. Reiserer, N. Kalb, M. Blok, J. Ruitenberg, R. Vermeulen, R. Schouten, C. Abellan, W. Amaya, V. Pruneri, M. Mitchell, M. Markham, D. Twitchen, D. Elkouss, S. Wehner, T. Taminiau, and R. Hanson, "Loophole-free Bell inequality violation using electron spins separated by 1.3 kilometres," Nature **526** (2015).

[122] A. Hamma, R. Ionicioiu, and P. Zanardi, "Ground state entanglement and geometric entropy in the Kitaev model," Phys. Let. A **337**, 22 (2005).

[123] M. Hermanns, "Entanglement in topological systems," arXiv:1702.01525.

[124] J. Eisert, M. Cramer, and M. B. Plenio, "Colloquium : Area laws for the entanglement entropy," Rev. Mod. Phys. **82**, 277 (2010).

[125] F. G. S. L. Brandão and M. Horodecki, "Exponential Decay of Correlations Implies Area Law," Commun. Math.. Phys. **333**, 761 (2014).

[126] A. Kitaev and J. Preskill, "Topological Entanglement Entropy," Phys. Rev. Lett. **96**, 110404 (2006).

[127] K. Van Acoleyen, M. Mariën, and F. Verstraete, "Entanglement Rates and Area Laws," Phys. Rev. Let. **111** (2013).

[128] S. Michalakis, "Stability of the Area Law for the Entropy of Entanglement," (2012), arXiv:1206.6900.

[129] Y. Ge and J. Eisert, "Area laws and efficient descriptions of quantum many-body states," ArXiv e-prints (2014), arXiv:1411.2995.

[130] N. Schuch, M. M. Wolf, F. Verstraete, and J. I. Cirac, "Computational Complexity of Projected Entangled Pair States," Phys. Rev. Lett. **98**, 140506 (2007).

[131] J. Haferkamp, D. Hangleiter, J. Eisert, and M. Gluza, "Contracting projected entangled pair states is average-case hard," (2018), arXiv:1810.00738.

[132] M. Schwarz, O. Buerschaper, and J. Eisert, "Approximating local observables on projected entangled pair states," Phys. Rev. A **95**, 060102 (2017).

[133] J. I. Cirac, J. Garre-Rubio, and D. Pérez-García, "Mathematical open problems in Projected Entangled Pair States," (2019), arXiv:1903.09439.

[134] S. Bravyi, M. B. Hastings, and F. Verstraete, "Lieb-Robinson Bounds and the Generation of Correlations and Topological Quantum Order," Phys. Rev. Lett. **97**, 050401 (2006).

[135] J. C. Bridgeman and C. T. Chubb, "Hand-waving and interpretive dance: an introductory course on tensor networks," J. Phys. A. **50**, 223001 (2017).

[136] I. Arad, A. Kitaev, Z. Landau, and U. Vazirani, "An area law and sub-exponential algorithm for 1D systems," (2013), arXiv:1301.1162.

[137] Z. Landau, U. Vazirani, and T. Vidick, "A polynomial time algorithm for the ground state of one-dimensional gapped local Hamiltonians," Nat. Phys. **11** (2015).

[138] S. R. White, "Density matrix formulation for quantum renormalization groups," Phys. Rev. Lett. **69**, 2863 (1992).

[139] U. Schollwöck, "The density-matrix renormalization group in the age of matrix product states," Ann. Phys. **326**, 96 (2011).

[140] F. Verstraete, V. Murg, and J. Cirac, "Matrix product states, projected entangled pair states, and variational renormalization group methods for quantum spin systems," Adv. Phys. **57**, 143 (2008).

[141] N. Schuch, "Condensed Matter Applications of Entanglement Theory," (2013), arXiv:1306.5551.

[142] T. Barthel, M. Kliesch, and J. Eisert, "Real-Space Renormalization Yields Finite Correlations," Phys. Rev. Lett. **105**, 010502 (2010).

[143] M. B. Hastings, "Entropy and entanglement in quantum ground states," Phys. Rev. B **76**, 035114 (2007).

[144] R. Orús and G. Vidal, "Simulation of two-dimensional quantum systems on an infinite lattice revisited: Corner transfer matrix for tensor contraction," Phys. Rev. B **80** (2009).

[145] M. Lubasch, J. I. Cirac, and M.-C. Bañuls, "Unifying projected entangled pair state contractions," New. J. Phys **16**, 033014 (2014).

[146] G. Evenbly, "Online ressource on tensor networks," https://www.tensors.net/peps.

[147] P. Corboz, T. M. Rice, and M. Troyer, "Competing States in the t-JModel: Uniformd-Wave State versus Stripe State," Phys. Rev. Let. **113** (2014).

[148] J. Jordan, R. Orús, G. Vidal, F. Verstraete, and J. I. Cirac, "Classical Simulation of Infinite-Size Quantum Lattice Systems in Two Spatial Dimensions," Phys. Rev. Let. **101** (2008).

[149] G. Evenbly, "Gauge fixing, canonical forms, and optimal truncations in tensor networks with closed loops," Phys. Rev. B **98** (2018).

[150] M. J. J. O'Rourke and G. K.-L. Chan, "A simplified and improved approach to tensor network operators in two dimensions," (2019), arXiv:1911.04592.

[151] P. Schmoll, S. S. S. Jahromi, M. Hörmann, K.P. Schmidt, and R. Orús, "Fine-Grained Tensor Network Methods," (2019), arXiv:1911.04882.

[152] M. Nightingale and C. Umrigar, *Quantum Monte Carlo methods in physics and chemistry*, Vol. 154 (Springer, 1999).

[153] P. Henelius and A. W. Sandvik, "Sign problem in Monte Carlo simulations of frustrated quantum spin systems," Phys. Rev. B **62**, 1102 (2000).

[154] V. Murg, F. Verstraete, and J. I. Cirac, "Exploring frustrated spin systems using projected entangled pair states," Phys. Rev. B **79**, 195119 (2009).

[155] A. Kshetrimayum, T. Picot, R. Orús, and D. Poilblanc, "Spin- 12 kagome XXZ model in a field: Competition between lattice nematic and solid orders," Phys. Rev. B **94** (2016).

[156] D. Poilblanc, M. Mambrini, and S. Capponi, "Critical colored-RVB states in the frustrated quantum Heisenberg model on the square lattice," SciPost Phys. **7** (2019).

[157] D. Perez-Garcia, F. Verstraete, J. I. Cirac, and M. M. Wolf, "PEPS as unique ground states of local Hamiltonians," ArXiv e-prints (2007), arXiv:0707.2260.

[158] J. I. Cirac, J. Garre-Rubio, and D. Pérez-García, "Mathematical open problems in Projected Entangled Pair States," (2019), arXiv:1903.09439.

[159] G. De las Cuevas, J. I. Cirac, N. Schuch, and D. Perez-Garcia, "Irreducible forms of matrix product states: Theory and applications," J. Mat. Phys. **58**, 121901 (2017).

[160] A. Kapustin and L. Fidkowski, "Local Commuting Projector Hamiltonians and the Quantum Hall Effect," Commun. Math. Phys. (2019).

[161] F. J. Wegner, "Duality in Generalized Ising Models and Phase Transitions without Local Order Parameters," J. Mat. Phys. **12**, 2259 (1971).

[162] J. B. Kogut, "An introduction to lattice gauge theory and spin systems," Rev. Mod. Phys. **51**, 659 (1979).

[163] D. Lidar and T. Brun, *Quantum Error Correction* (Cambridge University Press, 2013).

[164] H. Bombin, "An Introduction to Topological Quantum Codes," (2013), arXiv:1311.0277.

[165] A. Córcoles, E. Magesan, S. J Srinivasan, A. Cross, M. Steffen, J. M Gambetta, and J. Chow, "Demonstration of a quantum error detection code using a square lattice of four superconducting qubits," Nat. Comm. **6**, 6979 (2015).

[166] J. M. Gambetta, J. Chow, and M. Steffen, "Building logical qubits in a superconducting quantum computing system," npj Quant. Inf. **3** (2015).

[167] H. Bombin and M. A. Martin-Delgado, "Topological Quantum Distillation," Phys. Rev. Lett. **97**, 180501 (2006).

[168] S. Bravyi, M. B. Hastings, and S. Michalakis, "Topological quantum order: Stability under local perturbations," J. Mat. Phys. **51**, 093512 (2010).

[169] S. Bravyi and M. B. Hastings, "A Short Proof of Stability of Topological Order under Local Perturbations," Commun. Math.. Phys. **307**, 609 (2011).

[170] S. Michalakis and J. P. Zwolak, "Stability of Frustration-Free Hamiltonians," Commun. Math.. Phys. **322**, 277 (2013).

[171] M. Levin and X.-G. Wen, "Detecting Topological Order in a Ground State Wave Function," Phys. Rev. Lett. **96**, 110405 (2006).

[172] L. Fidkowski, M. Freedman, C. Nayak, K. Walker, and Z. Wang, "From String Nets to Nonabelions," Commun. Math. Phys. **287**, 805 (2009).

[173] S. MacLane, *Categories for the Working Mathematician*, Graduate Texts in Mathematics, Vol. 5 (Springer-Verlag, New York, 1971).

[174] E. Lake and Y.-S. Wu, "Signatures of broken parity and time-reversal symmetry in generalized string-net models," Phys. Rev. B **94**, 115139 (2016).

[175] L. Lootens, R. Vanhove, J. Haegeman, and F. Verstraete, "Galois conjugated tensor fusion categories and non-unitary CFT," (2019), arXiv:1902.11241.

[176] S. X. Cui and Z. Wang, "Universal quantum computation with metaplectic anyons," J. Mat. Phys. **56**, 032202 (2015).

[177] P. Bonderson, E. Rowell, Z. Wang, and Q. Zhang, "Congruence subgroups and supermodular categories," Pac. J. Math. **296**, 257 (2018).

[178] Y. Zhang, T. Grover, A. Turner, M. Oshikawa, and A. Vishwanath, "Quasiparticle statistics and braiding from ground-state entanglement," Phys. Rev. B **85**, 235151 (2012).

[179] A. Joyal and R. Street, "Tortile Yang-Baxter operators in tensor categories," J. Pure Appl. Algebra **71**, 43 (1991).

[180] A. Gruen, *Computing modular data for drinfeld centers of pointed fusion categories*, BA thesis, 2017.

[181] M. Thuresson, "Drinfeld Centers," MA thesis (Uppsala University, Algebra and Geometry, 2018), p. 73.

[182] M. Müger, "From subfactors to categories and topology II: The quantum double of tensor categories and subfactors," J. Pure Appl. Algebra **180**, 159 (2003).

[183] M. B. (https://mathoverflow.net/users/10718/marcel-bischoff), *Is the central charge of a Drinfeld center always 0?* eprint: https://mathoverflow.net/q/261827.

[184] C. Kassel, *Quantum Groups* (Springer, 2012).

[185] Z. Kádár, A. Marzuoli, and M. Rasetti, "Microscopic Description of 2D Topological Phases, Duality, and 3D State Sums," Adv. Mat. Phys. **2010**, 1 (2010).

[186] A. K. Jr, "String-net model of Turaev-Viro invariants," (2011), arXiv:1106.6033.

[187] B. Balsam and A. K. Jr, "Kitaev's Lattice Model and Turaev-Viro TQFTs," (2012), arXiv:1206.2308.

[188] K. Walker, "TQFT," http://canyon23.net/math/tc.pdf (2006).

[189] R. Dijkgraaf and E. Witten, "Topological gauge theories and group cohomology," Commun. Math. Phys. **129**, 393 (1990).

[190] V. Turaev and O. Viro, "State sum invariants of 3-manifolds and quantum 6j-symbols," Topology **31**, 865 (1992).

[191] J. Barrett and B. Westbury, "Invariants of piecewise-linear 3-manifolds," Trans. Amer. Math. Soc. **348**, 3997 (1996).

[192] M. Atiyah, *New invariants of 3- and 4-dimensional manifolds.* The mathematical heritage of Hermann Weyl, Proc. Symp. Pure Math. 48, 285-299 (1988). 1988.

[193] M. F. Atiyah, "Topological quantum field theory," Pub. Math. de l'IHÉS **68**, 175 (1988).

[194] E. Witten, "Quantum field theory and the Jones polynomial," Commun. Math. Phys. **121**, 351 (1989).

[195] O. Buerschaper and M. Aguado, "Mapping Kitaev's quantum double lattice models to Levin and Wen's string-net models," Phys. Rev. B **80**, 155136 (2009).

[196] L. Chang, "Kitaev models based on unitary quantum groupoids," J. Mat. Phys. **55**, 041703 (2014).

[197] C. Meusburger, "Kitaev Lattice Models as a Hopf Algebra Gauge Theory," Commun. Math. Phys. **353**, 413 (2017).

[198] J. Fuchs and C. Schweigert, "Symmetries and defects in three-dimensional topological field theory," (2015), arXiv:1501.01885.

[199] A. Davydov, M. Müger, D. Nikshych, and V. Ostrik, "The Witt group of non-degenerate braided fusion categories," J. reine u. angew. Math. (Crelles Journal) **2013** (2013).

[200] B. Bartlett, C. L. Douglas, C. J. Schommer-Pries, and J. Vicary, "Extended 3-dimensional bordism as the theory of modular objects," (2014), arXiv:1411.0945.

[201] N. Carqueville, C. Meusburger, and G. Schaumann, "3-dimensional defect TQFTs and their tricategories," (2016), arXiv:1603.01171.

[202] J. Collins and R. Duncan, "Hopf-Frobenius algebras and a Simpler Drinfeld double," (2019), arXiv:1905.00797.

[203] C.-H. Lin and M. Levin, "Generalizations and limitations of string-net models," Phys. Rev. B **89**, 195130 (2014).

[204] L. Chang, M. Cheng, S. X. Cui, Y. Hu, W. Jin, R. Movassagh, P. Naaijkens, Z. Wang, and A. Young, "On enriching the Levin–Wen model with symmetry," J. Phys. A. **48**, 12FT01 (2015).

[205] S.-M. Hong, "On symmetrization of 6j-symbols and Levin-Wen Hamiltonian," (2009), arXiv:0907.2204.

[206] T. Lan and X.-G. Wen, "Topological quasiparticles and the holographic bulk-edge relation in $(2+1)$-dimensional string-net models," Phys. Rev. B **90**, 115119 (2014).

[207] I. Runkel, "String-net models for non-spherical pivotal fusion categories," (2019), arXiv:1907.12532.

[208] J. W. Barrett and B. W. Westbury, Trans. Amer. Math. Soc. **348**, 3997 (1996).

[209] S. X. Cui and Z. Wang, "State sum invariants of three manifolds from spherical multi-fusion categories," J. Knot. Theor. Ramif. **26**, 1750104 (2017), eprint: https://doi.org/10.1142/S0218216517501048.

[210] Y. Hu, Y. Wan, and Y.-S. Wu, "Twisted quantum double model of topological phases in two dimensions," Phys. Rev. B **87**, 125114 (2013).

[211] D. E. Evans and Y. Kawahigashi, "On Ocneanu's theory of asymptotic inclusion for subfactors, topological quantum field theories and quantum doubles," Int. J. Math. **06**, 205 (1995).

[212] Y. Hu, N. Geer, and Y.-S. Wu, "Full dyon excitation spectrum in extended Levin-Wen models," Phys. Rev. B **97**, 195154 (2018).

[213] P. Bruillard, S.-H. Ng, E. C. Rowell, and Z. Wang, "Rank-finiteness for modular categories," J. Am. Math. Soc. **29**, 857 (2015).

[214] M. Mignard and P. Schauenburg, "Modular categories are not determined by their modular data," (2017), arXiv:1708.02796.

[215] X. Wen and X.-G. Wen, "Distinguish modular categories and 2+1D topological orders beyond modular data: Mapping class group of higher genus manifold," (2019), arXiv:1908.10381.

[216] A. Francuz, J. Dziarmaga, G. Vidal, and L. Cincio, "Determining topological order from infinite projected entangled pair states," (2019), arXiv:1910.09661.

[217] N. Kimura, "A generalization of the Dijkgraaf-Witten invariants for cusped 3-manifolds," (2018), arXiv:1805.05130.

[218] G. Dauphinais, L. Ortiz, S. Varona, and M. A. Martin-Delgado, "Quantum error correction with the semion code," New. J. Phys **21**, 053035 (2019).

[219] J. Magdalena, *Quantum error correcting codes from general topological quantum models*, Master's Thesis, in preparation.

[220] T. Tao, *Cayley graphs and the algebra of groups*, 2012, eprint: {https://terrytao.wordpress.com/}.

[221] U. Pachner, "Bistellare Äquivalenz kombinatorischer Mannigfaltigkeiten," Arch. Mat. **30**, 89 (1978).

[222] N. Reshetikhin and V. G. Turaev, "Invariants of 3-manifolds via link polynomials and quantum groups," Invent. Math. **103**, 547 (1991).

[223] T. B. Wahl, S. T. Haßler, H.-H. Tu, J. I. Cirac, and N. Schuch, "Symmetries and boundary theories for chiral projected entangled pair states," Phys. Rev. B **90**, 115133 (2014).

[224] S. Yang, T. B. Wahl, H.-H. Tu, N. Schuch, and J. I. Cirac, "Chiral Projected Entangled-Pair State with Topological Order," Phys. Rev. Lett. **114**, 106803 (2015).

[225] D. Poilblanc, J. I. Cirac, and N. Schuch, "Chiral topological spin liquids with projected entangled pair states," Phys. Rev. B **91**, 224431 (2015).

[226] D. Poilblanc, N. Schuch, and I. Affleck, "$SU(2)_1$ chiral edge modes of a critical spin liquid," Phys. Rev. B **93**, 174414 (2016).

[227] D. Poilblanc, "Investigation of the chiral antiferromagnetic Heisenberg model using projected entangled pair states," Phys. Rev. B **96**, 121118 (2017).

[228] J.-Y. Chen, L. Vanderstraeten, S. Capponi, and D. Poilblanc, "Non-Abelian chiral spin liquid in a quantum antiferromagnet revealed by an iPEPS study," Phys. Rev. B **98**, 184409 (2018).

[229] T. B. Wahl, H.-H. Tu, N. Schuch, and J. I. Cirac, "Projected Entangled-Pair States Can Describe Chiral Topological States," Phys. Rev. Lett. **111**, 236805 (2013).

[230] J. Dubail and N. Read, "Tensor network trial states for chiral topological phases in two dimensions and a no-go theorem in any dimension," Phys. Rev. B **92** (2015).

[231] T. Wahl and J. Eisert, *A no go theorem for Gaussian chiral PEPS*, in preparation.

[232] Z.-C. Gu, Z. Wang, and X.-G. Wen, "Lattice model for fermionic toric code," Phys. Rev. B **90**, 085140 (2014).

[233] N. Bultinck and M. Cheng, "Filling constraints on fermionic topological order in zero magnetic field," Phys. Rev. B **98**, 161119 (2018).

[234] J. Eisert, "Lecture Notes Advanced quantum mechanics," eprint: `https://www.physik.fu-berlin.de/.../ag-eisert/teaching/ws18-19`.

[235] A. Kapustin, A. Turzillo, and M. You, "Spin topological field theory and fermionic matrix product states," Phys. Rev. B **98**, 125101 (2018).

[236] A. Y. Kitaev, "Unpaired Majorana fermions in quantum wires," Physics-Uspekhi **44**, 131 (2001).

[237] R. Usher, "Fermionic 6j-symbols in superfusion categories," J. Algebra **503**, 453 (2018).

[238] D. Gaiotto and A. Kapustin, "Spin TQFTs and fermionic phases of matter," Int. J. Mod. Phys. A **31**, 1645044 (2016).

[239] Z.-C. Gu, "Efficient simulation of Grassmann tensor product states," Phys. Rev. B **88**, 115139 (2013).

[240] Z.-C. Gu and X.-G. Wen, "Symmetry-protected topological orders for interacting fermions: Fermionic topological nonlinear σ models and a special group supercohomology theory," Phys. Rev. B **90**, 115141 (2014).

[241] A. C. Balram, C. Tőke, A. Wójs, and J. K. Jain, "Fractional quantum Hall effect in graphene: Quantitative comparison between theory and experiment," Phys. Rev. B **92** (2015).

[242] J. I. A. Li, Q. Shi, Y. Zeng, K. Watanabe, T. Taniguchi, J. Hone, and C. R. Dean, "Pairing states of composite fermions in double-layer graphene," Nat. Phys. **15**, 898 (2019).

[243] J. S. Helton, K. Matan, M. P. Shores, E. A. Nytko, B. M. Bartlett, Y. Yoshida, Y. Takano, A. Suslov, Y. Qiu, J.-H. Chung, D. G. Nocera, and Y. S. Lee, "Spin Dynamics of the Spin-1/2 Kagome Lattice Antiferromagnet $ZnCu_3(OH)_6Cl_2$," Phys. Rev. Lett. **98**, 107204 (2007).

[244] T.-H. Han, J. S. Helton, S. Chu, D. G. Nocera, J. A. Rodriguez-Rivera, C. Broholm, and Y. S. Lee, "Fractionalized excitations in the spin-liquid state of a kagome-lattice antiferromagnet," Nature **492**, 406 (2012).

[245] D. V. Pilon, C. H. Lui, T. H. Han, D. Shrekenhamer, A. J. Frenzel, W. J. Padilla, Y. S. Lee, and N. Gedik, "Spin-Induced Optical Conductivity in the Spin-Liquid Candidate Herbertsmithite," Phys. Rev. Lett. **111**, 127401 (2013).

[246] S. Bravyi and A. Kitaev, "Universal quantum computation with ideal Clifford gates and noisy ancillas," Phys. Rev. A **71**, 022316 (2005).

[247] J. R. Wootton, J. Burri, S. Iblisdir, and D. Loss, "Error Correction for Non-Abelian Topological Quantum Computation," Phys. Rev. X **4**, 011051 (2014).

[248] J. R. Wootton and A. Hutter, "Active error correction for Abelian and non-Abelian anyons," Phys. Rev. A **93**, 022318 (2016).

[249] S. Burton, C. G. Brell, and S. T. Flammia, "Classical simulation of quantum error correction in a Fibonacci anyon code," Phys. Rev. A **95**, 022309 (2017).

[250] M. C. Bañuls, R. Blatt, J. Catani, A. Celi, J. I. Cirac, M. Dalmonte, L. Fallani, K. Jansen, M. Lewenstein, S. Montangero, C. A. Muschik, B. Reznik, E. Rico, L. Tagliacozzo, K. V. Acoleyen, F. Verstraete, U. .-.-J. Wiese, M. Wingate, J. Zakrzewski, and P. Zoller, "Simulating Lattice Gauge Theories within Quantum Technologies," (2019), arXiv:1911.00003.

[251] R. Oliveira and B. M. Terhal, "The Complexity of Quantum Spin Systems on a Two-dimensional Square Lattice," Quantum Info. Comput. **8**, 900 (2008).

[252] R. König, "Simplifying Quantum Double Hamiltonians Using Perturbative Gadgets," Quantum Info. Comput. **10**, 292 (2010).

[253] S. D. Bartlett and T. Rudolph, "Simple nearest-neighbor two-body Hamiltonian system for which the ground state is a universal resource for quantum computation," Phys. Rev. A **74**, 040302 (2006).

[254] S. Bravyi, D. P. DiVincenzo, and D. Loss, "Schrieffer–Wolff transformation for quantum many-body systems," Ann. Phys. **326**, 2793 (2011).

[255] D. Aharonov and T. Naveh, "Quantum NP - A Survey," (2002), arXiv:quant-ph/0210077.

[256] C. Bloch, "Sur la théorie des perturbations des états liés," Nucl. Phys. **6**, 329 (1958).

[257] J. R. Schrieffer and P. A. Wolff, "Relation between the Anderson and Kondo Hamiltonians," Phys. Rev. **149**, 491 (1966).

[258] C. Xu and L. Fu, "Fractionalization in Josephson junction arrays hinged by quantum spin Hall edges," Phys. Rev. B **81**, 134435 (2010).

[259] A. Roy, B. M. Terhal, and F. Hassler, "Quantum Phase Transitions of the Majorana Toric Code in the Presence of Finite Cooper-Pair Tunneling," Phys. Rev. Lett. **119**, 180508 (2017).

[260] Z. Nussinov, G. Ortiz, and E. Cobanera, "Arbitrary dimensional Majorana dualities and architectures for topological matter," Phys. Rev. B **86**, 085415 (2012).

[261] S. Plugge, A. Rasmussen, R. Egger, and K. Flensberg, "Majorana box qubits," New J. Phys. **19**, 012001 (2017).

[262] T. Karzig, C. Knapp, R. M. Lutchyn, P. Bonderson, M. B. Hastings, C. Nayak, J. Alicea, K. Flensberg, S. Plugge, Y. Oreg, C. M. Marcus, and M. H. Freedman, "Scalable designs for quasiparticle-poisoning-protected topological quantum computation with Majorana zero modes," Phys. Rev. B **95**, 235305 (2017).

[263] J. Alicea, "New directions in the pursuit of Majorana fermions in solid state systems," Rep. Prog. Phys. **75**, 076501 (2012).

[264] M. Leijnse and K. Flensberg, "Introduction to topological superconductivity and Majorana fermions," Semicond. Sci. Techn. **27**, 124003 (2012).

[265] C. W. J. Beenakker, "Search for Majorana Fermions in Superconductors," Annu. Rev. Con. Mat. Phys. **4**, 113 (2013).

[266] R. Aguado, "Majorana quasiparticles in condensed matter," Rivista del Nuovo Cimento **40**, 523 (2017).

[267] R. M. Lutchyn, E. P. A. M. Bakkers, L. P. Kouwenhoven, P. Krogstrup, C. M. Marcus, and Y. Oreg, "Majorana zero modes in superconductor–semiconductor heterostructures," Nat. Rev. Mat. **3**, 52 (2017).

[268] S. Das Sarma, M. Freedman, and C. Nayak, "Majorana Zero Modes and Topological Quantum Computation," npj Quant. Inf. **1** (2015).

[269] V. Mourik, K. Zuo, S. M. Frolov, S. R. Plissard, E. P. A. M. Bakkers, and L. P. Kouwenhoven, "Signatures of Majorana Fermions in Hybrid Superconductor-Semiconductor Nanowire Devices," Science **336**, 1003 (2012).

[270] S. M. Albrecht, A. P. Higginbotham, M. Madsen, F. Kuemmeth, T. Jespersen, J. Nygård, P. Krogstrup, and C. Marcus, "Exponential Protection of Zero Modes in Majorana Islands," Nature **531**, 206 (2016).

[271] M. T. Deng, S. Vaitiekenas, E. B. Hansen, J. Danon, M. Leijnse, K. Flensberg, J. Nygård, P. Krogstrup, and C. M. Marcus, "Majorana bound state in a coupled quantum-dot hybrid-nanowire system," Science **354**, 1557 (2016).

[272] F. Nichele, A. C. C. Drachmann, A. M. Whiticar, E. C. T. O'Farrell, H. J. Suominen, A. Fornieri, T. Wang, G. C. Gardner, C. Thomas, A. T. Hatke, P. Krogstrup, M. J. Manfra, K. Flensberg, and C. M. Marcus, "Scaling of Majorana Zero-Bias Conductance Peaks," Phys. Rev. Lett. **119**, 136803 (2017).

[273] S. Gazibegovich, D. Car, H. Zhang, S. C. Balk, J. A. Logan, M. W. A. de Moor, M. C. Cassidy, R. Schmits, D. Xu, G. Wang, P. Krogstrup, R. L. M. Op het Veld, J. Shen, D. Bouman, B. Shojaei, D. Pennachio, J. S. Lee, P. J. van Veldhoven, S. Koelling, M. A. Verheijen, L. P. Kouwenhoven, C. J. Palmstrøm, and E. P. A. M. Bakkers, "Epitaxy of advanced nanowire quantum devices," Nature **548**, 434 (2017).

[274] H. Zhang, C. X. Liu, S. Gazibegovich, D. Xu, J. Logan, G. Wang, N. van Loo, J. D. S. Bommer, M. W. A. de Moor, D. Car, R. L. M. Op het Veld, P. J. Veldhoven, S. Koelling, M. A. Verheijen, C. J. Palmstrøm, M. Pendharkar, D. J. Pennachio, B. Shojaei, J. S. Lee, E. P. A. M. Bakkers, and L. P. Kouwenhoven, "Quantized Majorana conductance," Nature **556**, 74 (2018).

[275] A. Andreev, "Thermal conductivity of the intermediate state of superconductors II," Sov. Phys. JETP **20**, 1490 (1965).

[276] A. Andreev, "Electron spectrum of the intermediate state of superconductors," Sov. Phys. JETP **22**, 18 (1966).

[277] J. A. Sauls, "Andreev bound states and their signatures," Philos. Trans. Royal Soc. A: Math. Phys. Eng. Sci. **376**, 20180140 (2018).

[278] R. V. Mishmash, B. Bauer, F. von Oppen, and J. Alicea, "Dephasing and leakage dynamics of noisy Majorana-based qubits: Topological versus Andreev," (2019), arXiv:1911.02582.

[279] E. Prada, P. San-Jose, M. W. A. de Moor, A. Geresdi, E. J. H. Lee, J. Klinovaja, D. Loss, J. Nygård, R. Aguado, and L. P. Kouwenhoven, "From Andreev to Majorana bound states in hybrid superconductor-semiconductor nanowires," (2019), arXiv:1911.04512.

[280] J. Manousakis, C. Wille, A. Altland, R. Egger, K. Flensberg, and F. Hassler, "Weak measurement protocols for Majorana bound state identification," (2019), arXiv:1910.10591.

[281] L. Fu, "Electron Teleportation via Majorana Bound States in a Mesoscopic Superconductor," Phys. Rev. Lett. **104**, 056402 (2010).

[282] T. Hyart, B. van Heck, I. C. Fulga, M. Burrello, A. R. Akhmerov, and C. W. J. Beenakker, "Flux-controlled quantum computation with Majorana fermions," Phys. Rev. B **88**, 035121 (2013).

[283] B. Béri, "Majorana-Klein Hybridization in Topological Superconductor Junctions," Phys. Rev. Lett. **110**, 216803 (2013).

[284] B. M. Terhal, "Quantum error correction for quantum memories," Rev. Mod. Phys. **87**, 307 (2015).

[285] S. C. Morampudi, C. von Keyserlingk, and F. Pollmann, "Numerical study of a transition between $\mathbb{Z}_2$ topologically ordered phases," Phys. Rev. B **90**, 035117 (2014).

[286] D. I. Tsomokos, T. J. Osborne, and C. Castelnovo, "Interplay of topological order and spin glassiness in the toric code under random magnetic fields," Phys. Rev. B **83**, 075124 (2011).

Summary

In this Thesis, we discuss non-chiral topological order from a tensor network perspective. The Thesis is divided into three parts. The first part introduces the necessary background material and provides the context of our work. The second part is devoted to the theory of non-chiral topological order, its various mathematical descriptions and the relations among the latter. The third part discusses how non-chiral topological order might be realized in artificial quantum matter by exploiting the tensor network structure of topologically ordered ground states.

We review the concept of *gapped local quantum phases* and discuss how they are classified according to their *entanglement* properties. Tensor network states are introduces as a suitable framework to characterize the latter. Turning to the main subject of our studies – topological order in two dimension, we present a conceptual introduction to the topic by discussing the paradigmatic example of the toric code and its tensor network ground state. Already at this stage we observe a crucial insight: Virtual symmetries of the tensor network give rise to topological order.

We complete the introduction to topological order by a general review of the *algebraic theory of anyons* in the language of braided fusion categories. We highlight a particular mathematical construction, which yields non-chiral anyon models called the Drinfeld center and comment on its importance for Hamiltonian models and tensor network descriptions of non-chiral topological order. Elaborating on the latter observation we discuss the connections between Levin–Wen string-net models and a particular class of tensor network states – so-called matrix product operator isometric projected entangled pair states (MPO-isometric PEPS). As an illustrative example, we present the twisted-quantum double models in the two aforementioned formalisms and review how they are related to state-sum constructions and topological manifold invariants.

As an extension to the established formalisms, we present a simple fermionic variant of string-net models and MPO-injective PEPS.

At last we discuss a scheme to realize topological order in a specific mesoscopic hardware platform – networks of tunnel coupled so-called Majorana Cooper boxes. We review different variants of low-energy effective theories and how they can be employed for *Hamiltonian design*. We discuss the effective theory of tunnel coupled MCB networks, design functional units composed of the latter and show how they can be assembled to yield effective Levin–Wen string-net phases. We discuss a blueprint for double semion phase in detail and sketch the additional effort needed to design a double Fibonacci phase, which is of particular interest due to its potential application as a universal topological quantum computer.

Zusammenfassung

Diese Arbeit diskutiert nichtchirale topologische Ordnung innerhalb eines Tensornetzwerk-Formalismusses. Sie ist in drei Teile gegliedert. Im ersten Teil wird notwendiges Hintergrundmaterial bereitgestellt und der Kontext dieser Arbeit erläutert. Der zweiten Teil widmet sich der theoretischen Beschreibung von nichtchiraler topologischer Ordnung mit verschiedenen mathematischen Formalismen und zeigt auf, wie diese miteinander in Verbindung stehen. Im dritten Teil wird ein Vorschlag diskutiert, wie topologische Ordnung in bestimmten synthetischen Materialien erzeugt werden könnte. Für diesen Vorschlag ist es zentral, die Tensornetzwerkstruktur topologischer Zustände auszunutzen.
Wir beginnen mit einer Diskussion von lokalen Quantenphasen mit einer Energielücke oberhalb des Grundzustands und erklären, wie diese anhand ihrer Verschränkungseigenschaften klassifiziert werden können. Tensornetzwerkzustände bieten hier einen geeigneten Zugang. Anschließend wenden wir uns dem zentralen Gegenstand unserer Arbeit zu – nichtchirale topologische Ordnung in zwei Dimensionen. Wir präsentieren eine konzeptionelle Einleitung in das Thema, indem wir das paradigmatische "toric code" Modell diskutieren und seinen Tensornetzwerk-Grundzustand erörtern. Bereits an dieser Stelle können wir eine zentrale Beobachtung machen, nämlich, dass virtuelle Symmetrien des Tensornetzwerks ursächlich sind für topologische Ordnung.
Wir beenden die Einleitung in das Thema mit einer Zusammenfassung der abstrakten algebraischen Anyonen-Theorie, welche durch bestimmte Fusionskategorien (braided fusion categories) beschrieben wird. Dabei heben wir eine bestimmte Konstruktion aus der Kategorientheorie hervor, die sogenannte Drinfeld center Konstruktion, welche zentral ist für die Hamiltonsche Formulierung von nichtchiraler topologischer Ordnung in sogenannten Levin-Wen Modellen und einer Klasse von Tensornetzwerkzuständen, den sogenannten "matrix product operator isometric projected entangled pair states (MPO-isometric PEPS)".
Wir erläutern die beiden letztgenannten Formalismen am Beispiel der sogenannten fermionischen twisted quantum double models und zeigen auf, wie diese mit Zustandssummen und topologischen Invarianten auf Mannigfaltigkeiten zusammenhängen.
Als eine Erweiterung der bisher präsentierten bereits existierenden Theorien präsentieren wir eine einfache Variante von fermionischen Modellen mit topologischer Ordnung und deren MPO-injective PEPS Grundzustände.
Zuletzt diskutieren wir einen Vorschlag, wie topologische Ordnung in spezifischen mesoskopischen Systemen aus tunnel-gekoppelten sogenannten Majorana-Cooper Boxen (MCBs) realisiert werden könnte. Dazu geben wir einen Überblick über verschiedene Varianten der von effektiven Niedrigenergie-Theorien und wie diese genutzt werden können um gezielt Hamiltonians zu erzeugen. Wir diskutieren die effektive Niedrigenergie-Theorie der gekoppelten MCBs, zeigen, wie kleine funktionale Bausteine in diesen Netzwerken gebaut werden können und wie diese so zusammen gebaut werden können, dass man effektiv eine Levin-Wen Phase erhält. Wir diskutieren eine Blaupause für das sogenannte double semion Modell im Detail und skizzieren, welcher zusätzlicher Aufwand notwendig wäre um eine sogenannte double Fibonacci Phase zu erzeugen. Diese Phase ist vor allem interessant, da sie prinzipiell als universeller topologischer Quantenrechner geeignet ist.

Anteil der Autorin bei Konzeption, Durchführung und Verfassung der zugrundeliegenden Arbeiten

Die Dissertation beruht auf den Publikationen [1–3]. Die Beiträge der Autorin zu den genannten Publikationen sind wie folgt:

[1] Die Autorin war federführend in diesem Projekt. Die Projektidee, sämtliche Herleitungen, Rechnungen und die Interpretationen der Ergebnisse ist Werk der Autorin. An der Verfassung der Publikation war sie maßgeblich beteiligt.

[2] Die Autorin war federführend in diesem Projekt. Die Kombination von Tensornetzwerkmethoden mit der Theorie von Majorana-Cooper-Box Netzwerken ist die Idee der Autorin. Sie hat die Entwicklung der Methoden und ihre Anwendung vorgenommen und war maßgeblich an der Verfassung der Publikation beteiligt.

[3] Die Autorin war an der Konzeption der Arbeit beteiligt und hat an der Formulierung der Publikation mitgewirkt. Sie hat sämtliche Ergebnisse des Erstautors detailliert mit dem Erstautor diskutiert und somit zur konzeptionellen Klarheit des Materials beigetragen.

Eigenständigkeitserklärung

Ich bestätige, die vorliegende Arbeit selbstständig und nur mit Hilfe der angegebenen Hilfsmittel verfasst zu haben. Alle Stellen der Arbeit, die wörtlich oder sinngemäßaus Veröffentlichungen oder aus anderweitigen fremden Quellen entnommen wur den, sind als solche kenntlich gemacht. Ich habe die Arbeit noch nicht in einem früheren Promotionsverfahren eingereicht.

Carolin Wille, Berlin, 6. Dezember 2019